KINGDOM OF CAMBODIA

NATION RELIGION KING

NATIONAL CLIMATE REPORT

PART I

CLIMATE CHANGE

PHYSICAL SCIENCE BASIS

January 2026

National Climate Report

About Authors

Lead Authors:

- Royal University of Phnom Penh (RUPP): LAY Chanthy, SEAK Sophat, CHOU Phanith, *et al.*
- Royal University of Agriculture (RUA): KIM Soben, SIEN Teamhy, *et al.*
- Institute of Technology of Cambodia (ITC): SOK Ty, SONG Layheang, *et al.*

Contributing Authors, Reviewer and Editors:

- **H.E. Dr. HENG Chanthoeun**, Deputy Director General, General Directorate of Policy and Strategy, Ministry of Environment.
- **H.E. MENG Monyrak,** Deputy Director General, General Directorate of Policy and Strategy, Ministry of Environment.
- **Mr. SUM Cheat,** Deputy Director of Department of Climate Change, General Directorate of Policy and Strategy, Ministry of Environment.
- **Mr. LEANG Sophal,** Deputy Director of Department of Climate Change, General Directorate of Policy and Strategy, Ministry of Environment.
- Officials of General Directorate of Policy and Strategy, Ministry of Environment.
- NAP Phase 1 Project Team
- Royal University of Phnom Penh
- Royal University of Agriculture
- Institute of Technology of Cambodia
- Members of Technical Working Group on Climate Change
- United Nations Development Programme (UNDP)
- Food and Agriculture Organization (FAO)
- United Nations Office for Project Services (UNOPS)

Compiler, Reviewers and Editors:

- NAP Phase 1 Project Team
- National Consultants

International Peer Reviewers and Editors:

- Dr. Sarah ROSE-JENSEN, PhD.

FOREWORD

The Royal Government of Cambodia recognizes climate change as one of the most profound and urgent challenges of our time. As one of the country's most vulnerable to its impacts, Cambodia remains steadfast in its commitment to addressing this global crisis, despite having contributed minimally to its historical and current causes. We believe that ambitious, science-based, and cooperative climate action is critical to safeguarding our people, ecosystems, and ensuring sustainable development.

This Cambodia National Climate Report (NCR) represents a significant milestone in Cambodia's climate response. It comprises two parts: *Part I- Physical Science-Basis* and *Part II - Climate Change Impacts, Vulnerability Assessment, and Adaptation*. Together, these components provide the most up-to-date scientific data and analysis on climate change in Cambodia. By offering reliable global, regional, and country-specific information, the report serves as a valuable resource for policymakers, decision-makers, planners, government officials, researchers, academics, practitioners and development partners. This data will support critical considerations and decisions made today to strengthen Cambodia's climate resilience and advance national efforts to build a sustainable, climate-resilient society.

The NCR forms as a strategic resource for advancing Cambodia's climate objectives. It supports the achievement of Nationally Determined Contributions (NDCs 3.0), which set a goal of reducing greenhouse gas emissions by 16-55 percent by 2035—under two different climate change scenarios (unconditional: 16 percent; and conditional: 55 percent)—and it also informs the development of NDC 3.0. The NDC 3.0 outlines Cambodia's climate change commitments and policies, including the Long-Term Strategy for Carbon Neutrality (LTS4CN), in which Cambodia aims to achieve a carbon-neutral and resilient society by 2050 as the first country in ASEAN and the second LDCs worldwide to submit a Long-Term Low Emission Development Strategy (LTLEDS). As noted in the NDC 3.0 and reiterated in this NCR, climate change is predicted to reduce Cambodia's economic growth by up to 10 percent, affecting the country's aim to transition to upper-middle-income status by 2030 and high-income status by 2050. The data presented in the NCR supports the ambitious development goals laid out in the NDC 3.0 by providing the most up-to-date data on climate change and its effects on the country.

Additionally, the NCR Part I provides key data that supports the implementation of the Cambodia Climate Change Strategic Plan 2024-2033 (CCCSP) and aligns with some of the national development strategies, including the Royal Government's Pentagonal Strategy Phase 1, 2024–2028 (Growth, Employment, Equity, Efficiency, and Sustainability) and the Ministry of Environment's Circular Strategy on Environment (Clean, Green, and Sustainable) 2023-2028. The CCCSP laid out three strategic objectives, promoting greenhouse gas mitigation, strengthening adaptation to climate change, and promoting good governance and digital transformation. The NCR provides up-to-date and actionable data on current and projected climate change, which supports the development of policies and plans to promote these strategic objectives and overall achievement of the goals outlined in the CCCSP.

Finally, the NCR Part I builds on scientific research data/information related to climate change and the status of emissions presented in the Initial Biennial Transparency Report 1 (BTR1) under the Paris Agreement and furthers the work begun in that report. The BTR1 outlined the information needed to track progress made in implementing and achieving

NDCs under Article 4 of the PA. The NCR Part I provides updated data on climate change effects and greenhouse gas emissions, allowing for tracking of progress and setting the next targets for limiting emissions. The BTR1 also outlined the financial, technology development and transfer and capacity-building support needed to achieve Cambodia's climate goals. The NCR Part I provides further information on next steps for research and policy development to support achievement of these goals.

I would like to express my sincere appreciation to the Ministry of Environment's Management Team and the General Directorate of Policy and Strategy (GDPS) for their effective leadership and coordination. I also gratefully acknowledge the valuable contributions of the Technical Working Group on Climate Change (TWGCC), relevant-line government ministries and institutions, academia, development partners, the private sectors, and community stakeholders. This work was made possible through the financial support of the Green Climate Fund (GCF) and the implementation support provided by the United Nations Office for Project Services (UNOPS).

Our efforts must continue with greater determination. To realize the vision set forth in this report, Cambodia will require sustained partnerships and strengthened support, particularly in the areas of financing, capacity development (capacity building or resource development), climate science-based knowledge sharing, and technology transfer. Crucially, we also need a shared commitment and a common goal of building the climate-resilient and low-emission development.

I do hope that the NCR Part I is very useful to all key stakeholders on climate in Cambodia and internationally. May the knowledge and insights contain within this document guide impactful and enduring climate action in Cambodia and beyond.

CHUOP Paris

Secretary of State

ACKNOWLEDGEMENT

The development of the National Climate Report (NCR) was supported by the Green Climate Fund (GCF) under the Preparatory Readiness Programme through the United Nations Office for Project Services (UNOPS), as part of a broader process of cooperation with the Ministry of Environment / National Council for Sustainable Development (NCSD), the General Directorate of Policy and Strategy, and the Department of Climate Change (DCC) in Cambodia.

The Ministry of Environment, through the General Directorate of Policy and Strategy, extends its sincere appreciation to: **H.E. Dr. EANG Sophalleth**, Minister of Environment and Chair of the NCSD; **H.E. Dr. CHUOP Paris**, Secretary of State and Chair of the Technical Working Group on Climate Change (TWGCC); **H.E. Dr. PHEAV Sovuthy**, Under Secretary of State and Chair of the Project Steering Committee; **H.E. SUM Thy**, Director General of the General Directorate of Policy and Strategy (GDPS) for valuable guidance. Special thanks to **H.E. Dr. HENG Chanthoeun**, Deputy Director General of GDPS and NAP National Project Director; **H.E. MENG Monyrak**, Deputy Director General of GDPS and National Project Director; **Mr. SUM Cheat**, Deputy Director of the Department of Climate Change and NAP National Project Manager; **Mr. LEANG Sophal**, Deputy Director of the Department of Climate Change and National Project Manager; and the NAP Project Coordination Team of GDPS for technical inputs.

We extend our heartfelt gratitude to the Royal University of Phnom Penh, the Royal University of Agriculture, the Institute of Technology of Cambodia, and the Prek Leap National Institute of Agriculture for their technical intribution and cooperation.

Profound thanks are also extended to the members of the Technical Working Group on Climate Change from line ministries including MoE, MAFF, MoWRAM, MoP, MoT, MEE, MISTI, MOWA, MRD, MoIn, MPWT, MoH, MoEYS, MEF, MLMUPC, MFA&IC, MoI, NCDM, and CDC; provincial departments; communities; concerned development partners such as UNDP, FAO, and UNOPS; as well as NGOs and the private sector for their credible and valuable inputs, comments, and suggestions.

Finally, our deepest gratitude goes to peer reviewers for their valuable comments and suggestions, which greatly contributed to the revision and finalization of this report.

TABLE OF CONTENTS

LIST OF TABLES

LIST OF FIGURES

LIST OF ACRONYMS

ADB	Asian Development Bank
AFOLU	Agriculture, Forestry and Other Land Use
AHE	Anthropogenic Heat Emission
ALT	Active-Layer Thickness
AR6	Sixth Assessment Report
BAU	Business as Usual
BCSD	Bias-Corrected Spatial Downscaling
CCCSP	Cambodia Climate Change Strategic Plan
CCN	Cloud Condensation Nuclei
CDD	Consecutive Dry Days
CDWQS	Cambodia Drinking Water Quality Standard
CEGIM	Climate Economic Growth Impact Model
CFC	Chlorofluorocarbon
CH_4	Methane
CMCCC	Euro-Mediterranean Center on Climate Change
CMIP5	Coupled Model Inter-comparison Project Phase 5
CO	Carbon Monoxide
CO_2	Carbon Dioxide
COP	Conference of the Parties
CWD	Consecutive Wet Days
ELC	Economic Land Concessions
ENSO	El Niño–Southern Oscillation
ESL	Extreme Sea level
ESMs	Earth System Models
ETCCDMI	Extreme Rainfall Detection Monitoring and Indices
FOLU	Forest and Other Land Use
FiA	Fisheries Administration
GCM	General Circulation Models
GMSL	The Global Mean Sea Level
GHG	Greenhouse Gases
GST	Global Surface Temperature
HCFC	Hydrochlorofluorocarbon
HFC	Hydrofluorocarbon
IN	Ice Nuclei
IOD	Indian Ocean Dipole
IPCC	Intergovernmental Panel on Climate Change

IPPU	Industrial Processes and Product Use
LGM	Last Glacial Maximum
LULC	Land Use and Land Cover
MAGT	Mean Annual Ground Temperature
MASL	Meters Above Sea Level
MBE	Mean Bias Error
NASA	National Aeronautics and Space Administration
NCSD	National Council for Sustainable Development
NEEP	National Energy Efficiency Policy
NMVOC	Non-Methane Volatile Organic Compounds
NOx	Nitrogen Oxide
OHC	Ocean Heat Content
ORP	Oxidation-Reduction Potential
PRCPTOT	Total Annual Precipitation
PPM	Part Per Million
PPB	Part Per Billion
RCPs	Representative Concentration Pathways
RMSE	Root Mean Square Error
SO_2	Sulphur Dioxide
SROCC	Special Report on the Ocean and Cryosphere in a Changing Climate
SSPs	Shared Socio-economic Pathways
SST	Sea-surface Temperature
TCs	Tropical Cyclones
TDs	Tropical Depressions
TDS	Total Dissolved Solids
TOA	Top of Atmosphere
UHI	Urban Heat Islands
UNCBD	United Nations Convention on Biological Diversity
UNCCD	United Nations Convention to Combat Desertification
UNEP	United Nations Environment Programme
UNFCCC	United Nations Framework Convention on Climate Change
UV	Ultraviolet
WBG	World Bank Group

LIST OF SCIENTIFIC UNITS

Name	Symbol name	Unit
Annual rainfall	Annual rainfall	mm
Amount	Million	M
Area size	Kilometer square	km^2
	Meter square	m^2
	Hectare	ha
Area volume	Area Volume	km^3, m^3, dm^3
Concentration	Concentration	ppm, ppb
	Microgram per liter	µg/L
Currency	US Dollar	USD
Decreasing	Decreasing	-
Increasing	Increasing	+
Increase or decrease	Increase or decrease	±
Length	Kilometer	km
	Meter	m
	Centimeter	cm
	Millimeter	mm
Percentage	Percentage	%
Temperature	Degree Celsius	^oC
Time duration	Second	s
	Minute	m
	Hour	Hr
	Day	D
	Month	M
	Year	Y
	Decade	s
	Century	th-c
Thickness and depth	Meter	m
	Meter	m
	Decimeter	dm
	Centimeter	cm
Weight	Gigaton	Gtv
	Ton	T
	Kilogram	Kg
	Gram	G

EXECUTIVE SUMMARY

The *Cambodia National Climate Report* (NCR) comprises two main parts: *Part I: Physical Science Based-Climate Report* and *Part II: Climate Change Impacts, Vulnerability Assessment and Adaptation Report*. The NCR report was developed with the aim of providing the most recent scientific climate change information, data, impacts, and adaptation strategies for Cambodia. It serves as a baseline and scientific input for the government, policymakers, decision-makers, planners, development partners, academia, researchers, and practitioners in making interventions and decisions for present and future responses to climate change impacts, as well as mainstreaming climate change adaptation and resilience in Cambodia.

Part I: Physical Science-based Climate Report seeks to compile the most up-to-date, scientific, and evidence-based climate change information and data for Cambodia, serving as a physical science baseline and providing scientific and technical input for informed decision-making in Cambodia's current and future climate change responses. The goals of Part 1 are to provide an overview of the latest global and regional scientific climate change; describe the current weather and climate conditions of Cambodia, including observed changes and variability; assess major trends in climate change that affect Cambodia; identify key physical drivers, observed impacts, and sectoral vulnerabilities related to climate change in Cambodia; and present climate projections and identify appropriate future climate scenarios for national adaptation planning and risk management.

Chapter 1 provides an in-depth physical science-based assessment of climate change, with a focus on its implications for broader global contexts. Climate change has led to rising global temperatures, altered precipitation patterns, more frequent extreme weather events, and sea-level rise. The Chapter 1 focuses on changes that have been observed globally in land surface and ocean temperatures, and the effects of these shifts on the environment, including changes to sea level and the El Niño Southern Oscillation, which affects weather conditions in Cambodia, particularly precipitation. The Chapter also covers projected future changes in temperature and resulting effects on weather and sea level, based on various climate and emissions scenarios. Most scenarios project further increases in global temperature, with potentially dramatic effects, particularly in Southeast Asia, which is disaster-prone and highly climate vulnerable. Many countries in the region, including Cambodia, experienced their hottest year on record in 2023, along with a barrage of extreme conditions, from droughts and heat waves to floods and storms. Climate change exacerbated the frequency and severity of such events, profoundly impacting societies, economies, and, most importantly, human lives and the environment that we live in.

Chapter 2 focuses on effects of climate change on Cambodia, including overall climate and weather data, and historical changes in climate. The Chapter covers Cambodia's unique and varied climatology; weather characteristics, including the effects of the El Niño Southern Oscillation; and the seasonal characteristics of Cambodia's wet and dry seasons. Cambodia has already experienced effects of climate change, which include increases in overall temperature; changes to precipitation and effects on the rainy and dry seasons; and increased extreme weather events, such as droughts, floods, and typhoon effects. The historical predictability of seasonal cycles is becoming more erratic, posing challenges for agriculture, water resources, and public health. The combined

impacts of rising temperatures, changing monsoon patterns, and the growing intensity of storms and droughts underscore the urgent need for effective climate adaptation strategies. As with the global climate change data, climate change in Cambodia and associated effects is projected to increase over the next decades, unless countries globally take strong action to reduce emissions and climate change.

The Chapter 2 concludes with knowledge gaps in climate change and recommendations for future research and study. Long-term data on climate in Cambodia is still limited, which in turn limits the ability to model future climate change and extreme weather. In particular, predicting extreme weather events, such as droughts and floods, is uncertain, which creates challenges for infrastructure planning and policy development. The chapter recommends enhancing data availability and quality and advancing information integration and sharing across various stakeholders involved as well as strengthening links between climate change researchers and communities which are most affected by climate change, to enable efficient adaptation and to increase resilience to climate and environmental change.

Chapter 3 examines changes in the sea level and coastal ecosystem in Cambodia. Coastal regions and marine ecosystems are particularly vulnerable to effects of global warming and changes to the cryosphere, the region of earth which is frozen, including glaciers and ice caps. These areas face significant threats from rising sea levels and changes in coastal ecosystems. The impacts of climate change in coastal regions include sea level rise, coastal erosion, salinity intrusion, ecosystem degradation, and socioeconomic impact. Sea level rise is a significant concern for Cambodia, particularly due to its extensive coastline and low-lying areas. Changing climate patterns affect mangrove forests, coral reefs, seagrass beds, salt marshes, and estuaries, which are facing degradation due to habitat loss, pollution, erosion, and shore collapse under climate change. This degradation can lead to reduced biodiversity, loss of ecosystem services, and increased vulnerability to natural disasters. Coastal communities are particularly vulnerable to the impacts of sea level rise and coastal erosion. These impacts can include loss of livelihoods, displacement, and increased poverty. Changes to the water cycle and salinity intrusion in coastal areas also affect freshwater availability in coastal areas, resulting in less available water for agriculture, irrigation, and human consumption, which will also have an effect on tourism and development in Cambodia's coastal regions.

Chapter 4 focuses on anthropogenic causes of climate change, particularly the increase in emissions of greenhouse gases (GHGs), and predictions of future climate change based on various emissions scenarios. The key drivers of climate change in Cambodia are a mix of global and local factors, including greenhouse gas emissions, deforestation, land-use changes, and other related economic activities. The main driver of the increase in GHG emissions is Deforestation and Forestry and Other Land Use (FOLU). Agriculture, a key economic pillar of Cambodia, is the second-largest GHG-emitting sector in the country. It also examines various socio-economic and emissions scenarios and their projected impact on Cambodia. Most climate prediction models indicate a global increase in GHG emissions and thus climate change. This would have a negative effect on terrestrial ecosystems, including increased disasters and loss of biodiversity. It would also affect human life, as increased heat will impact worker productivity and overall quality of life, especially for urban residents. The Chapter 4 concludes with research gaps and recommendations for future research. Limited high-quality, long-term, and spatially disaggregated data makes it difficult to accurately model and project climate impacts. Future research should focus on improving the availability and accessibility of data and

information. Transdisciplinary and participatory approaches are needed to ensure findings remain relevant across diverse decision-making contexts.

Chapter 5 presents likely scenarios for future climate change in Cambodia and effects of these scenarios. It also focuses on the need for improved models that are scaled and adapted to the Cambodian climate and context. Accurate information about future climate patterns helps make the strategic response plan more precise in responding to future climate scenarios. Because of Cambodia's size and geographic variability, most existing climate models cannot easily be applied to the country. In order to provide accurate data, models must be downscaled and adjusted. Meteorological networks in Cambodia also need to be improved to provide accurate and comprehensive data for climate models. This will necessitate building more weather stations and integrating satellite and remote sensing data to generate a comprehensive dataset that effectively captures the intricacies of both local and regional climate processes. This Chapter also details climate projections for Cambodia under various emissions scenarios and potential effects of temperatures, precipitation patterns, and extreme weather events. Most scenarios indicate increasing of temperatures, increased flooding and droughts, and increased extreme weather events and disasters. This connects the NCR Part I to Part II, which focuses on climate change impacts, vulnerability, and adaptation in Cambodia.

Overall, Part 1 of the NCR provides evidence for the current effects of climate change and expected future impacts in Cambodia. It further provides scientific evidence-based information/data for the government and key relevant stakeholders to take action to develop effective strategies to mitigate and adapt to effects of climate change in Cambodia.

CHAPTER 1
INTRODUCTION

Climate change is one of the most critical global concerns and challenges of both the present and the future. The Earth's climate has fluctuated primarily due to greenhouse gases emitted by human activities in recent decades. In particular, the burning of fossil fuels, deforestation, transportation, and industrial agriculture have accelerated these changes (IPCC, 2023). The rapid increase in greenhouse gas emissions has led to rising global temperatures, changing precipitation patterns, increased wind speed, rising sea levels, and more frequent extreme weather events (IPCC, 2022). Climate change impacts not only the environment but also has profound social, economic, and political consequences for human life. Its effects are complex and interconnected, affecting biodiversity as well as public health and exacerbating inequalities (IPCC, 2021a). Rising sea levels threaten coastal communities, altering ecosystems and habitats. Extreme weather events such as floods, droughts, storms, and heat waves disrupt food production, water resources, and energy systems, increasing the risk to vulnerable populations. Thus, failure to implement significant reduction of GHGs and adaptation measures today will render future adaptation to climate change impacts even more difficult (IPCC, 2022).

In response to these global concerns, international initiatives, debate, discussion, cooperation, and commitments have led to international treaties including the Paris Agreement, which aims to limit global temperature to increase at 2°C or lower by year 2100. Figure 1.1 below indicates key points of the Paris Climate Agreement.[1] The efforts to mitigate, adapt, and build resilience to climate change will shape the future of human civilization and the earth. The growing awareness of the urgency of climate action has prompted shifts toward renewable energy, sustainable agriculture, and circular economies. However, achieving these aims requires unprecedented global cooperation, technological innovation, and policy changes.

[1] Through the agreement, the world committed to: (i) limit temperature rise at 2°C or lower at year 2100; (ii) mobilize finance for 100 billion per year from 2020; (iii) deduct GHG for developed countries and increase adaptation for developing countries; (iv) target emission peak 2050; (v) developed countries provide help to developing countries; (vi) review agreement achievement in every five years; and (vii) recognize the need for adaptation and mitigation for vulnerable countries.

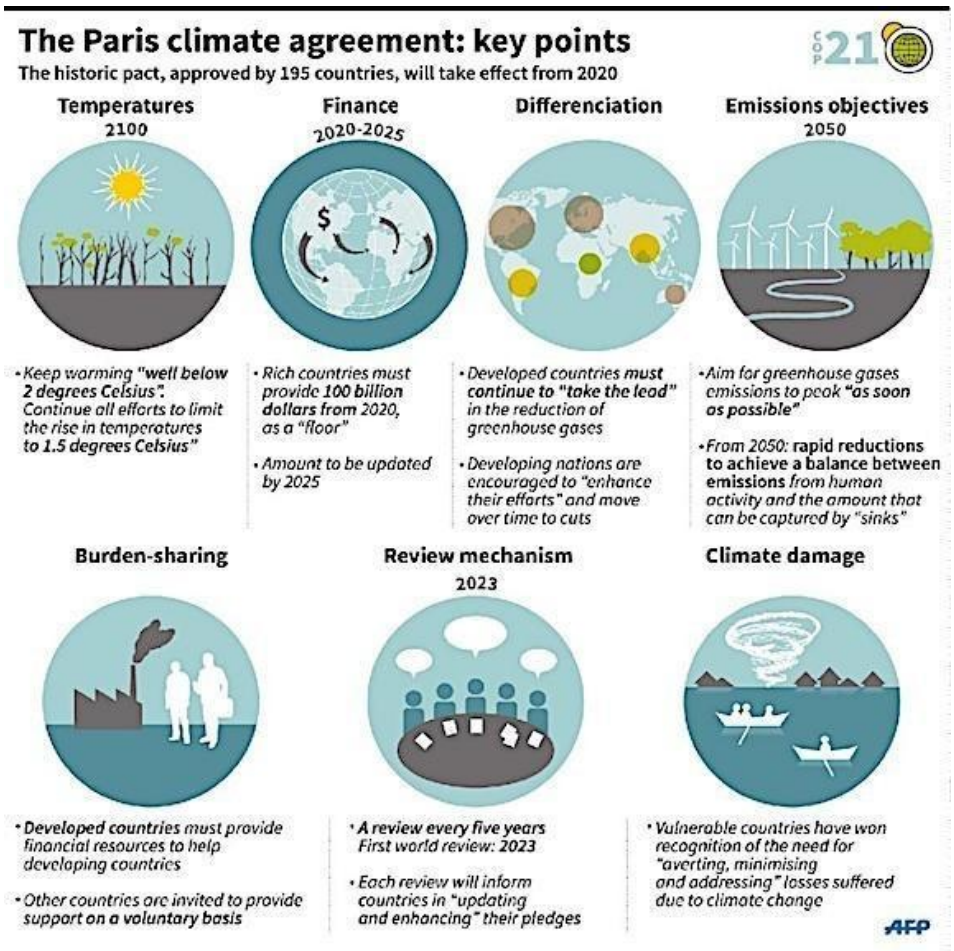

Figure 1.1: Key points of the Paris Climate Agreement
(Source: UNFCCC, 2015)

The United Nations Framework Convention on Climate Change Action (UNFCCC) is the UN mechanism for coordinating global agreements to limit global climate change. It coordinates member states for international treaties and commitments to combat global climate change, including the 2016 Paris Agreement. To review and evaluate the implementation of the agreement/treaty, the UNFCCC organizes Conference of the Parties (COP) once a year, with participation from all its member states to review the implementation of the Convention and any other legal instruments and adopt decisions necessary to promote the effective implementation of the Convention.

The Intergovernmental Panel on Climate Change (IPCC) is the leading international body for the assessment of climate change. The IPCC generates scientific information and technical guidance for the implementation of the UNFCCC and the Paris Agreement. The IPCC provides governments with specific information for use in developing climate policies. It generates regular comprehensive assessment reports on climate change (causes, impacts, and response options), methodology reports that provide practical guidance, and special reports on topics related to the assessment reports.

Cambodia has been a member state of the UNFCCC since 1995. As a member, Cambodia has made significant effort and commitments to respond to climate change. Cambodia also targets achieving the Sustainable Development Goals (SDGs), including goals relevant to climate change, environment, and sustainability. These climate change relevant SDG goals include SDG 9: build resilient infrastructure, promote inclusive and sustainable industrialization and foster intervention; SDG 11: making cities and human

settlement inclusive, safe, resilient, and sustainable; SDG 13: making urgent action to combat climate change and its impacts; SDG 14: conserve and sustainably use the ocean, seas, and marine resources for sustainable development; and SDG 15: protect, restore and promote sustainable use of terrestrial ecosystems, sustainable manage forests, combat diversification.

Cambodia has already made a strong commitment, through several policy instruments, to reducing GHG emissions and limiting climate change. Key among these is the Pentagonal Strategy Phase I of the Royal Government of Cambodia, specifically Pentagon #4, which focuses on resilient, sustainable and inclusive development through ensuring environmental sustainability, readiness to respond to climate change, and promotion of the green economy. The Cambodia Climate Change Strategic Plan (CCCSP: 2014-2023) came into effect in 2014 and CCCSP 2024-2033. This strategic plan outlines the objectives and directions for addressing climate change issues in Cambodia for a 10–year period.

Additionally, the Government of Cambodia has made other commitments and efforts through Cambodia's updated Nationally Determined Contributions (NDC) and NDC 3.0, National REDD+ strategy and program, a series of the Cambodia National Communication, Long-Term Strategy for Carbon Neutrality 2050, the Second National Communication and Third National Communication. Relatively, Cambodia is also a member state for the United Nations Convention on Biological Diversity (UNCBD) and the United Nations Convention to Combat Desertification (UNCCD).

Climate change in Cambodia has the potential to cause significant damage to the economy and natural resources, as well as impact human lives (NCSD, 2015). These impacts include intensified floods, droughts, saline intrusion, and extreme weather events. As a developing nation, Cambodia remains highly dependent on climate-sensitive sectors such as agriculture, water resources, forestry, fisheries, tourism, which form the critical foundation of its economic growth and support the livelihoods of a significant majority of its population (WBG and ADB, 2021 and WBG, 2023).

This physical science-based climate report is developed for Cambodia with the aim to present the most up-to-date scientific climate information and data for Cambodia. The report will serve as a baseline and provide scientific inputs for the government, policymakers, decision-makers, planners, practitioners, and researchers in making informed decisions regarding present and future responses to climate change impacts, as well as mainstreaming climate change adaptation and resilience. The report is organized into five chapters: Introduction, Global Climate Change, Climate Change in Cambodia, Coastal Ecosystem and Sea Level Change, Drivers of Key Emission and Climate Change in Cambodia, and Projections for Cambodia's Future Climate Change.

1.1 Objectives of the Report

The main objective of this report is to compile the most up-to-date, scientific, and evidence-based climate change information and data for Cambodia, serving as a physical science baseline and providing scientific and technical input for informed decision-making in Cambodia's current and future climate change responses. This main objective covers five specific objectives below:

1. To provide an overview of the latest global and regional scientific climate change information that Cambodia refers as a reference for national climate change actions in the present and future;

2. To describe the current weather and climate conditions of Cambodia, including observed changes and variability;
3. To assess changes in coastal ecosystems and sea level trends affecting Cambodia's coastal zones;
4. To identify key physical drivers, observed impacts, and sectoral vulnerabilities related to climate change in Cambodia; and
5. To present climate projections and identify appropriate future climate scenarios for national adaptation planning and risk management.

1.2 Chapter Summary

This chapter provides an in-depth physical science-based assessment of climate change, with a focus on its implications for broader global contexts. Climate change, driven predominantly by greenhouse gas (GHG) emissions from human activities, including fossil fuel combustion, industrial agriculture, deforestation, and transportation, has led to rising global temperatures, altered precipitation patterns, more frequent extreme weather events, and sea-level rise. The interconnected impacts span environmental, social, economic, and political dimensions, exacerbating biodiversity loss, public health challenges, and socio-economic inequality. These effects demand urgent and coordinated global and national responses.

The report's structure spans five sections, beginning with a comprehensive introduction to global climate dynamics, including scientific evidence of observed changes in temperature, GHG concentrations, and their respective roles in global warming. Key findings indicate that GHG levels, particularly carbon dioxide, methane, and nitrous oxide, have reached unprecedented levels, significantly influencing Earth's energy balance and climate patterns. This concentration increase is largely attributable to human activities since the Industrial Revolution. Projections based on climate models suggest further temperature increases, altered precipitation cycles, and amplified climate variability, which the report examines in the context of Cambodia.

Central to the report are detailed analyses of climate trends, coastal ecosystem dynamics, key emissions drivers, and projected climate scenarios. Sea surface temperature (SST) changes, ocean heat content, and greenhouse gas radiative forcing are examined to show the interconnections between climate systems.[2] Notably, ocean warming trends and sea-level rise, driven by thermal expansion and glacial melt, have direct implications for Cambodia's low-lying coastal areas, threatening infrastructure and livelihoods.

In addition, the report identifies significant sectoral GHG emissions from energy, agriculture, industry, and transportation sectors. Strategies for reducing emissions, enhancing carbon sequestration, and promoting climate-resilient practices are integral to mitigating future climate impacts. Efforts must prioritize renewable energy adoption, sustainable land management, and policy reforms that align with international climate goals.

Overall, this report serves as a critical scientific resource, guiding policymakers, researchers, and stakeholders in formulating evidence-based climate responses. By fostering collaboration and embracing innovation, Cambodia can strengthen its resilience

[2] Radiative forcing is a measure of how a particular factor changes the balance between incoming energy from the Sun and outgoing heat (infrared radiation) from Earth.

to climate impacts, mitigate emissions, and contribute to a sustainable future aligned with global climate targets.

1.3 Global Climate Changes

Global Climate Change encompasses the long-term shifts in Earth's climate patterns driven by both natural processes and human activities. While natural variability—such as volcanic eruptions, solar fluctuations, and ocean–atmosphere cycles—affects climate over time, the rapid changes observed since the mid-20th century are largely due to anthropogenic greenhouse gas emissions from energy production, industry, agriculture, and land-use change. These changes have intensified the greenhouse effect, warmed the atmosphere and oceans, altered precipitation patterns, and accelerated ice melt and sea level rise. Observations across multiple datasets confirm unprecedented global temperatures, ocean heat content, and shifts in the Earth's energy balance, underscoring the urgent need to monitor, understand, and respond to the evolving climate system.

1.3.1 Observations of Changes in the Global Climate

Greenhouse gases are the major source of climate change. Both human activities and natural events generate GHGs. Natural sources, accounting for about 40% of total emissions, are mainly wetlands, along with minor yet significant contributions from freshwater systems, wild animals, termites, and geological sources. Industrial activities such as gas and oil exploration, waste management, and biomass burning contribute to CH_4 emissions. Other anthropogenic sources include emissions from ruminant livestock and rice paddies; both associated with agriculture. Many of these methane sources are highly sensitive to climate change. Unlike its diverse sources, methane's primary sink is through its destruction via a reaction with hydroxyl (OH) radicals, which are abundant over oceans at low latitudes, where they form from the exposure of water vapor to ultraviolet (UV) radiation. This reaction determines methane's atmospheric lifetime. Several factors, including levels of traditional air pollutants, can influence OH abundance and therefore impact methane's lifespan in the atmosphere (WMO, 2024b). N_2O (nitrous oxide) sources include microbial processes such as nitrification and denitrification, emissions from oceans, the use of nitrogen fertilizers in agriculture, and fossil fuel or biomass combustion. Global human-induced emissions, primarily from nitrogen additions to croplands, have risen by 30 percent over the past four decades and are the main factor behind the increase in atmospheric N_2O levels (Tian et al., 2020). Globally, in 2019, 34% (20 GtCO2-eq) of the total 59 GtCO2-eq GHG emissions came from the energy sector, 24% (14 GtCO2-eq) from industry, 22% (13 GtCO2-eq) from agriculture, forestry, and other land use (AFOLU), 15% (8.7 GtCO2-eq) from transport, and 6% (3.3 GtCO2-eq) from buildings (Figure 1.2). The relative size of each sector varies depending on the specific definitions of sector boundaries (Lamb et al., 2021).

The largest individual subsector contributing to global GHG emissions in 2019 was electricity and heat generation, accounting for 14 GtCO2-eq (Creutzig et al., 2018). This subsector can be reallocated to consuming sectors as indirect emissions to highlight the role of final energy demand and demand-side solutions. This reallocation increases the emission share of the industry sector to 34 percent and the buildings sector to 16 percent (Creutzig et al., 2018).

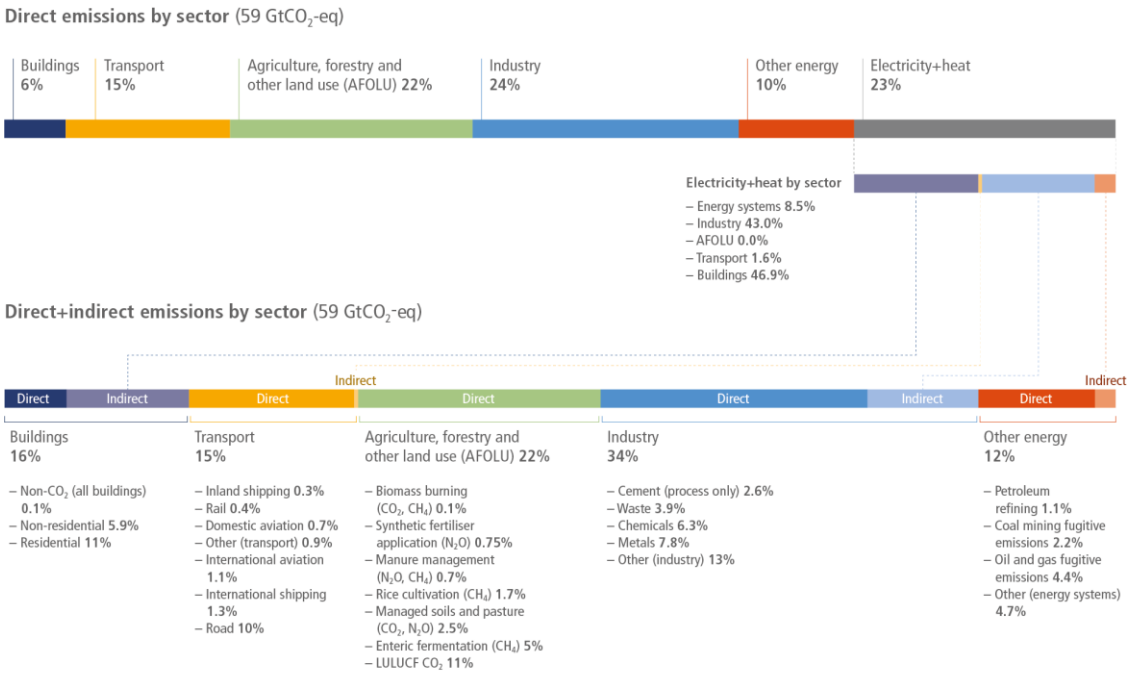

Figure 1.2: Total anthropogenic direct and indirect GHG emissions for the year 2019 (in GtCO2-eq) by sector and subsector
Source: (Parmesan et al., 2022)

From 2010 to 2019, average annual GHG emissions growth was fastest in the transport sector at about 1.8 percent, followed by direct emissions from industry (1.4 percent) and the energy sector (1 percent) (Figure 1.3). Between 2000 and 2009, the fastest GHG emissions growth occurred in industry (3.4 percent), followed by the energy sector (2.3 percent). Transport emissions growth remained steady at around 1.8 percent across both periods, while direct emissions from buildings grew at an average rate below 1 percent during 2010–2019 (Parmesan et al., 2022). Ranking high-emitting subsectors by direct emissions underscores the importance of CO_2 emissions from LULUCF (6.6 GtCO2-eq, though with low confidence in its magnitude and trend), road transport (6.1 $GtCO_2$-eq), metals (3.1 GtCO2-eq), and other industries (4.4 GtCO2-eq). Between 2010 and 2019, some of the fastest-growing sources of subsector emissions included international aviation (+3.4 percent), domestic aviation (+3.3 percent), inland shipping (+2.9 percent), metals (+2.3 percent), international shipping (+1.7 percent), and road transport (+1.7 percent) (Dhakal et al., 2022; Lamb et al., 2021).

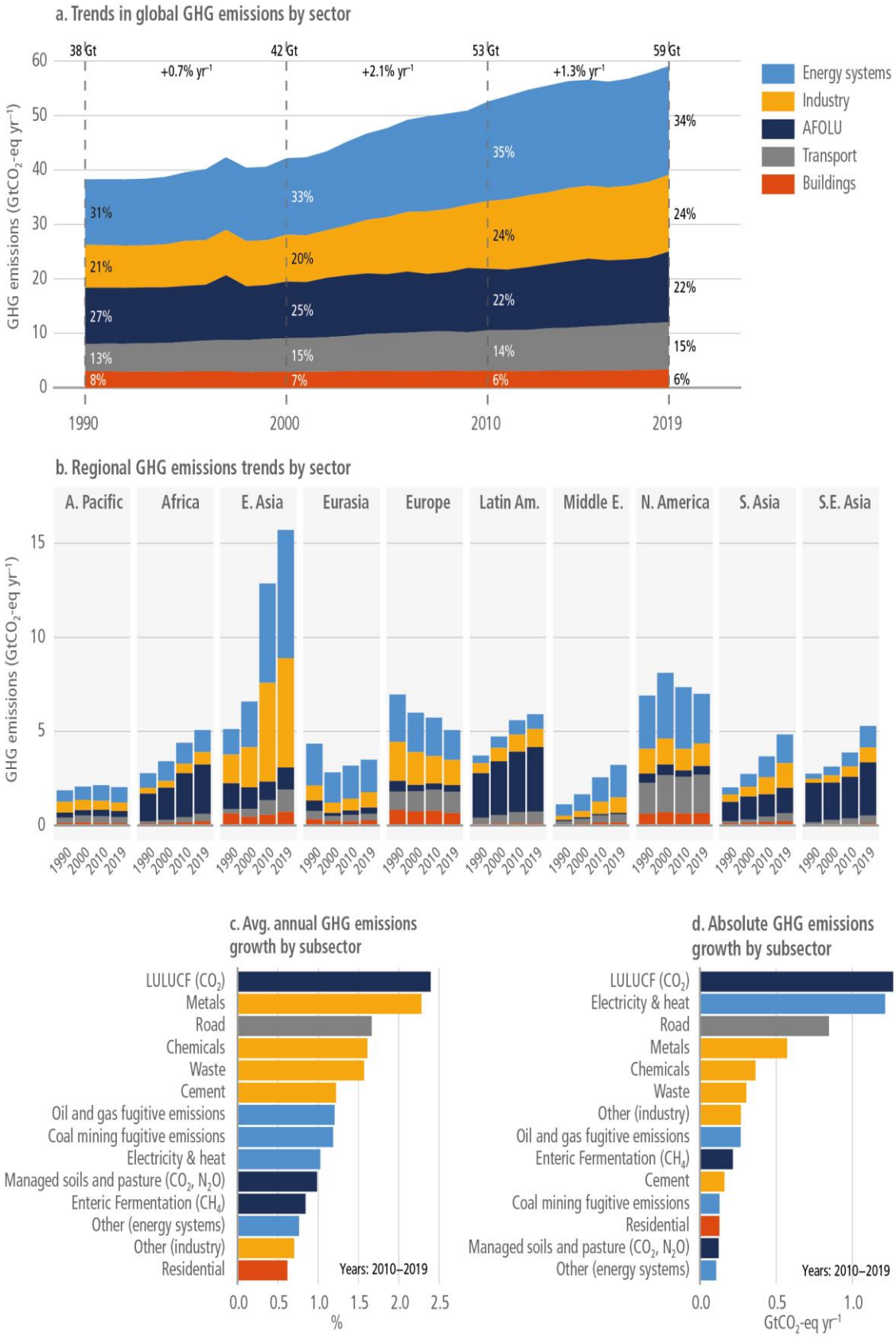

Figure 1.3: Total annual anthropogenic GHG emissions by major economic sector and their underlying trends by region
Source: (Parmesan et al., 2022).

Greenhouse effect

The sun powers Earth's climate by radiating energy, with about one-third of this energy being reflected to space and the rest absorbed by the Earth's surface and atmosphere (Figure 1.4). To balance the absorbed energy, Earth radiates it back to space as infrared radiation. This radiation is partially absorbed and reradiated by the atmosphere, creating the greenhouse effect, which warms the planet and makes life possible. Without this natural process, Earth's average temperature would be below freezing. However, human activities, such as burning fossil fuels and deforestation, have intensified the greenhouse effect, leading to global warming. Water vapor is the most significant greenhouse gas, followed by CO_2. The greenhouse effect is stronger in colder, drier regions, where small increases in CO_2 or water vapor have a larger impact, see Figure 1.4 (Le Treut et al., 2007).

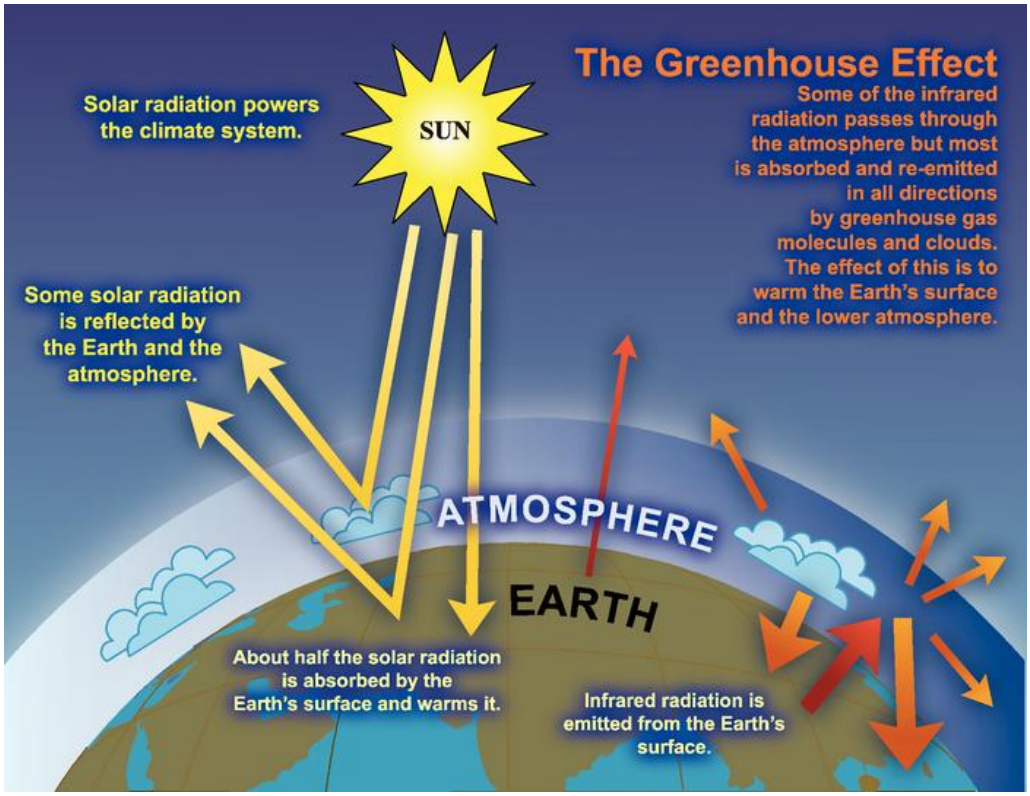

Figure 1.4: An idealized model of the natural greenhouse effect.

1.3.2 Observed Changes in Temperature

Observed changes in temperature refer to the measurable differences in the Earth's average surface temperatures over time. Scientists track these changes using historical records, satellite measurements, and other data sources to identify trends and patterns. This information helps us understand how global temperatures have shifted due to natural variability and human activities, such as greenhouse gas emissions. Observing these changes is critical for predicting future climate behavior and planning responses to mitigate and adapt to climate impacts (IPCC, 2021).

In 2023, the global average near-surface temperature was 1.45 ± 0.12 °C higher than the 1850–2023 average (Figure 1.5). This finding is based on a combination of six global temperature datasets. All six datasets confirm that 2023 was the hottest year in the 174-year instrumental record. The last nine years, from 2015 to 2023, were the warmest years

ever recorded. The warmest years were 2016, with a temperature anomaly of 1.29 ± 0.12 °C, and 2020, with 1.27 ± 0.13 °C (WMO, 2024a).

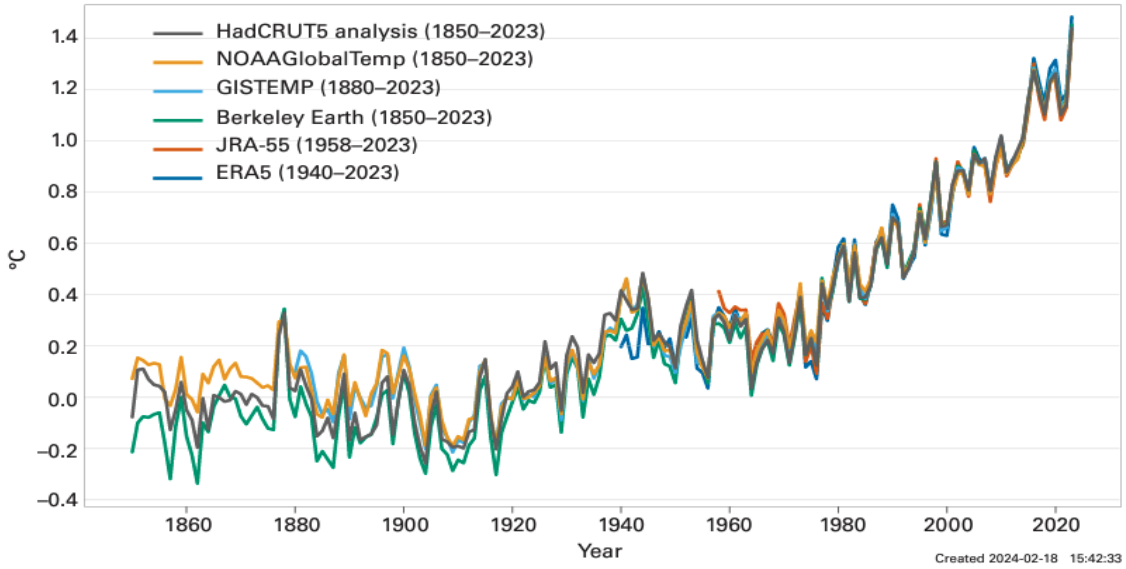

Figure 1.5: Annual global mean temperature anomalies (relative to 1850–2023)

Between June and December 2023, each month set a new global temperature record for that respective month. September 2023 was particularly noteworthy, surpassing the previous September record by 0.46–0.54°C across all datasets. For context, the second-largest temperature margin for September in the past 60 years was only 0.03–0.17°C, recorded in 1983. July 2023, typically the warmest month annually, also became the hottest month ever recorded. Additionally, the shift from a prolonged La Niña phase (mid-2020 to early 2023) to full El Niño conditions by September 2023 likely contributed to the sharp temperature increase from 2022 to 2023. However, certain regions, such as the north-east Atlantic (Figure 1.6), experienced unusual warming that does not align with typical El Niño warming or cooling patterns. Other factors, still under investigation, may also have played a role in the exceptional warming observed between 2022 and 2023, as it is unlikely to be explained by natural variability alone (Rantanen & Laaksonen, 2024).

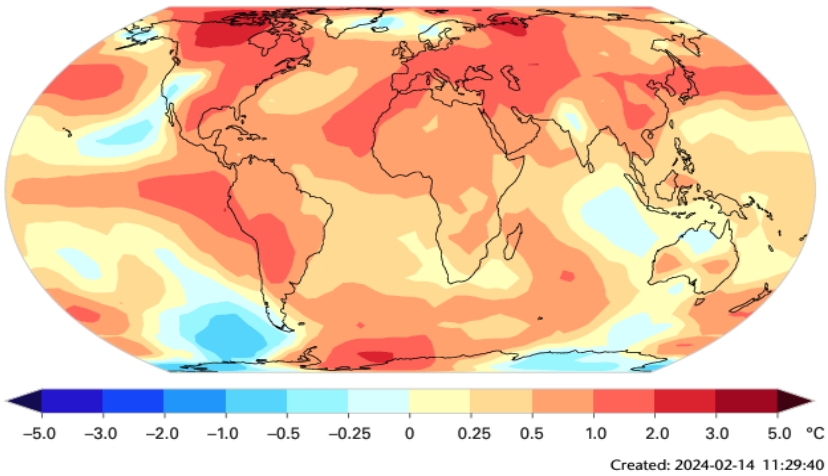

Figure 1.6: Mean near-surface temperature anomalies (difference from the 1991–2020 average) for 2023
Note: Data are the median of the six datasets indicated in the legend

The global average temperature over the decade from 2014 to 2023 was 1.20 ± 0.12°C higher than the 1850–1900 baseline, making this period the warmest 10-year span on

record across all six major datasets. Additionally, from late spring in the northern hemisphere through the end of 2023, global sea-surface temperatures (SSTs) reached unprecedented levels. Record-breaking SSTs were observed in July, August, and September, with temperature increases ranging from 0.21°C to 0.27°C above previous records. Exceptional warmth, relative to the 1991–2020 average, was particularly notable in several regions, including the eastern north Atlantic, the Gulf of Mexico, the Caribbean, the north Pacific extending from the Sea of Japan, the Arabian Sea, and large parts of the Southern Ocean. Global land temperature anomalies also reached record levels in July and August, slightly lagging behind the SST records, but September's land temperature set a new high, with a margin of 0.53°C–0.71°C. The second-largest record-breaking margin in the last 60 years was 0.22°C–0.27°C, set in September 2002. In 2023, most land regions experienced warmer-than-average temperatures compared to the 1991–2020 period. Areas with notable warmth included much of northern Canada, the southern United States, Mexico, Central America, and large parts of South America. Unusual warmth was also observed across wide areas from central Asia to western Europe, encompassing parts of North Africa and the Arabian Peninsula, as well as in Southeast Asia and Japan (WMO, 2024a).

1.3.3 Surface Temperatures

Global surface temperature (GST) refers to the average temperature of Earth's surface. Specifically, it is the weighted average of temperatures over both ocean and land. The ocean temperature is known as sea surface temperature, while the land temperature is referred to as surface air temperature (Consortium et al., 2019). Between 2011 and 2020, the global surface temperature was approximately 1.1°C higher than the 1850–1900 average (with an estimated range of 1.09°C). The temperature increase was more pronounced over land, rising by an average of 1.59°C [1.34°C to 1.83°C], compared to the ocean, which saw an average rise of 0.88°C [0.68°C to 1.01°C]. In the first two decades of the 21st century (2001–2020), global temperatures were on average 0.99°C [0.84°C to 1.10°C] higher than those of the late 19th century. Since 1970, the rate of warming has been faster than during any other 50-year period over the past 2000 years (high confidence). The human-caused increase in global surface temperatures from 1850–1900 to 2010–2019 is estimated to be between 0.8°C and 1.3°C, with a central estimate of 1.07°C. Greenhouse gases are likely responsible for warming by 1.0°C to 2.0°C, while other human activities (mainly aerosols) have likely contributed a cooling effect of 0.0°C to 0.8°C. Natural factors (solar and volcanic activity) are estimated to have caused temperature changes of ±0.1°C, and internal climate variability, driven by natural processes within the Earth's climate system, contributed ±0.2°C (Figure 1.7)(IPCC, 2021b).

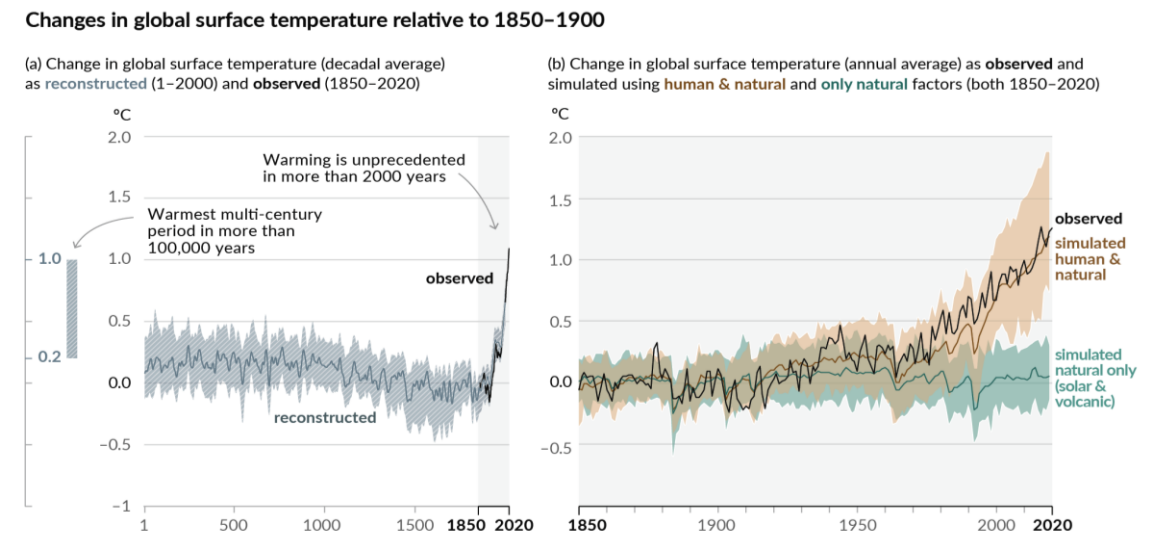

Figure 1.7: History of global surface temperature change and causes of recent warming; (a) changes in global surface temperature reconstructed from paleoclimate archives (solid grey line, years 1–2000) and direct observations (solid black line, 1850–2020); (b) changes in global surface temperature over the past 170 years (black line)
Source: (IPCC, 2021b)

1.3.4 Ocean Temperatures

Sea surface temperature (SST) is a critical climate system component because it significantly influences energy, momentum, and gas exchange between the ocean and the atmosphere. Heat and moisture exchanges driven by SST play a major role in global weather systems and climate patterns (NASA, 2023). Satellites enable the measurement of SST at depths ranging from approximately 10 µm below the surface (using infrared bands) to 1 mm (using microwave bands) through radiometers. SST's spatial distribution reveals underlying ocean dynamics, including ocean fronts, eddies, coastal upwelling, and exchanges between the coastal shelf and the open ocean.

In 2023, consolidated analyses from multiple datasets confirmed continued warming of the upper 2,000 meters of the ocean (von Schuckmann et al., 2020). This warming trend is expected to persist and is considered irreversible on centennial to millennial timescales (Cheng et al., 2017; IPCC, 2019). In 2023, OHC reached a new record, surpassing the 2022 levels by 13 ± 9 ZJ (Figure 1.8)[3], consistent with estimates released in early 2024 (Cheng et al., 2024). All datasets indicate that the rate of ocean warming has accelerated significantly over the past two decades. The average warming rate for the ocean's 0–2,000 meters layer was 0.7 ± 0.1 W m² from 1971 to 2023, but this increased to 1.0 ± 0.1 W m² from 2005 to 2023. This steady rise in ocean heat content (Miniere et al., 2023; von Schuckmann et al., 2020) is consistently observed through direct in situ measurements, remote sensing estimates, and satellite-based flux measurements at the top of the atmosphere (Miniere et al., 2023). The literature attributes this warming to a combination of factors, including anthropogenic climate forcing (Raghuraman et al., 2021) and natural variability (Loeb et al., 2021). Deep-ocean warming below 2,000 meters is estimated to be 0.07 ± 0.03 W m^{-2} from 1992 to 2022 (Purkey & Johnson, 2010).

[3] Ocean heat content is measured in zettajoules. A zettajoule is 1 021 joules, which is 1 000 000 000 000 000 000 000 joules.

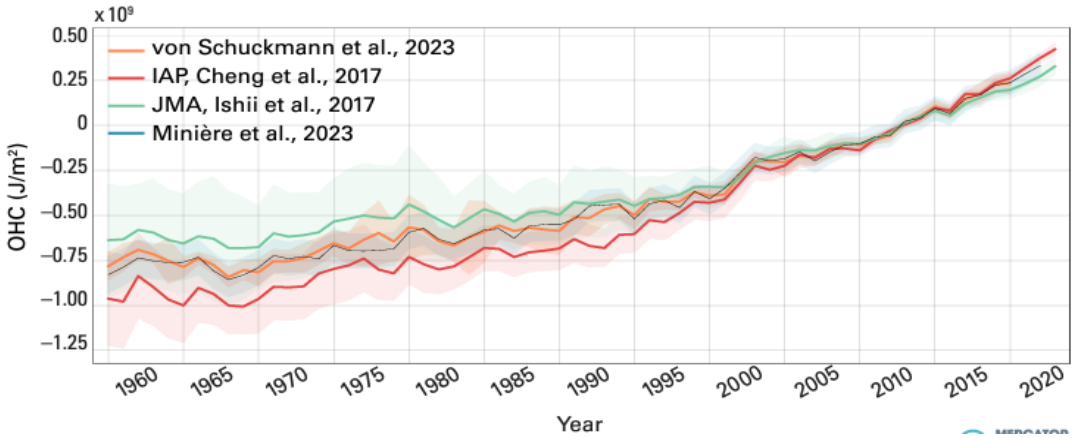

Figure 1.8: Global ocean heat content anomalies relative to the 2005–2021 average for the 0–2 000 m depth layer 1960–2023 (orange)
Source: Mercator Ocean international

Although ocean heat content has increased strongly through the entire water column, the rate of warming has not been the same everywhere (Cheng et al., 2023). The strongest warming in the upper 2,000 m occurred in the Southern Ocean (60° S–35° S), north Atlantic (20° N–50° N) and south Atlantic (60° S–0° S) (Figure 1.9). The Southern Ocean domain is the largest reservoir of heat, accounting for about 32 percent of the global OHC increase in the upper 2,000 m since 1958 (Cheng et al., 2024). The Atlantic Ocean accounts for approximately 31 percent of the global 0–2,000 m ocean heat content increase, and the Pacific Ocean for about 26 percent.

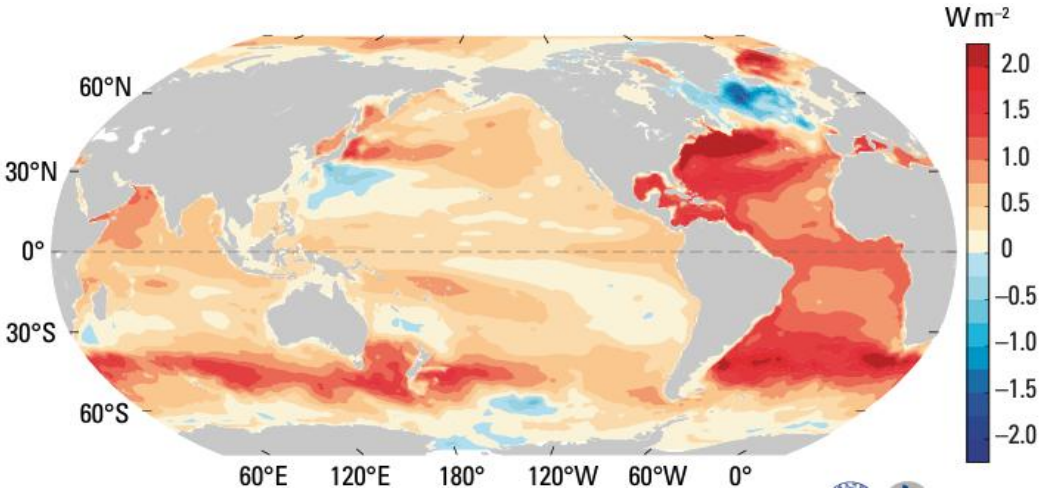

Figure 1.9: Observed upper 2000 m OHC trend from 1958 to 2023
Source: Data updated from Cheng et al. (2017)

Some relatively small regions are cooling, including the subpolar north Atlantic Ocean, extending from near the surface to a depth of over 800 m (also the only area to show centennial cooling at the surface). The contrasting pattern of cooling (50° N–70° N) and warming (20° N–50° N) in the north Atlantic has been associated with a slowing of the Atlantic Meridional Overturning Circulation and local interactions between the air and sea (Cheng et al., 2022). Other cooling regions include the north-west Pacific, the south-west Pacific, and the south-west Indian Ocean.

Since March 2023, the average surface temperature of global oceans has consistently risen above the long-term average, culminating in a new record high in August 2023. The trend has continued with sea surface temperatures reaching an unprecedented global average of 21.09°C in February and March 2024. As illustrated by the graph in Figure 1.10,

each day since May 4, 2023, has set a new daily temperature record for that time of year, with some days showing significant deviations from previous records (Copernicus, 2024a).

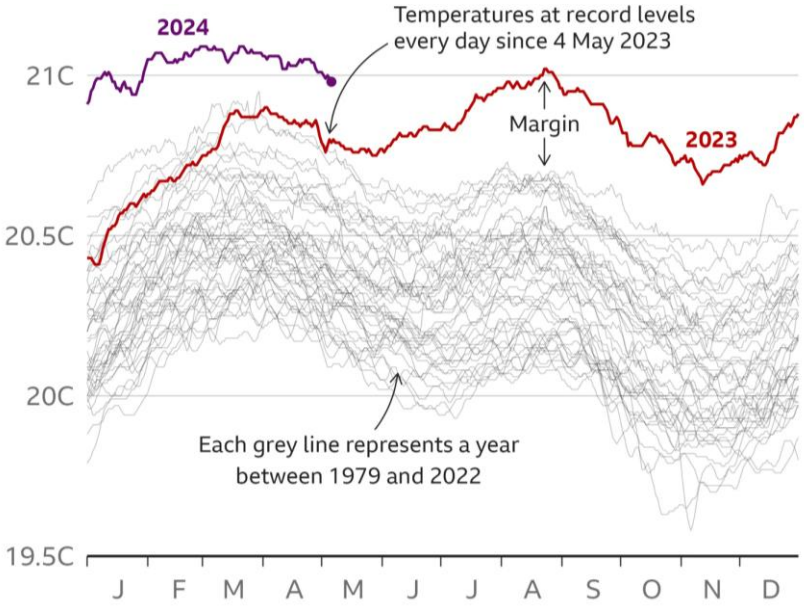

Figure 1.10: A year of record-breaking ocean temperatures: daily average sea surface temperatures, 1979-2024 (note: temperature measured between latitude 600 North and 600 South)
Source: ERA5, C3S/ECMWF

Rising ocean temperatures have serious consequences for marine ecosystems, including:

Coral Bleaching: Corals are highly sensitive to temperature increases; a rise of just 1°C can trigger coral bleaching. This process occurs when corals expel their symbiotic algae, losing both their vibrant colors and essential energy sources. If bleaching persists, it can lead to coral death, severely affecting the biodiversity that depends on coral reefs (USGS, 2024). Healthy coral reefs provide critical habitat, nursery grounds, and food for countless marine species, and their decline disrupts the balance and resilience of entire marine ecosystems.

Marine Heatwaves: The number of marine heatwave days rose by over 50 percent in the last century, with these extreme temperature events are becoming more frequent and severe. Marine heatwaves place immense stress on marine life, causing mass die-offs, disrupting reproductive cycles, and shifting species' habitats (Diwyanjalee, 2024).

Increased Storm Intensity: Warmer oceans fuel more powerful and frequent storms. NASA (National Aeronautics and Space Administration) reports that hurricanes and tropical cyclones are expected to grow stronger, with more rainfall and higher wind speeds (Colbert, 2022).

Sea Level Rise: The combination of thermal expansion and the melting of ice sheets and glaciers is causing significant sea level rise. This increase threatens coastal habitats and human communities through flooding and erosion (WMO, 2024b).

Changes in Ocean Ecosystems: Climate change is also altering ocean color and ecosystem dynamics. Phytoplankton populations, which are vital to marine food webs, are shifting, indicating broader changes in ocean ecosystems. These changes reflect a transformation in global carbon cycles and marine biodiversity (Bindoff et al., 2019).

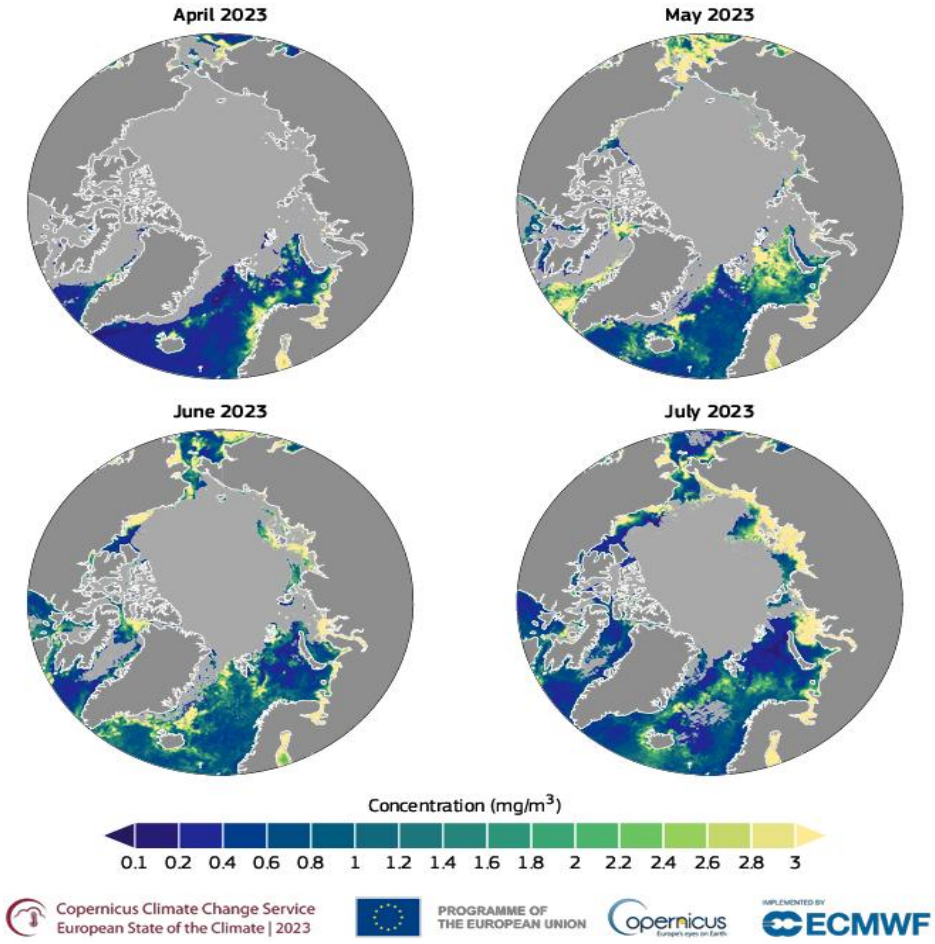

Figure 1.11: Monthly chlorophyll a concentration in 2023
Source: Data: C3S Ocean Colour v6.0. Credit:C3S/ECMWF/Brockmann Consult) (Copernicus, 2024b)

1.3.5 Observed Changes in Energy Budget and Heat Content

The Earth's climate system is driven by a continuous exchange of energy between the Sun, the atmosphere, the oceans, and space. Acting like a global heat engine, the planet not only moves heat across its surface but also transfers excess heat from the surface and lower atmosphere back into space. This ongoing exchange of incoming solar radiation and outgoing heat energy is referred to as the Earth's energy budget. The Earth's climate system balances its energy budget through processes at three levels: the surface, the atmosphere, and the top of the atmosphere. Approximately 71 percent of incoming solar energy is absorbed by the Earth system, with 23 percent absorbed by the atmosphere and 48 percent by the surface. The surface loses energy through evaporation (25 percent), convection (5 percent), and thermal infrared radiation (17 percent). The atmosphere radiates 59 percent of incoming solar energy back to space as thermal infrared radiation, sourced from the absorption of sunlight (23 percent), and energy transferred from the surface through evaporation, convection, and radiation. For Earth's temperature to remain stable over long periods, the amount of energy coming in must equal the energy going out. This balance at the top of the atmosphere is referred to as radiative equilibrium.

Approximately 29 percent of the solar energy that reaches the top of the atmosphere (TOA) is reflected into space by clouds, atmospheric particles, or reflective surfaces like snow and sea ice. This portion of energy does not contribute to Earth's climate system. Around 23 percent of incoming solar energy is absorbed by the atmosphere, primarily by

water vapor, dust, and ozone. As shown in Figure 1.12, the remaining 48 percent pass through the atmosphere and is absorbed by Earth's surface. In total, about 71 percent of the incoming solar energy is absorbed by the Earth system, playing a critical role in driving the planet's climate (NASA Earth Observatory, 2009).

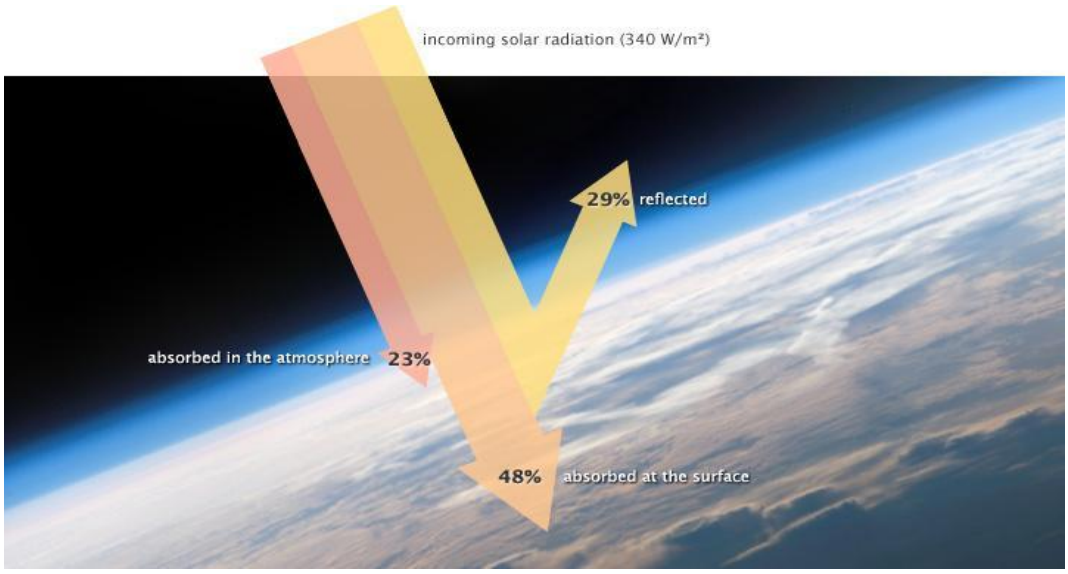

Figure 1.12: Earth's energy budget

A key aspect of the energy balance is the natural greenhouse effect, where greenhouse gases like water vapor and CO_2 absorb and radiate thermal infrared energy, raising Earth's surface temperature to an average of 15°C—over 30°C warmer than it would be without an atmosphere (NASA Earth Observatory, 2009). This greenhouse effect is regulated by the fact that as surface temperatures increase, more heat is radiated, preventing uncontrolled warming. The surface emits heat upward (117 percent of incoming solar energy), with 100 percent being "back radiation" from the atmosphere. This balance ensures that the energy leaving Earth equals the energy arriving from the Sun.

The Top of Atmosphere (TOA) energy budget is determined by the balance between incoming solar (shortwave) radiation and outgoing radiation, which includes both reflected solar radiation and emitted thermal (longwave) radiation from the Earth's climate system. In a stable climate, these incoming and outgoing radiative components are generally balanced over the long-term global average, maintaining Earth's overall energy equilibrium. However, short-term fluctuations can occur due to internal climate variability, which may temporarily disrupt this balance without necessarily indicating long-term shifts in the climate system (Brown et al., 2014).

The Earth's climate system is currently out of energy balance, leading to a continuous accumulation of heat over recent decades. This has caused warming in the oceans, land, cryosphere, and atmosphere, shaping the Earth's heat inventory (von Schuckmann et al., 2020). This planetary warming is driven by human activities and is causing unprecedented and long-term changes to the Earth system (IPCC, 2021a), with detrimental effects on both ecosystems and human systems (IPCC, 2022). As long as this energy imbalance persists or worsens, Earth will continue to absorb excess energy, further intensifying global warming (Hansen et al., 2005; Hansen et al., 2017).

This imbalance leads to gradual increases in global surface temperatures, with the oceans' high heat capacity causing a delay in the full manifestation of climate change. Despite this lag, Earth's average surface temperature has already risen between 0.6 and

0.9°C over the past century. Even if greenhouse gas levels stabilize, the global temperature will remain higher than pre-industrial levels. However, if greenhouse gas concentrations continue to rise, the energy imbalance will grow, leading to further increases in surface temperatures (IPCC, 2022).

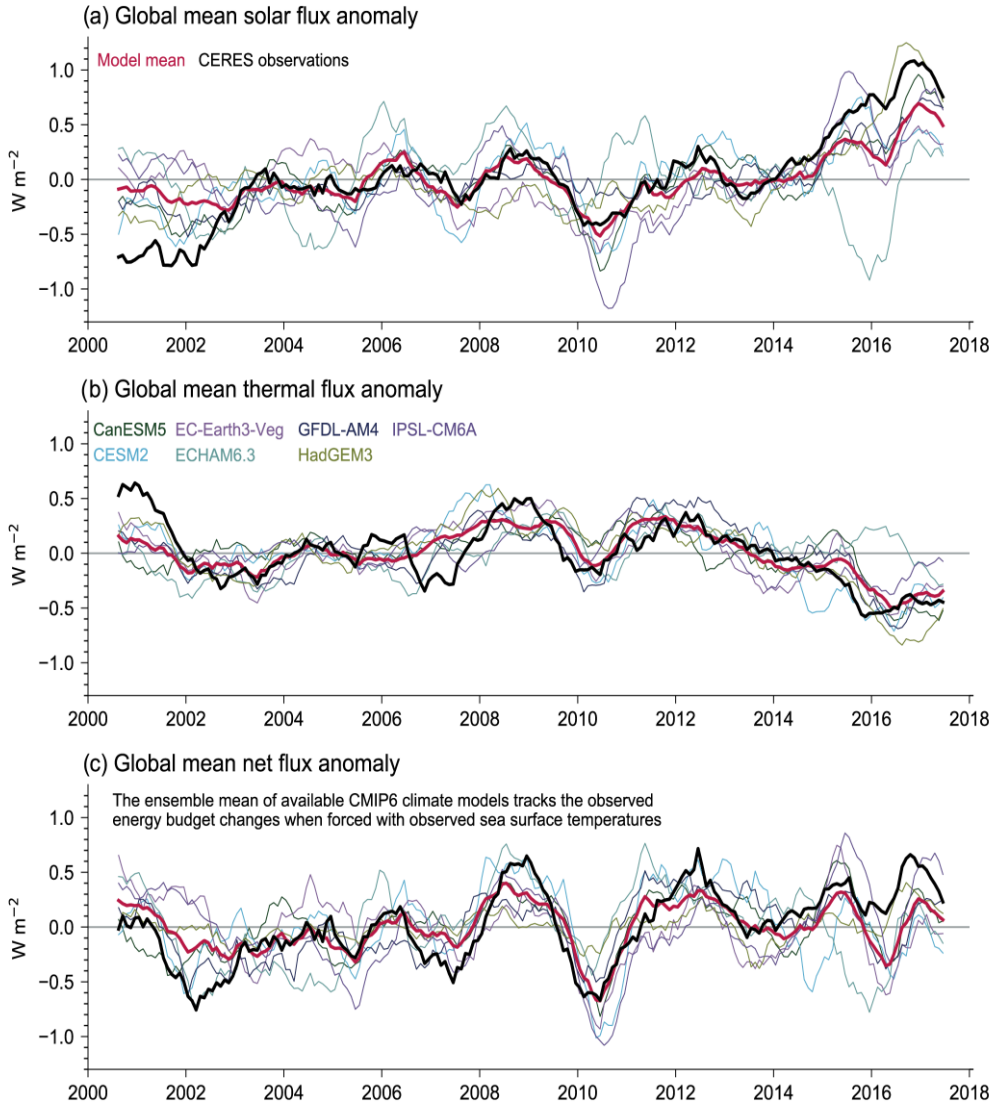

Figure 1.13: Anomalies in global mean all-sky top-of-atmosphere (TOA) fluxes from CERES-EBAF Ed4.0 (solid black lines) and various CMIP6 climate models (colored lines) in terms of (a) reflected solar, (b) emitted thermal and (c) net TOA fluxes
Source: (Forster et al., 2021).

Over the past 50 years (since 1971), the Earth has accumulated nearly 0.5 watts (0.48 + 0.1) of heat per square meter of its surface. More recently, from 2006 to 2020, this heating rate increased to over 0.75 watts (0.76 + 0.2) per square meter. The majority of this heat (89 percent) has been absorbed by the ocean, with the remaining energy distributed among land (6 percent), ice (4 percent), and the atmosphere (1 percent). This global assessment of energy gained and disbursed is a key indicator of climate change, reflecting its impacts on the ocean, land, atmosphere, and cryosphere. Such assessments require sustained international cooperation in monitoring and research (von Schuckmann et al., 2020).

Changes to Earth's climate system that affect the balance between incoming and outgoing energy disrupt its radiative equilibrium, influencing global temperatures. These changes, known as climate forcings, can be natural or manmade. Natural forcings include variations in the Sun's brightness, Milankovitch cycles (small changes in Earth's orbit and axis over thousands of years), and volcanic eruptions, which reflect sunlight by releasing particles into the atmosphere. Manmade forcings include aerosols that absorb and reflect sunlight, deforestation that alters surface reflectivity, and increased greenhouse gases like carbon dioxide that trap heat by reducing the amount radiated back to space. These forcings can trigger feedback mechanisms, such as ice loss at the poles, further intensifying their effects. Carbon dioxide is a particularly potent forcing agent. While water vapor absorbs many thermal infrared wavelengths, there are "windows" in the spectrum where it allows heat to escape. Carbon dioxide absorbs thermal infrared energy in wavelengths that water vapor does not, effectively "closing" some of these windows and trapping more heat. This absorption creates an energy imbalance, as Earth continues to absorb around 70 percent of incoming solar energy, but less heat can escape. The resulting imbalance—currently estimated at just over 0.8 watts per square meter—is inferred through satellite and ocean-based observations.

1.3.6 El Niño Southern Oscillation

The El Niño–Southern Oscillation (ENSO) is a climate phenomenon that involves fluctuations in ocean temperatures and atmospheric conditions over the tropical Pacific Ocean. It has three phases (L'Heureux, 2014):

El Niño: This phase involves a rise in sea surface temperatures in the central and eastern tropical Pacific Ocean. It typically leads to decreased rainfall in Indonesia and increased rainfall over the tropical Pacific. The usual east-to-west winds along the equator weaken or sometimes reverse direction, blowing from west to east.

La Niña: This phase is characterized by a decrease in sea surface temperatures in the same regions. It generally results in more rainfall in Indonesia and less in the central tropical Pacific. The typical easterly winds along the equator become even stronger.

Neutral: This phase occurs when sea surface temperatures in the tropical Pacific are close to average. Sometimes, the ocean may appear to be in an El Niño or La Niña state, but the atmospheric conditions do not match, or vice versa.

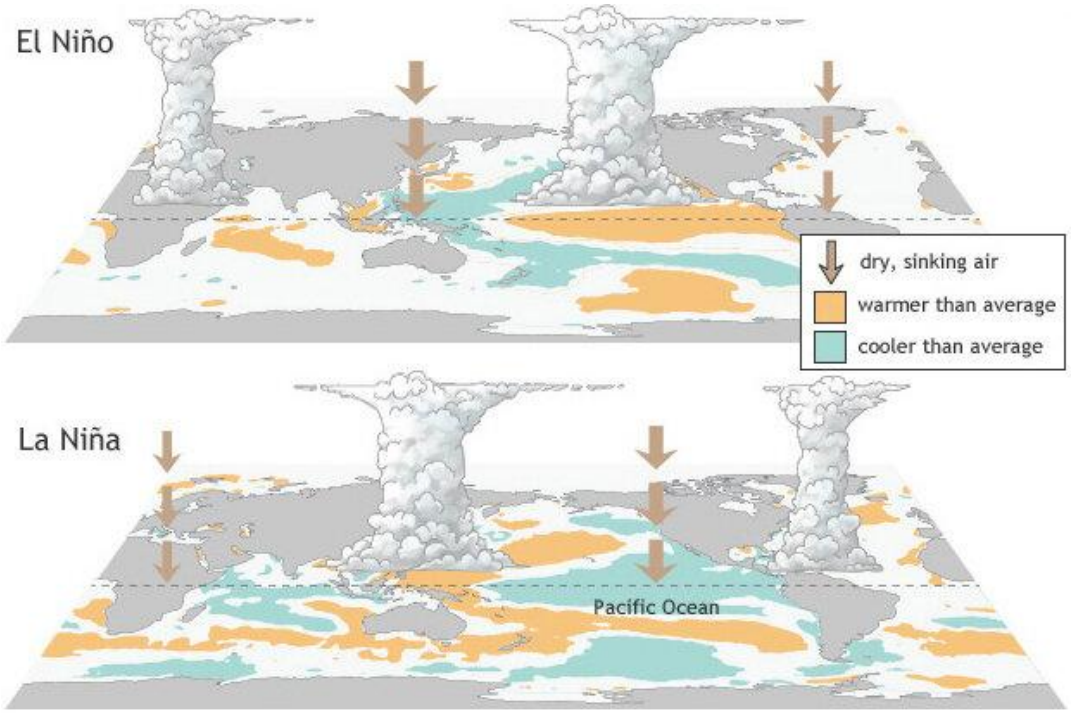

Figure 1.14: El Nino-La Nina Phenomenon
Source: (L'Heureux, 2014)

El Niño significantly influences regional rainfall patterns. Typical precipitation anomalies associated with El Niño included drier-than-usual conditions in maritime Southeast Asia and from southern Mexico to northern South America, while parts of Chile experienced wetter-than-normal conditions (Figure 1.14). In Southeast Asia, El Niño is also linked to reduced monsoon rainfall. For instance, the monsoon onset over Kerala, India, occurred on June 8, seven days later than normal. By the end of September, India had received 94 percent of its usual monsoon rainfall, although higher-than-average rainfall was observed along the lower Indus River and in central India (WMO, 2024a).

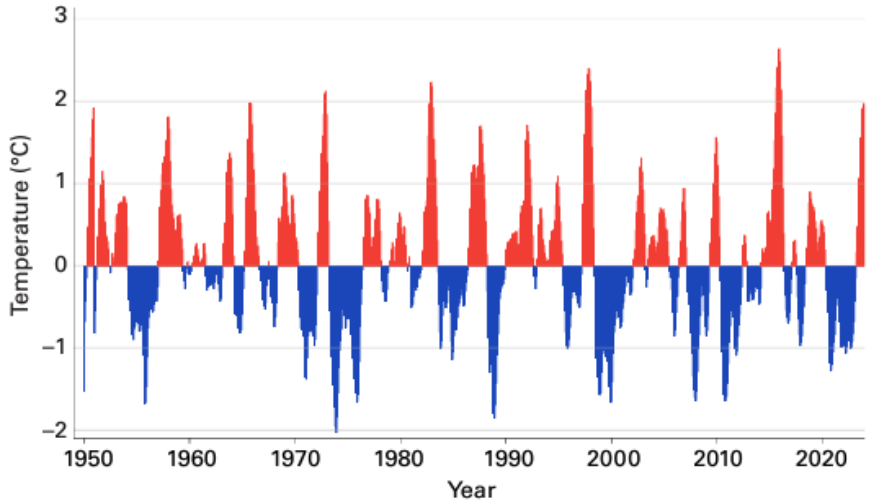

Figure 1.15: Time series of NOAA's Oceanic Niño index from January 1950 to December 2023 showing the presence of cooler-then-average conditions (blue) and warmer-than-average conditions (red) during 3-month average time periods. Anomalies are with respect to the 1991–2020 average sea-surface temperature
Source: NOAA NCEP

The Indian Ocean Dipole (IOD), also known as the “Indian Niño,” is a climate phenomenon characterized by the oscillation of sea surface temperatures between the western and eastern parts of the Indian Ocean. IOD significantly impacts weather patterns across the Indian Ocean region. The Indian Ocean Dipole (IOD) has only been recognized for about 20 years, making it significantly less studied than other climate patterns, such as ENSO (Saji et al., 1999; Webster et al., 1999). During a positive IOD phase, as observed in the southern hemisphere winter and spring of 2019, cooler-than-normal sea surface temperatures develop in the eastern Indian Ocean near Java and Sumatra, while warmer-than-normal conditions occur in the western tropical Indian Ocean. This east-west ocean temperature contrast, or "dipole," alters regional wind, temperature, and rainfall patterns, often causing floods in eastern Africa and droughts and bushfires in eastern Asia and Australia, among other ecological and socio-economic effects. During the negative IOD phase, the warm and cool temperature patterns—and their associated impacts—reverse. Similar to ENSO, the development of these IOD conditions requires interaction between the atmosphere and ocean. In a positive IOD phase, cooler sea temperatures west of Indonesia and warmer conditions in the western Indian Ocean shift atmospheric patterns, often causing dry, bushfire-prone weather in Indonesia and Australia and increased flooding in eastern Africa. The neutral phase of the Indian Ocean Dipole shows neither positive nor negative features (Johnson, 2020).

1.3.7 Observed Changes in the Water Cycle

The water cycle refers to the constant circulation of water within the Earth’s atmosphere and surface. Understanding these processes, shown in Figure 1.16, helps in managing water resources and predicting changes in weather and climate patterns (NASA, 2024). Human-caused climate change has significantly altered the global water cycle since the mid-20th century. This includes increased atmospheric moisture, more intense precipitation, heightened evapotranspiration, and changes in aridity. Additionally, ocean surface salinity patterns have shifted due to the imbalance between precipitation and evaporation.

The water cycle includes several key processes: evaporation, where water changes from liquid to vapor, mainly from oceans; transpiration, the release of water vapor from plants; and condensation, where vapor cools to form clouds and eventually falls as precipitation. After precipitation, water then either runs off into oceans or infiltrates into the ground, contributing to groundwater. Ice, such as glaciers and permafrost, also plays a significant role. Despite the fixed total water volume, water distribution among these processes shifts continuously, affecting water availability for human activities, such as agriculture (Bates et al., 2008).

Evaporation occurs primarily over oceans but also from snow and ice through sublimation (direct conversion from solid to vapor). This process is influenced by factors such as temperature, humidity, and wind speed. Water vapor is crucial for forming clouds, fog, and precipitation. Condensation happens when air becomes oversaturated with moisture, typically due to cooling. Precipitation, including rain and snow, redistributes water, and its runoff flows into rivers, lakes, and oceans. Runoff refers to water flowing back to the sea, while infiltration allows some water to enter the soil and eventually reach streams through groundwater flow. The water cycle and water availability are shifting as a result of climate change. Ice masses like glaciers and permafrost are key to the water cycle. In the past, glaciers covered a third of Earth’s surface; today, ice covers about 12 percent of Earth’s surface.

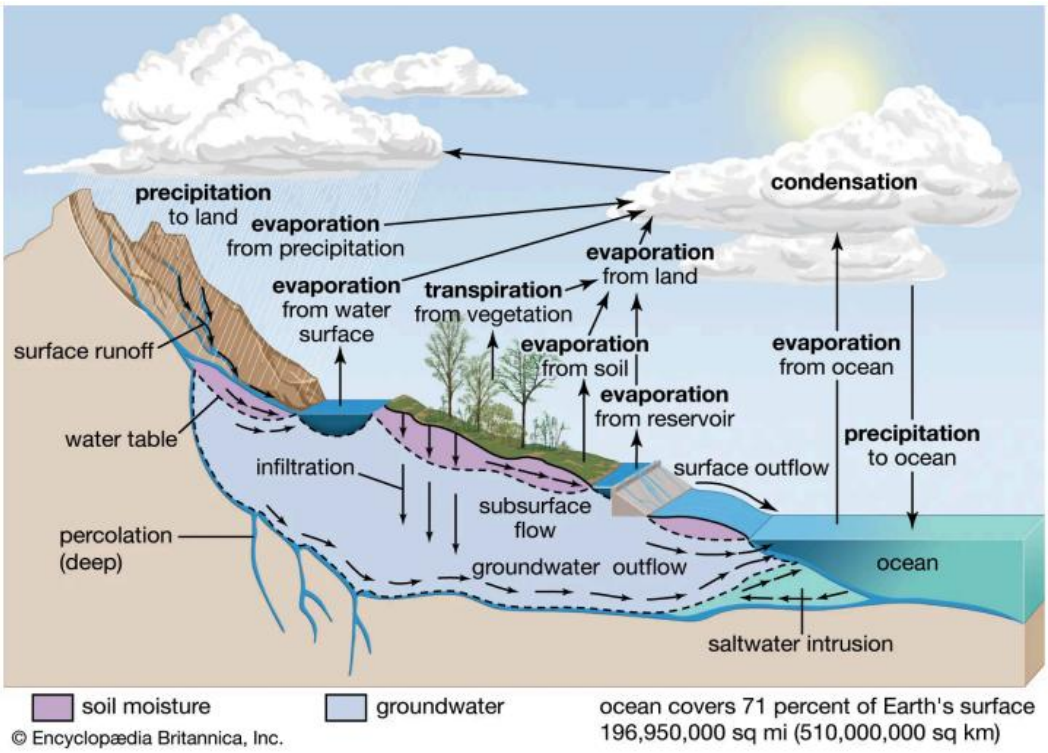

Figure 1.16: Water cycle
Source: (NASA, 2024)

Causes of changes in the water cycle

1.Greenhouse Gas Impacts: Greenhouse gases have influenced precipitation patterns, increasing the contrast between wet and dry seasons. Drying trends in summer climates are evident in regions like the Mediterranean and western North America, with streamflow changes due to earlier snowmelt and glacier melt.

2.Aerosol Effects: Anthropogenic aerosols have driven notable changes in the water cycle, influencing the tropical rain belt and contributing to the Sahel drought of the 1970s–1980s. These aerosols have also counteracted greenhouse gas-driven increases in monsoon precipitation across regions like South Asia and West Africa.

3.Land Use & Water Extraction: Large-scale deforestation has altered local water cycles by reducing evapotranspiration and increasing runoff. Urbanization has raised local precipitation and intensified runoff, while irrigation has depleted groundwater, particularly in dry regions such as northwest India and the USA's Central Valley.

4.Storm Track Shifts: Since the 1970s, storm tracks in the southern hemisphere have shifted poleward, particularly in the austral summer. These shifts are linked to greenhouse gas emissions and stratospheric ozone depletion. Expansion of the Hadley circulation has also been observed, though its contribution to subtropical drying is less certain (Douville et al., 2021).

Observed changes in precipitation

Recent decades have seen changes in the frequency and intensity of precipitation events globally. An analysis of rain gauge data from 1961 to 2018 shows an increased likelihood of precipitation exceeding 50 mm/day, mainly due to heightened rain intensity (Benestad et al., 2019). While these changes haven't been explicitly linked to human activity, they

align with CO_2-induced warming effects on daily precipitation rates (Fischer & Knutti, 2014; Konapala et al., 2017).

In the tropics, there has been an observed increase in precipitation in convergence zones and a decrease in descending branches of atmospheric circulation since 1979. This trend is consistent with increased moisture transport due to global warming. Over tropical land, the pattern of "wet regions getting wetter" and "dry regions getting drier" shows significant variability, influenced by changes in ENSO, as shown in Figure 1.17 (Gimeno et al., 2020).

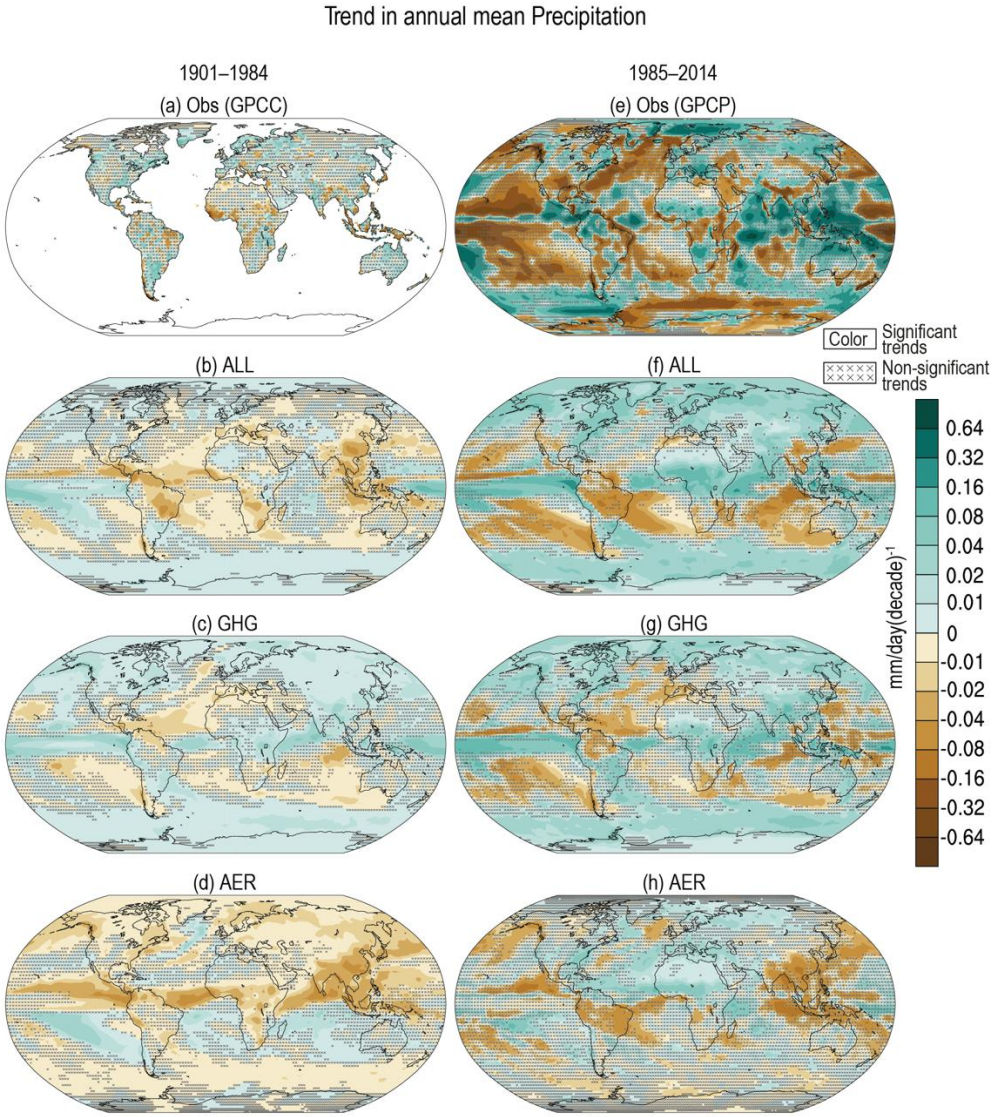

Figure 1.17: Linear trends in annual mean precipitation (mm day–1per decade) for 1901–1984 (left) and 1985–2014 (right): (a, e) observational dataset, and the CMIP6 multi-model ensemble mean historical simulations driven by: (b, f) all radiative forcings; (c, g) GHG-only radiative forcings; (d, h) aerosol-only radiative forcings experiment
Source: (D]ouville et al., 2021)

Observed changes in evapotranspiration

Evapotranspiration describes the transfer of water from land to the atmosphere via two main processes: evaporation from water bodies and soil and transpiration from plants. This phenomenon is crucial in various fields such as hydrology, agriculture, energy balance, and climate research. Observed changes in evapotranspiration (ET) have shown

significant variability due to several factors, including climate change, land use changes, and atmospheric conditions. Climate change significantly impacts evapotranspiration.

Recent studies indicate that anthropogenic factors significantly influence observed trends in evapotranspiration. Douville et al. (2012) linked the post-1960 rise in evapotranspiration in mid-latitudes and northern high latitudes to anthropogenic radiative forcing. The fifth phase of the Coupled Model Intercomparison Project (CMIP5) simulations suggest that such forcing accounts for a substantial portion of the global mean trend from 1982 to 2010 (Dong & Dai, 2016). Additionally, Padrón et al. (2020) found that increases in evapotranspiration primarily drive the trends in dry-season water availability since 1984, supported by CMIP6 results indicating GHG forcing's role in recent increases. The global long-term mean evapotranspiration (ET) from 2003 to 2019 is 423 mm yr^{-1}, with a temporal standard deviation of 98 mm yr^{-1}. This value is generally comparable to estimates in the literature, including those from water-balance studies (450–470 mm yr^{-1})(Fasullo et al., 2007; Wood et al., 2015), model-based estimates (415–586 mm yr^{-1}) (Haddeland et al., 2011), and upscaled flux estimates (325–510 mm yr^{-1}) (Hobeichi et al., 2018; Jung et al., 2019).

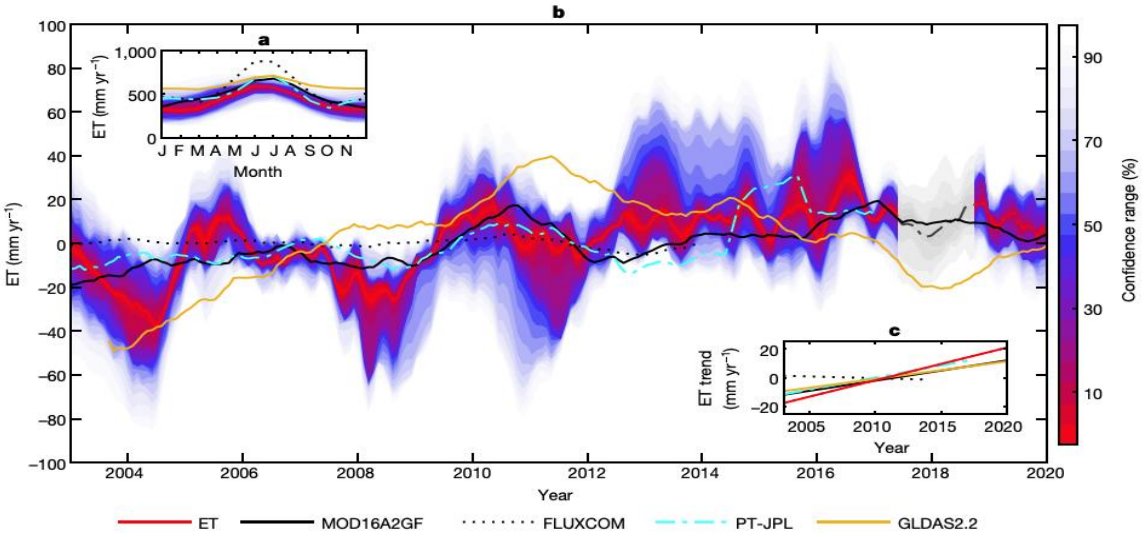

Figure 1.18: Comparison of ET with other products. **a**, Long-term mean (2003– 2019) seasonal cycle of ET compared with other ET products. **b**, Time series of ET with seasonal cycle removed and a moving average of 15 months applied for ET (red line), FLUXCOM (dotted black), GLDAS2.2 (orange), MOD16A2GF (black) and PT-JPL (dashed cyan). **c**, The trend in ET for each of the smoothed
Source: (Pascolini-Campbell et al., 2022).

1.3.8 Observed Changes in Sea Level

In 2023, the global mean sea level (GMSL) reached its highest point since satellite monitoring began in 1993, driven by ongoing ocean warming and the melting of glaciers and ice sheets. The pace of sea-level rise over the past decade (2014–2023) has more than doubled compared to the first decade of satellite measurements (1993–2002). Global warming is causing global mean sea level to rise in two ways. First, glaciers and ice sheets worldwide are melting and adding water to the ocean. Second, the volume of the ocean is expanding as the water warms. The oceans take in 90 percent of the excess heat caused by greenhouse gases. As climate change warms the oceans, the water expands, even if the overall volume stays the same. Since the ocean basins are not increasing in size, this expansion forces water levels to rise, similar to how mercury rises in a thermometer. NOAA researchers estimate that since 2004, about one-third of global sea level rise could be attributed to this warming effect. A third, much smaller contributor to

sea level rise is a decline in the amount of liquid water on land. As groundwater from aquifers, lakes and reservoirs, rivers, soil moisture is depleted by human activity, liquid water shifts from land to ocean (Figure 1.20) (NASA, 2025).

El Niño cycles have a strong effect on sea level. From January to March 2023, sea levels in the western tropical Pacific were above the long-term average (1993–2012), reflecting the presence of warm seawater during El Niño-Southern Oscillation (ENSO)-neutral conditions (Figure 1.19). In contrast, sea levels in the north Atlantic and eastern tropical Pacific were below the long-term average. As surface waters in the eastern tropical Pacific began warming during the early stages of the 2023 El Niño, sea levels rose above the long-term mean in that region between April and June. By July to September, the El Niño pattern became more pronounced, with elevated sea levels extending from the central tropical Pacific to the coasts of Central and South America. Above-average sea levels were also observed in the tropical and north-east Atlantic, linked to anomalous warming during the northern hemisphere summer. From October onwards, the El Niño pattern continued to intensify, and the shift to the positive phase of the Indian Ocean Dipole (IOD) resulted in higher-than-normal sea levels in the western Indian Ocean, while sea levels in the eastern Indian Ocean dropped below average.

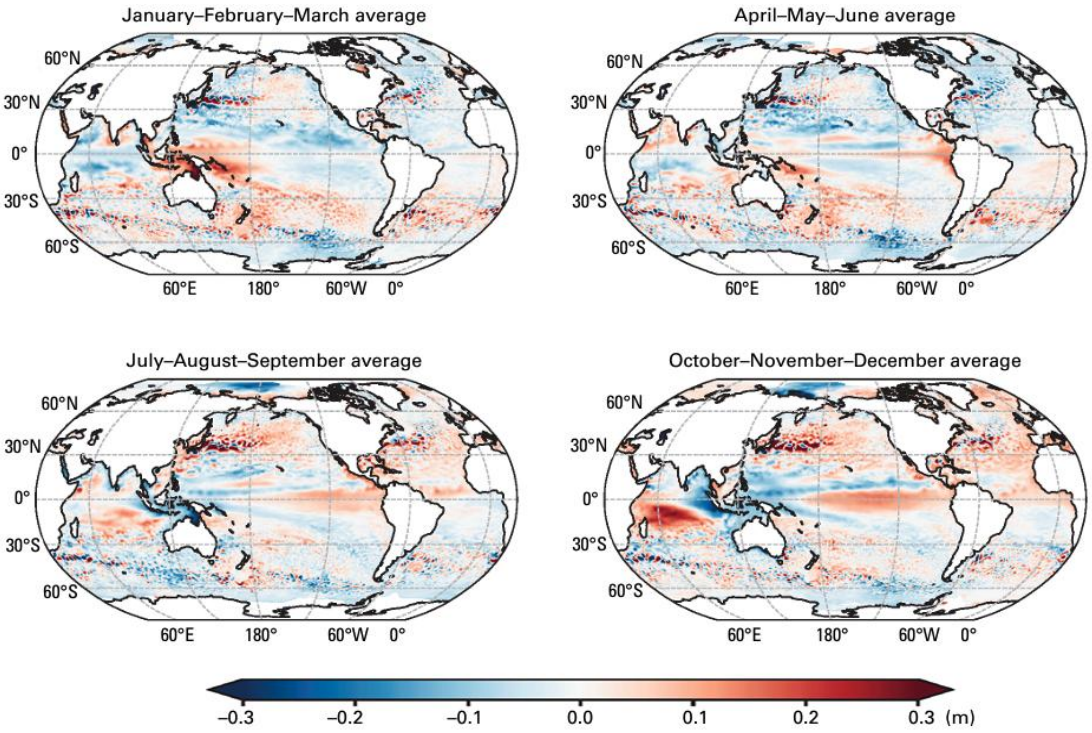

Figure 1.19: Three-month averages of altimetry-based sea-level anomalies (relative to the 1993–2012 average, which is the product climatology) for (top left) January–March 2023, (top right) April–June 2023, (bottom left) July–September 2023 and (bottom right) October–December 2023
Source: Copernicus Marine Service

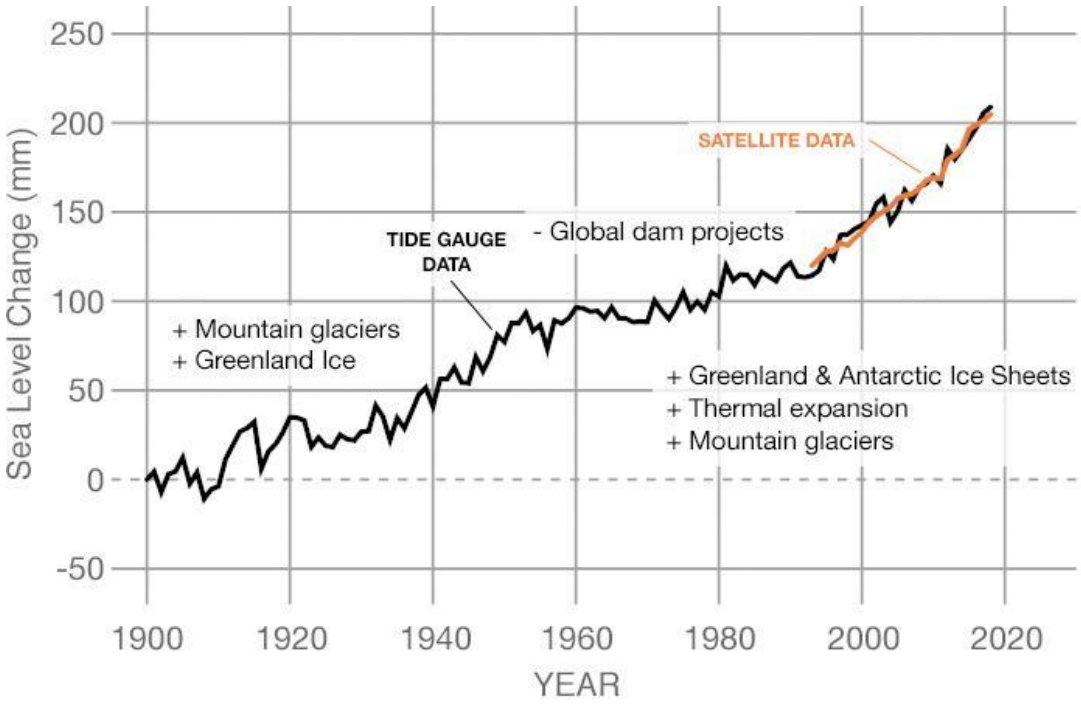

Figure 1.20: Sea level changed from about 1900 to 2018. Items with pluses (+) are factors that cause global sea level to increase, while minuses (-) are what cause sea level to decrease. These items are displayed at the time they were affecting sea level
Source: (Frederikse et al., 2020)

1.3.9 Observed Changes in Carbon and Other Biogeochemical Cycles

Human-induced GHG activities have caused significant changes to carbon and biogeochemical cycles. While natural processes like tectonic activity and biological sources impact greenhouse gas levels over long timescales, human activities, particularly burning fossil fuels, changing land use, and using limestone to make concrete increased carbon dioxide in the atmosphere by 40 percent since pre-industrial times.

Greenhouse gases, such as carbon dioxide, methane, and water vapor, absorb and re-radiate infrared radiation from Earth's surface, contributing to the greenhouse effect. These gases trap heat, slowing its release back into space and helping to regulate Earth's temperature (Mann, 2024). Though they comprise only a small fraction of the atmosphere, these gases greatly influence Earth’s climate by affecting its energy balance. Their concentrations have varied throughout history, with higher levels during warmer periods and lower levels during cooler ones (Mann, 2024).

Atmospheric concentrations of greenhouse gases represent a balance between emissions from human activities and natural sources and sinks, which remove and sequester GHGs. Since the Industrial Revolution, the rise in greenhouse gas levels due to human activities has been the primary driver of climate change. In 2022, the levels of the three primary greenhouse gases—carbon dioxide, methane, and nitrous oxide—hit unprecedented highs, according to the most recent consolidated global data (from 1984 to 2022). Current measurements from various locations indicate that these greenhouse gas levels continued to rise in 2023 (WMO, 2024a).

In 2022, global atmospheric concentrations of greenhouse gases reached record levels: CO_2 averaged 417.9 ± 0.2 ppm (150 percent above pre-industrial levels), CH_4 reached

1,923 ± 2 ppb (264 percent above pre-industrial levels), and N_2O was 335.8 ± 0.1 ppb (124 percent above pre-industrial levels). N_2O saw its highest recorded rate of increase, while CH_4 was the second highest on record. CO_2 growth was influenced by La Niña conditions in 2022, which typically result in lower growth compared to El Niño years (Betts et al., 2016). Real-time monitoring from various locations suggest these gases continued rising in 2023 (NOAA, 2024; CSIRO, 2024[4]).

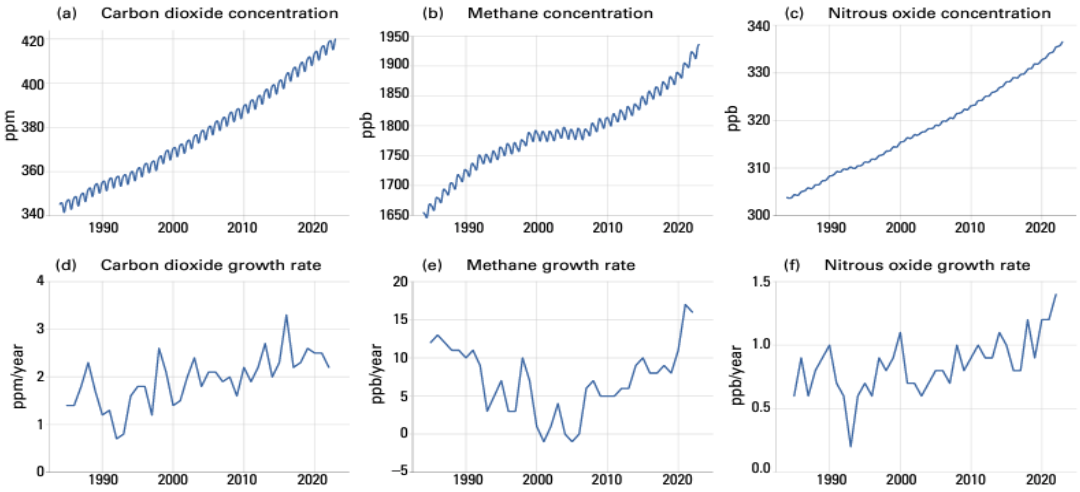

Figure 1.21: Top Row: Monthly globally averaged mole fractions (a measure of atmospheric concentration) from 1984 to 2022 for (a) CO_2 in ppm, (b) CH_4 in ppb, and (c) N_2O in ppb. Bottom Row: Growth rates showing annual increases in the mole fractions for (d) CO_2 in ppm per year, (e) CH_4 in ppb per year, and (f) N_2O in ppb per year.
Source: (WDCGG, 2024)

The impact of each greenhouse gas on the climate depends on its chemical properties and atmospheric concentration. Some gases are highly effective at absorbing infrared radiation and are found in significant amounts, while others are less effective or present only in trace quantities. Radiative forcing, as defined by the Intergovernmental Panel on Climate Change (IPCC), measures the effect of a greenhouse gas or other climatic factors (like solar irradiance or albedo) on the radiant energy reaching the Earth's surface. To compare the influence of different greenhouse gases, forcing values (measured in watts per square meter) for the period from 1750 to today are provided below (Figure 1.22) (Arias et al., 2021).

[4] PPM (parts per million) and PPB (parts per billion) measure the concentration of a substance in air. PPM means 1 part per million parts of air. For instance, 400 ppm of CO_2 means 400 molecules of CO_2 per million molecules of air. PPB is 1 part per billion parts of air, used for trace gases present in smaller amounts.

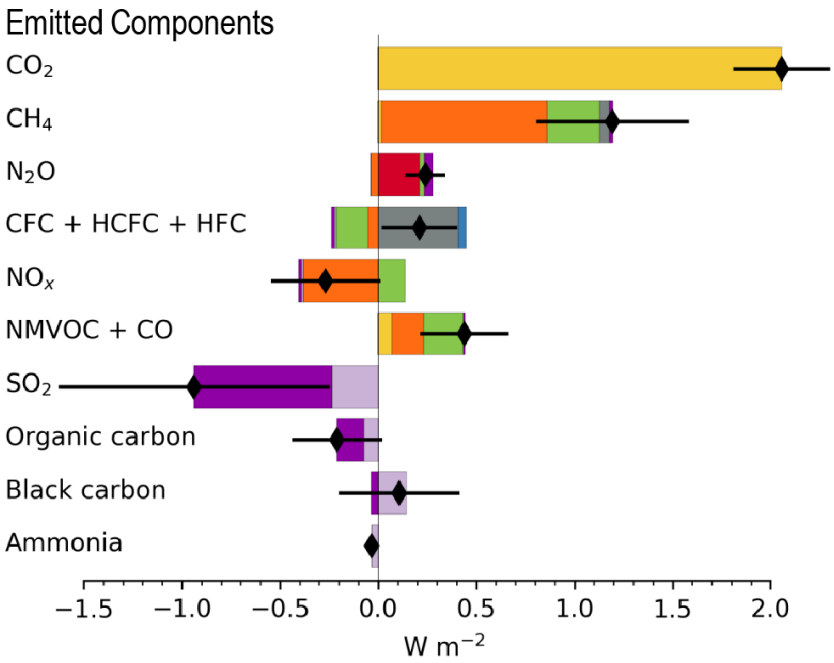

Figure 1.22: Effective radiative forcing 1750 to 2019
Sources: (Arias et al., 2021)

1.3.10 Global Climate Projections

The IPCC released the Sixth Assessment Report (AR6) on the physical science basis of climate change in 2021. The IPCC projects that under different emissions scenarios, global temperatures are expected to continue to rise by 1.5°C to over 4°C by the end of the 21st century (IPCC, 2021). The IPCC primarily uses models from the Coupled Model Intercomparison Project Phase 6 (CMIP6), encompassing advanced Earth System Models (ESMs) and General Circulation Models (GCMs) created by global research organizations. These models replicate intricate climatic processes with enhanced resolution and precision, integrating elements such as aerosol interactions and carbon cycle feedback.

The AR6 incorporates Shared Socioeconomic Pathways (SSPs), which depict various socio-economic possibilities, and Representative Concentration Pathways (RCPs) for many emissions scenarios, facilitating comprehensive forecasts of climate change across different global contexts. There are five SSPs to describe the societal changes influenced by climate change. These SSPs represent five different scenarios of climate change and emissions, ranging from SSP1, Sustainability, which is highly optimistic, to SSP5, Fossil-Fueled Development, which represents the most extreme climate change outcome:

- SSP1 - Sustainability: A world focused on sustainable development and environmental consideration with low challenges for mitigation and adaptation, limiting global warming to below 1.5°C.
- SSP2 - Middle of the Road: Continuation of historical trends and current trends without significant change, resulting in moderate challenges for mitigation and adaptation, aiming with efforts to limit global warming to below 2°C.
- SSP3 - Regional Rivalry: A Fragmented world with regional conflict and high challenges for mitigation and adaptation.
- SSP4 - Inequality: A world with growing inequalities between and within countries, resulting in high adaptation challenges but low mitigation challenges for wealthy countries.

- SSP5 - Fossil-Fuelled Development: Focus on rapid economic growth driven by fossil fuels, resulting in low adaptation challenges but high mitigation challenges due to high emissions.

Throughout the report, SSP2-4.5 and SSP5-8.5 are used to indicate a moderate and a severe climate change scenario. SSP2-4.5 is a climate change scenario that assumes moderate socioeconomic development and moderate climate change mitigation. The number 4.5 refers to the radiative forcing of 4.5 watts per square meter by the year 2100. SSP5-8.5 is the worst-case climate change scenario that assumes high greenhouse gas emissions and high temperatures. The number 8.5 refers to the radiative forcing of 8.5 watts per square meter by the end of the year 2100. NASA used the results from IPCC Sixth Assessment Report for visualization. Figure 1.23 below illustrates global temperature anomalies for meteorological summer 2023, which was much warmer compared to the baseline average from 1951 to 1980.

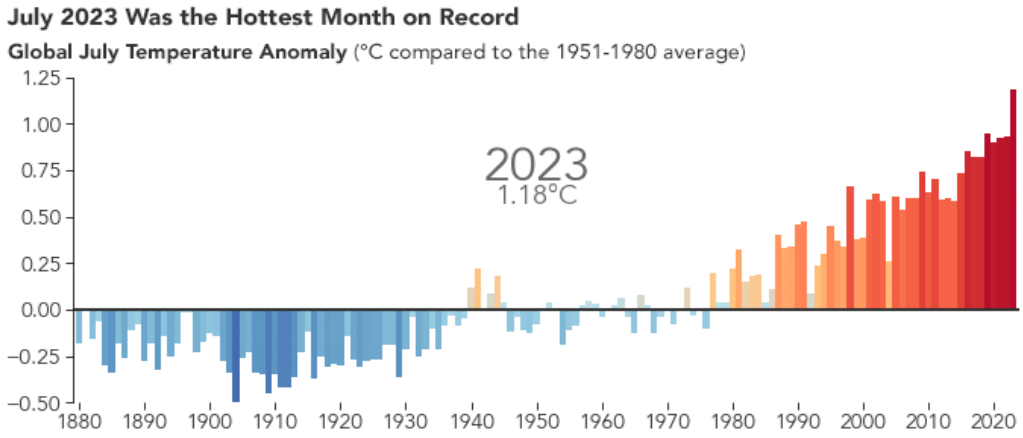

Figure 1.23: Global temperature from 1880 to 2023
Source: NASA (2023)

1.3.11 Projection of Global Temperature

According to the report from the Coupled Model Intercomparison Project Phase 6, global temperatures are projected to rise between 1.5°C and 5.7°C by 2100, depending on different SSPs. Under a low-emission scenario (SSP1-1.9) that aligns with the goals of the Paris Agreement, temperatures are projected to increase by 1.5°C to 2°C by 2100 if significant emissions reductions occur. However, under business-as-usual high-emission scenario (SSP5-8.5), the global temperatures could increase by 3.3°C to 5.7°C by the end of the century (Copernicus Climate Change Service, 2024).

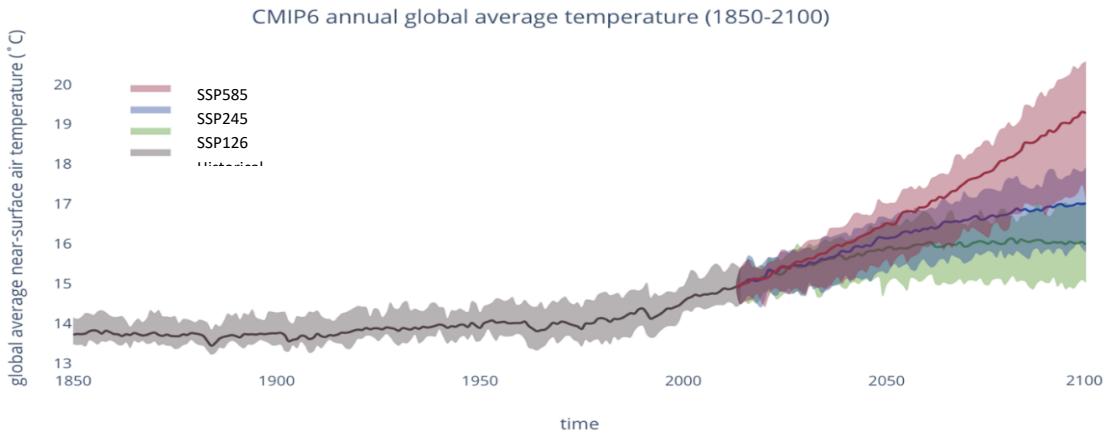

Figure 1.24: Annual global average temperature from 19850 to 2100 used Coupled Model Intercomparison Project – phase 6 (CMIP)
Source: Copernicus Climate Change Service (2021)

1.3.12 Projection of the Global Water Cycle

The Earth is a watery place, with 71 percent of the Earth's surface covered by water and the ocean holding about 96.5 percent of that water. Only about 2.5 percent of Earth's water is freshwater, of which 68.7 percent is in glaciers and ice caps, 30.1 percent is groundwater, and just 1.2 percent is surface water (USGS, 2019). This small proportion of freshwater amounts to approximately 835,000 km³, with the majority (630,000 km³) stored in groundwater, while the remaining 205,000 km³ is retained in lakes, rivers, marshes, and soils. Although the natural cycling rate of this freshwater is theoretically sufficient to meet global human and ecosystem requirements, significant geographical and seasonal variations affect its availability to fulfil regional demands (Douville, 2021).

Figure 1.25 illustrates the global classification of precipitation regimes based on atmospheric pressure systems and agricultural emissions, using the percentile threshold and entropy method (Konapala et al., 2020). The following description highlights the geographical extent and climatic characteristics of one of the dominant regimes. High-pressure, Low Agricultural Emission and Medium-pressure, Low Agricultural Emission regimes are widespread across the Indian subcontinent, northeast Asia, northern Australia, and north-central and south-central Africa, collectively encompassing approximately 15 percent of the global land area. These regions are predominantly influenced by monsoonal climate systems, which drive strong seasonal precipitation variability.

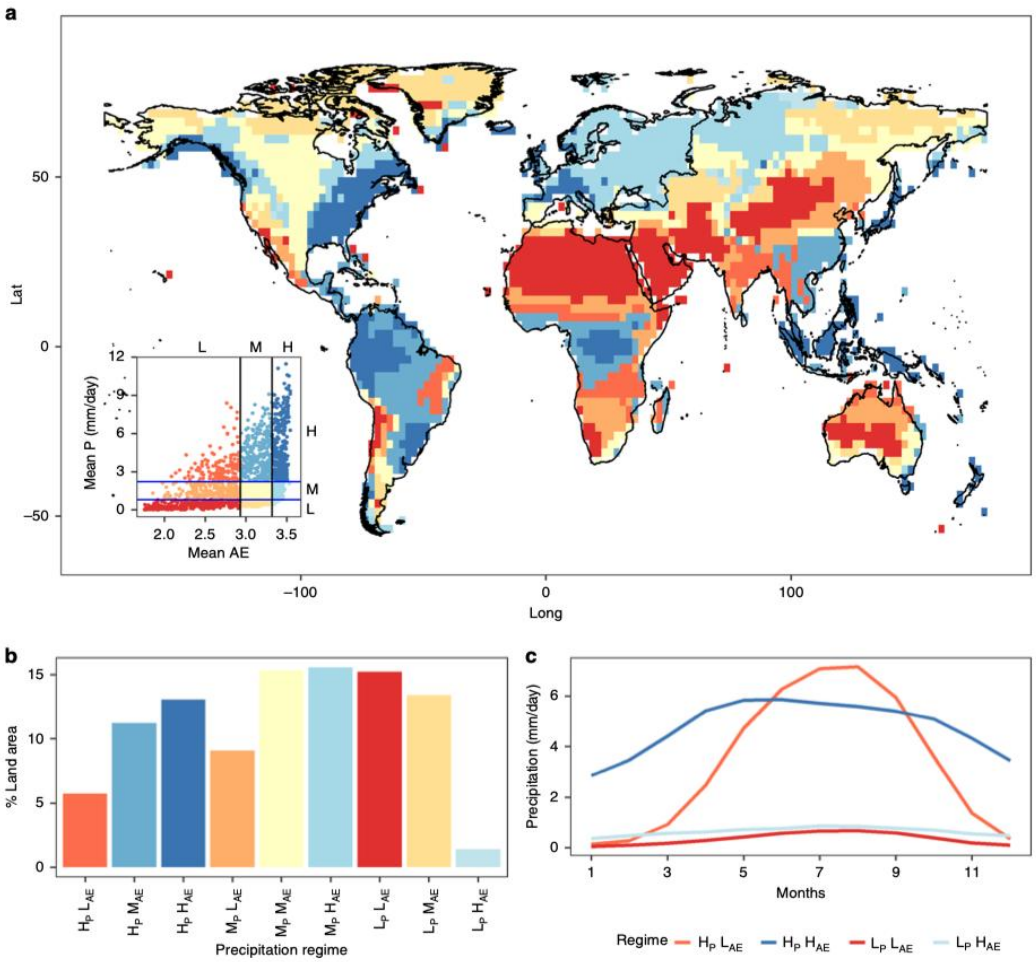

Figure 1.25: Classification of the global precipitation regime based on the percentile threshold concept using mean apportionment entropy
Source: Konapala et al. (2020)

Global mean precipitation and evaporation rise with global warming (high confidence), while the predicted rate is contingent upon the model used (very likely range of 1–3 percent per 1°C). The worldwide rise in precipitation is influenced by a strong correlation with global mean surface air temperature (very probable range of 2–3 percent per 1°C), which is partially counterbalanced by rapid atmospheric responses to warmth from greenhouse gases and aerosols. The cumulative impact of anthropogenic aerosols is to diminish global precipitation and modify extensive atmospheric circulation patterns due to their established surface radiative cooling effect (high confidence). Land use and land cover alterations also affect regional hydrological cycles by impacting surface water and energy budgets, as illustrated in Figure 1.26.

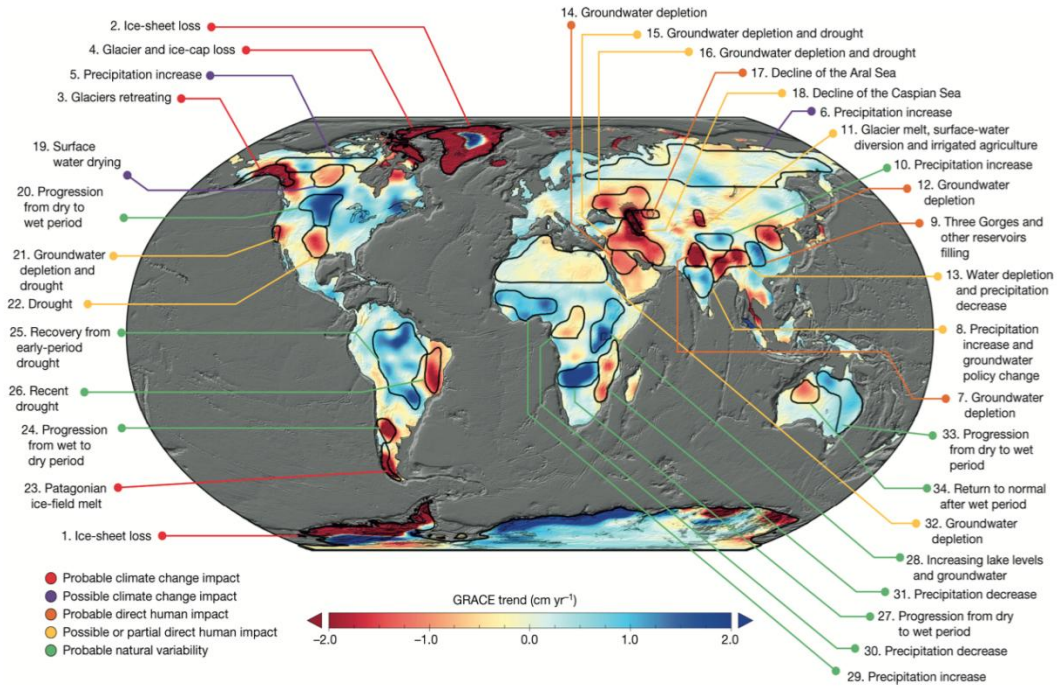

Figure 1.26: Trends in terrestrial water storage obtained on the basis of Grace observation from April 2002 to March 2016
Source: Douville (2021)

Figure 1.27 indicates that precipitation changes to precipitation levels will likely vary across continents. The tropical Pacific and high latitudes, particularly the Arctic, are expected to experience increasing precipitation. In subtropical Africa and Asia, substantial percentage gains are mostly due to low baseline precipitation rather than major improvements. The Mediterranean, Central America, the Amazon, southern Africa, and western Australia will likely experience lower levels of precipitation and thus significant drying. The reliability of these projections is determined by analyzing the variability among models and scenarios. Regions exhibiting considerable diversity, especially in temperature patterns, include areas near the poles where models demonstrate inconsistencies due to differing ice melt timelines. The most uncertainty for precipitation is noted at the low latitudes of the Pacific, Africa, and Asia. (Tebaldi et al., 2021).

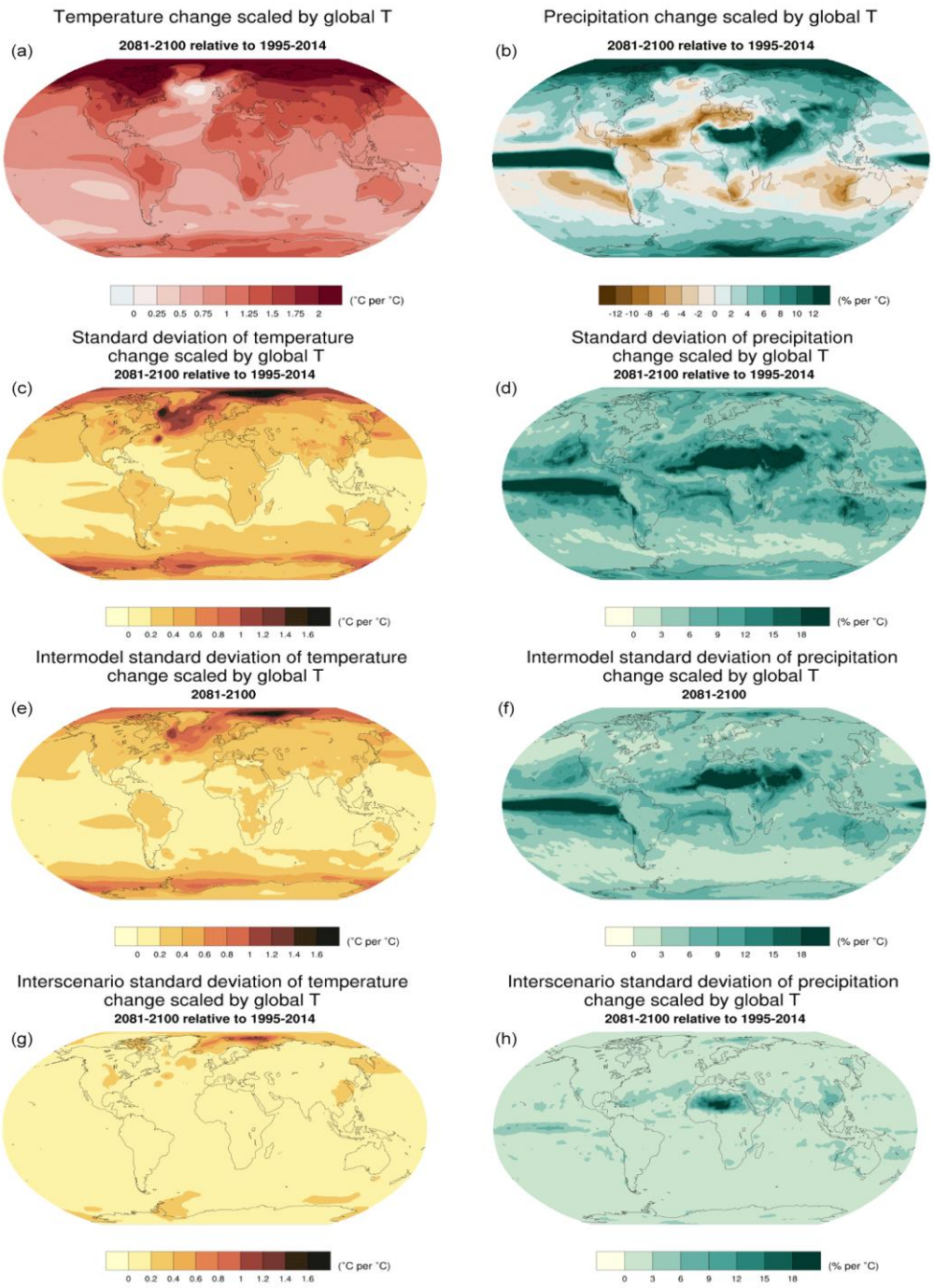

Figure 1.27: Trends in terrestrial water storage obtained on the basis of Grace observation from April 2002 to March 2016
Source: Tebaldi et al. (2021)

CMIP6 modelling in the IPCC report indicates that global and continental precipitation, together with precipitation and evaporation, as well as runoff, will exacerbate the water cycle in both the mid-term and long-term, with emissions scenarios amplifying the magnitude of change. CMIP6 global mean precipitation simulations indicate a systematic multi-model mean increase of 1.6 to 2.9 percent per °C of warming by 2081–2100 compared to the present day across the SSP scenarios. Despite the variability of different scenarios, it is very likely that the intensity of the global water cycle, assessed through global and continental average precipitation, evaporation, and runoff, would escalate with ongoing global warming. The projected changes are outlined below:

- The increase in precipitation across scenarios is negligible, 2.6–4.0 percent, in the medium term (2021-2024, can be extended to 2041-2060), and thereafter escalates to 2.6–8.8 percent in the long-term globally. Global annual precipitation over land is projected to rise by 2.4 [–0.2 to +4.7] percent (likely range) in the SSP1-1.9 low-emissions scenario and 8.3 [0.9 to 12.9] percent in the SSP585 high-emissions scenario by 2081–2100 compared to 1995–2014.
- Due to heightened ocean-to-land moisture transport, land precipitation and evapotranspiration (P–E) rises by 2–3 percent in the medium-term (excluding SSP5-8.5) and by 1–12 percent in the long-term. Global land P-E is anticipated to increase in the medium-to-long-term. Glacier melt and alterations in groundwater storage enhance runoff, albeit with varying reliability. All mid- and long-term projections forecast heightened worldwide precipitation and runoff.
- Precipitable water vapor increases over land by 6–15 percent in the mid-term and 5–36 percent in the long-term across all scenarios; nevertheless, predictions exhibit inconsistency. This indicates that mid-term extreme precipitation increases depend on mitigating strategies.

These projected changes are summarized in Table 1.1, which presents global annual mean water cycle indicators for both the mid-term (2041–2060) and long-term (2081–2100) periods relative to 1995–2014 (Douville, 2021).

Table 1.1 Global annual mean water cycle projections in the mid-term (2041-2060) and long term (2081-2100) relative to present day (1995-2014)

		Mid-term: 2041–2060 Minus Reference Period					Long Term: 2081–2100 Minus Reference Period				
	1995–2014 reference period	SSP119	SSP126	SSP245	SSP370	SSP585	SSP119	SSP126	SSP245	SSP370	SSP585
Global Annual											
Precipitation (mm day^{-1})	2.96 [2.76 to 3.17]	0.06 [0.03 to 0.11]	0.07 [0.03 to 0.12]	0.07 [0.04 to 0.12]	0.06 [0.03 to 0.11]	0.08 [0.03 to 0.14]	0.06 [0.02 to 0.11]	0.09 [0.04 to 0.17]	0.12 [0.07 to 0.21]	0.15 [0.08 to 0.24]	0.2 [0.1 to 0.33]
Precipitable Water (kg m^{2})	24.79 [23.06 to 26.82]	1.42 [0.7 to 2.26]	1.84 [1.03 to 2.62]	2.29 [1.6 to 3.09]	2.7 [1.92 to 3.92]	3.15 [2.13 to 4.38]	1.11 [0.28 to 2.13]	2.11 [0.98 to 3.15]	3.76 [2.41 to 5.08]	6.2 [4.24 to 8.83]	7.92 [5.21 to 10.69]
Global Land Annual											
Precipitation (mm day^{-1})	2.27 [1.98 to 2.58]	0.07 [0.02 to 0.11]	0.07 [–0.0 to 0.13]	0.06 [0.01 to 0.13]	0.06 [0.02 to 0.12]	0.09 [0.01 to 0.16]	0.06 [0.01 to 0.1]	0.08 [0.02 to 0.16]	0.11 [0.02 to 0.19]	0.14 [0.03 to 0.22]	0.2 [0.07 to 0.32]
Precipitation – Evaporation (mm day^{-1})	0.87 [0.49 to 1.26]	0.02 [0.0 to 0.03]	0.02 [–0.01 to +0.05]	0.02 [–0.02 to +0.06]	0.03 [–0.0 to +0.06]	0.04 [0.0 to 0.1]	0.01 [–0.0 to +0.03]	0.03 [–0.01 to +0.08]	0.04 [–0.01 to 0.07]	0.07 [0.0 to 0.12]	0.1 [0.01 to 0.22]
Runoff (mm day^{-1})	0.79 [0.54 to 1.0]	0.02 [0.0 to 0.05]	0.04 [–0.0 to +0.1]	0.04 [–0.0 to +0.11]	0.04 [0.01 to 0.08]	0.06 [0.01 to 0.14]	0.02 [–0.0 to +0.03]	0.04 [–0.0 to +0.13]	0.06 [0.0 to 0.17]	0.1 [0.02 to 0.2]	0.15 [0.04 to 0.27]
Precipitable Water (kg m^{2})	18.86 [17.12 to 21.28]	1.23 [0.57 to 1.96]	1.58 [0.77 to 2.42]	1.96 [1.34 to 2.76]	2.33 [1.63 to 3.46]	2.72 [1.79 to 3.84]	0.95 [0.19 to 1.95]	1.78 [0.8 to 2.77]	3.18 [2.04 to 4.34]	5.33 [3.57 to 7.5]	6.81 [4.35 to 9.32]

1.3.13 Projection of Oceanic Change

The ocean absorbs significant amounts of heat that results from elevated levels of greenhouse gases in the atmosphere, primarily from fossil fuel usage. Two-thirds of this heat is absorbed by the surface level of the ocean, at 0-700 m. The Fifth Assessment Report released by the IPCC in 2013 indicated that the ocean had absorbed over 93 percent of the surplus heat from greenhouse gas emissions during the 1970s. This is resulting in an increase in water temperatures (IUCN, 2017).

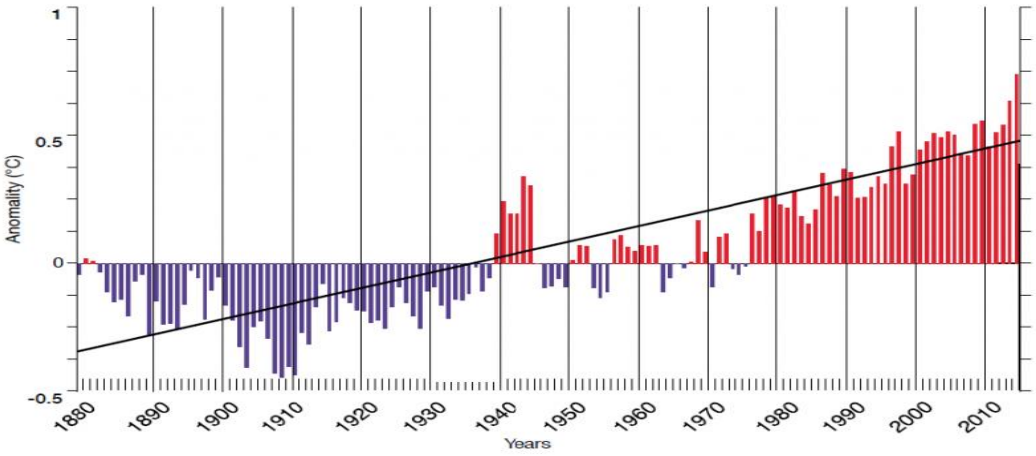

Figure 1.28: Average global sea surface temperature

Modelling studies presented in the IPCC's 2013 Report forecast a probable increase in mean worldwide ocean temperature of 1-4°C by 2100. This trend is illustrated in Figure 1.28, which shows the observed and projected increase in global sea surface temperature. The deep ocean is also affected, with one-third of the excess heat absorbed below 700 meters beneath the sea surface. Ocean warming leads to deoxygenation, characterized by reduced dissolved oxygen levels, and sea-level rise, resulting from the thermal expansion of seawater and the melting of continental glaciers. These interconnected changes within the ocean and cryosphere system are summarized in Figure 1.29, which depicts the feedback and exchanges of heat, water, and carbon across Earth's systems. Rising temperatures, coupled with ocean acidification (the decrease in ocean pH due to CO_2 absorption), affect marine creatures and ecosystems, hence impacting the vital benefits humans derive from the ocean (IPCC, 2019).

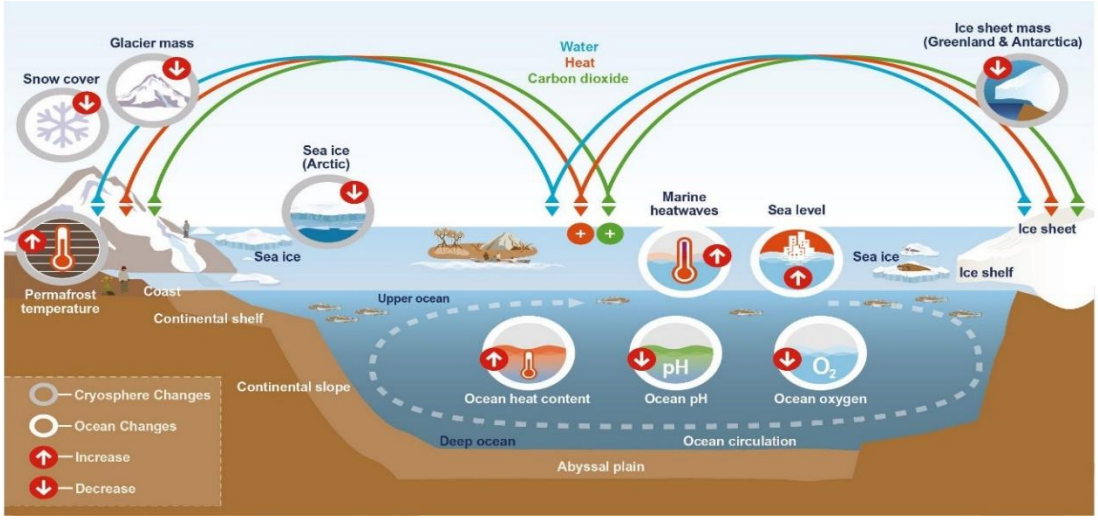

Figure 1.29: Key components and changes of the ocean and cryosphere, and their linkages in the Earth system through global exchange of heat, water, and carbon
Source: IPCC (2019)

The IPCC estimates through CMIP5 that changes and dangers to the ocean and cryosphere by the end of the century (2081–2100) will be more significant under high greenhouse gas emission scenarios than under low emission scenarios (very high confidence). Forecasts and evaluations of forthcoming alterations in climate, oceans, and

cryosphere in the Special Report on the Ocean and Cryosphere in a Changing Climate (SROCC) are typically derived from synchronized climate model experiments from the Coupled Model Intercomparison Project Phase 5 (CMIP5), utilizing Representative Concentration Pathways (RCPs) for future radiative forcing. Current emissions continue to rise, suggesting a trajectory aligned with high-emission futures such as RCP8.5. The SROCC assessment compares a future characterized by elevated greenhouse gas emissions with a low-emission, high-mitigation scenario (designated as RCP26), which offers a two-thirds probability of restricting warming to below 2°C cover pre-industrial levels by the century's end (IPCC, 2019).

1.3.14 Projection of Sea Level

Data indicates that the global mean sea level (GMSL) is rising and that this rise is accelerating (high confidence). The primary factor contributing to the rise in Global Mean Sea Level (GMSL) since 1970 is anthropogenic influence (Oppenheimer, 2019). The combined contributions of glaciers and ice sheets are currently the primary source of global mean sea level rise (extremely high confidence), according to SSP models. GMSL, which is derived from tide gauges and altimetry data, rose from 1.4 mm per year during 1901–1990 to 2.1 mm per year from 1970–2015, further increasing to 3.2 mm per year from 1993–2015, and reaching 3.6 mm per year from 2006–2015 (high confidence).

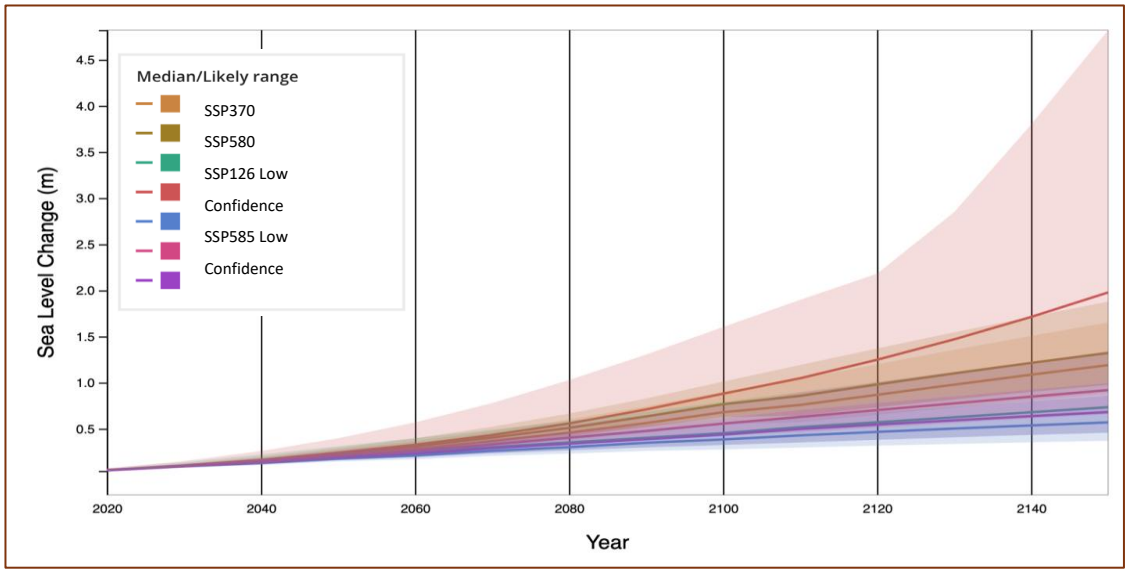

Figure 1.30: Projected Sea Level Rise Under Different SSP Scenarios
Source: NASA

Presently, 267 million individuals globally reside on land situated less than 2 meters above sea level. Hooijer and Vernimmen (2021) used a remote sensing technique known as Lidar, which emits laser light across coastal regions to assess elevation on the Earth's surface, to determine that by 2100, with a 1-meter rise in sea level and no population growth, the affected population may escalate to 410 million individuals. Their maps indicated that 62 percent of the most vulnerable land is located in the tropics, with Indonesia exhibiting the greatest area of at-risk land globally. The forecasts indicated an increased risk of land loss in the future, with 72 percent of the at-risk population located in the tropics, and 59 percent in tropical Asia specifically.

Thermal expansion, glacial and ice sheet melting, and alterations in terrestrial water storage will elevate the Global Mean Sea Level (GMSL) contingent upon the Representative Concentration Pathway (RCP) emission scenario. All the SSP scenarios in

CMIP6 anticipated that sea level will rise by the end of the century. The Global Mean Sea Level (GMSL) is projected to increase by 0.43 m, under RCP2.6, to 0.84 m, under RCP8.5, by 2100, with moderate confidence, relative to the period of 1986–2005. Owing to profound oceanic heat absorption and the mass reduction of the Greenland Ice Sheet (GIS) and Antarctic Ice Sheet (AIS), sea levels are projected to increase for millennia post-2100 (high confidence). In RCP8.5, the forecasts for 2100 are elevated, and the uncertainty range is broader compared to AR5. Melting in Antarctica might elevate sea levels by 28 cm (RCP8.5, upper limit of probable range) by the conclusion of the century (medium confidence). Estimates of sea level rise that surpass the likely range are also presented for risk-averse decision-makers.

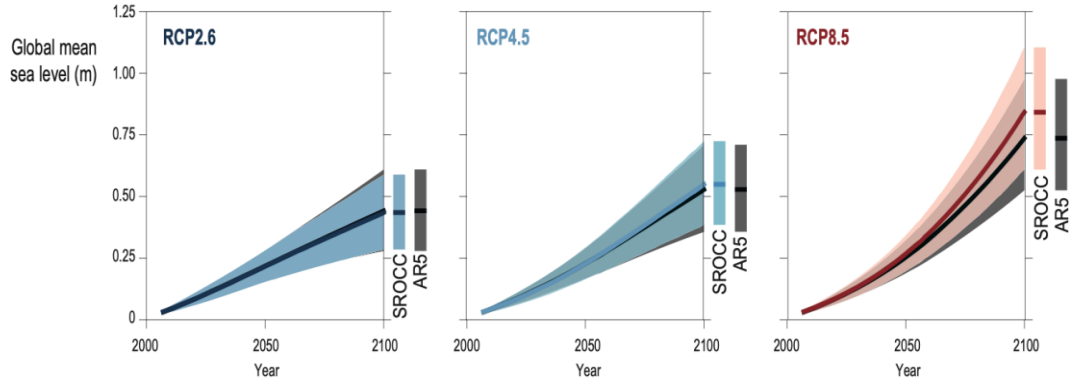

Figure 1.31: Global mean sea level (m)
Source: Oppenheimer (2019)

The projected impacts of sea level rise on coastal ecosystems throughout the century include habitat loss, reduced functionality, and loss of biodiversity, along with lateral and inland migration of human and non-human populations. The effects will be exacerbated in cases of land reclamation and where anthropogenic barriers hinder the interior movement of marshes and mangroves, hence limiting sediment supply and relocation (high confidence). Marshes and mangroves can adapt to rapid sea-level rise (e.g., >10 mm yr –1) under optimal conditions, albeit this capacity varies significantly due to factors such as wave exposure, tidal range, sediment retention, sediment supply, and coastal squeezing (high confidence).

In the absence of adaptation, the frequency and intensity of ESL occurrences, coupled with coastal development trends, will increase projected annual flood damages by 2 to 3 orders of magnitude by 2100 (high confidence). Nevertheless, effectively engineered coastal protection substantially reduces expected damage and is economically viable for urban and densely populated areas, but it is generally expensive for rural and economically disadvantaged regions (high confidence). Effective protection requires global expenditures between tens and maybe hundreds of billions of USD each year (high confidence). Expenditures are generally cost-effective in densely populated metropolitan areas (high confidence). Rural and economically disadvantaged regions face challenges in financing such expenditures, with annual costs for specific small island nations amounting to several percent of GDP (high confidence). Notwithstanding strong preventive measures, the risk of catastrophic consequences in the event of defense failure remains (Oppenheimer, 2019).

Without considerable additional adaptation measures, dangers linked to sea level rise, including erosion, floods, and salinization, are expected to significantly increase by the

end of the century along all low-lying beaches (very high confidence). Urban atoll islands and specific Arctic communities are expected to experience moderate-to-high risk under a low emission scenario, while all low-lying coastal regions are predicted to face high-to-very high risks at the upper threshold of the probable range for high emission scenarios (medium confidence). The transition from moderate to high risk and from high to extremely high risk will vary among different coastal habitats (high certainty). A diminished rate of sea-level rise enables improved adaptation strategies; nonetheless, the benefits of adaptation are expected to vary among coastal ecosystems (Oppenheimer, 2019).

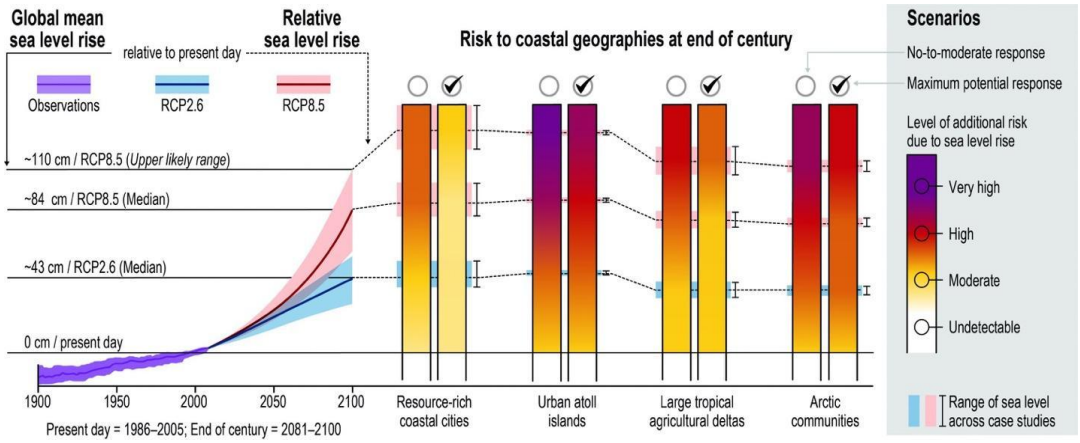

Figure 1.32: Risk related to sea level rise for low-lying coastal areas
Source: Oppenheimer (2019)

Sea-level rise results in risks and effects that are also partially intrinsic to other processes, such as sediment depletion from rivers, permafrost thawing, glacier retreat, and the alteration of natural dynamics due to land reclamation or sediment extraction. Six primary concerns for low-lying coastal areas include:

- Permanent land submersion due to mean sea levels or mean high tides
- Increased frequency or severity of flooding
- Enhanced erosion
- Loss and changes in ecosystems
- Salinization of soils, groundwater, and surface water and impeded drainage

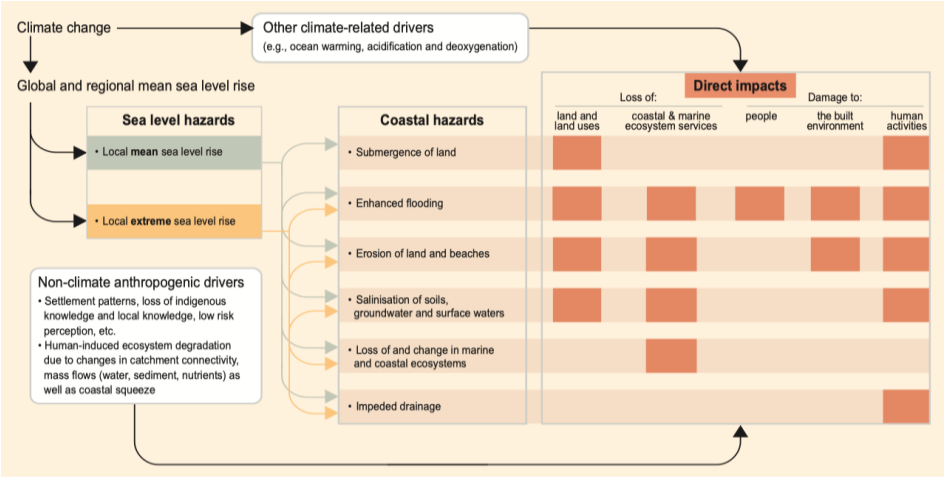

Figure 1.33: Overview of the main impact from sea level rise
Source: Oppenheimer (2019)

1.3.15 Projection of Carbon and Other Biogeochemical Cycles

The three greenhouses gases (GHGs)—CO_2, CH_4, and N_2O—have increased in the atmosphere since pre-industrial times. Together, they comprise 80 percent of the total radiative forcing from homogenized greenhouse gases. The increase in CO_2, CH_4, and N_2O is ascribed to human-induced emissions from fossil fuel use for energy and changes in land use, particularly in agriculture. The observed change in atmospheric levels of CO_2, CH_4, and N_2O results from the interplay between human emissions and the interruption of natural processes that partially eliminate these gases from the atmosphere. Natural processes are interrelated with physical conditions, chemical reactions, and biological transformations, responding to changes in air composition and climatic change. Thus, the physical climate system and the biogeochemical cycles of CO_2, CH_4, and N_2O are interrelated (Ciais, 2013).

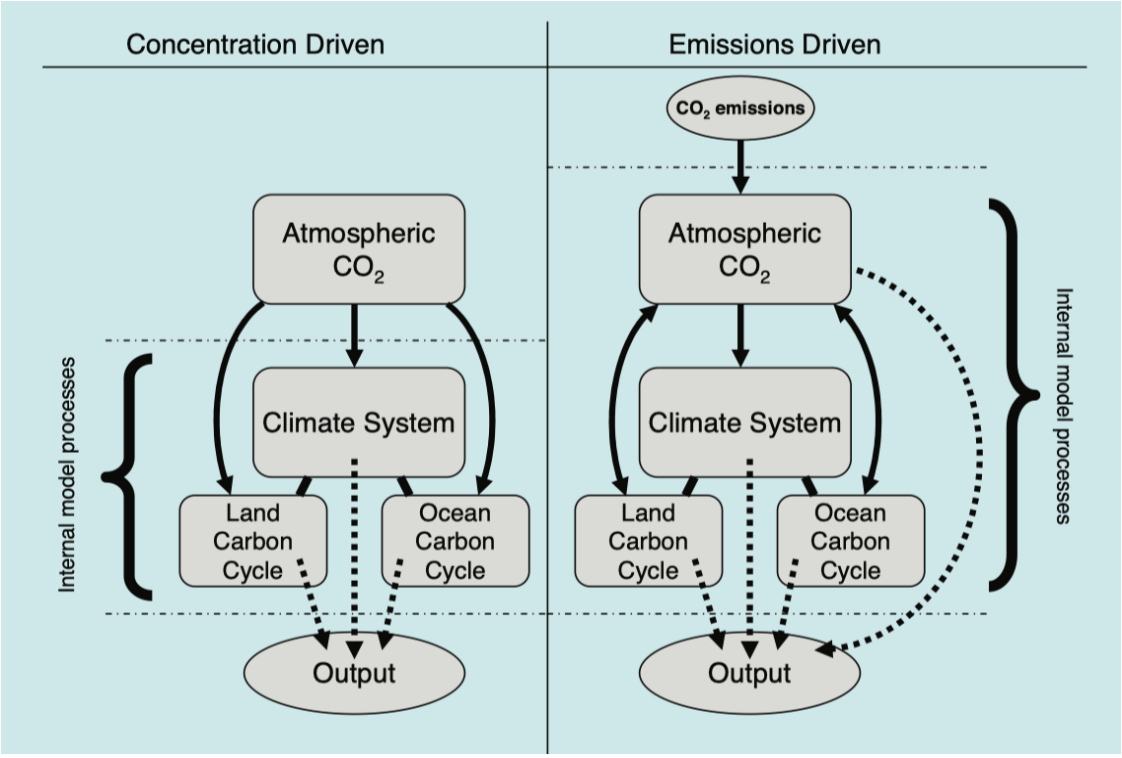

Figure 1.34: Carbon cycle - concentration driven (left) and emissions driven (right)
Source: Ciais (2013)

Figure 1.34 illustrates the carbon cycle under both concentration-driven (left) and emissions-driven (right) scenarios. The carbon cycle plays a crucial role in regulating Earth's temperature, and its interaction with climate feedback mechanisms has substantial implications for future warming:

- Anthropogenic activities, including burning of fossil fuels and deforestation, have augmented atmospheric CO_2 concentrations, resulting in global temperature increase.
- Natural carbon sinks, such as forests and oceans, presently sequester approximately fifty percent of these emissions; however, as global temperatures rise, their efficacy is anticipated to diminish.

- This feedback, wherein heat diminishes the capacity of natural systems to sequester carbon, could intensify climate change by increasing atmospheric CO_2 levels. Moreover, alterations in other greenhouse gases, like methane (CH_4) and nitrous oxide (N_2O), further exacerbate this feedback loop.

The degradation of carbon sinks and the possible release of sequestered carbon from ecosystems (e.g., via wildfires or permafrost thawing) may expedite warming, underscoring the necessity for immediate emission reductions to avert catastrophic climate consequences (Ciais, 2013).

1.3.16 Southeast Asian Climate Change & Projection

Asia remains the most disaster-prone region globally concerning weather, climate, and water-related dangers in 2023. Floods and storms resulted in the greatest number of documented casualties and economic damage, while the effects of heatwaves intensified. According to WMO (2024), Asia is warming faster than the global average. The warming trend has nearly doubled since the 1961–1990 period. Many countries in the region experienced their hottest year on record in 2023, along with a barrage of extreme conditions, from droughts and heatwaves to floods and storms. Climate change exacerbated the frequency and severity of such events, profoundly impacting societies, economies, and, most importantly, human lives and the environment that we live in.

Temperature

In 2023, the annual mean near-surface temperature over Asia was the second-highest recorded, at 0.91 °C [0.84 °C–0.96 °C] above the 1991–2020 average and 1.87 °C [1.81 °C–1.92 °C] above the 1961–1990 average. Significantly elevated average temperatures were documented from western Siberia to central Asia and from eastern China to Japan. Japan and Kazakhstan experienced unprecedentedly warm years.

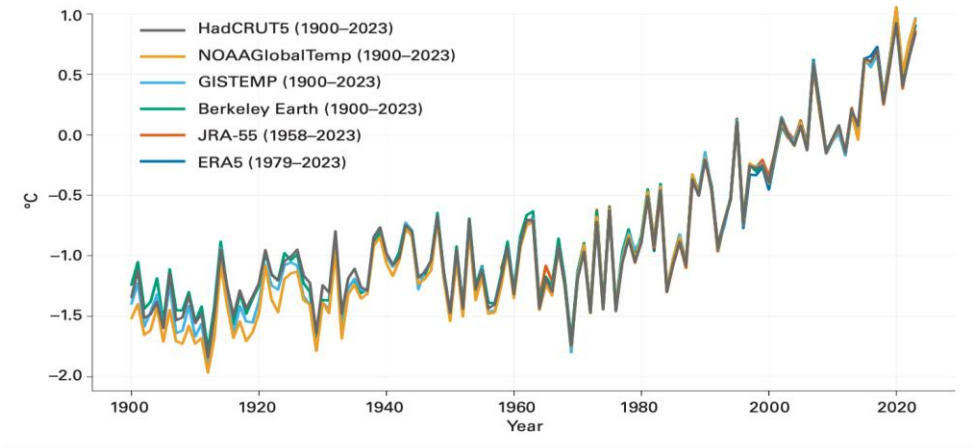

Figure 1.35: Annual mean temperature anomalies (0C), 1900 - 2023, averaged over Asia, relative to 1991 - 2020 average
Source: WMO (2024)

Over the long term, a clear warming trend has emerged in Asia in the latter half of the twentieth century. During the two recent intervals (1961–1990 and 1991–2023), Asia, the continent with the greatest land area stretching to the Arctic, has experienced a rate of warming that surpasses the world average for land and ocean. This indirectly indicates that the temperature rise over land exceeds that over the ocean, as noted in the IPCC AR6 assessment. The warming trend across Asia from 1991 to 2023 was nearly twice that

of the 1961–1990 period and significantly exceeded the trends of the preceding 30-year intervals.

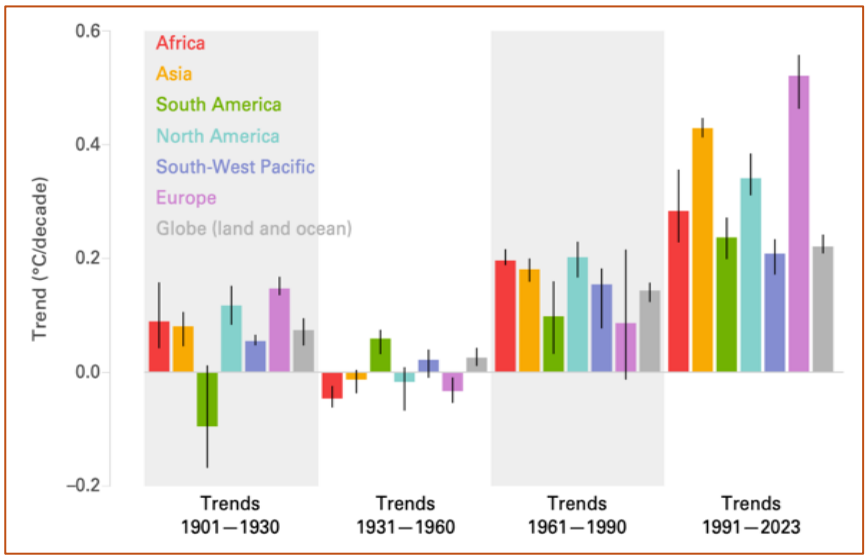

Figure 1.36: Trend in mean surface air temperature

Precipitation

Asia has experienced unusual levels of precipitation in recent years, both excess and below average in various regions. In 2023, precipitation was subnormal in extensive regions Asia, including the lower reaches of the Mekong River, the Arakan Mountains (Myanmar) the Turan Lowland (Turkmenistan, Uzbekistan, Kazakhstan), the Hindu Kush (Afghanistan, Pakistan), the Himalayas, and the vicinity of the Ganges and lower reaches of the Brahmaputra Rivers (India and Bangladesh). Southwest China experienced a drought, characterized by subnormal precipitation in almost every month of 2023, with rainfall linked to the Indian Summer Monsoon being below average. Other regions of the continent experienced above average precipitation. Significant absolute precipitation excesses were recorded in the lower reaches of the Indus River (Pakistan), the Tenasserim Range (Myanmar), and the Kamchatka and Kolyma Ranges (Russian Federation). Significantly elevated precipitation levels were seen in Manchuria and the northern China plain (China); between the Yamal and Taymyr peninsulas (Russian Federation); the Kazakh steppe (Kazakhstan); and the Arabian peninsula (Saudi Arabia) (WMO, 2024).

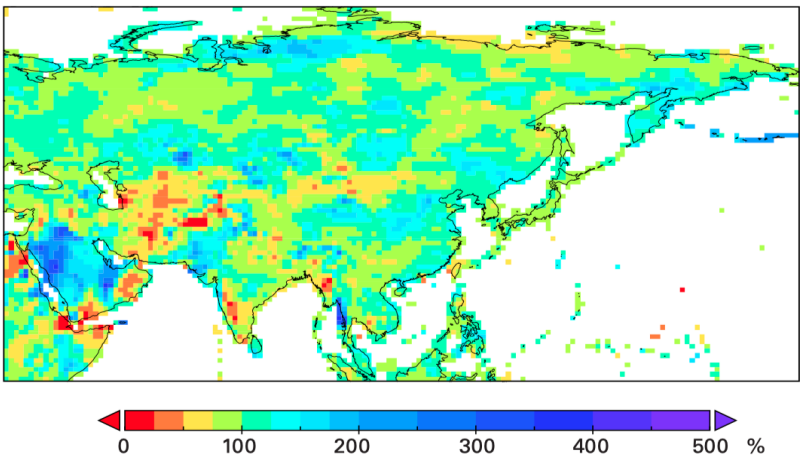

Figure 1.37: Precipitation anomalies for 2023 in Asia

Sea surface temperature and ocean heat

In 2023, the area-averaged sea surface temperature anomalies in the north-west Pacific Ocean reached the highest levels recorded (WMO, 2024). The sea surface in the regions of the Kuroshio current system (western north Pacific Ocean basin), the Arabian Sea, the southern Barents Sea, the southern Kara Sea, and the south-eastern Laptev Sea are experiencing warming at a rate exceeding three times that of the global average sea surface temperature. The Barents Sea is recognized as a climate change hotspot due to ocean surface warming significantly affecting sea-ice cover. This creates a feedback loop where the reduction of sea ice further accelerates ocean warming, as darker sea surfaces absorb more solar energy than the highly reflective sea ice.

Marine heatwaves have been extended durations of high thermal conditions impacting the ocean, transpired in extensive regions of the Arctic Ocean, the eastern Arabian Sea, and the northern Pacific, enduring for three to five months. The upper-ocean warming (0 m–700 m) is notably pronounced in the north-western Arabian Sea, the Philippine Sea, and the waters east of Japan, occurring at a rate exceeding the global average by more than threefold (WMO, 2024).

Sea level rise

In 2023, the global average sea level persisted in its ascent at a consistent rate of 3.43 ± 0.3 mm/year from January 1993 to May 2023, attributable to ocean warming through thermal expansion and the ablation of glaciers, ice caps, and ice sheets. Nonetheless, the rate of increase is not uniform across all locations. The discerned heterogeneous regional patterns in sea level are mostly attributable to uneven ocean thermal expansion coupled with variations in salinity in certain areas. The regional sea-level time series has significant interannual variability, primarily influenced by the El Niño–Southern Oscillation (ENSO), particularly in the eastern Indian Ocean and tropical Pacific Ocean. Figure 1.38 below shows coastal sea-level trends from January 1993 to May 2023 over six subregions in Asia. The sea-level rise rates in all six subregions exceed the global average pace from 1993 to 2023 (WMO, 2024).

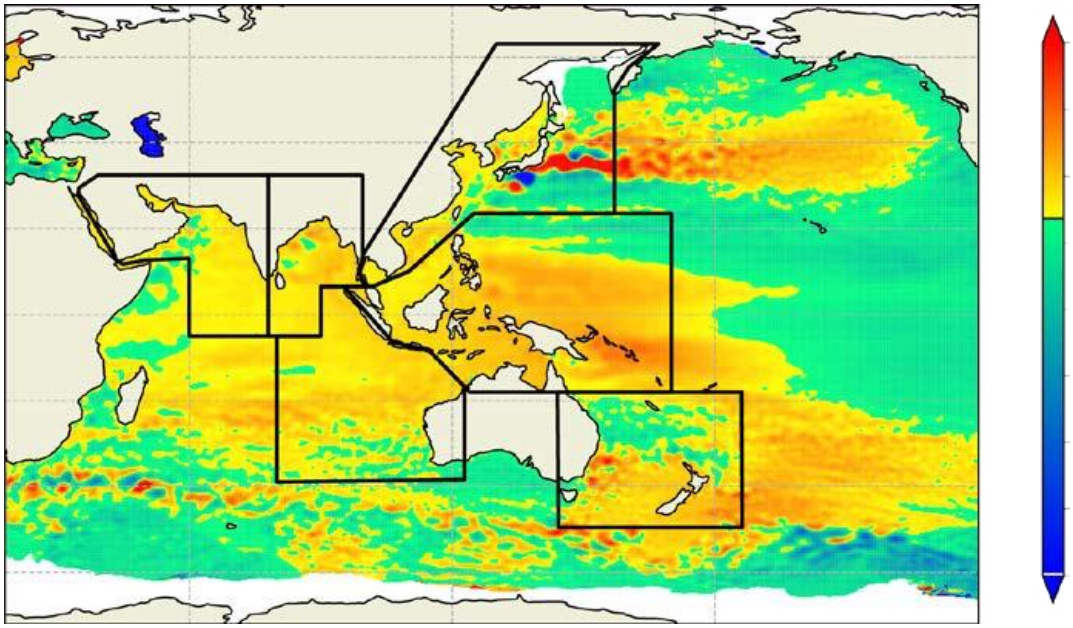

Figure 1.38: Spatial patterns in sea-level trends observed by altimeter satellites over the period from January 1993 to May 2023

Source: WMO (2024)

Impact from climate change through extreme events

In 2023, more than 80 percent of documented hydrometeorological hazards in Asia were attributed to flood and storm occurrences, as per the EM-DAT dataset. In 2023, flooding was the predominant cause of mortality in reported incidents, by a significant margin. In India, Yemen, and Pakistan, floods were the natural hazard event which resulted in the highest fatalities, underscoring Asia's persistent vulnerability to such catastrophes, particularly floods (WMO, 2024).

A total of 17 named tropical cyclones formed over the western north Pacific Ocean and the South China Sea in 2023. This was below average but there were still major impacts and record-breaking rainfall in countries including China, Japan, the Philippines and Republic of Korea. Several extreme precipitation events took place in 2023. In June, July and August, several floods and storm events resulted in more than 600 reported deaths across India, Pakistan, and Nepal (WMO, 2024).

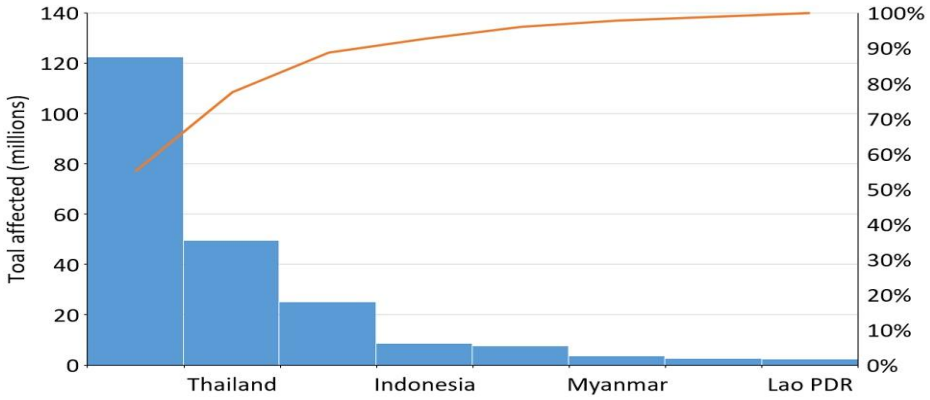

Figure 1.39: ASEAN countries in the order of total number of affected by natural hazards
Source: ASEAN (2023)

The ASEAN Status of Climate Change Report indicates that ASEAN is the world's second-largest open market, following the EU, due to initiatives promoting the unrestricted movement of products, services, and individuals within the area, which positively impacts regional economic integration. Nonetheless, this integration encounters a fundamental danger related to its designation as the 'rice basket of the globe.' Approximately 28 percent of the worldwide rice production and 31 percent of Asia's rice output originates from the region, making fluctuations in rainfall patterns potentially detrimental to food security both locally and globally. As illustrated in Figure 1.39 above, hundreds of millions of individuals in ASEAN nations were impacted by climate change.

Numerous regions in Asia had severe heat episodes in 2023. A significant and extended heatwave impacted a substantial portion of Southeast Asia during April and May, reaching westward to Bangladesh and eastern India, and northward to southern China, accompanied by unprecedented temperatures.

Japan recorded its warmest summer to date. During the summer, China encountered 14 extreme heat events, with almost 70 percent of national meteorological stations surpassing 40°C and 16 sites setting new temperature records.

Table 1.2 Climate change impacts of the sea level rise and heat stress in the ASEAN region

Source: ASEAN (2023)

Country	Sea Level Rise						Heat stress	
	Inundated area (Km2)		Affected population		Economic impact (Billion USD)		Heat mortality (Number of deaths per 1,000 Km^2)	
	RCP 4.5	RCP 8.5	RCP 4.5	RCP 8.5	RCP 4.5	RCP 8.5	RCP 4.5	RCP 8.5
Brunei Darussalam	7	95	60 (60-60)	53 (50-60)	78 (78-78)	62 (54-88)	0.88 (0.5-1.44)	0.86 (0.47-1.35)
Cambodia	1495 (1364-1784)	1474 (1343-1784)	205703 (183950-265700)	213745 (190640-280910)	676 643-766)	660 (486-1054)	4.26 (3.16-4.88)	4.11 (2.36-5.4)
Indonesia	20671 (20304-21260)	19968 (18642-20541)	1540802 (1527442-1561680)	1644018 (1371680-1837870)	3155 (3142-3176)	2783 (2045-4821)	3.06 (1.55-6.83)	2.70 (1.03-3.75)
Lao PDR	0	0	0	0	0	0	2.38 (1.88-3.43)	2.85 (1.74-4.18)
Malaysia	2689 (2662-2726)	2630 (2513-2684)	105103 (104460-105870)	104495 (100910-107000)	1743 (1738-1749)	1465 (1224-2109)	1.13 (0.91-1.4)	1.06 (0.57-1.69)
Myanmar	3851 (3654-4269)	3649 (3471-3725)	471695 (456590-513090)	427150 (379000-568780)	1261 (1227-1356)	682 (449-1334)	1.23 (0.7-1.69)	1.18 (0.55-1.75)
Philippines	4720 (4626-4815)	4606 (4292-4815)	315440 (310500-320760)	342158 (279600-375550)	1198 (1176-1243)	652 (496-1042)	5.50 (4.16-7.49)	5.67 (4.34-8.01)
Singapore	128 (128-128)	128 (128-128)	89170 (89170-89170)	89350 (84790-90870)	1630 (1630-1630)	1382 (1202-1922)	0.22 (0.03-0.4)	0.31 (0.06-0.65)
Thailand	2012 (1933-2122)	1985 (1869-2164)	680468 (670570-694160)	615013 (563350-761530)	3157 (3135-3188)	2482 (1817-4431)	6.90 (5.37-8.18)	6.84 (3.67-10.02)
Vietnam	37810 (36700-38334)	37720 (36700-38353)	17517443 (16174133-18097448)	16685083 (15044492-19245000)	6482 (6241-6585)	8621 (8146-9490)	7.82 (4.93-11.14)	7.85 (4.08-11.79)

CHAPTER 2
CAMBODIA CLIMATE CHANGE

2.1 Chapter Summary

Cambodia is bordered by Thailand to the west and northwest, Lao PDR to the northeast, Vietnam to the east and southeast, and the Gulf of Thailand to the southwest. The country's weather is categorized into two distinct seasons: the rainy season from May to October and the dry season from November to April, each of which is characterized by distinctly differing rainfall, sunshine, and temperature patterns. The country is located on low-lying plains covering an area of 181,035 km², consisting of central plains, which are surrounded by high mountainous regions. Three major water bodies exist in Cambodia: the Mekong River, Tonle Sap, and Bassac River. More than 70 percent of the country is situated in the lowland basin of the Mekong River and several hundred tributaries. Cambodia's population is 17.09 million people, with males representing approximately 48.9 percent and females 51.1 percent. The population growth rate is 1.5 percent as of 2023. The water supplies are seriously threatened by climate stressors such as prolonged droughts, shifting rainfall patterns, and an increase in the frequency of storms. The issues associated with effective food production, water supply management, irrigation, and climate change adaptation have gotten worse due to economic growth, particularly in rural areas. It is anticipated that surface water availability in rural Cambodia will further decline as temperatures rise and climate unpredictability increases. The objectives of this chapter are: i) to provide an overview of Cambodia's climate, such as the frequency and intensity of extreme weather events, climatology, topography, weather patterns, and seasonal characteristics; and ii) to address the drivers of climate changes, including the anthropogenic activities and natural factors, as well as the implications for socio-economic emission pathways and future uncertainty in climate modelling and suitable scenarios. This chapter reports on the effects of climate change in Cambodia, focusing on the general overview of climatology, geographical area, topography, weather, and seasonal characteristics, together with the natural and human-induced drivers of climate change.

The El Niño-Southern Oscillation (ENSO) is one of the most extensively studied climate phenomena. The type of tropical sea surface temperature (SST) anomaly that characterizes the ENSO, that is, a warm (El Niño) or cold (La Niña) SST, affects most of the globe and is involved in radiative and/or water vapor teleconnections far beyond the tropics (Haszpra et al., 2020). In Cambodia, El Niño and La Niña events caused fluctuations in temperature of about +0.28°C to +0.36°C and -0.1°C to -0.31°C, respectively (Williams et al., 2019). Rainfalls and water levels in the Tonle Sap Lake can vary from year to year due to the interannual climate oscillation, particularly the El Niño-Southern Oscillation (ENSO). Effects of ENSO on mainland Southeast Asia are limited; however, there are some studies on the influence of dry-spell patterns in rainfall on rice crop yields in Thailand. However, those earlier studies generally focus on local rainfall variations rather than on the links with sea surface temperature (SST) change and the underlying mechanism. Many important rivers (such as the Mekong and Mun), lakes (like Tonle Sap), and wetlands (such as Boeung Tonle Sap) are located in Cambodia, which experiences a monsoonal climate directly influenced by ENSO events. Rainfall levels in Cambodia are monitored through 200 rainfall stations across Cambodia, operated by the Department

of Meteorology of the Ministry of Water Resources and Meteorology (MoWRAM, 2009). All data indicates that temperature variability in Cambodia will be examined by using temperature datasets from 33 weather stations. A total of 840 monthly average temperatures, ranging from January 1995 to December 2014, were analyzed to assess temperature changes by using Mann–Kendall test and Sen's slope estimator. The temperature trend is gradually increasing. This analysis provides information for evaluating and predicting possible impacts on some areas of life, especially on agriculture and ecosystem health deterioration due to biodiversity changes, floods, and human health hazards in Cambodia (Abdolrahimi, 2016).

The El Niño-Southern Oscillation (ENSO) influences weather patterns, including temperature and precipitation. Rainfall variability patterns in the world, including Cambodia, were strongly related to ENSO events. Variations in temperature affect ecosystem health, crops, and diseases (Yeh et al., 2018).

2.2 Introduction

The majority of Cambodia, in mainland Southeast Asia, is located on low-lying plains. Topographically, approximately three-fourths of the nation's 181,035 km^2 area consists of central plains, which are surrounded by high mountainous regions. The country is bordered by Thailand to the west and northwest, Lao PDR to the northeast, Vietnam to the east and southeast, and the Gulf of Thailand to the southwest. Cambodia has ambitious development goals, aiming to become an upper-middle-income country by 2030 and a high-income country by 2050 (RGC, 2023). The country's robust economic growth, especially in rural areas, has intensified the challenges related to efficient food production, water supply management, irrigation, and climate change adaptation. Climate stressors, such as prolonged droughts, shifting rainfall patterns, and increased storm frequency, pose significant threats to the country's water resources. As temperatures continue to rise and climate variability intensifies, surface water availability in rural Cambodia is projected to decrease further.

2.2.1 Objective

The climate on Earth is changing, and it is anticipated that changes will continue and potentially accelerate in the next century. The amount of greenhouse gases (heat-trapping gases) released into the atmosphere globally, along with the uncertainty surrounding the Earth's climate sensitivity to these emissions, will be the key factors in determining the extent of climate change beyond the next few decades. The global annual average temperature rise could be limited to 2°C or below with significant reductions in greenhouse gas (GHG) emissions. The general objectives of this section are as follows:

- To provide an overview of Cambodia's climate, such as the frequency and intensity of extreme weather events, climatology, topography, weather patterns, and seasonal characteristics; and
- To address the drivers of climate changes, including the anthropogenic activities and natural factors, as well as the implications for socio-economic emission pathways and future uncertainty in climate modelling and suitable scenarios.

2.2.2 Scope of the Chapter

This chapter reports on the effect of climate change in Cambodia, focusing on the general overview of climatology, geographical area, topography, weather, and seasonal characteristics, together with the natural and human-induced drivers of climate change. Concentrations of CO_2, CH_4, and N_2O have increased significantly due to human activities and are now far exceeding pre-industrial levels. Important climate drivers over the industrial era include both those associated with anthropogenic activities and, to a lesser extent, those of natural origin. The only significant natural climate drivers in the industrial era are changes in solar irradiance, volcanic eruptions, and the El Niño–Southern Oscillation. While natural emissions and sinks of GHGs and tropospheric aerosols have varied over the industrial era, they have not contributed significantly to climate change.

2.3 Cambodia Climate

2.3.1 Cambodia Climatology

Cambodia has two distinct seasons, each of which is characterized by distinctly differing rainfall, sunshine, and temperature patterns. The southwest monsoon brings the rainy season from mid-May to November, and the northeast monsoon flow of drier and cooler air lasts from early November to April. These two seasons of relatively equal length are defined largely by precipitation, as temperatures and humidity are generally high and steady throughout the year.

Cambodia has a fairly predictable climate, given that the nation's physical and geographic situation is at mid-latitudes and affected by the Indian Ocean monsoon system. The country is characterized by a tropical savanna climate and monsoons. The mechanism by which the monsoon shapes Cambodia's climate is driven by the intense seasonal heating of the Tibetan Plateau. This creates a pronounced thermal contrast between the Asian landmass and adjacent oceans, spanning from the Indian Ocean to the South China Sea. This gradient subsequently regulates the Indian and western Pacific monsoon systems, ultimately driving low-level, moisture-laden air currents from the Indian Ocean toward the South China Sea (Chen et al., 2023). These moist maritime flow systems regularly impact Cambodia. The dry season is a period of wet and dry airflow from Central Asia to the southern part of Indo-China, the western Pacific, and the South China Sea, which is accompanied by an influx of continental anticlockwise air flows that keep the humidity levels extremely low within the region (Zhu et al., 2021). During the end of the northeast monsoon season, the temperature increases and the velocity of the wind from the sea is reduced. The advection of dry and cool air, together with extremely high solar radiation during this period, are the major reasons behind the drastic reduction of relative humidity values over Cambodia (Alvar-Beltrán et al., 2022).

Cambodian climatology is also highly dependent on how maritime air masses converge with the above air masses. During the South Asian monsoon season, coastal sea breeze circulations dominate central Indo-China, bringing large amounts of moist and maritime air masses inland over Cambodia. During the north Asian monsoon season, circulation linked with the coastal pressure trough caused by the Siberian High, a massive, semi-permanent area of high atmospheric pressure that develops over Siberia during the winter months, occasionally drives extremes of humid southeast wind with large amounts of moisture to upper central Cambodia, especially in the northern region (Lohani et al., 2020). In general, Cambodia has warm and humid air for much of the year from the

Indian-Eurasian land surface. The surface temperature of the western Pacific Ocean, a component of the Indian western Pacific monsoons, is also a major factor affecting Cambodia's climate and environment.

2.3.2 Geographical Location

Cambodia is located in mainland Southeast Asia lies between latitudes 10° and 15° N and longitudes 102° and 108° E. The country borders Thailand to the west and northwest, Laos to the northeast, and Vietnam to the east and southeast. The entire land area of Cambodia is 181,035 km^2, including 176,515 km^2 of land and 4,520 km^2 of water, with an approximate east-west distance of 580 km and a north-south distance of 450 km, and 435 km of coastline to the south along the Gulf of Thailand (Figure 2.1). The country consists of 25 provinces, with a population around 17.09 million in 2023 (MoP, Population Projection 2020-2033, 2023). Phnom Penh, the capital city, is located in south-central Cambodia, at the confluence of the Mekong, Tonle Sap, and Bassac River.

Figure 2. 1. Geography location of Cambodia
Source: (MFAIC, 2025)

Major Water Bodies in Cambodia

The water resources of the Kingdom of Cambodia are crucial for ecology and economic and social development. More than 70 percent of the country is situated in the lowland Mekong basin and freshwater bodies vary in terms of surface area, water depth,

shoreline, drainage patterns, physicochemical characteristics, and biological attributes (Soukhaphon et al., 2021).

The hydrological regime of many Cambodian lowland landscapes is significantly influenced by seasonal flooding, where lake ecosystems play an important role. The many lake basins act as compensatory water storage, dampening disturbing events and fluctuations of rainfall. This allows them to resist severe disturbances, constrain turbulent runoff events during the rainy season, support much richer and more diverse flora, and provide resources to larger fish and wildlife populations. Furthermore, the large amount of freshwater wetlands in the river basins are beneficial for farmers and are of international importance for water bird migration and maintaining a natural flow of nutrients and energy via the fish populations. Many other small, seasonal water bodies contribute directly to this food web by supporting fish populations and by offering breeding sites to fish, shrimps, and other species living in the larger rivers. Wildlife in these aquatic environments enriches local food for people and wildlife, as well as providing an alternate food source for wildlife, like mammals and reptiles, during droughts when natural vegetation on the banks of rivers and wetlands diminishes.

Three major water bodies exist in Cambodia: the Mekong, Tonle Sap, and Bassac River. These water bodies play a crucial role in economic development, fishery resources, and social development (Figure 2.2). Each water body is illustrated in the sections below.

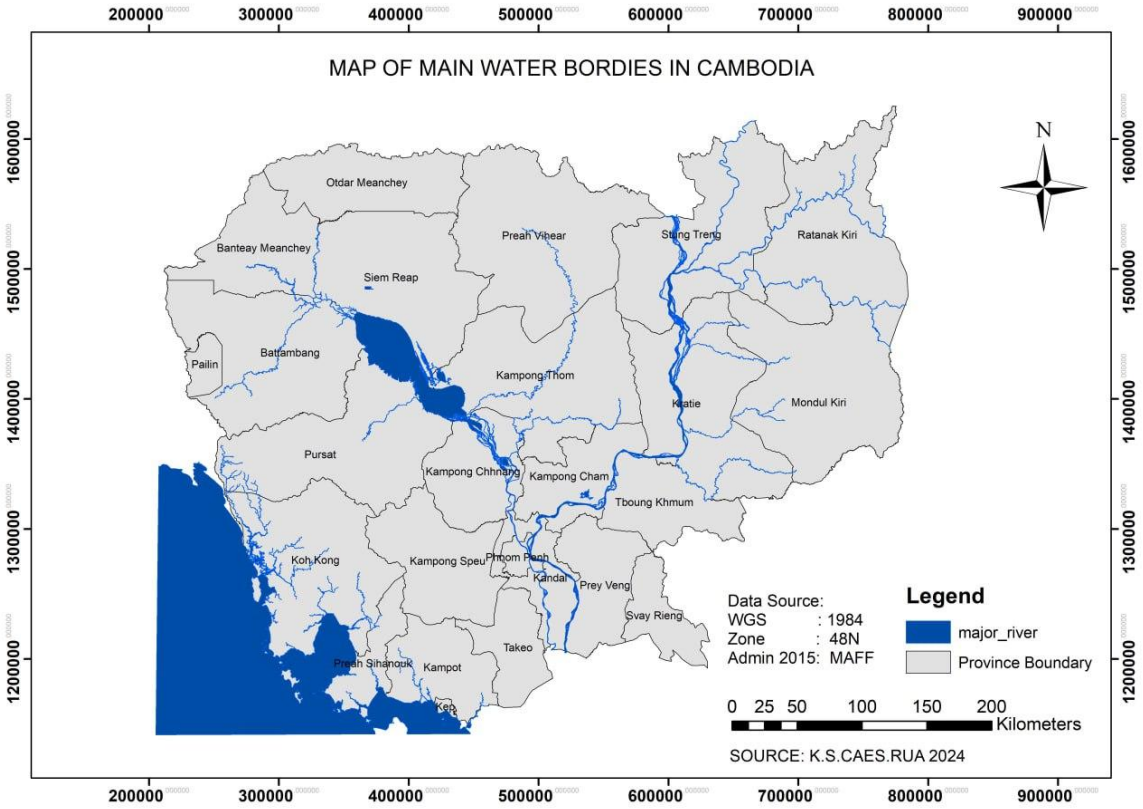

Figure 2. 2 Main water bodies in Cambodia
Source: (CAES-RUA, 2024)

Mekong River

The Mekong River flows from the Tibet Plateau through six countries, including China, Myanmar, Thailand, Lao PDR, Cambodia, and Vietnam, before reaching the South China Sea. The river lies between longitudes 95° E and 106° E and between latitudes 27° N and 14° N. The total length of the river is 4,909 km from its source and 4,400 km from its confluence at the Mun River in Amphoe Phon Sawan, Nakhon Phanom Province, Thailand (Morovati et al., 2023). The Mekong River flows through Cambodia for approximately 486 km before entering the Mekong Delta in Vietnam (Figure 2.2). The Mekong River in Cambodia is home to a unique hydrological feature called the Tonle Sap Reverse Flow. During the flood season, when the Mekong water level is high, the water flows into the Tonle Sap Great Lake; the flow is reversed back to the Mekong River during the dry season from the Tonle Sap Great Lake. This remarkable hydrologic phenomenon gives birth to the Tonle Sap Lake flood pulse, which supports the environment and fisheries by providing breeding and safe growth space for many fish species in seasonally flooded areas, as well as nurturing plant species in the floodplain and providing nutrients, via sediment flows, for agriculture (MRC, 2018).

Tonle Sap River

The Tonle Sap River serves as the primary outlet for the Tonle Sap Lake. It connects the lake to the Mekong River at the northern border of Phnom Penh city (Figure 2.2). The river flow and volume change seasonally according to the volume of water transferred between the Mekong and the lake. The river width varies, but it can cover as much as 900 m at its widest. The course of the river runs in a northwest-to-southeast direction and covers nearly 100 km from where the river diverts from the Mekong to where it arrives at the lake. The course also forms a U-turn just before it arrives at the lake. The average annual discharge is 328 m^3/s over the last decade but can reach 500 m^3/s during wet years (Morovati et al., 2023).

Because of the Mekong flood pulse and Tonle Sap reverse flow, the area has unique biodiversity that is crucial for human and animal life in the region. The flooded forest and a diverse range of aquatic plant and tree species along the river, combined with the presence of bird nests and bird roosts, have created ideal breeding environments for many species of fish and wildlife. The natural flooding regime of the river is crucial to its fish productivity. The river carries water and breeding fish from the Mekong River to the lake between May and October and then dissipates the water out again from October to May, draining out fish from the lake. The wet season flow is accompanied by an inflow of nutrients that sustains the lake's productivity for the rest of the year. Around mid-January, water starts to flow back into the lake via the river, peaking between May and June, after which the water level recedes, returning to the Mekong River by November (Avijit, 2022). Human encroachment has changed the river course, which has had negative impacts on wildlife and local communities.

Bassac River

The Bassac River, a distributary of the Tonle Sap and Mekong Rivers, starts in Phnom Penh, Cambodia, and flows southerly, crossing the border into Vietnam over a distance of 190 km (Figure 2.2). The Bassac River is an important transportation corridor between Cambodia and Vietnam (Mak, 2021). It plays a critical role in the lives and livelihoods of riparian residents, in general, and particularly for fishing communities. Its free-flowing water provides year-round fertile floodplains and wetlands for extensive rice cultivation,

fish habitat, and water management. The availability of diversified water levels and habitats facilitates the breeding of rich aquatic biodiversity and serves as a variety of habitats to support extensive sedentary or agro-based communities in agriculture, small-scale rice cultivation, vegetable gardens, and fruit trees in the lowland along the river.

2.3.3 Topography of Cambodia

Cambodia is a country renowned for its rich history, culture, and stunning landscape. Much of this has been facilitated by Cambodia's unique geography and hydrological features. The country's topography consists of center plains, surrounded by mountains and highland areas, and coastal lowlands. Hydrology is dominated by the Mekong River and its tributaries. The Tonle Sap Lake, an outlet of the Mekong during the rainy season covering up to 10,400 km^2 in the northwest, is one of the main geographical characteristics of Cambodia. Natural borders are formed by the Cardamom Mountains in the southwest and the Dangrek mountain range in the north. Cambodia's forest cover has decreased over the years, it still retains a significant amount of forest; however, it remains one of the countries having the densest forests in the area as of 2022, forest cover remained at 40.10 percent (MAFF's Annual Report, 2023). Phnom Aural is the tallest peak at 1,813 meters above sea level. Each of these regions plays a significant role in the country's development and should be studied in detail (Keir Chapman, 2024).

The central plains of Cambodia, averaging less than 50 m above sea level, extend from the northwest to the southeast of the country. These areas are characterized by flatlands that stretch across the country's central region. These plains are essential for agriculture as they provide fertile soil for farming. The Mekong River flows through these plains, providing water for irrigation and transportation.

In the highland regions, elevation ranges from 100-500 m above sea level on average, while some highlands reach to 1,000 m above sea level. In the mountainous area, the average altitude is approximately 1,000 m above sea level. These areas comprise natural borders in the southwest, north, northeast, and east parts of Cambodia. The most well-known mountainous areas are the Cardamom Mountains in the southwest and the Dangrek Mountains in the north. The highest peak is Phnom Aural, in the Cardamom range, sitting 1,813 meters above sea level. These mountainous regions are not only visually stunning but also serve as important habitats for a diverse range of flora and fauna. They are home to many endangered species, making them crucial for biodiversity conservation efforts (Tran Canh, 2000).

Cambodia's coastal regions, located along the Gulf of Thailand, are known for their beautiful beaches and vibrant marine life. These regions are essential for the fishing industry, providing livelihoods for many coastal communities. The coastal regions are rich in marine resources, making them attractive for both local and international fishermen (Keir Chapman, 2024). The topographic conditions of Cambodia are shown in Figure 2.3 below.

Topography plays an important role in influencing local climate. It has an impact on local temperature, precipitation, wind, and humidity. Mountains can block the movement of air on the side facing the incoming air, which forces the air to rise. Rising air cools and water vapor condenses into clouds and falls as precipitation. Hence, the windward side of mountains often has higher precipitation, while the leeward side of mountains, also known as the rain shadow area, often has less precipitation. Moreover, topography can influence temperature in the local area. Temperature inversion often occurs in

topographic areas such as valleys, where temperatures increase as height increases. Changes in temperature, particularly in relation to topographic features, can indicate shifts in air mass characteristics. Due to these effects, local climate may differ in terms of temperature and precipitation corresponding to topographic areas (Hu et al., 2020).

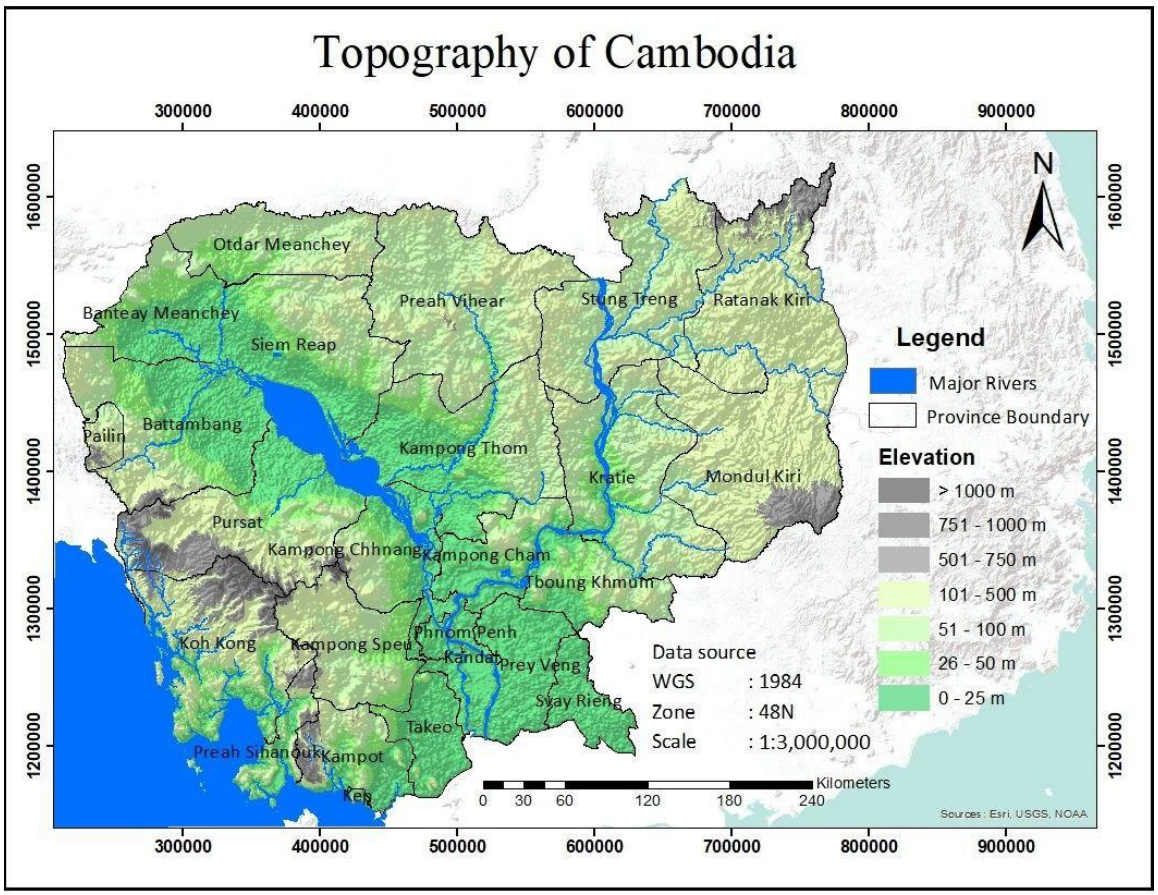

Figure 2. 3 Elevation map of Cambodia
Source: (CAES-RUA, 2024)

2.3.4 Sea Currents

Sea current, or marine current, is the flow or movement of seawater in the sea, the ocean, or other larger bodies of water affected by solid earth. Sea currents are an important branch of physical oceanography, responsible for carrying energy and spreading water salinity and heat, as well as moving marine animals and plants. In smaller or closed seas, such as Cambodia's coastal waters, local factors further influence the surrounding currents, including longshore currents and strong flows such as tides and floodwaters. These coastal currents then affect sediment shifting and land formation in the area. Three main sea currents maneuver marine water across Cambodia's geographical zone. The most influential current originates from the Pacific Ocean through the southern part of Japan enters from the South China Sea. It passes the western rim of Vietnam and the eastern rim of Xiaosha and Wanshan Islands, eventually turning toward the Philippine Sea due to the repelling force exerted by other currents. A second major current is established by two currents from the Pacific Ocean and Indian Ocean. It passes through the South China Sea south of Surabaya, Java and approaches Peninsular Malaysia. The current flows are created by a complex and convoluted eddy over the Gulf of Thailand. The third main current follows the Thai peninsula and course of the extensive coastline of the Gulf of Thailand, before entering Cambodia's coastal waters. As the current moves

southwestward, it forms a micro-cyclonic spin of water north of Koh Kong and then moves in a more southerly direction. It becomes banded with more currents coming from the Pacific Ocean, and together, they finally exit via the southwest into the Indian Ocean. The currents that affect Cambodia's waters are mutually related: they come from different directions and, through their merging and divisions, form a complex internal flow system of the Gulf of Thailand.

Movement of surface oceanic currents plays a major role in ENSO. Other influences on oceanic currents can be air, Earth's rotation, and underwater geography (Timmermans, 2020). This structure or movement in seawater is one of the factors that influence the dynamics and ecological balance of a region. The location of the existence of sea currents also has an impact on the weather and climate. Changes in currents affect ecosystems, especially related to marine biodiversity and communities that depend on coastal natural resources. Moreover, the existence of strong oceanic currents can provide opportunities for environmental protection and can influence marine and nautical spatial arrangements, especially when related to the protection of species and marine biological resources.

The environmental parameters in Cambodia's coastal region, such as water temperature, salinity, and nutrients, are driven by the interactions of local, regional, and global sea currents. The above currents are driven primarily by the monsoon but are also influenced by sea waves in the open ocean. Adding to the regional monsoon-driven effects, the general patterns of Indochina Sea circulation are also indirectly impacted by global changes in sea level and winds. Even though climate variability and climate change contribute to atmospheric variation (including temperature and rainfall in mountainous upstream areas), sea currents may also influence the distribution of temperature and precipitation in coastal lowland areas, which have significant impacts on the choice of plant species and techniques for agriculture in farming practice. Marine ecology may be affected by the variation in sea currents. Nutrient distribution is related to currents, and the stability of habitats is transboundary, which may affect marine ecosystems and natural resources. For example, many fish species in the Kep archipelago move toward the northwestern areas to lay their eggs, and the fingerlings then enter the mangrove zone for the nursery. If the sea currents affect both areas, it is likely that the species numbers may decrease during the egg hatching to fingerling phase, which would affect aquatic resources and food security and lead to local economic deficiency in communities that rely on adult species for income and nutrition.

Fast dynamic changes in local currents can influence the distribution and existence of different invertebrates and may lead to large changes in the community composition of these species (Saeedi et al., 2022). Human activities either have caused or will cause ecological changes in many coastal areas, and since the coastal zone is not only transboundary but also transdisciplinary, it is important to understand marine current dynamics on a broad scale.

2.3.4.1 El Niño Southern Oscillation

El Niño Southern Oscillation (ENSO) is a naturally occurring ocean and atmospheric temperature fluctuations across the east-central equator of the Pacific Ocean. ENSO regularly appears every two to seven years and consists of El Niño—a “warm phase” or a large warming in the equatorial Pacific Ocean—and La Niña—a “cool phase” in which surface waters of the central Pacific Ocean are colder than normal. El Niño is a periodic

oceanographic phenomenon in which strong and extensive warming occurs in the upper ocean in the tropical eastern Pacific, affecting weather patterns globally.

ENSO events are characterized by positive and negative differences in sea surface temperature in the central and eastern Pacific Ocean, coupled with interactions among the atmosphere, ocean, and marine biology. El Niño events disturb rainfall patterns and wind fields and influence hydrological processes such as drought and monsoons. The resulting droughts and water shortages impact agriculture and water resources, leading to economic and societal impacts. Conversely, La Niña is characterized by a cooling of surface waters of the central and eastern Pacific Ocean. This cooling shifts the region of deep convection to the western Pacific, causing stronger trade winds and higher rainfall in Cambodia (Kosal Chim, et al., 2021). The Southern Oscillation is a phenomenon that is closely connected with the ENSO cycle. Rainfall patterns change, trade winds increase, high clouds and high atmospheric pressure form over Indonesia, and low clouds and low-pressure form over the eastern tropical Pacific (Thanh Duc Dang et al., 2020).

ENSO variability affects the climate of Cambodia and Mekong River flow based on its impacts on sea surface temperatures over the Pacific region. The Asian region is divided into nine sub-regions based on spatial characteristics of ENSO-related climate factors. The Indian Ocean and the equatorial Pacific display an ENSO relationship through intertropical convergence zones, wind fields, and ocean factors. For Cambodia, the ENSO impact is significant because in the Southeast Asian region annual rainfall variability is pronounced. Overall, the impact of ENSO on Cambodia's climate can be seen through annual changes in temperature and precipitation, including the well-known effect of warming during the dry and developing stages of El Niño, and the cooling effect during the wet stage.

The ENSO index is widely accepted as a regional climatic signal of a physical phenomenon that affects local weather, temperature, and seasonality. Monthly or annual ENSO can be examined. Local variations in ENSO are due to changes in the relationship between climatic factors and the main characteristics of ENSO, such as ocean temperature, changes in flow fields, and their evolutions. Rainfall is detrimental to developing and accumulated patterns in the Mekong River, not only for the floods in the capture zone but also for subsequent reservoir injection and the El Niño drought. Sunny weather occurs in Southeast Asia during the cold phase of La Niña, and rainfall occurs during the warm phase of El Niño (Nguyen-Thanh et al., 2023).

A. Pacific Decadal Oscillation

The Pacific Decadal Oscillation (PDO) is a pattern of climate variability similar to ENSO in the Pacific. The PDO has been described by some researchers as a long-lived El Niño-like pattern of Pacific climate variability, and by others as a combination of two occasionally separate modes with different temporal and spatial features of north Pacific Sea surface temperature (SST) fluctuation. Widespread variations in the Pacific Basin and the climate of North America are indicators of El Niño/Southern Oscillation (ENSO) extremes in the PDO cycle. Accordingly, the ENSO phenomenon, the extreme phases of the PDO have been classified as either warm or cool, as defined by ocean temperature anomalies in the northeast and tropical Pacific Ocean. The PDO has a positive value when sea level pressures are below average over the North Pacific and when SSTs are abnormally warm along the Pacific Coast and cold in the interior North Pacific. The PDO has a negative value when the patterns of climate anomalies are reversed, with warm SST anomalies in the

interior and cool SST anomalies along the coast of North America, or when the North Pacific experiences above-normal sea level pressures (Mantua, 1999).

B. Madden-Julian Oscillation

The Madden Julian Oscillation (MJO) is an intra-seasonal fluctuation (30-90 days) occurring in the global tropics, responsible for most weather variability. It is characterized by eastward propagation of regions of enhanced and suppressed tropical rainfall, primarily over the Indian and Pacific Oceans. It results in variations in atmospheric and oceanic parameters such as wind speed, cloudiness, rainfall, sea surface temperature, and ocean surface evaporation (Martin, 2021).

MJO influences weather patterns significantly in terms of rainfall, temperatures, floods and droughts. The MJO influences the timing and intensity of rainfall which can lead to cooler conditions through changes in atmospheric circulation patterns. This can have a significant impact on agriculture, water resources, and overall livelihoods in Cambodia (Martin, 2021). Figure 2.4 illustrates the structure of the MJO across the Indian Ocean and west-central Pacific Ocean.

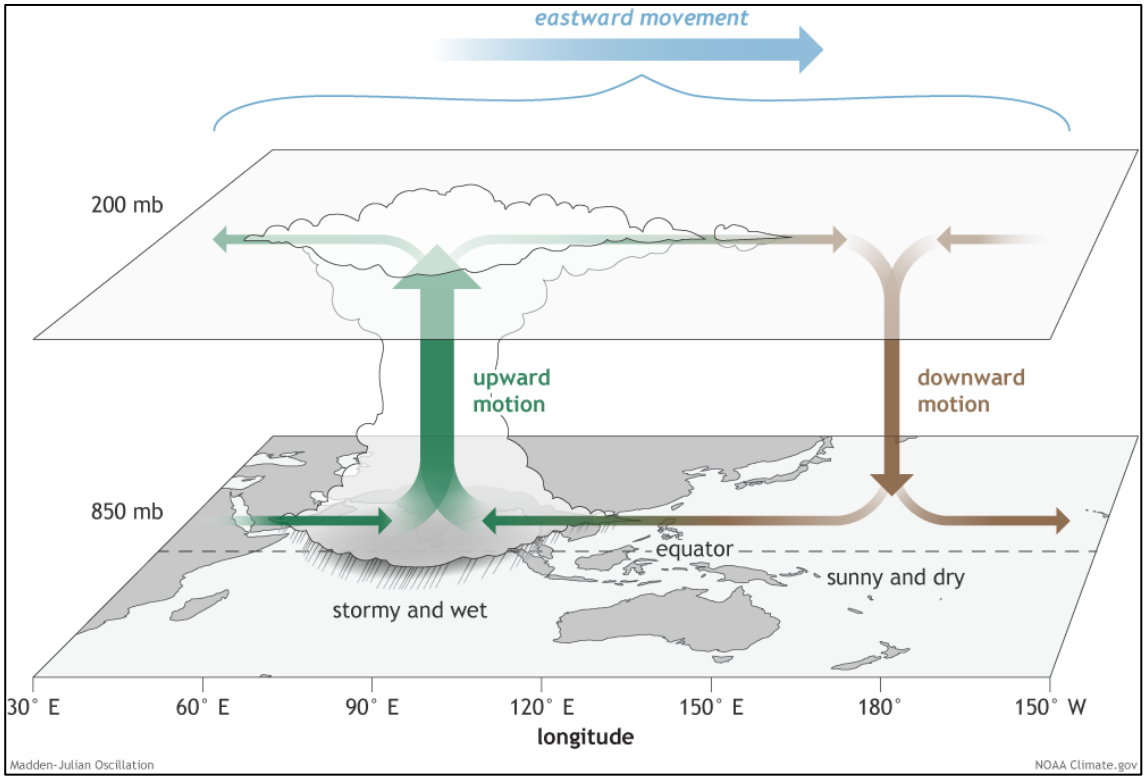

Figure 2. 4 The structure of the MJO for a period when the enhanced convective phase is centered across the Indian Ocean and the suppressed convective phase is centered over the west-central Pacific Ocean Source: (Martin, 2021)

C. Impact of ENSO on Cambodia Rainfall

The ENSO has particular and specific climate effects on the Kingdom of Cambodia, particularly on Cambodian rainfall patterns. These effects are characterized by excessive rain during El Niño events and deficient rain during La Niña. The effects of ENSO, through changes in Cambodian rainfall, have implications for Cambodian farmers. The specific ENSO signal for Cambodian rainfall was defined using a number of large-scale sea surface temperature variabilities in combination with other atmospheric parameters. Rainfall variation was measured through a weighted rainfall station index that helped to identify

ENSO effects on rainfall throughout Cambodia. The seasonal patterns cause a later onset of wet and dry seasons in the north of Cambodia relative to the southern region (Sutton et al., 2019). ENSO's main climate impact in Cambodia is on average rainfall, which declines during El Niño and increases during La Niña. In Cambodia, the warm El Niño phase is generally drier than the cold La Niña phase, particularly between October and May (Figure 2.5).

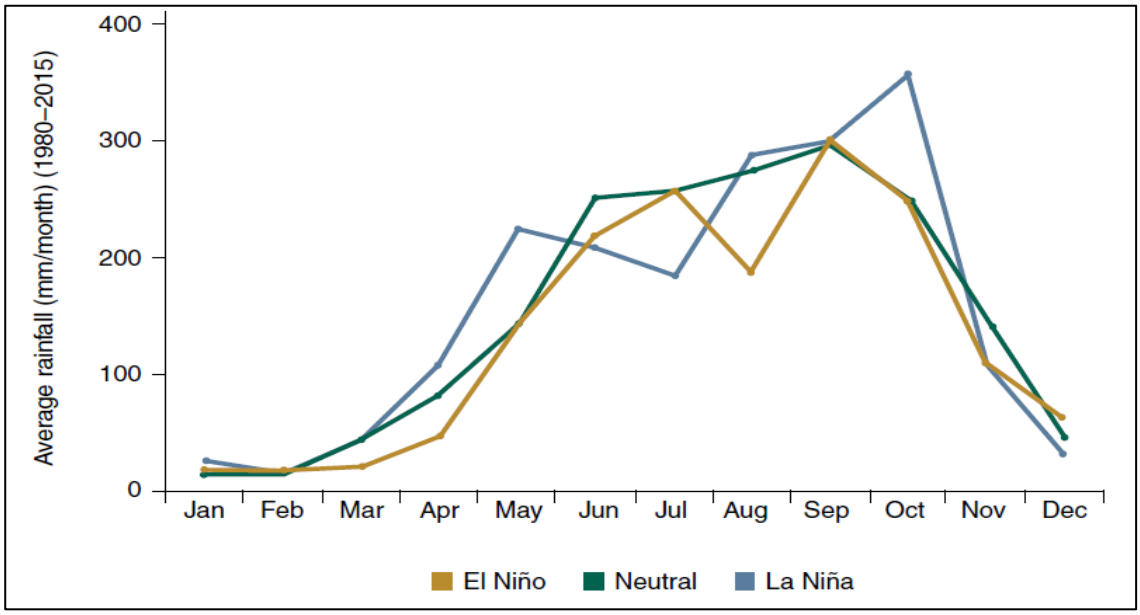

Figure 2. 5 Monthly average of rainfall amount in ENSO Phases During 1980-2015
Source: (Li et al., 2021)

D. Impact of ENSO on Cambodia's Tropical Pattern

El Niño Southern Oscillation (ENSO) influences tropical weather patterns, including storms and monsoons in the Greater Mekong Subregion. Understanding El Niño and its impacts can help countries manage risks associated with climate change by developing community response and action plans. Normally, the Inter-Tropical Convergence Zone (ITCZ) occurs during the onset of the southwest monsoon around the end of March. The region experiences the dry and hot season until the first rain brought by the monsoon in May and June. Thus, El Niño tends to strongly affect the Southeast Asian dry season, lengthening the period of little or no rainfall. However, when La Niña develops, the ITCZ positions itself over Cambodia's southern part, leading to the heavy rains the country experiences from the beginning of the wet season in May and June until the early months of the new year (Abdul Azim Amirudin, et al., 2020). Cambodia is in the process of implementing the climate change and adapation policy, particularly the National Climate Change Strategy and the National Adaptation Plan, it is crucial to understand seasonal activities, including monsoon intensity and length. The synoptic-scale low-pressure trough forming in the north becomes the interface through which surge after surge of cold air travels into equatorial Southeast Asia. It forms the dry season for Indo-China countries, and El Niño tends to extend the period across the season, particularly in central and southern parts of Vietnam. Information about each monsoon's characteristics and activities, as well as the causes of their year-to-year variations, is valuable (Table 3.1). This information is necessary for developing the response scenarios for risk management plans for different sectors, households, and communities. These should be include activities for smallholder dry season rice growth, household water management in dry months, and flood warning systems. Local and national disaster management authorities

will also benefit from more timely information for flood and drought planning (Li et al., 2021).

Table 2.1 El Niño events and droughts in Cambodia, 1982–2016.

Drought event	El Niño event	El Niño strength	Peak Oceanic Niño Index (ONI)	El Niño duration (months)	Impacts
1982–1983	1982–1983	Strong	2.1	15	120,000 ha of crop area damaged
1986–1987	1986–1987	Moderate	1.6	18	N/A
1994	1994–1995	Moderate	1	6	5 million people affected by food and water shortages
1997–1998	1997–1998	Strong	2.3	13	N/A
2002	2002-2003	Moderate	1.2	9	2 million people affected by food and water shortages; $22 million in economic losses
2005	2004-2005	Week	0.7	10	2 million people affected; 62,700 ha of crop damage; $21 million in economic losses
2010	2009-2010	Moderate	1.3	10	12 provinces affected by drought; about 23,000 ha of crop area damaged
2012	No El Niño	N/A	N/A	N/A	11 provinces affected by drought; over 14,000 ha of rice fields damaged of which 3,151 ha were totally damaged
2016	2014-2016	Strong	2.3	18	18 provinces affected by drought; 2.5 million people affected by food and water shortages

Source: (Sutton et al., 2019)

Note: Summarized from Vathana et al, 2013; Leng, 2014; Chhinh, 2015; Miyan, 2015; El Niño information from http://ggweather.com/enso/oni.htm

2.3.5 Cambodia Weather Characteristics

Cambodia's tropical monsoon climate, characterized by high temperatures, includes a rainy season and a dry season, influenced by El Niño Southern Oscillation (ENSO) and La

Niña. Cambodia has a tropical climate with high temperatures and two distinct seasons: the rainy season, driven by the monsoon, lasts from May to October. It brings south-westerly winds ushering in clouds and moisture that account for anywhere between 80–90 percent of the country's annual precipitation. Annual average rainfall is typically 1,400–2,000 mm with higher rates in the coastal and highland areas and lower rates in other inland region (Figure 2.6). The dry season (November–April) brings cooler temperatures, especially between November and January (World Bank, 2021a). Average temperatures are relatively uniform across the country with the highest temperatures occurring in the early summer, just before the start of the rainy season, when highs frequently reach 32°C and remain between 25°C–27°C throughout the rest of the year. The El Niño Southern Oscillation affects the region's monsoon patterns, causing interannual fluctuations in the climate. Southeast Asia often experiences higher and drier winter temperatures during El Nino occurrences, whereas La Niña episodes bring lower temperatures than usual. The observed spatial variation for temperature and precipitation across Cambodia are show in Figure 2.7.

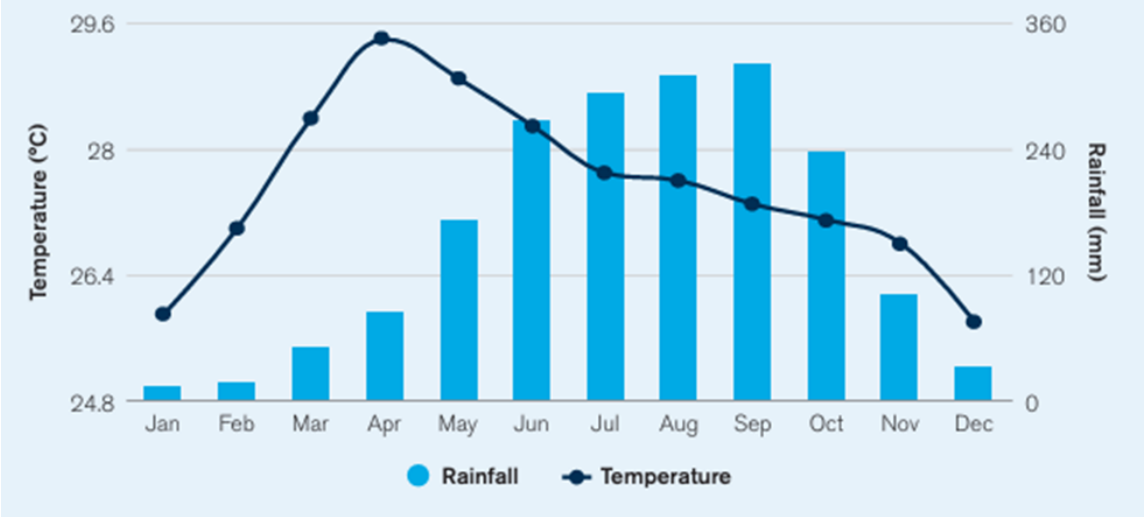

Figure 2. 6 Average monthly temperature and rainfall in Cambodia (1991–2020)
Source: (World Bank, 2021a)

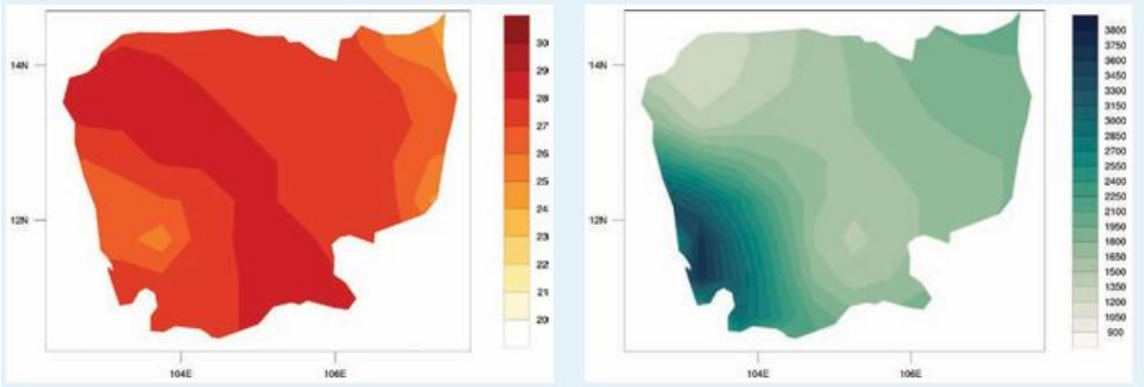

Figure 2. 7 Annual mean temperature (°C) (left), and annual mean rainfall (mm) (right) in Cambodia over the period 1991–2020
Source: (World Bank, 2021a)

2.3.5.1 Temperature

The annual temperature of Cambodia is generally hot, exceeding 32°C, with the mean annual temperature between 25°C to 27°C. Average maximum and minimum

temperature ranges from 30°C to 35°C and a large diurnal range is always observed (Alvar‐Beltrán, 2022). In the low-altitude basin, the mean annual temperature is over 27°C. The highest temperature may occasionally soar up to 41°C. The provinces in the northeastern and central areas are relatively hotter than the coastal area. In the upland, it is cooler. In general, temperatures in Cambodia vary from 26°C to 38°C between the wet and dry or hot seasons. March, April, and May are generally the hottest months of the year, whereas December, January, and February are the cooler months (Fujihara et al., 2021) .

The climate of Cambodia is additionally affected by the local geography of the country, such as the Cardamom Mountains, Tonle Sap Lake, and flowing rivers, resulting in the formation of distinct microclimates. The northwestern monsoon delivers a significant portion of the annual rainfall during the rainy season. The southeastern monsoon begins after a short transitional period of two months from dry to wet, which is not as obvious as the change from wet to dry. The months may be completely dry, and this dry period is potentially applicable for the use of both the rainfed lowland and the upland. It forms the requirement not to interfere with the annual seasonal activities.

2.3.5.2 Humidity

Cambodia's principal humid areas are the Siem Reap-Angkor area, the eastern and central parts of the country, the upper part of the western plain, and the lower part of the Mekong Delta. As a part of the diversity in climate across the country, Cambodia also experiences a wide range of humidity (Lin et al., 2023). The humidity is also higher in a forest than in agricultural areas in the same area because of the canopy of trees, which prevents evaporation of water by the sun. However, at about 10:00 AM, the humidity is lower in the forest than in agricultural areas because the plant leaves in the forest have absorbed water from the atmosphere better due to the higher sunlight compared to the crop field. As can be expected, for geographical impact, humidity is higher in lower elevation regions compared with those at higher elevations. It is also noted that the humidity in the western region is higher than in the eastern region of the country and is in the range of 80 percent, particularly in the wet season. The central region has humidity levels from 75—80 percent in the morning, which is near the boundary of the low and high humidity regions. The northeastern region is usually the least humid and, in the dry season, is very low, at 60–65 percent in the morning and 55–60 percent in the afternoon (Cox et al., 2020). In the wet season, during the months of May through October, the hot and wet air brings humidity levels of over 90 percent to the country. Humidity affects human activities, particularly for agricultural workers who work outside during the day, and also affects tourist activities, a main source of income. Then, as the wet season ends, November through April brings the dry season, with humidity levels around 50 percent.

2.3.5.3 Cloudiness

Cloudiness, commonly referred to as cloud cover, is the quantity of clouds in the sky. Typically, it is expressed as a percentage or fraction of the sky covered by clouds. An overcast day has almost all the clouds present, whereas a clear day has little to none. The average percentage of cloud cover ranges from 40 percent to 60 percent, with up to 200 days experiencing overcast conditions. Overall cloudiness in Cambodia largely depends on geographical location and the behavior of moisture flow. Also, in some parts, cloud generation times vary strongly and exert a local influence (Soulard et al., 2020).

In general, clouds consist of four main types: high clouds, medium clouds, low clouds, and fog. The wet season in Cambodia can be characterized by less cloud cover, with a prevalence of cloud-free conditions, low clouds, and fog. However, in the dry season, the number of medium clouds, high clouds, and total cloud cover is much lower than in the wet season. The temperature and the amount of sunlight that reaches the ground can both be impacted by cloudiness. The sunniest places are those with the least amount of cloud cover, and the cloudiest places have the least amount of sunlight. Sunlight can be blocked by clouds, particularly around sunrise and sunset.

Cambodia's monsoon seasons, which are marked by alternating winds and precipitation, have an impact on cloudiness. The southwest monsoon, from the middle of May until the beginning of October, brings powerful winds from the southwest, with high humidity and a lot of rain. The northeast monsoon, which lasts from early November to mid-March, is characterized by varying cloud cover and reduced humidity due to lighter and drier winds from the northeast. Thus, each region may experience different types of clouds or local weather patterns (Dadashazar et al., 2021).

2.3.5.4 Atmospheric Pressure

Atmospheric pressure or barometric pressure plays an important role in the weather patterns of any particular location. In Cambodia, low pressure causes the wet season's rain and high pressure produces the dry season. When the atmospheric pressure decreases relative to the surrounding area, the air rises and eventually cools. During the cooling process, a certain amount of water vapor in the rising air can condense into water droplets, and clouds are formed (Abhishek et al., 2021; Huang et al., 2024). This process can also produce vertical air movement and make the air currents accelerate and become convective (Smirnov, 2020).

At the Earth’s surface, air pressure may be either high or low. High pressure refers to an area where the atmospheric pressure is higher than the surrounding areas, and the air slowly descends (O’Rourke, et al., 2023). Generally, high pressure leads to subsidence, temperature increase, and the reduction of relative humidity (López et al., 2021). Furthermore, the air’s moisture drops to the surface in the form of dew and fog to create a clear sky. Conversely, low pressure occurs where the pressure drops significantly relative to the surrounding areas and is characterized by rising air currents that move towards low-pressure regions with a higher risk of producing storm or tempest activity (Sheposh, 2024). For example, whenever tropical cyclones approach the coast of Cambodia, low atmospheric pressure can lead to a rapid rise in surface water or flooding.

2.3.6 Cambodia Seasonal Characteristics

Cambodia has distinct wet and dry seasons. According to the Cambodian Climate Change Strategic Plan, the seasonal properties currently include the wet season—roughly May to November, with 80 percent of all rainfall, high fields flooded, increased pollutants in rivers, and non-harvest season; and the dry season—roughly December to April, with only 20 percent of all rainfall, agriculture dependent on irrigation, vulnerable in drought years, temperatures rise, and less water for everyday life and activities. Unfortunately, the changing wet/dry season pattern has proven to be the biggest challenge for the country. If seasonal characteristics change, it can threaten food security and human livelihoods across the globe, especially in developing and resource-strained countries like Cambodia.

Cambodia has one of the most unique wet and dry seasonal characteristics. Between mid-May and early October, Cambodia experiences its wet season, governed by the southwest monsoon winds. Heavy rains and humid conditions result from the strong prevailing winds carrying moisture-laden airflow along the same path (MoE, 2024). As a result, this time of year sees the heaviest rainfall, with the most severe flooding conditions impacting those living along the Tonle Sap system and Mekong River side. The vast rivers, wetlands, and lower traversable plains are flooded for months as the Tonle Sap River naturally reverses direction during the rainy season. With the northern plains as the water drainage outlet, Cambodia receives, on average, nearly 80 percent of its total annual rainfall. This water plays a large role in irrigation for the country's agriculture and helps maintain the water table and ecosystems of the vast wetlands.

The transition from the southwest monsoon to the drier northeast monsoon usually occurs in late October, marking the start of the nation's cool or dry season, which lasts from early November to mid-April. Most of the country receives little to no rain during these months, with an average of less than 3 percent of total annual rainfall. The last month of the rainy season still experiences some residual flooding due to the formidable current of the Mekong River, while Cambodia's vast wetlands act as natural retention lakes. The dry season typically begins with the arrival of cool weather in early November, when temperatures drop to around 14-16 ^{o}C in the central highlands from November to mid-March. The shift in winds from southwest to northeast also brings drier air and high pressure into the region, along with relatively clear skies. As a result, there is a large diurnal temperature variation, with high temperatures reaching around 33-36 ^{o}C . During March and April, temperatures gradually increase as Cambodia transitions into the pre-monsoon season, characterized by pattering thunderstorms in the early parts of May.

Cambodia, home to millions of people and diverse ecosystems, is experiencing both climate change causes (such as rising carbon dioxide concentrations in the atmosphere, deforestation, and fossil fuel use) and characteristics (such as rising sea levels, shortening of wet seasons, droughts, and increased frequency of extreme events). Even the slightest rise in temperature and change in precipitation can turn into disasters because Cambodia is already borderline in climate and access to resources (Suddhiyam et al., 2013).

2.3.6.1 Precipitation

Precipitation is defined as the form of rain, snow, mist, or dew that falls from the sky. Climate change can alter precipitation amount, distribution (spatially and temporally), frequency, and intensity. Temperature changes can alter mechanism precipitation development depends on, indirectly altering precipitation amounts. Climate change include changing precipitation patterns, impacting not only the total amount of rainfall but also its distribution throughout the year, which changes the seasonality of precipitation. This means that some areas might experience more intense rainfall during shorter periods, leading to potential flooding, while others could experience prolonged droughts.

Changes in precipitation patterns have been observed globally in the last decades, including Cambodia, and projected through global climate models (GCMs) (Suddhiyam et al., 2013). Global climate models project a general southward movement of the East Asian monsoon, affecting regions characterized by monsoon, including Cambodia. In addition, the increased variability of precipitation as expressed on the inter-annual timescale has also been reported (Attavanich, 2011). In Cambodia, the effect of climate change on precipitation is manifested by a shift in a mega hydro-meteorological regime.

The consequences of climate change for precipitation are yet unclear, but trends discussed in Chapter 3 seem to indicate increasing variability. Over the 50 years of 1971–2020, Cambodia experienced seasonally varied and significant decreases in precipitation per decade across its central and eastern provinces but significant increases per decade across some western provinces (Figure 2.8). Average annual rainfall could be as low as 1,400 mm in the central lowlands and as high as 4,000 mm near the Cardamom Mountains and nearby coastal areas in the southwest. The country's eastern plains receive approximately 2,000 to 2,600 mm of rainfall annually and may exceed those amounts in the mountainous areas in the northeast (USAID, 2019). While rainfall was observed to increase in some areas since the 1960s, no statistically significant changes were detected over the 20th century, either in terms of annual rainfall or extreme events. However, precipitation variability is linked to the ENSO, with years of strong El Niño correlated with years of moderate and severe drought over the 20th century (ADB, 2021; World Bank, 2021b).

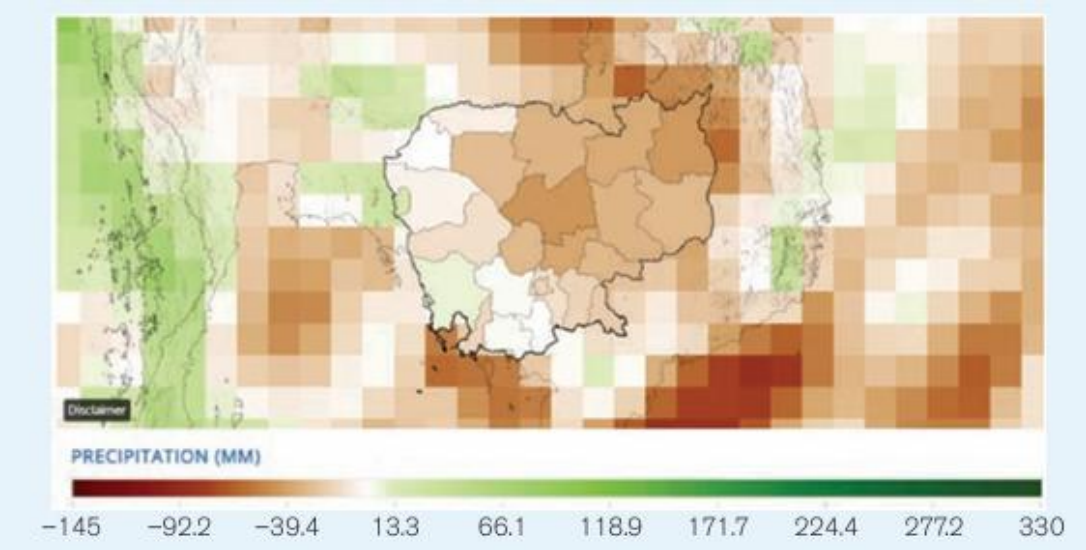

Figure 2. 8 Observed precipitation trend per decade (1971–2020) annually
Source: (World Bank, 2024)
Noted: significant decreases in most of the countries except in parts of the western and southern provinces

2.3.6.2 Monsoons

The Asian Summer Monsoon is a complex process of seasonal change and is one of the most prominent and important climate systems in the world. It influences the weather systems across two continents and drives water and energy exchanges between land and atmosphere over different time scales. The energy exchange results in the reversal of prevailing winds, which transports moisture from the ocean to the continent and induces a consistent pressure system and circulation pattern (Limsakul, 2010).

Cambodia is characterized by a tropical monsoon climate, resulting in two main seasons: the wet season (monsoon) and the dry season. The monsoon winds, which establish these distinct seasons, control Cambodia's climate. The southwest monsoon's powerful prevailing winds bring high humidity and significant rainfall from mid-May to early October. In contrast, the northeast monsoon's lighter and drier winds provide variable cloudiness, less precipitation, and reduced humidity from early November to mid-March. Transitional weather occurs between these seasons. Year-round high temperatures range from approximately 28 °C in January, the coldest month, to around 35 °C in April, with

occasional peaks of 38 °C to 40 °C. The country's annual precipitation varies significantly across regions, from 1,270 to 1,400 mm in the central lowland region to over 5,000 mm on the seaward slopes of the southwestern highlands. Approximately three-fourths of the annual rainfall occurs during the southwest monsoon months (World Atlas, 2025).

2.3.6.3 Wind Patterns

Prevailing wind patterns in Cambodia vary seasonally, including the northeast monsoon, which brings dry, cool air from November to March, and the southwest monsoon, which brings warm, wet conditions from May to October. The annual change in seasons is associated with the shifting of the Intertropical Convergence Zone (ITCZ) between the northern and southern tropics (Ratanak & Dong, 2018). Climate change may also affect wind patterns. Changes in wind patterns can significantly affect weather, agriculture, and ecosystems.

The northeast wind occurs from November to the following April and causes dry weather across the country due to the northeast trade system. This wind first blows over Cambodia in November and lasts until the end of the following April. In the dry season, winds are generally weak and variable, with low rainfall and high sunshine, resulting in decreased humidity. During this time, the country experiences a variety of weather patterns controlled by the northeast monsoon system.

The southwest wind occurs from May to October and induces a wet and rainy season across the country due to the southwest monsoon system. The wet season is characterized by the prevailing southwesterly winds, bringing humidity, cloudiness, and rains to Cambodia. The southwesterly monsoon system commences in May and lasts until October. During this period, wind speeds are generally strong. The greatest wind speeds occur at the beginning of the southwest monsoon, and the monthly average wind speeds are higher than those of the northeast trade system.

2.4 Historical Changes in Cambodia Climate

2.4.1 Changes in Temperature

2.4.1.1 Trends and Changes in Temperature

The temperature data presented are historical, running from 1950 to 2023, and derived from ERA5 (ECMWF Reanalysis v5) dataset from the European Centre for Medium-Range Weather Forecasts (ECMWF) (Hersbach, et al., 2023). The long-term mean of the model was removed to obtain the anomalous field (by dividing the data by the daily long-term mean). The anomalous field of the bias-corrected model data was then interpolated to a fine scale that matches that of the observation. The interpolated anomalous field was subsequently scaled by the long-term mean of the observation to align the model's spatial feature with the spatial pattern of the observation. The observed data was obtained from the Ministry of Water Resources and Meteorology (MOWRAM) from 1990-2023.

Utilizing ERA-5 temperature data, the warming situation in Cambodia was evaluated. The dataset covers around 80 years, from 1940 to 2022. The first 30 years of data (1940–1969) were used as the baseline or reference period for calculating the warming level, while the last 20 years (2003–2022) were selected to represent the current climate in Cambodia. The degree of warming in Cambodia can be determined by adjusting these time parameters.

The warming level based on the ERA5 dataset is shown in Figure 2.1 using the previously described calculation method. The average temperature increase in Cambodia is 1.42°C when considering the entire country. The map shows that Kampong Speu, Kampong Chhnang, Kampong Thom, Kampong Cham, Tboung Khmum, Kratie, Mondulkiri, Ratanakiri, Stung Treng, Pursat, Battambang, and Banteay Meanchey have the warmest temperatures, which range from 1.40 to 1.60 °C. The coastal regions get the least amount of warming, which is between 0.80 and 1.10 °C. This indicates that Cambodia's temperature is 1.23 °C warmer than the global average.

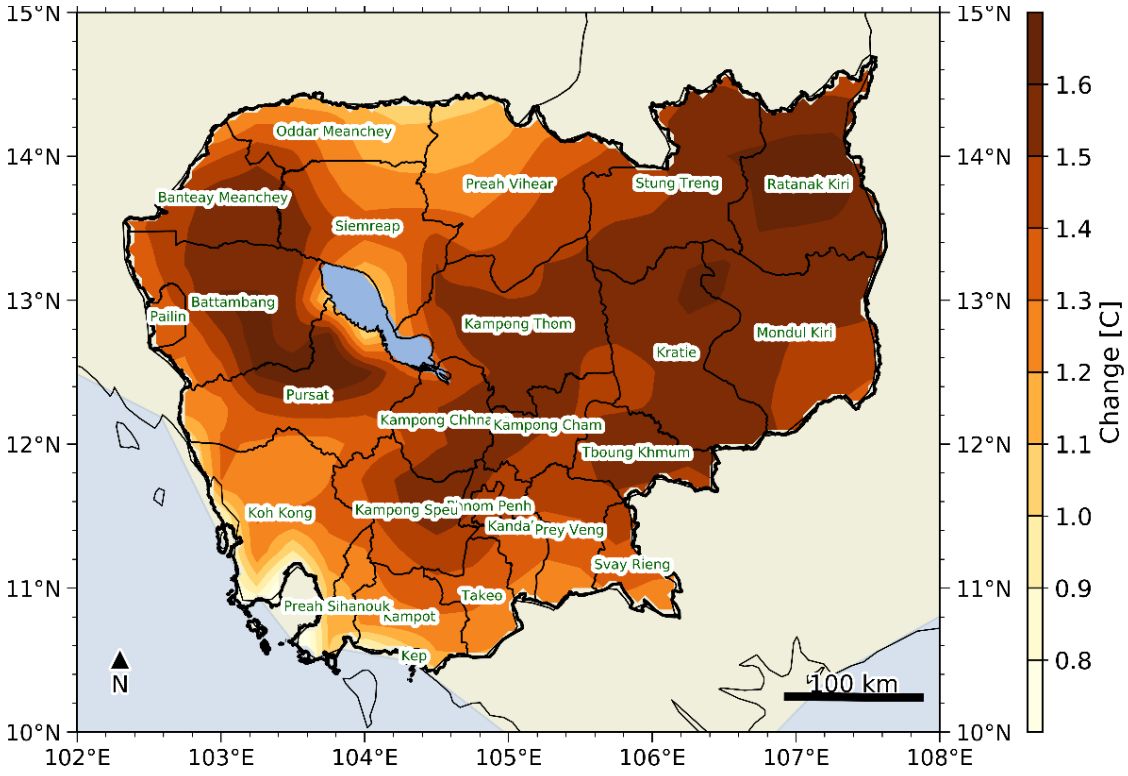

Figure 2.1: Average Spatial Annual Mean Temperature Trends Nationally per Decade. Warming Status in Cambodia: A Comparative Analysis using ERA5 Data. The reference climate period is 1940-1969, while the current climate status is analyzed for the period 2003-2022.

2.4.1.2 Extreme Daily Temperature Indices

Climate change has significantly altered temperature patterns globally, with noticeable shifts in the frequency and intensity of extreme temperature events. The IPCC's Sixth Assessment Report (2021) highlights that anthropogenic activities have been the primary drivers of these changes, leading to an increase in the occurrences of hot days, warm nights, cool days, and cold nights. These indices are critical for assessing the impacts of climate change on various sectors, including agriculture, health, and infrastructure.

Extreme daily temperature indices are metrics used to measure deviations in temperature patterns from historical norms. The key indices under review include:

- Maximum temperature (TXx): The annual value of daily maximum temperature.
- Minimum temperature (TXn): The annual minimum value of daily minimum of temperature.
- Hot Days (TX90p): Days where the daily maximum temperature exceeds the 90th percentile of a reference period.
- Warm Nights (TN90p): Nights where the daily minimum temperature exceeds the 90th percentile of a reference period.

- Cool Days (TX10p): Days where the daily maximum temperature falls below the 10th percentile of a reference period.
- Cold Nights (TN10p): Nights where the daily minimum temperature falls below the 10th percentile of a reference period.

Table 3.2 provides descriptions of the four temperature indices that were chosen. To create a distribution of the daily maximum temperatures, all of the wintertime daily maximum temperature data from 1990 to 2023 are used. The detailed calculation and formula have been included in Annex A1: Method for calculating the temperature indices and detecting change in temperature and Annex A2: Method for detecting the trend of annual rainfall and magnitude of the trend.

Table 2.2: Definitions of the temperature indices used in this study

Variable	Indicator Name	Definition	Unit
Tmax	Hot Days	No. of days with the daily maximum temperature exceeding the 90th (95th) percentile	Day
	Cool Days	No. of days with the daily maximum temperature below the 10th (5th) percentile	Day
Tmin	Warm Nights	No. of nights with the daily minimum temperature exceeding the 90th (95th) percentile	Day
	Cold Nights	No. of nights with the daily minimum temperature below the 10th (5th) percentile	Day

Overall trends indicate increased temperature variability. In the western highlands and coastal plain, provinces like Kampong Speu, Pursat, and Kep have experienced decreases in maximum temperatures, with Kampong Speu showing the largest drop at -0.25°C per decade (Table 3.2 and Figure 2.2). In contrast, Kampot has seen an increase of 0.06°C per decade. Minimum temperatures in this region are consistently decreasing, with Battambang (-0.42°C/decade) and Kep (-0.43°C/decade) showing significant declines.

In the central Cambodia plains, maximum temperatures are also decreasing, particularly in provinces as such Kampong Thom (-0.30°C/decade), while Kandal and Svay Rieng are experiencing slight increases of 0.02°C and 0.06°C per decade, respectively. Minimum temperatures are mostly falling, with Banteay Meanchey (-0.48°C/decade) and Oddar Meanchey (-0.59°C/decade) having the largest decreases. Kampong Thom, however, shows a slight increase in minimum temperatures (+0.07°C/decade).

In the eastern highlands and plains, the decrease in maximum temperatures is even more pronounced, especially in provinces as such Mondulkiri (-0.40°C/decade). Minimum temperatures in the region are also dropping, with Preah Vihear showing the largest decrease (-0.77°C/decade). However, Kratie shows a slight increase in minimum temperatures (+0.07°C/decade), contrasting with the overall cooling trend.

Most provinces are experiencing decreases in both maximum and minimum temperatures, particularly in the highlands and plains. Some urbanized areas like Kampot, Kandal, and Svay Rieng are seeing slight increases, likely due to factors such as urbanization.

Table 2.3: Trends in temperature changes across various provinces and areas in Cambodia

Provinces and area	Maximum Temperature (TXx) (°C/decade)	Minimum Temperature (TXn) (°C/decade)
Western Highlands and Coastal Plain		
Pailin	0	▼ -0.34
Battambang	0	▼ -0.42
Pursat	▼ -0.08	▼ -0.32
Koh Kong	0	▼ -0.20
Kampong Speu	▼ -0.25	▼ -0.22
Preah Sihanouk	0	▼ -0.36
Kampot	▲ 0.06	▼ -0.26
Kep	▼ -0.14	▼ -0.43
Central Cambodia Plains		
Banteay Meanchey	▼ -0.14	▼ -0.51
Oddar Meanchey	▼ -0.09	▼ -0.61
Siem Reap	0	▼ -0.21
Kampong Chhnang	0	▼ -0.41
Kampong Thom	▼ -0.30	▲ 0.11
Kampong Cham	0	▼ -0.21
Kandal	▲ 0.02	▼ -0.21
Phnom Penh	▼ -0.11	▲ 0.01
Takeo	▼ -0.22	▼ -0.41
Prey Veng	0	▼ -0.31
Svay Rieng	▲ 0.06	▼ -0.31
Tboung Khmum	▼ -0.14	▼ -0.21
Eastern Highlands and Plains		
Preah Vihear	▼ -0.12	▼-0.77
Stung Treng	0	▼-0.60
Ratanakiri	0	▼-0.53
Mondulkiri	▼ -0.40	▼-0.26
Kratie	0	▲ 0.07

Note: It is divided into two main parameters: Maximum Temperature (TXx) and Minimum Temperature (TNx). Each parameter displays the magnitude of temperature change in degrees Celsius (°C per decade) with directional indicators. Red arrows pointing down indicate a decrease in temperature, while green arrows pointing up represent an increase.

In the western highlands and coastal plain, most provinces show minimal changes in extreme temperatures (Table 2.3 and Figure 2.2). Notably, Koh Kong shows an increase in hot day maximum (+0.15 days/decade) and a decrease in warm night maximum (-0.25 days/decade), indicating more frequent hot days and fewer warm nights. Kampong Speu province exhibits a decline in both hot day maximum (-0.07 days/decade) and cold day minimum (-1.00 days/decade). Kep experiences an increase in cold nights (+0.71 days/decade), while Battambang shows a decrease (-0.67 days/decade).

In the central Cambodia plains, varied temperature trends are observed. Banteay Meanchey province has declines in both hot day maximum (-0.06 days/decade) and warm night maximum (-0.14 days/decade), as well as decreases in cold day minimum (-0.56 days/decade) and cold night minimum (-0.46 days/decade). Oddar Meanchey exhibits a decrease in hot day maximum (-0.25 days/decade) but an increase in warm night maximum (+0.13 days/decade) and cold night minimum (+0.77 days/decade). Kampong

Thom shows a decline in hot day maximum (-0.16 days/decade) and a reduction in cold days (-0.91 days/decade). Phnom Penh has an upward trend in a maximum of warm nights (+0.08 days/decade). Interestingly, Takeo displays mixed trends, with a decrease in hot day maximum (-0.04 days/decade) but increases in warm night maximum (+0.04 days/decade), cold day minimum (+1.50 days/decade), and cold night minimum (+2.22 days/decade).

In the eastern highlands and plains, Stung Treng and Kratie both show decreasing trends in hot day maximum (-0.17 days/decade). Kratie also shows significant decreases in both cold day minimum (-1.15 days/decade) and cold night minimum (-2.27 days/decade). Preah Vihear, on the other hand, shows a minor increase in cold night minimum (+0.50 days/decade).

Table 2.4: Temperature trends in different regions of Cambodia,

Provinces and area	Hot day maximum (TX90p)	Warm night maximum (TN90p)	Cold day minimum (TX10p)	Cold night minimum (TN10p)
	(day)	(day)	(day/decade)	(day)
Western Highlands and Coastal Plain				
Pailin	0	0	0	0
Battambang	0	0	0	▼ -0.67
Pursat	▲ 0.01	0	0	0
Koh Kong	▲ 0.21	▼ -0.25	0	0
Kampong Speu	▼-0.07	▼ -0.03	▼ -1.00	0
Preah Sihanouk	0	▼ -0.25	0	0
Kampot	0	▲ 0.01	0	0
Kep	0	▼ -0.06	0	▲ 0.71
Central Cambodia Plains				
Banteay Meanchey	▼ -0.06	▼ -0.14	▼ -0.56	▼ -0.45
Oddar Meanchey	▼ -0.25	▲ 0.11	▼ -0.71	▲ 0.81
Siem Reap	0	0	0	0
Kampong Chhnang	▼ -0.07	▼ -0.11	0	▼ -0.83
Kampong Thom	▼ -0.16	0	▼ -0.91	0
Kampong Cham	0	▼ -0.12	0	0
Kandal	0	0	▲ 1.61	0
Phnom Penh	0	▲ 0.11	0	0
Takeo	▼ -0.04	▲ 0.01	▲ 1.51	▲ 2.21
Prey Veng	0	0	0	0
Svay Rieng	▼ -0.14	0	0	▼ -0.59
Tboung Khmum	0	0	0	▼ -0.71
Eastern Highlands and Plains				
Preah Vihear	0	0	0	▲0.51
Stung Treng	▼ -0.17	0	0	0
Ratanakiri	0	0	0	0
Mondulkiri	0	0	0	0
Kratie	▼ -0.17	▼ -0.26	▼ -1.15	▼ -2.27

Note: Focusing on the following indicators: Hot Day Maximum (TX90p), Warm Night Maximum (TN90p), Cold Day Minimum (TX10p), and Cold Night Minimum (TN10p). Red arrows signify decreases, while green arrows indicate increases. The number after arrow refers to the magnitude of change as day per decade

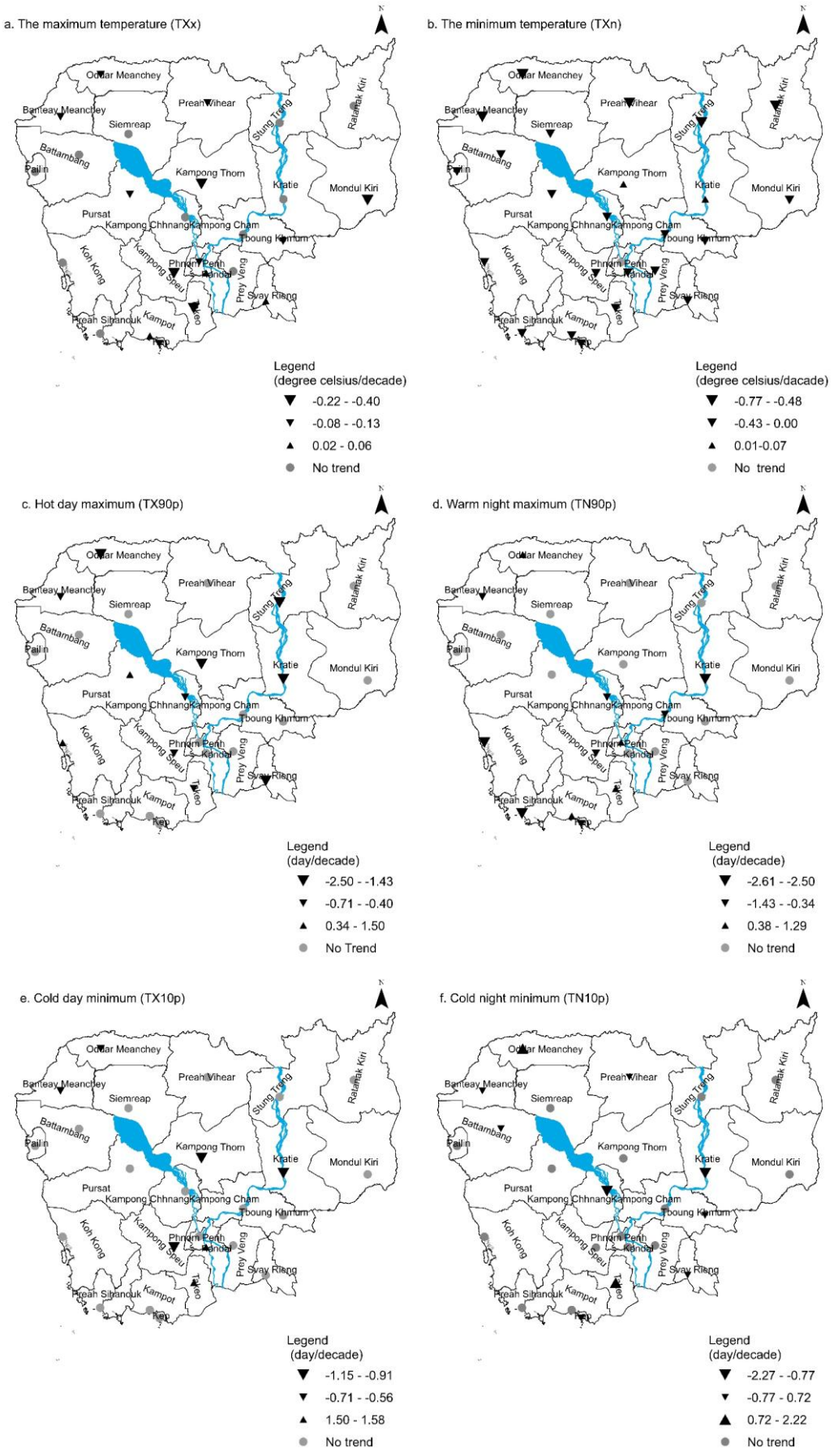

Figure 2.2: Spatial temperature trends in different regions of Cambodia per decade for annual, focusing on the following indicators: (a). maximum, (b). annual minimum, (c). hot day maximum, (d). warm night maximum, (e). cold day minimum, and (f). cold night minimum.

2.4.2 Changes in Precipitation Patterns

2.4.2.1 Trends and Changes in Rainfall

From 1979 to 2023, Cambodia experienced substantial variability in decadal rainfall trends across its diverse geographical regions, as shown in the current analysis (Figure 2.3). To detect the trends and magnitudes of rainfall, the study utilized historical climate rainfall data from MOWRAM and ERA5 reanalysis data (Hersbach, et al., 2023), incorporating bias corrections for observed data. The detailed calculations and formulas have been included in Annex A1: Method for calculating the temperature indices and detecting change in temperature and Annex A2: Method for detecting the trend of annual rainfall and magnitude of the trend. This period marked significant increases in rainfall in the western highlands and coastal plain, while mixed trends were observed in the central Cambodia plains, and decreases were recorded in the eastern highlands and plains.

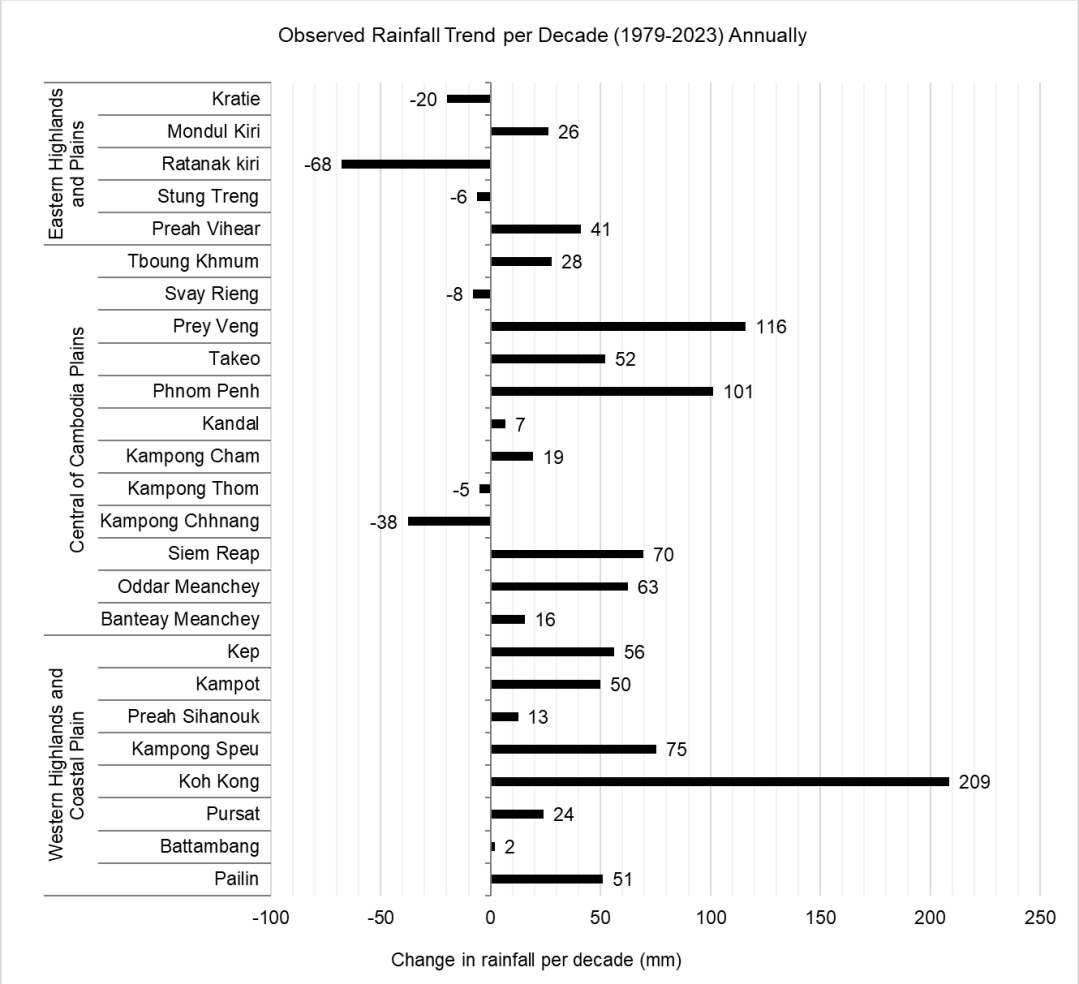

Figure 2.3: Observed rainfall trend per decade (1979-2023) annually across various province and Cambodian regions. This bar chart represents the magnitude of rainfall changes per decade, highlighting the variability in decadal from 1979 to 2023.

In the western highlands and coastal plain, Koh Kong province observed the most significant increase in rainfall per decade (+209 mm/decade), followed by Kampong Speu (+75 mm/decade). Other significant increases in the central Cambodia plains included Prey Veng (+116 mm/decade), Phnom Penh (+101 mm/decade), Siem Reap (+70 mm/decade), Oddar Meanchey (+63 mm/decade), and Takeo (+52 mm/decade). In contrast, the eastern highlands and plains showed mixed trends; Ratanakiri experienced

a decrease per decade (−68 mm/decade), whereas MondulKiri recorded an increase (+26 mm/decade).

2.4.2.2 Extreme Rainfall Indices

Extreme rainfall indices, i.e., Maximum 1-day precipitation (RX1day), Number of days with precipitation larger than 50 mm (R50mm), Number of days with precipitation larger than 100 mm (R100mm), Consecutive dry days (CDD), and consecutive wet days (CWD) (Table 2.4)- are used to analyze the magnitude, frequency and extreme of rainfall events. Precipitation data from 25 stations across Cambodia between 1990 and 2023 was analyzed using the Mann-Kendall Test and Sen's Slope. The detailed calculation and formula have been included in Annex A3: Method for calculating extreme rainfall indices.

Table 2.5: Definitions of extreme rainfall indices used in this study

Index	Index name	Definition	Unit
RX1day	Maximum 1-day precipitation	Annual maximum 1-day precipitation	mm
R50mm	Number of days with precipitation higher than 50 mm	Annual count of days when daily precipitation ≥ 50 mm	day
R100mm	Number of days with precipitation higher than 100 mm	Annual count of days when daily precipitation ≥ 100 mm	day
CDD	Consecutive dry days	Number of consecutive dry days	day
CWD	Consecutive wet days	Number of consecutive wet days	day

Between 1990 and 2023, Cambodia experienced a general trend of increasing maximum daily precipitation, more days with very heavy precipitation, shorter dry spells, and longer wet spells. In the western highlands and coastal plains, there is a mixed trend in maximum 1-day precipitation (Figure 2.4). Some provinces like, Koh Kong, Kep, and Kampong Speu, saw a large increase of more than 8 mm/decade, whereas areas along the coast, such as Kampot and Preah Sihanouk, experienced a decrease. The central plains show a slight trend toward both decreasing and increasing precipitation, with a notable decrease of more than 4 mm/decade in Kampong Chhnang. In the eastern highlands and plains, there is a general trend of increasing precipitation, especially in the northeastern provinces like Ratanakiri and Preah Vihear. Stung Treng is an exception, showing a decreasing trend.

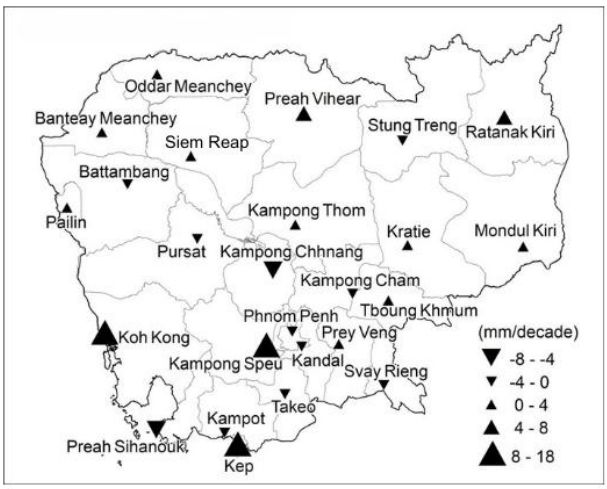

Figure 2.4: Change trend (day per decade) of at the station of each province in Cambodia between 1990 and 2023. Normal triangles indicate an increasing trend of Maximum 1-day Precipitation, while upside-down triangles indicate a decreasing trend. The size of each triangle indicates the magnitude of an increasing or a decreasing trend. Grey circles indicate no trend.

Only coastal provinces like Koh Kong, Preah Sihanouk, and Kampong Speu in the western highlands and coastal plains show an increase in the number of days with precipitation greater than 50 mm (Figure 2.5a). In contrast, the other provinces did not experience major change in trends. The central plains show no change in precipitation trend except in Kampong Chhnang, Prey Veng, and Oddar Meanchey. There is only a notable increase in Mondulkiri and Preah Vihear in the eastern highlands and plains. Most regions show no significant trend in days with precipitation greater than 100 mm over the past three decades (Figure 2.5b). However, Koh Kong stands out in the coastal plain with a marked increase in day with precipitation greater than 100 mm.

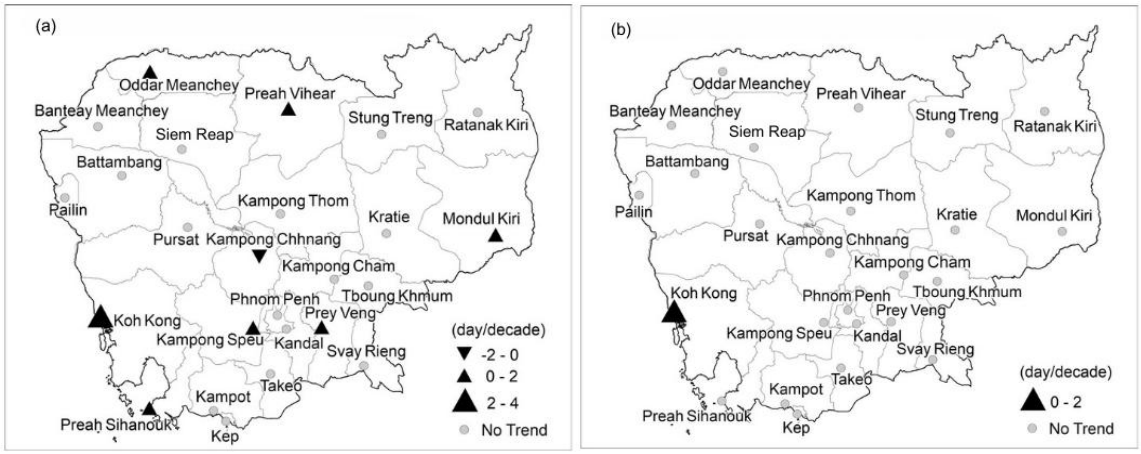

Figure 2.5: Change trend (day per decade) of (a) Number of days with precipitation larger than 50 mm and (b) Number of days with precipitation larger than 100 mm at the station of each province in Cambodia between 1990 and 2023. Normal triangles indicate an increasing trend of Maximum 1-day Precipitation, while upside-down triangles indicate a decreasing trend. The size of each triangle indicates the magnitude of an increasing or a decreasing trend. Grey circles indicate no trend.

Except for Kratie, all provinces show a decreasing trend in consecutive dry days. The central plains experienced a significant decrease of more than 8 days/decade (Figure 2.6a). In the western highlands and coastal plains, there is a notable increase in consecutive wet days, particularly in Koh Kong, Preah Sihanouk, and Kep (Figure 2.6b). In the central plains, only Takeo experienced a significantly increasing trend, whereas the same trend occurred in Mondulkiri in the eastern highlands and plains. In general, rainfall

in Cambodia has become more variable, with decreases in rainfall in the central and eastern regions and increases in western regions.

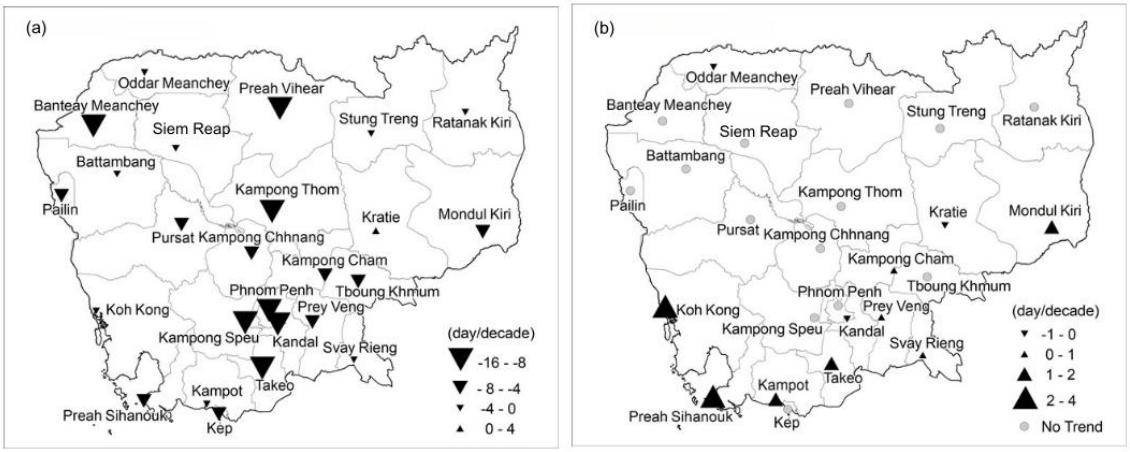

Figure 2.6: Change trend (day per decade) of (a) Number of consecutive dry days and (b) Number of consecutive wet days at the station of each province in Cambodia between 1990 and 2023. Normal triangles indicate an increasing trend of Maximum 1-day Precipitation, while upside-down triangles indicate a decreasing trend. The size of each triangle indicates the magnitude of an increasing or a decreasing trend. Grey circles indicate no trend.

2.4.3 Climate Extremes

Cambodia, like much of Southeast Asia, is recognized as a disaster-prone area due to its heightened exposure to extreme weather events (Lee, Kim, & Choi, 2019). Cambodia is highly vulnerable to climate-related hazards, including river floods, droughts, extreme heat, wildfires, and sea level rise (European Commission, 2023). From 1987 to 2007, major floods and droughts significantly impacted Cambodia's provinces and are expected to become more frequent in the future (Ministry of Environment, 2022). Without proper risk planning, flooding by midcentury could cause billions of dollars in damage, increasing the risks of landslides and other hazards (World Bank, 2023). Provinces with productive agricultural activities face the greatest climate hazard risks from droughts, which have affected millions and challenge water resource management (Word Bank, 2024). Additionally, extreme heat, wildfires, and sea level rise pose threats to biodiversity and human health.

2.4.3.1 Floods and Drought

Cambodia experiences a complex hydrological cycle characterized by distinct wet and dry seasons, with associated risks of floods and droughts that significantly impact communities, infrastructure, and the economy. The country is highly vulnerable to flooding, particularly in the Mekong River Basin and the Tonle Sap Basin. Floods are most common during the monsoon season, which runs from May to October, while droughts are most common during the dry season, which runs from November to April.

Figure 2.7 presents the Standardized Precipitation Index (SPI) for Cambodia based on precipitation data from the 25 stations between 1990 and 2023. Data was measured across three timescales: 3-month, 6-month, and 12-month, ending in June, August, and November. According to average rainfall patterns, the wet season typically begins around June, reaches its driest point in August, and finishes in November. These specific months also align with the timings of early, mid-season, and late seasonal droughts documented in the literature (Chhinh & Millington, 2015). The selection of June, August, and November aims to capture critical points within Cambodia's distinct seasonal and

agricultural calendar. June reflects conditions during the crucial early wet season, vital for rice planting and establishment. August provides insight into moisture availability midway through the main growing season, while November represents the cumulative annual rainfall picture near harvest time, indicating overall water resource status heading into the dry season. For the 3-month SPI, all three months show significant fluctuations, with frequent swings between wet and dry periods. There is no consistent long-term trend towards wetter or drier conditions for any of the months (Figure 2.7a). November shows an increasing trend, indicating rising rainfall during the late rainy season. However, August exhibits more pronounced wet events compared to June and November. The 6-month SPI for November shows the same increasing trend (Figure 2.7b). The trend towards wetter conditions in recent years is even more evident in the 12-month SPI, particularly for August and November (Figure 2.7c). The detailed calculation and formula have been included in Annex A4: Method for flood and drought assessment at country scale.

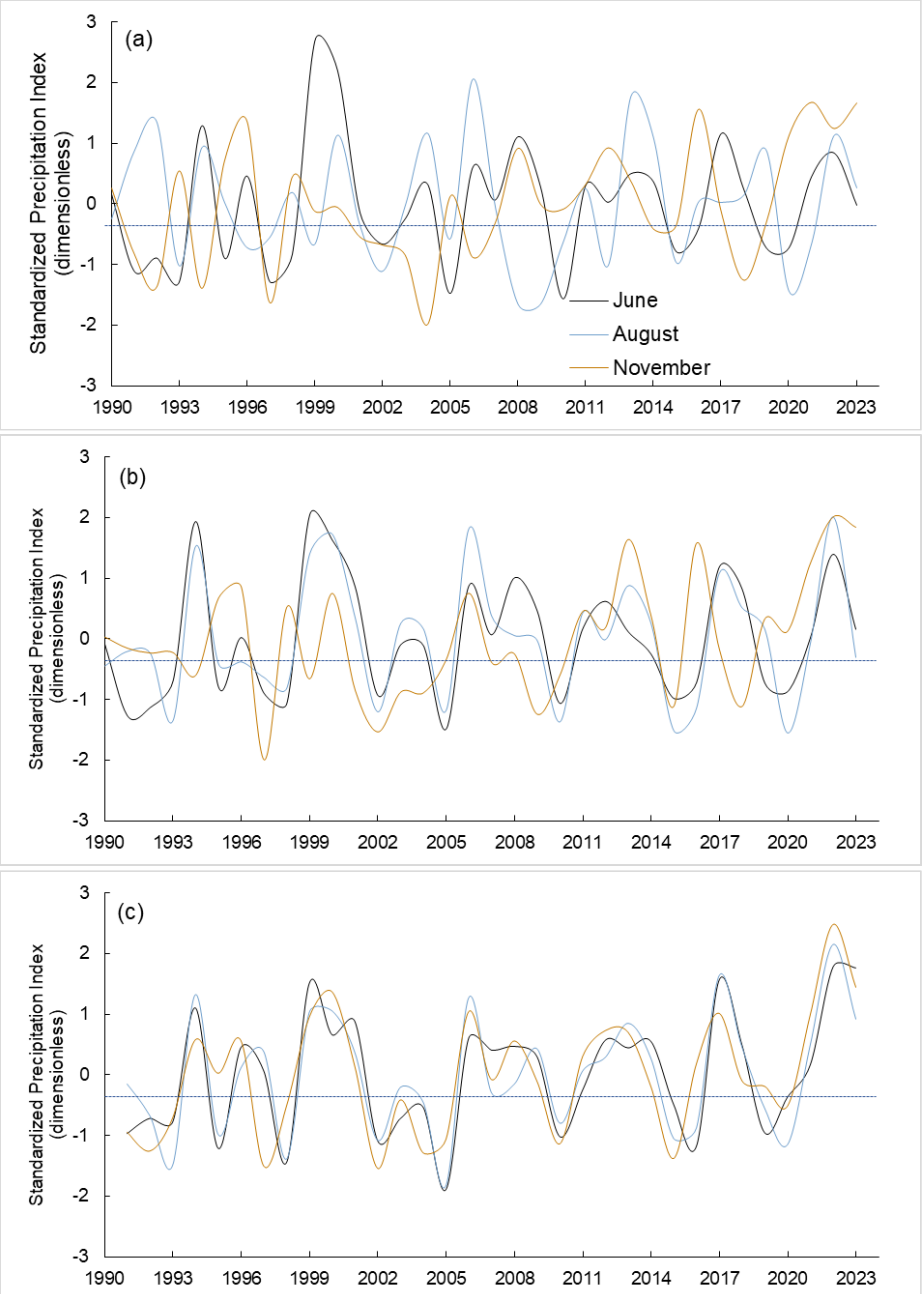

Figure 2.7: Standardized Precipitation Index for June, August, and November for the average precipitation of Cambodia between 1990 and 2023. (a) 3-month timescale Standardized Precipitation Index; (b) 6-month timescale Standardized Precipitation Index; (c) 12-month timescale Standardized Precipitation Index. June, August, and November are the base months of each timescale; for example, the 3-month timescale Standardized Precipitation Index for June means the total precipitation from April to June of a specific year compared to the average between 1990 and 2023.

Floods occur more frequently than any other natural hazard in Cambodia and have affected the largest number of people compared to other hazards (World Bank, 2021). There was a notable spike in flood impact around the year 2000 due to exceptionally intense rainfall events. Droughts occur less frequently than floods but also have a significant impact. Between 1990 and 2020, substantial numbers of people were affected.

2.4.3.2 Precipitation-Related Events

In recent decades, Cambodia has experienced an increase in the frequency and intensity of extreme precipitation events, including hailstorms, thunderstorms, and tornadoes. These events, historically less common, appear to be growing in both number and severity, posing new challenges to the country's water resources, infrastructure and agricultural sectors. Climate change could result in rising temperatures that impact the water cycle by altering the timing, duration, and intensity of rainfall patterns and seasons. These alterations may lead to more frequent droughts and extended dry periods, delayed rainy seasons with heavy downpours and flash floods, reduced river flow during the dry season and increased flow during the rainy season. Such changes ultimately affect the hydrology of major rivers, tributaries, and groundwater systems (Oudry, Pak, & Chea, 2016). This section examines the patterns and impacts of these extreme weather events, considering whether their frequency is on the rise and what implications this trend holds for Cambodia's future.

- ☀ Heavy monsoonal rainfall events leading to flash floods

One of the most impactful changes has been the rise in the number of heavy rainfall events, often resulting in flash floods, especially in urban areas with inadequate drainage systems (Huang, Park, Wang, & Sophal, 2024). For instance, Phnom Penh has experienced multiple instances of severe flooding in recent years due to torrential rains that overwhelm the city’s infrastructure (Huang, Park, Wang, & Sophal, 2024). These floods cause widespread damage to homes, roads, and public infrastructure, leading to significant economic losses and posing barriers to development (Yang, Keating, & Sourn, 2024).

Besides flash floods lasting a few hours to a few days, river floods driven by high moisture from monsoon winds and elevated water levels due to heavy rainfall in the upstream regions of the Mekong River are also causing significant challenges for Cambodia (World Bank & Asian Development Bank, 2021). Since the 1990s, Cambodia has experienced flooding at a relatively frequent interval, roughly every two years (Mekong River Commission, 2012). Notably, the 2000 flood was the most severe in 70 years (Flower & Fortnam, 2015). Early monsoon rains were followed by torrential downpours, which led to prolonged flooding (IFRC, 2002). 374 people were killed and 2.7 million were adversely affected; agricultural damage was estimated at 402,940 ha (Ros, Nang, & Chhim, 2021). Another devastating flood occurred in 2011, resulting from tropical storms including Typhoon Ketsana, which caused economic damages of USD 500 million, as estimated by National Committee for Disaster Management (NCDM) and the World Bank in 2014 (RCRC, 2014). This event ravaged 400,000 ha of agricultural land, disrupted

transportation, caused 250 fatalities, and affected 1.6 million people (ADB, 2012). It remains the largest flood since 2000, although Phnom Penh was spared severe flood damage (JICA, 2015). In October 2020, another major flood impacted 19 out of 25 provinces (76 percent), with severe river and flash floods affecting over 175,000 households and damaging 300,000 ha of agricultural land (Humanitarian Response Forum, 2020). Another significant flood occurred in October 2024, impacting 11 of the 25 provinces (44 percent). 22,752 ha of agricultural land were damaged and 12,295 families were affected by severe river and flash floods (Humanitarian Response Forum, 2024).

☀ Typhoons and tropical storms

Although typhoons never make direct landfall in Cambodia, their transition into decaying typhoons or weakened tropical storms has caused extensive damage to civil infrastructure, agriculture, and livelihoods. These impacts are felt over both short periods due to immediate effects and long periods required for recovery (Phy et al., 2022). Decaying typhoons often bring powerful, deadly rotating winds and intense precipitation, which frequently lead to flash floods (Regional Integrated Multi-Hazard Early Warning System, 2011).

Table 2.5 catalogs typhoons from 1997 to the present to measure their frequency and briefly discuss their impacts on Cambodia. The first recorded typhoon, Linda, struck in November 1997. While primarily affecting Vietnam, it caused around 25 deaths in Cambodia. Between late September and late October 2009, the remnants of Typhoon Ketsana triggered flash floods across more than 14 provinces, resulting in 43 deaths, numerous injuries, and significant damage and losses (Royal Government of Cambodia, 2010). The typhoon destroyed 40,136 ha of rice crops and damaged 67,355 ha just before harvest (Royal Government of Cambodia, 2010). Productive sectors were the most affected, with agriculture, livestock, fisheries, and industry experiencing estimated losses of USD 60 million. The social sector, including housing, health, and education, incurred USD 43 million in damages and losses, followed by infrastructure, primarily transport and irrigation, with USD 29 million in damages and losses (Royal Government of Cambodia, 2010). Four years later, in 2013, three typhoons—Wutip, Usagi, and Nari—struck the lower Mekong Basin (LMB) between September and October, evolving into major tropical storms as they entered Cambodia. These typhoons caused flash floods and claimed nearly 190 lives nationwide.

The list provided in Table 2.5 is not exhaustive and excludes tropical storms that passed through Cambodia, which if included, would increase the list greatly, as tropical storms (excluding decaying typhoons) occur more frequently. While tropical storms often result in flash floods and strong winds, their impacts are typically less deadly and devastating than typhoons. Nonetheless, it is noteworthy that the severe flooding of 2011 was intensified by prolonged weeks of rain caused by a series of tropical storms (Son, Chen, & Chen, 2021).

Table 2.6: Catalogue of typhoons, dates of occurrence, and their impacts over Cambodia since 1997

Typhoon	Date	Key Impact
Linda	November 1997	• Directly hit Vietnam (Australian Broadcasting Corporation, 1997; Reliefweb, Typhoon Linda - Nov 1997. https://reliefweb.int/disaster/st-1997-000267-vnm#overview, 1997) • 25 dead with over 200 missing (HKO, 1998)

Typhoon	Date	Key Impact
Ketsana	September 2009	• 14 provinces affected (Kampong Thom was most badly hit) • 43 dead and 67 severely injured • 49,000 families or 180,000 people affected • Total damage and loss of USD 132 million
Mirinae	November 2009	• Mainly affected the Philippines and Vietnam • Two people dead due to strong winds (NBC News, 2009)
Wutip	September 2013	• Over 30 people dead (Deutsche Welle, 2013) • 13 out of 24 provinces affected with the number of affected families around 100,000 (FloodList, 2013)
Usagi	September 2013	• Brought heavy rains and subsequent flooding (Reliefweb, 2013) • At least 12 dead (Reliefweb, 2013)
Nari	October 2013	• 152 people lost to flash floods • Over half a million people affected in 16 of 24 provinces (The International Charter: Space And Major Disasters, 2013)
Molave	October 2020	• 121 districts in 20 out of 25 provinces affected • At least 44 dead and 175,872 families affected (Reliefweb, 2020)
Noru	September 2022	• Northern Cambodia affected (Banteay Meanchey, Otdar Meanchey, Preah Vihear, Siem Reap, and Stung Treng) • 16 people dead (Reliefweb, 2022)

Thunderstorms

Thunderstorms are a common phenomenon across Cambodia, especially during the rainy season. They occur most frequently in the afternoon and early evening when surface heating is at its peak (Dai, 2001). The distribution of thunderstorms varies across the country, with higher frequencies observed in the central plains and mountainous regions due to orographic lifting, where moist air is forced to rise over terrain, enhancing thunderstorm formation (Tsujimoto, Ohta, Aida, Tamakawa, & So Im, 2018). In simple terms, the combination of high surface temperatures, abundant moisture, and atmospheric instability creates ideal conditions for thunderstorm development.

Thunderstorms bring several associated hazards, including lightning, heavy rainfall, and strong winds (LaDochy & Witiw, 2023). Lightning, often used as a proxy to count the occurrence of thunderstorms, poses significant risks (Allen & Allen, 2016). While not all lightning reaches the ground, strikes can threaten lives, damage property, and cause power outages, particularly in areas with limited protection from thunderstorms (LaDochy & Witiw, 2023). Intense rainfall, often lasting up to six hours, can lead to flash

floods, especially in urban areas with poor or underdeveloped drainage systems, as in some urban areas in Cambodia (Huang, Park, Wang, & Sophal, 2024). Additionally, the strong downdrafts and gust fronts produced by these storms can caused localized wind damage, uproot trees, and damage buildings.

Climate change on a global scale has influenced shifts in weather patterns across the Mekong region (Lee, Kim, & Choi, 2019). Rising in temperatures, driven by global climate change, are widely believed to intensify thunderstorms and result in heavier precipitation events (Schefczyk & Heinemann, 2017). Cambodia has taken steps to minimize the impacts of thunderstorms through regular warnings issued by the Ministry of Water Resources and Meteorology (MOWRAM). These warnings, which form an important part of meteorological forecasts, are disseminated via digital forecast bulletins and news outlets. Efforts to improve in monitoring system are also underway.

2.4.3.3 Temperature-Related Events

Cambodia is also experiencing significant temperature-related extremes, primarily driven by global climate change. Heat waves have become more frequent and intense, particularly during the dry season from November to April. As a result of urbanization, urban heat islands are becoming common in both developed and developing countries, as heat is trapped in cities full of high-rise buildings. As mentioned in previous sections, droughts become more intense due to rising temperature, compounded by El Nino events. These extreme heat events pose serious health risks, especially for vulnerable populations such as the elderly, children, and those with pre-existing health conditions. Moreover, these temperature-related events will continue to generate challenges for agriculture and the economy.

Heat waves

Heat waves in Cambodia have become increasingly frequent and severe, posing significant challenges to human health, agriculture, and the overall economy (World Bank, 2021) Recent years have seen temperatures reach as high as 42°C, with extreme heat waves becoming more common due to global warming (Khmer Times, 2024). Urban areas, particularly Phnom Penh, are especially vulnerable due to the urban heat island effect, which exacerbates the intensity of these heat waves. As temperatures rise, there are growing concerns about the direct health impacts on the population, such as heat stress, dehydration, and heat-related illnesses like heatstroke.

The agricultural sector has also been hit hard by these heat waves. For example, Cambodia’s famous Kampot pepper industry has been severely affected, with farmers reporting drastically reduced yields due to scorching temperatures (Phys Org, 2024)**.** Many pepper plants have died, and those that survive often produce lower-quality crops, leading to both economic losses and a reduction in food security. With little rainfall to counterbalance the high heat, farmers are increasingly struggling to maintain their livelihoods, particularly as they rely heavily on seasonal weather patterns for their crops (Khmer Times, 2024).

Additionally, the growing energy demand due to rising temperatures is straining Cambodia's infrastructure. Currently, cooling accounts for around 45 percent of the country's electricity consumption and this figure is expected to nearly double by 2040 if heatwave trends continue. To address this, Cambodia is adopting passive cooling strategies in building design, aiming to reduce reliance on energy-intensive mechanical cooling systems (Khmer Times, 2024). These strategies are part of the country’s broader

effort to adapt to climate change, improve energy efficiency, and reduce the environmental impact of growing urbanization.

Urban heat island

Urban heat islands (UHI) are becoming more prominent in rapidly growing cities like Phnom Penh. Compared to surrounding suburban or rural regions, urban areas tend to have darker surfaces and less vegetation, which generally have a higher capacity to absorb incoming solar radiation. This disparity contributes to the development of the UHI effect (Kaloustian & Diab, 2015). This phenomenon is associated with the rapid rise in land surface temperature, coupled with land use changes like the loss of green spaces and human activities. Thus, UHI leads to higher temperatures in urban areas compared to surrounding rural regions (Weng, 2009). This phenomenon exacerbates the effects of heat waves, leading to higher energy demand for cooling, increased air pollution, and a greater risk of heat-related illnesses (Santamouris, 2014).

Phnom Penh experiences UHI and the intensity is stronger during daytime than nighttime, likely attributed to the reduced humidity during the dry season, which allows surfaces to absorb and retain more heat (Bunleng et al., 2024). Heightened UHI intensity in Phnom Penh significantly increases human thermal discomfort, particularly during the day, which can lead to various health issues such as heat cramps, exhaustion, and heat stroke (Bunleng, et al., 2024).

Droughts

Droughts in Cambodia are primarily characterized by a reduction in water sources due to the early end or delayed onset of the expected seasonal rains during the rainy season (UNCCD, 2019). Mini-droughts between late July and early August are a common occurrence and significantly affect both rural and urban communities. These mini-droughts are often driven by climate variability, particularly the El Niño Southern Oscillation (ENSO), which leads to prolonged dry seasons and extreme heat. While short-term adaptation mechanisms have improved, such as managing mini-droughts, extended periods of drought remain a significant concern for livelihoods, especially in the agricultural sector (UNCCD, 2019; MAFF, 2016). The National Committee for Disaster Management (NCDM) and the United Nations Development Programme (UNDP) reported in 2014 that although drought does not directly result in human fatalities like other natural disasters, it greatly impacts agriculture, livestock, and water resources, undermining food security and rural economies.

Cambodia's rising temperatures exacerbate drought conditions, with mean annual temperature anomalies increasing by 0.8°C since 1960, with the fastest increases occurring in the dry seasons at rates of 0.20–0.23°C per decade (Thoeun, 2015). Higher temperatures contribute to increased evaporation, reducing water availability and raising the demand for crop irrigation (Srinivasan, Agarwal, & Bandara, 2024). This has profound implications for Cambodia's agricultural sector, where rice yields are projected to decline by 10–15 percent by the 2040s due to rising temperatures (World Bank & Asian Development Bank, 2021). Moreover, labor productivity is also affected, with studies indicating a potential 20 percent drop in productivity by the 2050s if current temperature trends continue (Srinivasan, Agarwal, & Bandara, 2024). The combined impact of increased temperature and prolonged drought poses significant challenges to Cambodia’s food security and economic stability.

2.4.3.4 Other Extreme Phenomena

Cambodia's seasonal climate is recurrently influenced by El Niño Southern Oscillation (ENSO), which consists of El Nino and La Nina, two cyclical climate phenomena that can disrupt weather patterns across the globe. Cambodia is vulnerable to ENSO-related climate shocks in a multifaceted way, encompassing interrelated climate, agriculture, economy, and society. Interventions during ENSO years can range from short- to medium-term and be discontinued in non-ENSO years (Sutton, et al., 2019). Landslides are also included in this section since they are indirectly linked to precipitation-related events and are a common extreme phenomenon in the country. The approach for calculating and determining the extreme phenomena is detailed in Annex A5: Approach for determining precipitation events and other extreme phenomena.

El Niño

El Niño, characterized by warmer-than-average sea surface temperatures in the central and eastern Pacific Ocean, often leads to below-average rainfall and thus, drier conditions in Cambodia. El Nino causes an early end to the rainy season or an early start to the dry season, contributing to droughts (Sutton, et al., 2019). The lack of rainfall during such events not only affects rice cultivation, which is the country's staple food, but also depletes water resources, exacerbating the challenges in both rural and urban areas.

Between 1980 and 2015, there were eight El Niño events in Cambodia, resulting in severe droughts in 1982–83, 1986–87, 1994, 1997–98, 2002, 2005, 2010, and 2016, and leaving 2.5 million people with water shortages. Rainfall during the El Nino years dropped by 10 to 30 percent, compared to neutral years (Sutton, et al., 2019). From 1997 to 2002, droughts caused a 20 percent decline in rice production (NAPA, 2016). In addition, 2010's El Niño–related droughts damaged 14,000 ha of transplanted rice, 3,500 ha of rice seedlings, and 5,500 ha of other crops (Leng, 2014). Another 2015-2016 El Niño event caused widespread drought, a 17 percent reduction in fish production, and crop failures in many parts of Cambodia, leading to significant economic losses and humanitarian crises (Sutton, et al., 2019). By 2016, water levels in Cambodia's rivers fell to 50 to 70 percent of the inter-annual average, rendering the 2016 drought the worst drought in 50 years (ODC, 2016).

La Niña

Conversely, La Niña, characterized by cooler-than-average sea surface temperatures in the same region, can bring increased or above-average rainfall and thus wetter conditions in Cambodia (Phy et al., 2022). La Nina is often associated with flooding and associated consequences such as landslides and damage to infrastructure. However, La Nina can have positive effects on agricultural production, in contrast with El Nino events, by contributing to flooding in the Cambodian floodplains where most agricultural production takes place. On average, rice production drops by 10 percent during El Niño episodes and rises by 5 percent during La Niña periods (Sutton, et al., 2019). In fact, Cambodia suffers considerable economic losses during El Niño events, but these are nearly offset by the economic gains brought by La Niña, which enhances agricultural productivity through increased rainfall (Sutton, et al., 2019).

Despite benefits, flooding as a result of La Nina causes damage to agriculture and other sectors. The 2000 and 2011 are prime examples of severe flooding and repercussions under the La Nina influence, not only in Cambodia, but in the entire Lower Mekong Basin (Cosslett, Cosslett, Cosslett, & Cosslett, 2018). Recently, another 2020-2021 La Niña event

covered 60 percent of the country, bringing heavy rain and flooding (Phnom Penh Post, 2020).

Landslides

Landslides, which are a byproduct of flooding resulting from precipitation-related events, are also considered in the context of extreme phenomena. Landslides in Cambodia often occur in regions with high rainfall and steep terrains, especially during the monsoon season (Lee & Sambath, 2006). Since mountainous regions are often sparsely populated, landslides tend to have minimal impact on private property, but they can still significantly disrupt transportation, particularly by damaging road networks that traverse the highlands and mountain valleys (Lee & Sambath, 2006). The region's most susceptible to landslides are the mountainous regions in the northeastern and southwestern provinces. Pursat, Koh Kong, and Preah Sihanouk are ranked as highly susceptible. In 2023, six landslides occurred in Pusat. They were triggered by intense rainfall and, in combination with flooding, resulted in displacement of hundreds of residents and damage to agricultural lands and infrastructure (Reliefweb, 2023).

2.4.4 Changes in Monsoons and Wind Patterns

Cambodia's monsoon rainfall, driven by seasonal wind patterns, is undergoing significant shifts. These changes, impacting the timing, duration, intensity, and distribution of rainfall, are largely influenced by factors such as climate change, shifts in atmospheric circulation, and rising sea surface temperatures.

Monsoon Rainfall Trends

Typically, Cambodia's rainy season begins in May and extends until late October or early November. Around 5-20 percent of the annual rainfall occurs during the pre-monsoon season (March-April), with the bulk of the rainfall (50-78 percent) occurring during the summer monsoon season (May-September) and a smaller percentage (12-36 percent) during the post-monsoon season (October-November) (Tsujimoto, Ohta, Aida, Tamakawa, & So Im, 2018). As temperatures continue to rise in the late 21st and early 22nd centuries, frequent changes and shifts in monsoon precipitation are anticipated, potentially leading to precipitation reductions of up to 70 percent below normal levels. This shift will not only impact the Indian summer monsoon but could also delay the onset of the monsoon over Southeast Asia by up to 15 days in the future (Ashfaq, et al., 2009).

Wind Speed Changes

From May to September, Cambodia is affected by a large-scale southwesterly wind. In October and November, northeasterly winds dominate the Gulf of Tonkin and the northern South China Sea, while from December to February, these northeasterly winds strengthen, bringing drier air (Tsujimoto, Ohta, Aida, Tamakawa, & So Im, 2018) (Figure 2.8). A notable decrease in wind speed has been observed in the northern mid-latitudes, impacting wind energy yields, especially in countries where wind power is crucial for electricity generation and the replacement of conventional energy sources. One potential contributor to this trend is the increasing surface roughness caused by biomass growth, which can disrupt wind patterns (McVicar et al., 2012). These changes in monsoon rainfall and wind patterns underscore the significant influence of climate change on Cambodia's weather and climate dynamics.

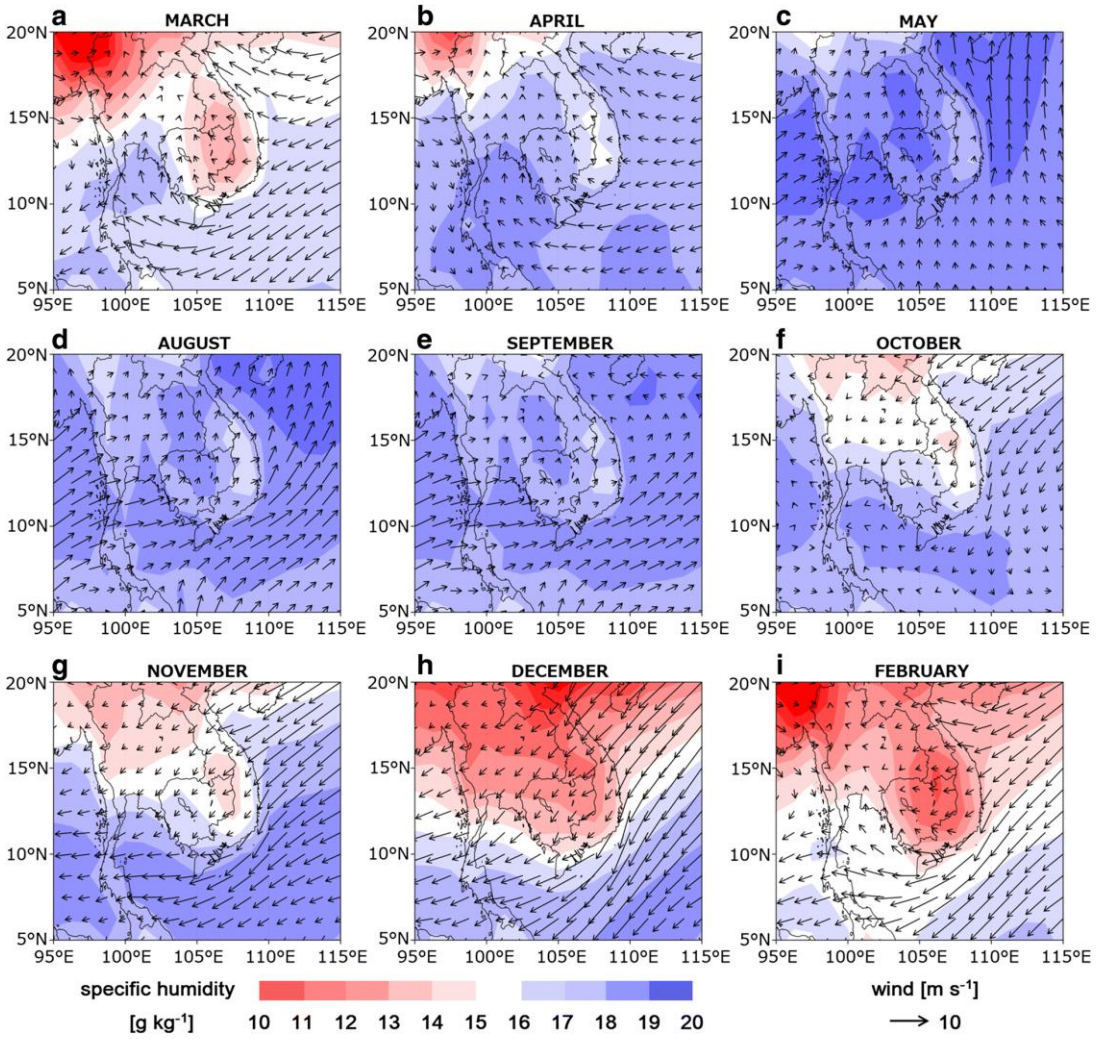

Figure 2.8: Wind and specific humidity at 1000 hPa over the Indochina Peninsula which covers Cambodia. Monthly mean data for March (a), April (b), May (c), August (d), September (e), October (f), November (g), December (h), and February (i) as 6-year (2010–2015) averages are shown. Data are from JRA-55 historical reanalysis. Reprinted from (Tsujimoto, Ohta, Aida, Tamakawa, & So Im, 2018) with modifications

2.4.4.1 Extreme Monsoon Performance

Cambodia's climate is heavily influenced by the monsoon cycle, which brings a distinct rainy and dry season. The rainy season, which stretches from May to October, contributes 85 percent of Cambodia's annual rainfall. It is driven by southwesterly winds which bring in clouds and moisture, creating the conditions for abundant rainfall. As the Intertropical Convergence Zone (ITCZ) shifts southward, northeasterly winds become dominant, marking the beginning of the cooler dry season, which typically lasts from November to April. This transition brings the lowest monthly precipitation totals of the year.

ENSO Influence

Interannual variations in precipitation are heavily influenced by the El Niño Southern Oscillation (ENSO). El Niño events typically bring warmer and drier winter conditions to Southeast Asia, while La Niña events bring cooler, wetter conditions. Climate change is expected to intensify the effects of the monsoon cycle, increasing the frequency and severity of hazards such as flooding and drought. These hazards already have significant impacts on Cambodia's population (Word Bank, 2024).

Over the past 50 years (1971-2020), Cambodia has experienced significant changes in precipitation trends across its diverse regions. The central and eastern provinces have generally seen decreases in rainfall per decade, while some western provinces have seen increases. The most notable decreases in precipitation per decade occurred in the central province of Kampong Thom (-44.71 mm) and the eastern province of Ratanakiri (-43.44 mm), with the most pronounced effects occurring during the summer wet monsoon months. Cambodia is likely to experience even more intense precipitation in the future, although the timing and severity of extreme rainfall events will vary by region. This will likely lead to more frequent extreme precipitation events, leading to increased flooding and impacts of agriculture and human lives (Word Bank, 2024).

2.4.4.2 Trends and Changes in Winds

In the second half of the 20th century and the first decade of the 21st century, wind speed has decreased in many regions. Open areas like offshore regions, coastal areas, deserts, and exposed mountain locations typically experience high mean wind speeds. Conversely, sheltered forested areas usually have much lower average wind speeds (Jung & Schindler, 2020). Wind speeds fluctuate significantly on daily, seasonal, and interannual timescales. To understand long-term trends in wind patterns, studying changes over multiple years is crucial (Jung & Schindler, 2018). The temporal variability of wind speed is mainly characterized by daily, seasonal, and inter-annual fluctuations. Wind speed also varies on multi-year time scales. Thus, investigations of long-term wind speed trends are crucial.

Analysis of annual average wind speed trends in Cambodia, spanning from 1990 to 2023, reveals distinct variations across different geographical zones. Data derived from ERA5 dataset (ECMWF Reanalysis v5) from the European Centre for Medium-Range Weather Forecasts (ECMWF) (Climate Engine, 2023) was used to assess these trends (Figure 2.9). The western highlands and coastal plains exhibited the highest annual average wind speed, registering 2.68 m/s. In contrast, the central Cambodia plains recorded the lowest average wind speed, measuring 1.12 m/s. Over the study period, a slight decrease in annual average wind speed was observed in the western highlands and coastal plains, with a linear trend of -0.0003 m/s per year. The central Cambodia plains also experienced a slight decrease, with a linear trend of -0.001 m/s per year. In contrast, the eastern highlands and plains showed a slight increase in average wind speed, with a linear trend of +0.0006 m/s per year.

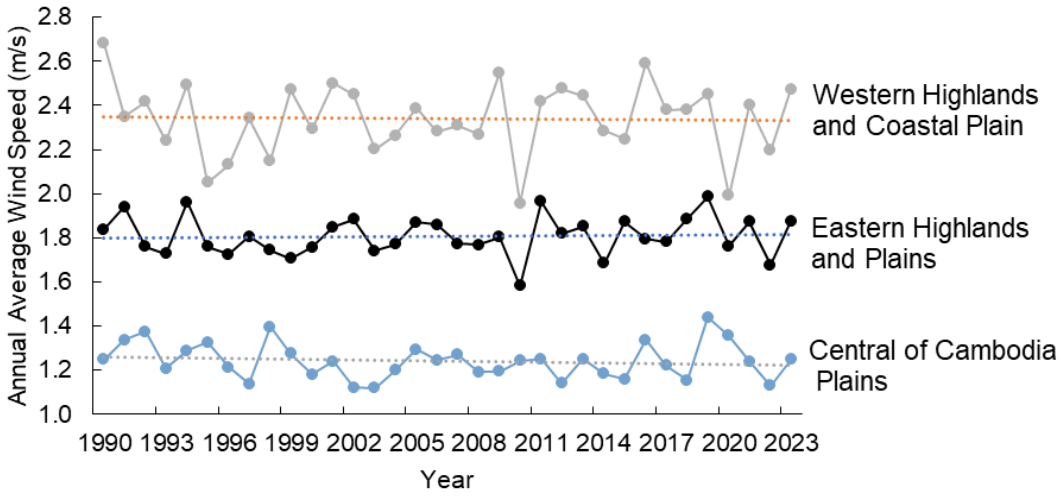

Figure 2.9: Trends in annual average wind speed changes each region in Cambodia from 1990–2023

Figure 2.10 shows that trends in the annual average wind speed for all regions in Cambodia decreased slightly during the same period. The linear wind speed trends declined from 0.015 m/s per decade in 1990-1999 to 0.011 m/s per decade in 2000-2009, before dramatically increasing to 0.017 m/s per decade in 2010-2019. Between 1990 and 2023, Cambodia witnessed substantial variability in decadal wind speed trends across its diverse geographical regions, as shown in the current analysis. This period marked significant increases in wind speed in the central plains, while mixed trends were observed in the western highlands and coastal plain, and decreases were recorded in the eastern highlands and plains (Table 2.6).

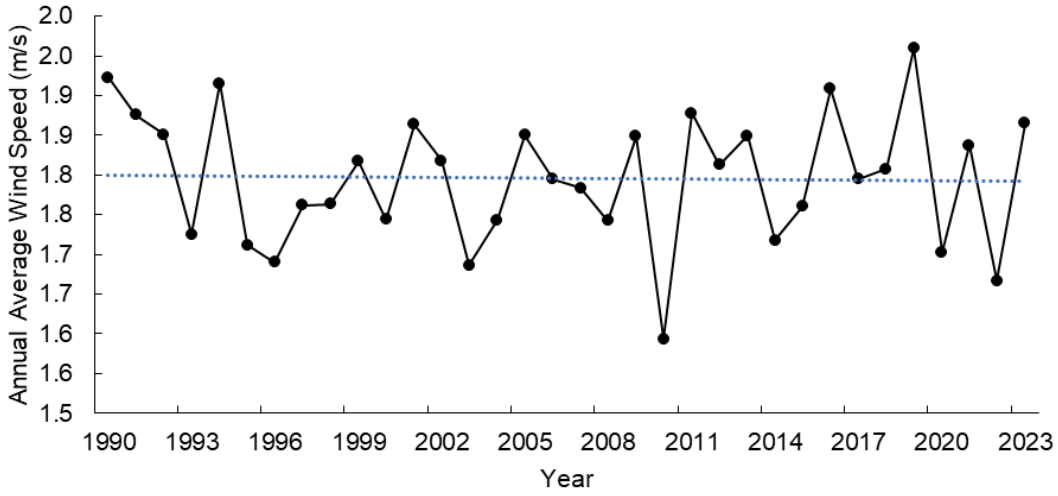

Figure 2.10: Trends in annual average wind speed changes. across region in Cambodia from 1990–2023

Table 2.7: Trends in wind speed changes across region in Cambodia.

Region	Mann–Kendall test	Sen's slope
Western Highlands and Coastal Plain	▲ 0.027	▲ 0.0010
Central Cambodia Plains	▼-0.116	▼-0.0015
Eastern Highlands and Plains	▲ 0.123	▲ 0.0012
Cambodia	▼-0.030	▼-0.0002

Note: It is divided into two main methods: Mann–Kendall and Sen's slope tests. Each method displays the magnitude of wind speed change in meter per second (m/s) with directional indicators. Red arrows pointing down indicate a decrease in wind speed, while green arrows pointing up represent an increase.

2.4.4.3 Trends and Changes in Tropical Storms, Typhoons,and Cyclones Frequency, Intensity, and Trajectory

Southeast Asia is facing an increasing number of cyclones and tropical depressions. 123 tropical cyclones (TCs) and tropical depressions (TDs) made landfall in Indochina from 1979-2021 (Ho, Wang, & Yoon, 2024), Figure 2.11). The number of TC/TD in the latter period is slightly higher than that in the former period (59 from 1979-2000 and 64 from 2001-2021), partly due to a noticeable increasing trend in annual precipitation patterns. The same study examined seasonal mean precipitation, sea surface temperature (SST), sea level pressure, and wind patterns for 2001-2021 to better understand the climatic drivers of the observed trends. Higher precipitation values were observed in 2001–2021, with notable increases in open oceans, suggesting more water vapor transport to Indochina. Warmer SSTs in the South China Sea and Philippine Sea, particularly in the

northern region, also indicate warmer air holding more moisture. Additionally, a low-pressure system from eastern China to northern Indochina during 2001–2021 is linked to a stronger westerly wind pattern from the Indian Ocean, indicating a robust Asian monsoon channeling increased moisture to Indochina.

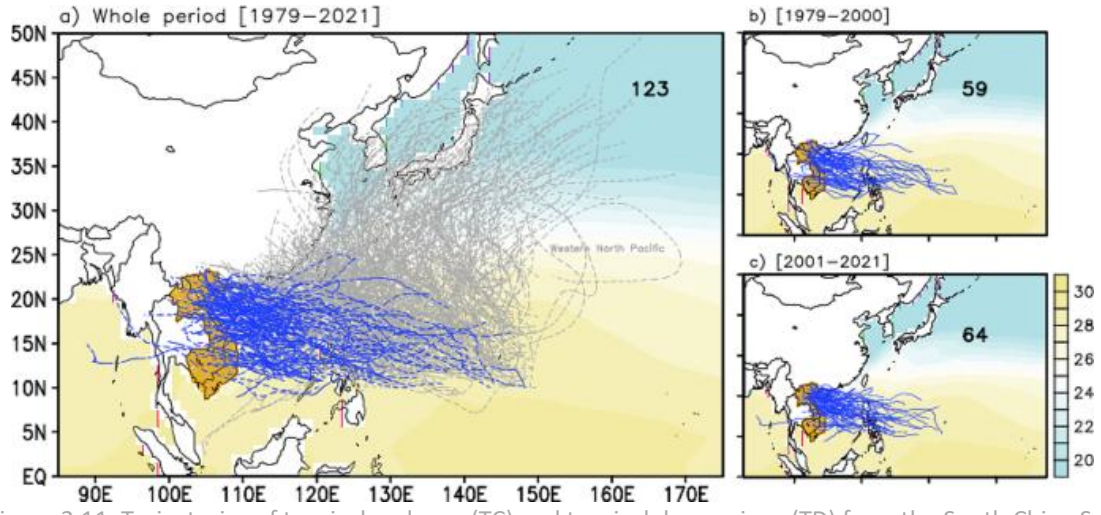

Figure 2.11: Trajectories of tropical cyclones (TC) and tropical depressions (TD) from the South China Sea and the Philippine Sea (1979-2021) are shown in (a). Blue lines indicate TCs and TDs that made landfall in Indochina (Cambodia, Laos, and Vietnam), while grey lines show those moving northward or elsewhere. The corner number shows TCs and TDs landing in the mainland. Shading represents the long-term mean sea surface temperature (1979-2021), and the orange polygon outlines Indochina. Panels (b) and (c) display the landfall trajectories in Indochina from May to December for 1979–2000 and 2001–2021, respectively (Ho, Wang, & Yoon, 2024).

Using data from 1979–2021, TC contributions to the annual precipitation are 6 percent in Cambodia, increasing to 7 percent when TD were taken into account (Figure 2.12). In southern Cambodia, TC contributes only about 3 percent of annual rainfall (around 50 mm), as those originating in the South China Sea and Philippine Sea rarely track far enough south to significantly affect the region.

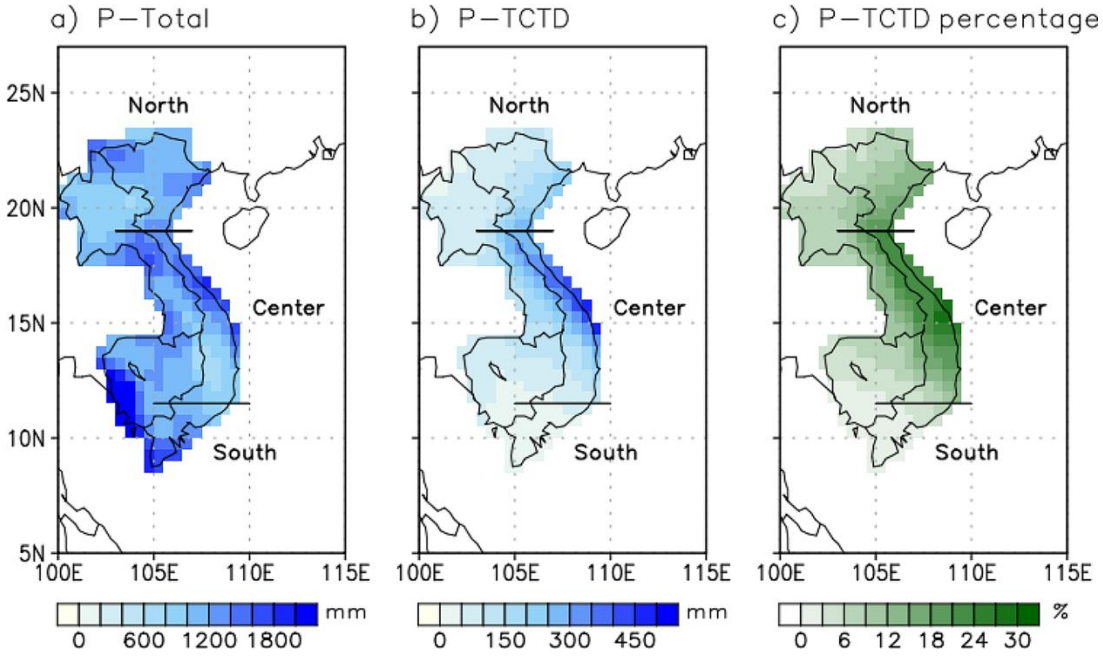

Figure 2.12: Spatial distribution of climatological precipitation displaying a) annual precipitation, b) precipitation induced by TCTD (P-TCTD), and c) its contribution to the climatology (P-TCTD percentage) (Ho, Wang, & Yoon, 2024).

While tropical cyclones do occur, they are relatively rare when considering the country's overall size – Cambodia has experienced 29 TCs that made landfall, with a relatively low density (1.6 x 10^{-4}) of landfall TCs per square kilometer, fewer than in other regions of Southeast Asia (Table 2.7). However, there were 33 recorded landfall events in which the storm's strength changed category during landfall; 24 were classified as tropical depressions and 9 as tropical storms. Possibly because of its geographical location and the natural path of storm systems in the region, Cambodia is not commonly affected by the most severe cyclonic events, characterized by wind speeds of 119 km/h and 240 km/h, respectively, possibly due to its geographical location and the natural path of storm systems in the region. However, Cambodia experiences a large number of tropical depressions, similar to Thailand and Laos

Table 2.8: Number of Land falling TCs, Land falling TCs per a Square Kilometer

Type of Extreme Disaster	Number
Landfalling TCs	29
Landfalling TCs/ km^2 x 10^{-4}	1.6
Entries	34
Landfalling Intensity Values	33
Tropical Depression	24
Tropical Storm	9
Typhoon	0
Super Typhoon	0

Note: Actual Landfalls (Including Multiple Landfalls by a Single TC), Intensity at Landfall Values from the JTWC Best Track Archive, and Number of Landfalls by JTWC Intensity Categories for Cambodia (Tran, Ritchie, & Perkins-Kirkpatrick, 2022).

Inland countries in Area 3 of Southeast Asia, such as Laos and Cambodia, are typically impacted by TCs that first make landfall along the Vietnam coastline (Figure 2.13) (Tran, Ritchie, & Perkins-Kirkpatrick, 2022). To a certain extent, tropical storms, traversing westward from Vietnam, usually hit the northeastern and eastern Cambodia provinces. Based on the same figure, no typhoons and super typhoons have been observed in the country.

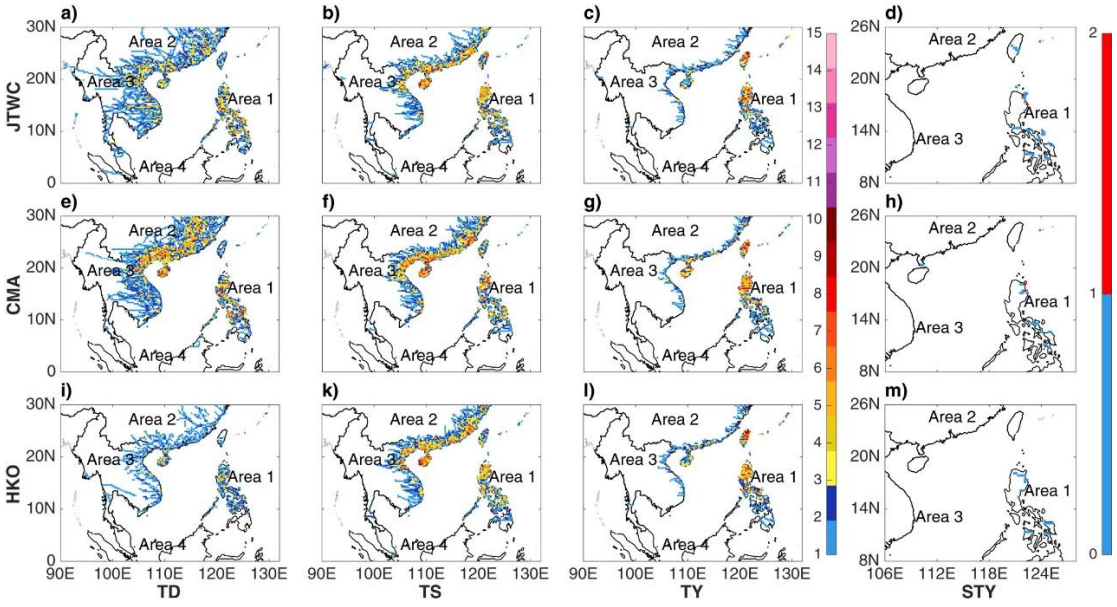

Figure 2.13: TC landfall frequency in 0.25° × 0.25° grids sorted by the Joint Typhoon Warning Center (JTWC) intensity classification for: (a) Tropical Depression; (b) Tropical Storm; (c) Typhoon; and (d) Super typhoon in the JTWC dataset; and (e)-(f)-(g)-(h); (i)-(k)-(l)-(m) as in (a)-(b)-(c)-(d) but for the China Meteorological Administration (CMA), and Hong Kong Observatory (HKO) agency records (Tran, Ritchie, & Perkins-Kirkpatrick, 2022).

TC density is scattered in the Mekong countries, with a greater density of TCs in the eastern of the lower Mekong River Basin, which includes Cambodia (Figure 2.14) (Chen, Ho, Chen, & Azorin-Molina, 2019). Generally, the spatial coverage of the Mekong region affected by TC rainfall for 1983–2016 at annual scale shows high variability with a mean percentage of 66.6 percent; while 2002 is an extreme year of the lowest TC rainfall influence (23.9 percent).

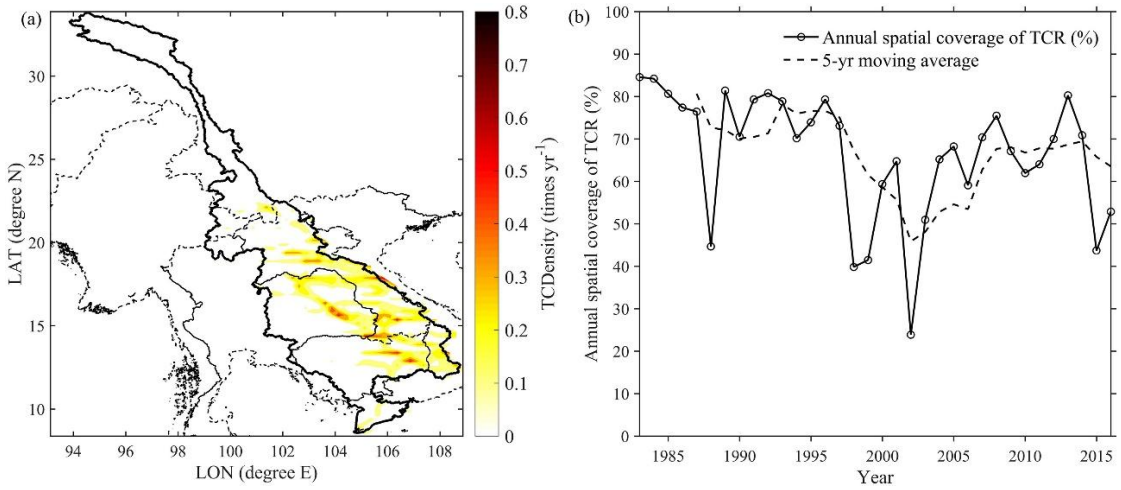

Figure 2.14: (a) Spatial patterns of annual mean TC Density (times yr−1) and (b) annual spatial coverage of TC rainfall (TCR in percent) across the Mekong River Basin for 1983–2016 (Chen, Ho, Chen, & Azorin-Molina, 2019).

2.5 Directions for Future Studies

This section presents challenges in data availability and suggested directions for future study. Generally, the lack of comprehensive understanding regarding climate change impacts on ecosystems and biodiversity is exacerbated by the poor quality and limited accessibility of relevant information.

2.5.1 Challenges: Data Availability and Variability

One of the primary challenges in modeling climate extremes in Cambodia is the difficulty of collecting long-term data. Additionally, the distribution of rain gauge stations across the country is limited. Furthermore, research and data are scarce on observed changes and the impacts of climate change on various socio-ecological systems, socio-economic and sectors at both national and sub-national levels.

2.5.2 Research Gaps and Directions for Future Studies

Extreme Events Prediction Uncertainty

As climate extremes like droughts and floods increase, their impact on water quality poses significant risks for drinking water and health (Fabian, Kwon, Vithanage, & Lee, 2023). Research gaps in water quality prediction underscore the need for comprehensive monitoring and a national strategy for water quality management during these events. Additionally, the role of surface hydrology in water quality dynamics warrants further

investigation.

The design of infrastructure in Cambodia, such as water drainage and flood control systems, is impacted by extreme precipitation probabilities (Zhao, Abhishek, & Kinouchi, 2022). However, the country faces challenges due to insufficient sub-daily gauge observations for predicting floods. This uncertainty hampers flood risk mitigation. Future studies should explore high-accuracy climate models and investigate the physical reasons behind observed changes in extreme weather events.

2.5.3 Ways Forward

Improving the availability and accessibility of data and information

To perform a qualitative and quantitative assessment of climate change impact, vulnerability assessment and risk, the future study requires enhancing data availability and quality and advancing information integration and sharing across various stakeholders involved.

Enriching knowledge of climate change

It is important to acknowledge the existing knowledge gaps in climate change science and its impacts on both natural and human systems. Climate change science research should be rooted in participatory approaches, promote social sciences, and adopt a transdisciplinary framework to ensure that findings are relevant across diverse decision-making contexts.

Strengthening the links, the science-based climate, adaptation, and communities

Climate change research aims to better inform users to enable efficient adaptation and to increase resilience to climate and environmental change. Two-way interaction between scientists and communities should be enhanced and strengthened.

CHAPTER 3
OBSERVED CHANGES IN SEA LEVEL & COASTAL ECOSYSTEM IN CAMBODIA

3.1 Chapter Summary

Chapter 3 delves into the intricate relationship between Cambodia's coastal ecosystems and the mounting pressures they face. Cambodia's coastal areas encompass various ecosystems, including upland forests, mangroves, seagrass, coral reefs, and rich fisheries resources. These resources play a crucial role for the nation's economic growth. Beyond their ecological significance, they are integral to Cambodia's economic prosperity, contributing substantially to sectors like fisheries and tourism and directly impacting the livelihoods of coastal communities. These ecosystems also provide essential services that bolster human well-being, support national defense strategies, and facilitate connections to international markets.

However, the chapter underscores that rapid development and the escalating effects of climate change are jeopardizing this delicate balance. Sea level rise, a particularly concerning consequence, is meticulously documented using satellite data, revealing a consistent increase in peak sea levels over recent decades. This trend, corroborated by projections from the IPCC's AR6 CMIP6, suggests that coastal areas will continue to experience heightened water levels, potentially inundating low-lying regions and damaging critical infrastructure.

Coastal erosion is another prominent threat. The chapter highlights the varying degrees of land loss along the coastline. This erosion is not solely a natural phenomenon; it is exacerbated by human activities such as unregulated coastal development, excessive sand mining, and deforestation in upland areas. These actions weaken the natural defenses of the coastline, making it more susceptible to the erosive forces of waves and tides.

The intrusion of salinity into freshwater sources is a further consequence of rising sea levels and altered river flow patterns. This salinization contaminates agricultural lands, reduces the availability of potable water, and disrupts the delicate balance of coastal ecosystems. The chapter emphasizes the far-reaching implications of this intrusion, particularly for coastal communities reliant on agriculture and freshwater resources.

Furthermore, the chapter meticulously documents the degradation of vital coastal ecosystems, including mangroves, seagrasses, and coral reefs. Habitat loss, pollution from land-based sources, and the direct impacts of climate change, such as increased water temperatures and ocean acidification, are contributing to this degradation. The loss of these ecosystems not only diminishes biodiversity but also compromises the essential ecosystem services they provide, such as storm protection, local microclimate regulation, water filtration, and fisheries support. This ecosystem degradation increases the vulnerability of coastal areas to natural disasters.

Crucially, the chapter highlights the profound socioeconomic impacts of these environmental changes on coastal communities. These communities, often heavily reliant on coastal resources for their livelihoods, face the risk of displacement, health

problems, loss of income, and increased poverty due to sea level rise and coastal erosion. The chapter stresses that these impacts are not merely environmental concerns, but also pose significant challenges to social stability and economic development. Therefore, the chapter serves as a call to action, emphasizing the urgent need for sustainable management practices and climate adaptation strategies to protect Cambodia's valuable coastal resources and the communities that depend on them.

3.2 Cryosphere and Sea Level Change

The cryosphere, encompassing vital frozen components such as snow, glaciers, permafrost, and lake and river ice, is a crucial component of high mountain regions, which are home to approximately 10 percent of the global population. Cambodia is not directly impacted by changes in the cryosphere, as these frozen regions are geographically distant from the country's location in Southeast Asia. However, Cambodia continues to experience the effects of global cryosphere changes, particularly through rising sea levels. The melting of glaciers and ice sheets contributes to this rise by adding freshwater to the oceans. Cambodia's coastline is particularly vulnerable to the negative impacts of rising sea levels.

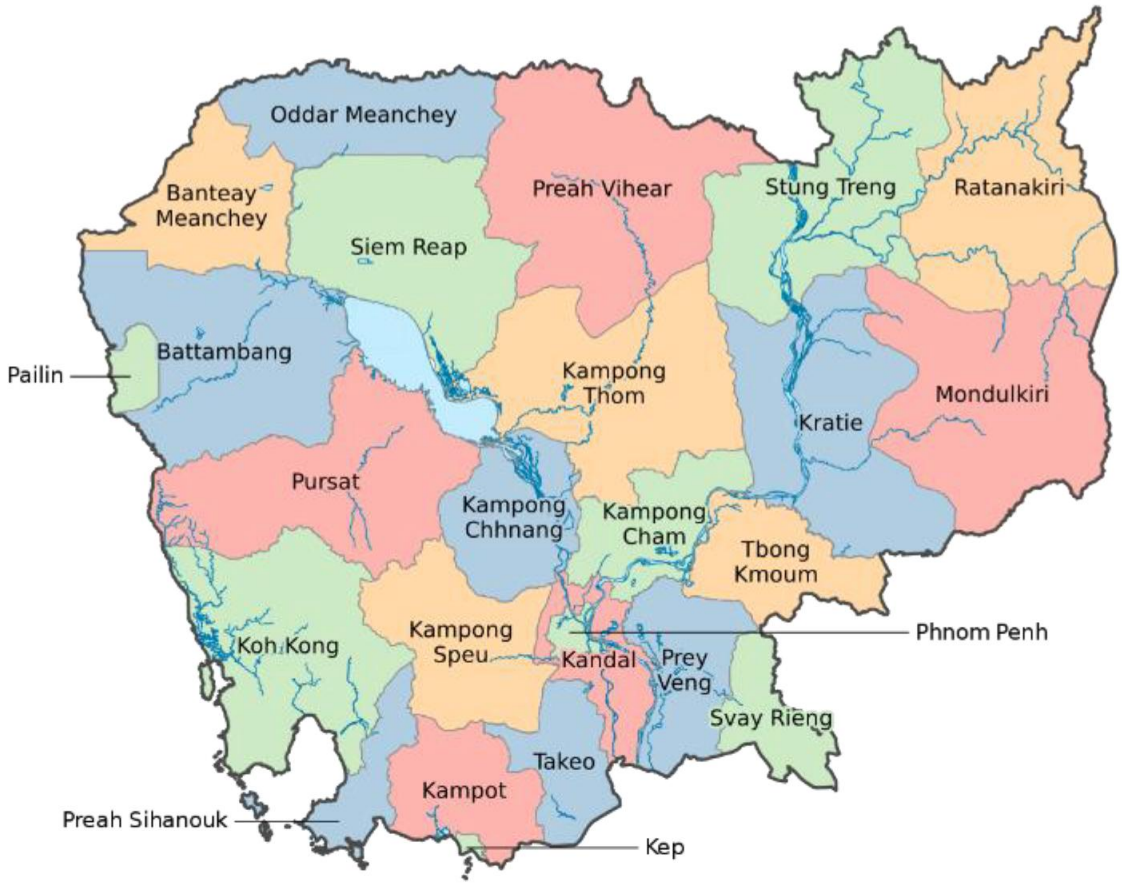

Figure 3.1: Coastal areas of Cambodia
Source: NCSD/MOE (2020)

3.2.1 Sea Level & Sea Surface Temperature

3.2.1.1 Sea Surface Temperature

Sea surface temperature (SST) is a crucial indicator of climate change, particularly in coastal regions like Cambodia. Over the past few decades, the SST in the Gulf of Thailand has been rising due to global warming. Warmer sea surface temperatures can have a variety of detrimental effects, including more intense and frequent storms, coral bleaching, and disruptions to marine ecosystems (McField, M. 2017).

Cambodia is affected by sea temperatures in the Gulf of Thailand. The sea level temperature is hot, around 30°C. The sea surface temperature in Cambodia's coastal regions remains warm and conducive for marine activities. For instance, the SST in Koh Rong is around 30.2°C, while in Krong Kep, it is approximately 29.9°C (Climate Change Institute and University of Maine, 2024). These temperatures are consistent with the general warming trend observed in the region, as seen in Figure 3.2.

The SST in the Gulf of Thailand, including the coastal waters of Cambodia, exhibits notable seasonal variations. During the northeast monsoon (November to March), cooler water temperatures are observed, while the southwest monsoon (May to October) brings warmer temperatures. The Cardamom Mountains' influence is particularly evident during the rainy season when the warm pool forms, with core temperatures being 0.5–0.8°C higher than the surrounding waters (Li et al., 2014).

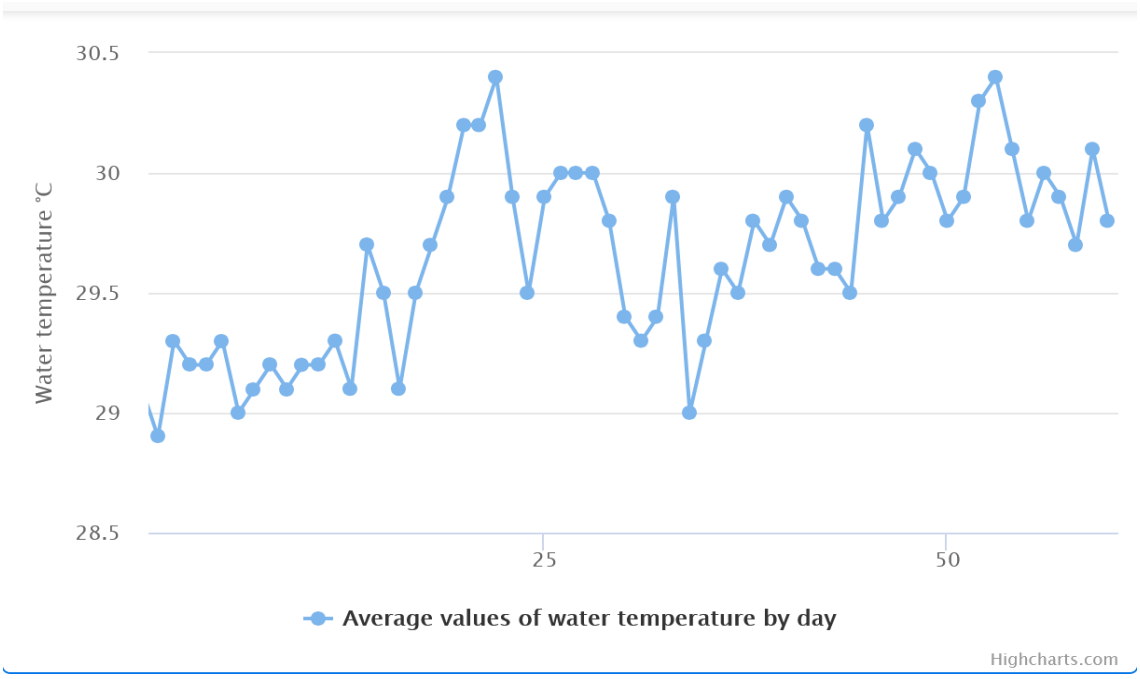

Figure 3.2: Average Values of Water Temperature by Day
Source: Climate Reanalyzer, Climate Change Institute, University of Maine. Retrieved March 27, 2025, from https://climatereanalyzer.org/clim/sst_daily/?dm_id=world2

3.2.1.2 Sea Level Rise

Sea level rise is a significant concern for Cambodia, particularly due to its extended coastline and low-lying areas. According to the Intergovernmental Panel on Climate Change (IPCC), global mean sea level has risen by approximately 20 cm since the beginning of the 20th century, with the rate of increase accelerating in recent decades (IPCC, 2022). This rise is primarily driven by two factors: the thermal expansion of

seawater as it warms and the melting of glaciers and ice sheets (Vinayachandran et al., 2022).

Cambodia's coastal zone, covering 17,237 km², is increasingly at risk from sea level rise and coastal inundation. Based on dataset from the Physical Oceanography Distributed Active Archive Center (PO.DAAC), sea level rise has increased from 194 mm in 1997 to 321 mm in 2024 with annual average fluctuation level at about 23.22 mm (Beckley et al., 2024). The projected sea level across Cambodia's four coastal provinces at three timeframes (2050, 2075, and 2100) under different SSPs reveals significant trends. For instance, under the SSP3-7.0 scenario, the projected SLR increases from 21 cm in 2050 to approximately 45 cm in 2075 and reaches 69 cm by 2100, based on a historical baseline from 1995 to 2014 (Fox-Kemper et al., 2021). This indicates an accelerating rate of sea level rise over time, particularly under higher emission scenarios. Similarly, the SSP2-4.5 and SSP1-2.6 scenarios also show an increasing trend in SLR across the decades, but with lower overall magnitudes compared to SSP3-7.0. The differences in projections between the low-emission SSP1-2.6 and the higher-emission SSP3-7.0 become more pronounced towards the end of the century, highlighting the potential benefits of implementing aggressive climate change mitigation efforts. The divergence in SLR projections between different scenarios increases with time, emphasizing that the long-term consequences of current emission choices will become increasingly evident in the latter half of the 21st century. The rate of SLR is projected to increase over time, especially under higher emission scenarios, indicating that the challenges associated with SLR will likely intensify in the coming decades. For instance, a one-meter rise in sea level could permanently inundate approximately 25,000 ha of land, with Koh Kong being the most affected area (MoE, 2015). The impacts include the loss of mangrove forests and marine ecosystems, salinization of agricultural lands, and seawater intrusion, particularly in Kampot and Kep provinces. Additionally, critical infrastructure and coastal tourism activities in Preah Sihanouk and Kampot provinces would face significant adverse effects (MoE, 2022).

The rate of sea level rise varies under different climate models, influenced by local land subsidence (National Aeronautics and Space Administration, n.d.). Under SSP3-7.0, sea levels near Preah Sihanouk are expected to rise by 0.50 meters above the historical baseline after 2080. This increase is slower under the SSP2-4.5 and SSP1-2.6 scenarios, with the 0.50-meter threshold being reached around 2090 and after 2100, respectively, both with high uncertainty (Figure 3.3). By 2100, sea levels are projected to rise by 0.69 meters under SSP3-7.0, 0.57 meters under SSP2-4.5, and 0.45 meters under SSP1-2.6, with much uncertainty due to potential land subsidence or vertical land motion.

In summary, by 2050, under a medium to high emissions scenario (SSP3-7.0), a mean rise of 21 cm is projected, with a likely range of 7 to 36 cm. By 2075, under similar scenarios, the rise is inferred to be around 45 cm. By the end of the century, in 2100, the projections show a substantial increase, ranging from a mean of 45 cm under a low emissions scenario (SSP1-2.6) to 69 cm under a high emissions scenario (SSP3-7.0), with likely ranges extending beyond one meter in the most severe case.

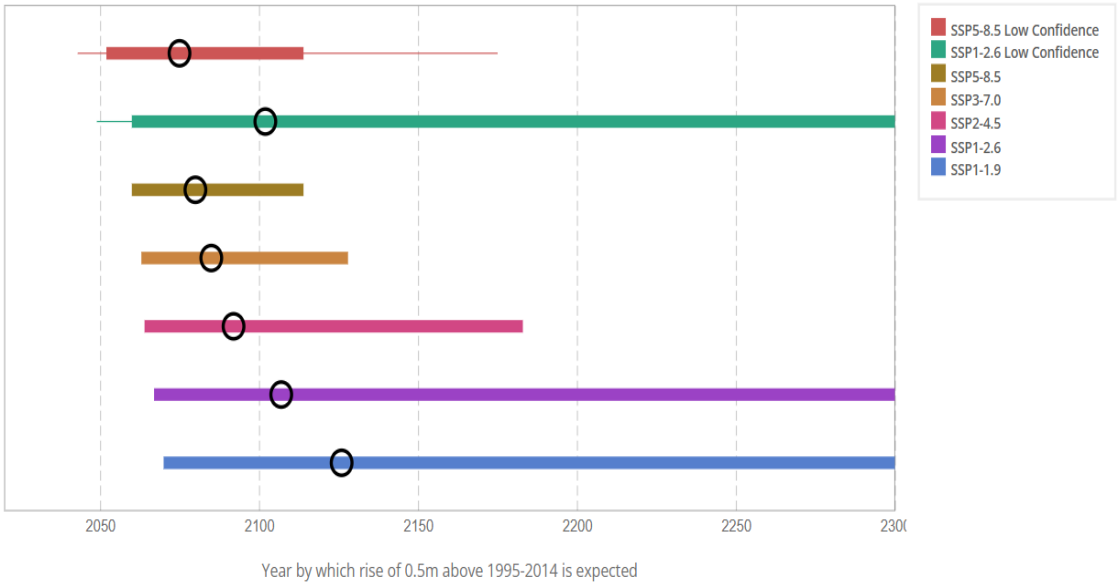

Figure 3.3: Projected Timing of 0.5-Meter Sea Level Rise Along Cambodia's Coast Under Various Scenarios (1995–2014)

Source: National Aeronautics and Space Administration. (n.d.)

Note: Timing of exceedance of different thresholds (increments of 0.1 m) under different SSPs. Thick bars show 17th-83rd percentile ranges, and black circles show median value. Thin bars also show 5th–95th percentile ranges for SSP1-2.6 Low Confidence and SSP5-8.5 Low Confidence scenarios.

3.2.2 Cambodia Coastal Climate

Cambodia has a tropical climate, with high temperatures and two seasons: a rainy monsoon season (May-October), contributing 80-90 percent of annual rainfall, and a dry season (November-April) with cooler temperatures. Annual rainfall averages 1,400-2,000 mm, varying by region, but coastal zone receives about 4,000 mm. Climate is influenced by ENSO, bringing drier conditions during El Niño and wetter conditions during La Niña (World Bank, 2021). The annual average temperature is 28 °C, with an average maximum temperature of 38 °C in April and an average minimum temperature of 17 °C in January (Thoeun, 2015). Data from the World Bank (2021) added that temperatures have risen by 0.18°C per decade since the 1960s, with the dry season warming faster (Figure 3.4). The number of hot days has increased by 46 per year. Precipitation trends show no significant changes, but droughts are linked to El Niño events.

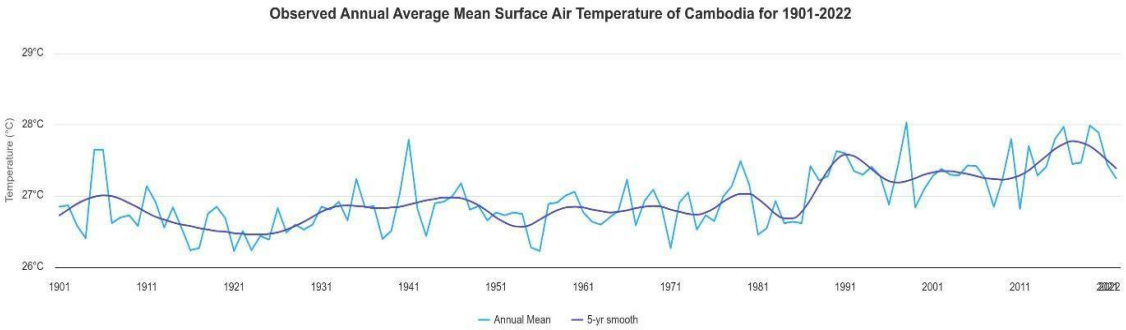

Figure 3.4: Observed Annual Average Mean Surface Air Temperature of Cambodia for 1901-2022

Source: World Bank (2021)

Cambodia's coastal provinces— Kep, Kampot, Preah Sihanouk, and Koh Kong— experience a tropical monsoon climate, characterized by distinct wet and dry seasons. In

the coastal areas of Cambodia, the minimum temperature ranges from 21°C in January to 24°C in May (Figure 3.5). The average temperature fluctuates between 26°C in January and 29°C in May. The maximum temperature varies from 31°C in January to 34°C in April.

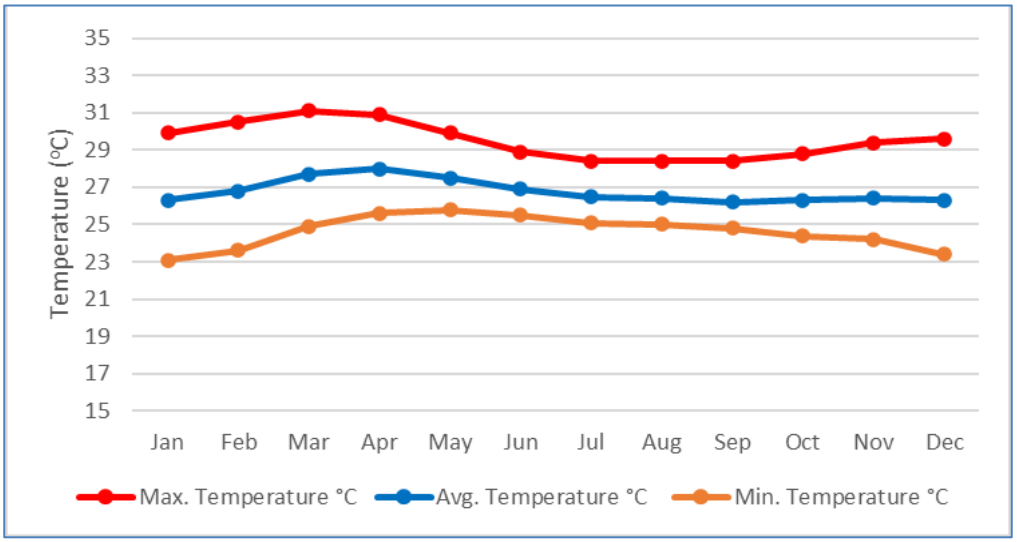

Figure 3.5: Average Monthly Temperature for Coastal Provinces (1991-2021)
Source: Climatedata.org

Table 3.1 shows that the month with the highest relative humidity is September (87.96 percent). The month with the lowest relative humidity is January (71.41 percent). The months with the highest number of rainy days are July, August, and September (20 days). The months with the lowest number of rainy days are January and February (5 days), which are considered the driest months of the year.

Table 3.1: Temperature, Precipitation/Rainfall, Humidity, Rainy Days and Average Sun Hours by month in Coastal Provinces of Cambodia

	January	February	March	April	May	June	July	August	September	October	November	December
Avg. Temperature °C (°F)	26.3 °C (79.3) °F	26.8 °C (80.3) °F	27.7 °C (81.8) °F	28 °C (82.4) °F	27.5 °C (81.5) °F	26.9 °C (80.4) °F	26.5 °C (79.6) °F	26.4 °C (79.4) °F	26.2 °C (79.2) °F	26.3 °C (79.3) °F	26.4 °C (79.6) °F	26.3 °C (79.3) °F
Min. Temperature °C (°F)	23.1 °C (73.6) °F	23.6 °C (74.5) °F	24.9 °C (76.8) °F	25.6 °C (78.2) °F	25.8 °C (78.4) °F	25.5 °C (77.8) °F	25.1 °C (77.2) °F	25 °C (77) °F	24.8 °C (76.6) °F	24.4 °C (76) °F	24.2 °C (75.5) °F	23.4 °C (74.1) °F
Max. Temperature °C (°F)	29.9 °C (85.8) °F	30.5 °C (87) °F	31.1 °C (87.9) °F	30.9 °C (87.7) °F	29.9 °C (85.8) °F	28.9 °C (84.1) °F	28.4 °C (83.2) °F	28.4 °C (83) °F	28.4 °C (83.1) °F	28.8 °C (83.9) °F	29.4 °C (84.9) °F	29.6 °C (85.3) °F
Precipitation / Rainfall mm (in)	29 (1)	27 (1)	69 (2)	108 (4)	217 (8)	242 (9)	265 (10)	248 (9)	266 (10)	238 (9)	91 (3)	36 (1)
Humidity(%)	71%	73%	76%	80%	85%	87%	87%	88%	88%	86%	80%	72%
Rainy days (d)	5	5	10	15	19	19	20	20	20	19	11	6
avg. Sun hours (hours)	9.0	8.9	8.8	9.3	9.3	9.4	9.3	9.2	9.0	8.7	8.9	9.2

Source: Climatedata.org

Figure 3.6 illustrates the monthly temperature variations in Preah Sihanouk. The minimum temperature ranges from 24°C in January to 26°C in April. The average temperature fluctuates between 27°C in January and 30°C in April. The maximum temperature varies from 30°C in January to 33°C in April.

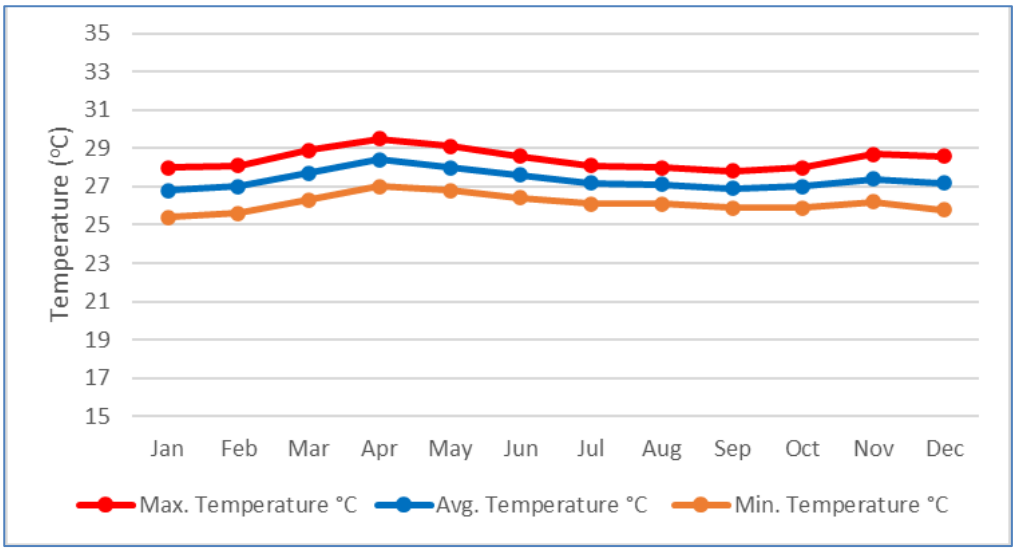

Figure 3.6: Average Monthly Temperature for Coastal Zone in Cambodia (1991-2021)
Source: Climatedata.org

3.2.3 Extreme Water Levels (Tides, Surges, and Ocean Waves)

3.2.3.1 Astronomic Tidal Range

Cambodia lacks comprehensive studies and measurements of tides, with no tidal gauges or publicly available data. According to ADB (2023), the maximum tidal range is estimated at 1.60 meters, with an additional 0.20 meters added to account for low atmospheric pressure, resulting in a total of approximately 1.80 meters. The tides are considered semi-diurnal, with occasional diurnal patterns during spring tides, and are classified as micro-tidal.

3.2.3.2 Ocean Climate (Wind and Swell Waves)

Cambodia's location in the Gulf of Thailand provides it with a sheltered shoreline, resulting in low-energy swell and wind waves, and a low risk of tsunamis. However, extreme wind events, particularly continuous southwesterly winds outside the gulf, can generate swell or tsunami waves that reach Cambodia. At the shoreline, wave energy increases water levels, a phenomenon known as wave setup, which should be considered in wave climate estimations. Wave height is limited by fetch (distance over which wind blows) and wind duration. High-energy wave events are most likely to come from the south, specifically from the south-southeast to south-southwest directions. Natural features like islands, mangroves, coral reefs, and sandbanks, including seagrass beds, help dissipate wave energy (James et al., 2021).

According to Chadwick (2023), in deep water, surface waves and the seabed interact minimally due to the exponential decrease in wave orbital motion with depth. Deep water is defined as areas beyond the shoreface, typically beyond the "depth of closure," which is approximately 10 times the maximum significant wave height that reaches the shoreline. In Cambodia, this depth is likely around the -30 mDL (meter Depth Level) contour line. Due to uncertainties, a conservative approach is recommended, considering deep water areas to be -10 mDL and deeper. Shallow water, where waves are most influenced by shoaling and breaking processes, is considered landward of the -10 mDL contour.

Table 3.3 provides valuable insights into how different fetch lengths influence wave heights under a constant wind speed of 11 m/s (40 km/hr) over a duration of 12 hours.

The data reveals that as the fetch length increases, the maximum significant wave height (Max Hs) also increases. For instance, with a fetch length of 5 kilometers, the Max Hs is 0.25 meters, while for fetch lengths of 10 and 15 kilometers, the Max Hs rises to 0.4 and 0.6 meters, respectively. This trend continues, with fetch lengths of 20, 50, and 100 kilometers resulting in Max Hs values of 1.0, 1.5, and 2.0 meters, respectively. The highest wave heights are observed for fetch lengths of 500 kilometers and greater than 1,000 kilometers, with Max Hs values of 3.0 and 3.5 meters, respectively (ADB, 2023).

Table 3.2 below highlights the importance of fetch length and wind speed in determining wave heights, which can significantly affect coastal erosion, sediment transport, and the design of coastal infrastructure. The use of the wave spectrum for deep-water fetch-limited situations provides a reliable basis for these estimates, ensuring that they are applicable to real-world conditions. Overall, this table serves as a valuable tool for coastal engineers and planners in assessing and mitigating the risks associated with wave activity along Cambodia's shores (Janswap, 1969).

Table 3.2: Significant Wave Height from Various Fetch Lengths at Maximum Wind Speed Experienced by Cambodia

Fetch length (kilometers)	Wind speed (meters/second)	Duration (hours)	Max H_s (meters)
5	11 m/s = 40 km/hr	12	0.25
10	11	12	0.4
15	11	12	0.6
20	11	12	1.0
50	11	12	1.5
100	11	12	2.0
250	11	12	2.5
500	11	12	3.0
1,000	11	12	3.5
Hr = hour, H_s = significant wave height, km = kilometers, m/s =meters/second Note: Estimates performed using Jonswap (1969) wave spectrum for deep water fetch-limited situations.			

Source: ADB (2023)

3.2.3.3 Storm Surges

When a hurricane or major storm strikes, the water level rises, and strong winds send the water surging inland, what's known as storm surge. When the water levels are already high to begin with, storm surge and flooding will be more frequent and dangerous (NRDC, 2024). The table below provides a comprehensive overview of extreme water levels in Preah Sihanouk, Cambodia, considering both current conditions and future projections for 2060, including the impacts of climate change. The table compares tidal ranges and combined wave levels under semi-diurnal, diurnal, and occasional diurnal conditions.

Under climate change, the sea level is predicted to rise. This predicted sea level rise can be factored into the calculation of the future combined water level. Table 3.3 demonstrates an approximation of the total water level above the datum line in Preah Sihanouk province and shows a more significant overall flood risk than the sea level rise figure for the most extreme events likely to reach the exposed shores of Preah Sihanouk.

Table 3.3: Rule of Thumb Extreme Water Levels Based on the Tides at Preah Sihanouk; An Exposed Coastal Region

	Combined Water Level, 2022 (meters)	Combined Water Level 38-year Design Life; 2060, including Climate Change (meters)
Tidal Range	Semi-diurnal, occasionally diurnal, 0.0 mDL to **1.8 mDL**	Semi-diurnal, occasionally diurnal, 0.00 mDL to **1.80 mDL**
Swell Waves	6.00 m in deep water	6.60 m (plus 10% under CC)
Wind Waves[a]	**3.50 m** (in deep water) **1.20 m** (=3.5/3 in shallow water) 0.00 m sheltered from ocean	**3.85 m** (plus 10% under CC, deep) **1.30 m** (=3.85/3 in shallow) 0.00 m sheltered from ocean
Storm Surge	**0.50** m	**0.55 m** (plus 10% under CC)
Sea Level Rise	0.00 m	**0.50 m** (0.32 m +/-0.2m under H^{++})
Tsunami[a]	Low risk 0.25-2.0 m (not included)	Low risk 0.25-2.0 m (not included)
Above Datum Line (Z_0)[b]	Max. 5.80 mDL exposed deep water **Max. 3.50 mDL exposed shoreline** Max. 2.20 mDL sheltered shoreline	Max. 6.70 mDL exposed deep water **Max. 4.15 mDL exposed shoreline** Max. 2.75 mDL sheltered shoreline

CC = climate change, DL = datum line, H++ = extreme prediction of future sea level (presently on track), m = meters, Z_0 = height above datum.

Notes:

These are the most exposed areas (non-sheltered) to open ocean waves along the Cambodian shoreline and therefore represent the worst-case scenario. Table produced for this report.

[a] Tsunami hazard is classified as low according to the information that is available as of 2023. This means that there is more than a 2% chance of a potentially damaging tsunami occurring in the next 50 years.

[b] The datum line (DL) will be different at each location around the shoreline, following the example provided in section 2.4.3. For example, at Sihanoukville subtracting 0.99 m from the combined water levels above will correct relative to mean sea level (mMSL).

Sources: JICA. 2015. Tidal analysis 2013–2014, in Sihanoukville Cambodia; and UNFCC. 2015. Cambodia's Second National Communication. Government of Cambodia, Ministry of Environment.

Source: ADB (2023)

Focusing on storm surges in the coastal area of Cambodia, the table indicates that the current storm surge risk is relatively low, with a height of 0.50 meters for both semi-diurnal and diurnal conditions. However, when considering the effects of climate change by 2060, the storm surge height is projected to increase slightly to 0.55 meters. This increase, though modest, highlights the potential for more significant impacts on coastal areas due to rising sea levels and changing weather patterns. Sea level rise escalates the threat of extreme weather. The data underscores the importance of preparing for future changes in storm surge levels, as even small increases can exacerbate coastal erosion, flooding, and damage to infrastructure. The projections suggest that while the current risk is manageable, ongoing monitoring and adaptive measures will be crucial to mitigate the impacts of climate change on Cambodia's coastal regions. This information is vital for coastal planners and engineers to develop resilient infrastructure and implement effective coastal management strategies.

3.3 Observed Changes in Coastal Ecosystems

3.3.1 Past and Future Changes in Marine and Terrestrial Cryosphere

Alterations within the cryosphere have far-reaching consequences for physical, biological, and human systems, affecting not only mountainous terrains but also adjacent lowlands. Certain impacts extend even further, reaching the ocean and coastal zones (Hock et al., 2019). Cambodia, for instance, is significantly influenced by changes in the cryosphere as it receives a substantial portion of its water supply from the Mekong River, which originates from the Tibetan Plateau, fed in part by meltwater from mountain glaciers (MRC, 2023). Shifts in the cryosphere can lead to both increased flooding and

prolonged droughts, setting off a chain reaction with profound effects on Cambodia's key economic sectors, including water resources, agriculture and fisheries, tourism and culture, transport infrastructure, and industry.

3.3.1.1 Atmospheric Drivers of Changes in the Mountain Cryosphere

1. **Surface Air Temperature**

Recent observations indicate that mountain surface air temperatures in western North America, the European Alps, and High Mountain Asia have been rising at an average rate of 0.3 C per decade, with a likely range of ±0.2 C. This rate surpasses the global average warming rate of 0.2 ± 0.1 C per decade (IPCC, 2018). Figure 3.7 compiles data from various global and regional studies, highlighting these mountain warming trends, primarily based on in situ observations.

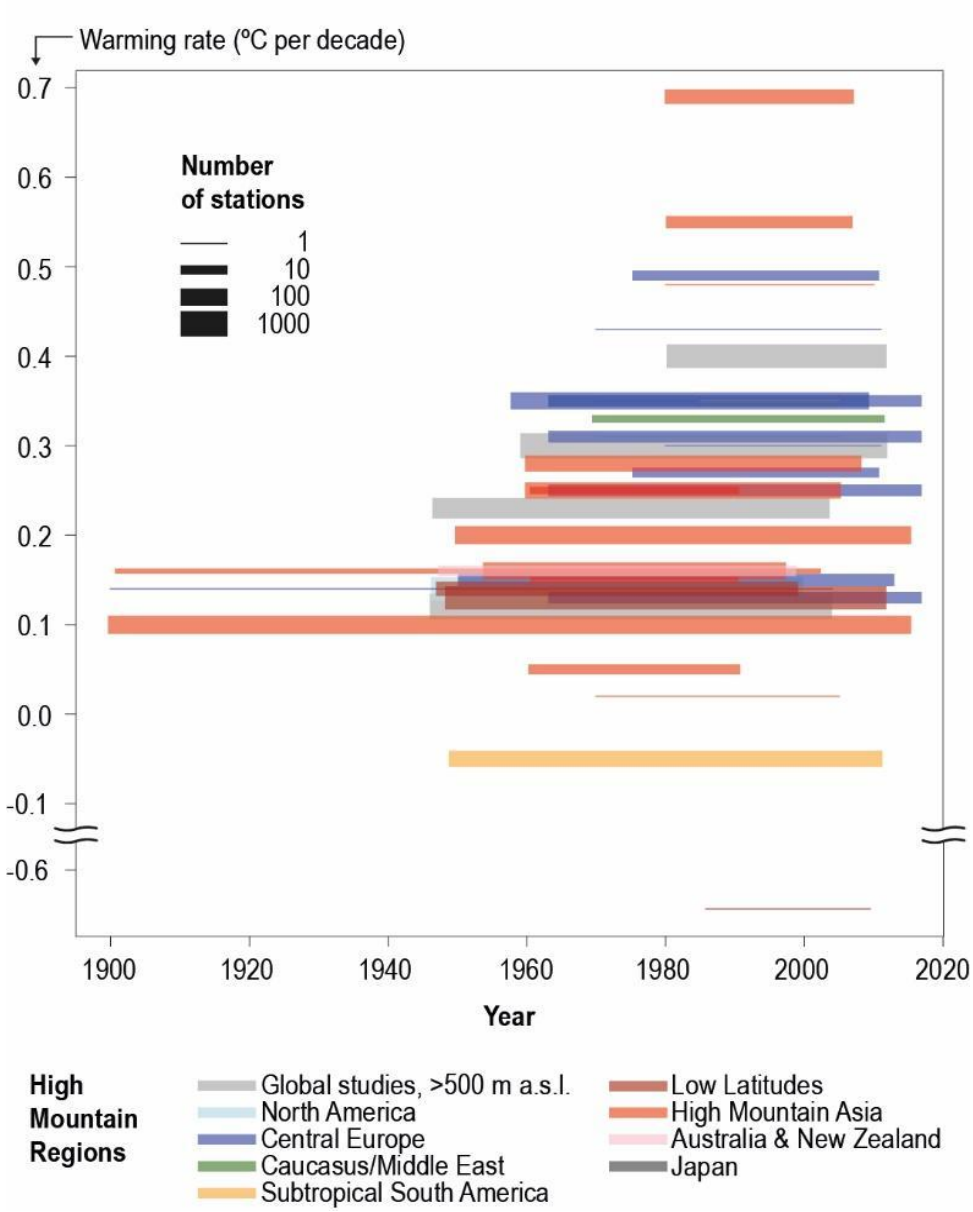

Figure 3.7: Trends in mean annual surface air temperature in mountain regions, based on 4672 observation stations from 38 datasets in 19 studies.
Source: IPCC (2019)
Note: Synthesis of trends in mean annual surface air temperature in mountain regions, based on 4,672 observation stations (partly overlapping) aggregated into 38 datasets reported in 19 studies. Each line

represents a warming rate from one dataset, calculated over the time period indicated by the extent of the line. Colors indicate the mountain region (Figure 3.8), and line thickness corresponds to the number of observation stations used. Detailed references are found in Table SM2.2 in the Intergovernmental

On the Tibetan Plateau, combining in situ observations, which are often limited at high elevations, with remote sensing and modeling approaches reveals that warming is more pronounced around 4,000 meters above sea level, but not above 5,000 meters (Tang et al., 2018). Research in the Italian Alps (Tudoroiu et al., 2016) and the southern Himalaya (Nepal, 2016) also shows greater warming at lower elevations. Figure 3.8 also provides additional information on trends for individual seasons and other temperature indicators (daily minimum or maximum temperature).

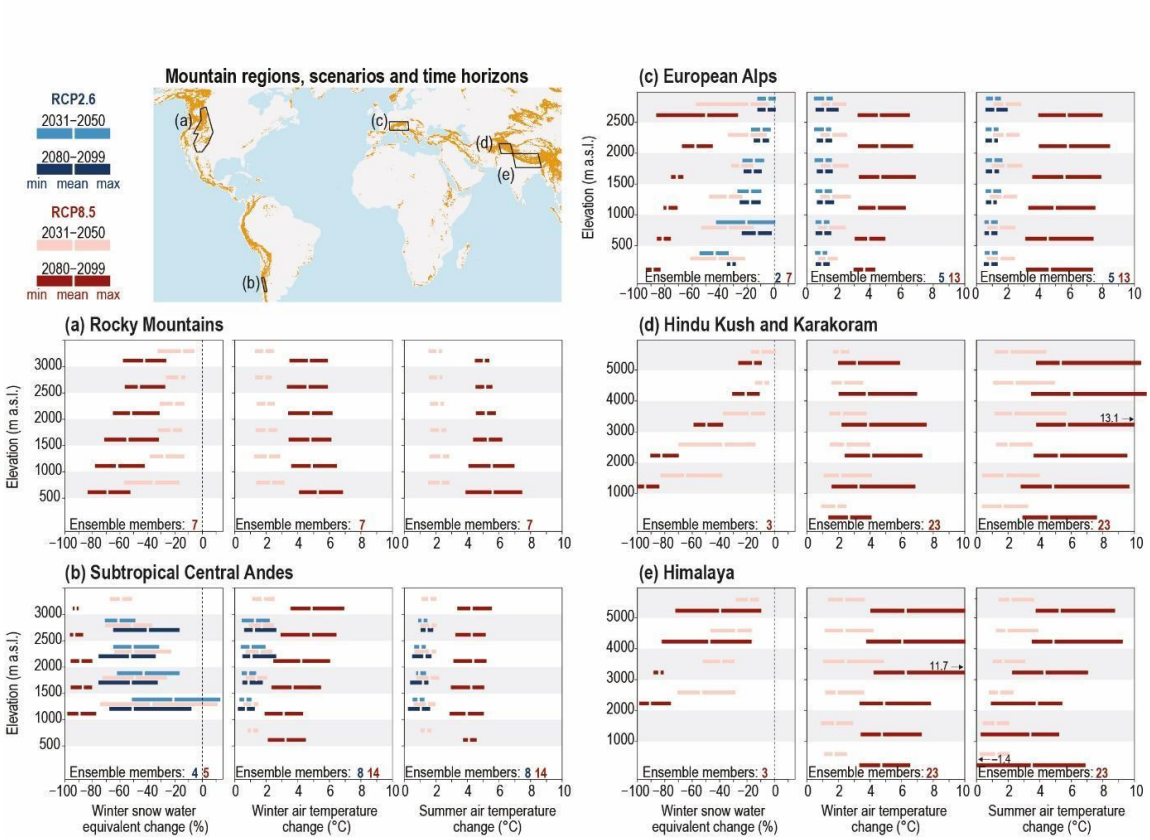

Figure 3-.8: Projected changes (1986–2005 to 2031–2050 and 2080–2099) in mean winter snow water equivalent, winter air temperature, and summer air temperature in five high mountain regions under RCP8.5 (all regions) and RCP2.6 (European Alps and Subtropical Central Andes).
Source: IPCC (2019)
Note: Projected change (1986–2005 to 2031–2050 and 2080–2099) of mean winter (December to May; June to August in Subtropical Central Andes) snow water equivalent, winter air temperature, and summer air temperature (June to August; December to February in Subtropical Central Andes) in five high mountain regions for RCP8.5 (all regions) and RCP2.6 (European Alps and Subtropical Central Andes). Changes are averaged over 500 m (a, b, c) and 1,000 m (d, e) elevation bands. The numbers in the lower right of each panel reflect the number of simulations (note that not all models provide snow water equivalent).

2. Rainfall and Snowfall

Past changes in precipitation are less well-documented than temperature changes and show more variability within mountain regions (Hartmann & Andresky, 2013). While there is medium confidence that no clear trend in annual precipitation exists, snowfall has decreased, particularly at lower elevations due to higher temperatures (high confidence).

Future projections indicate a 5-20 percent increase in annual precipitation in many mountain regions, including the Hindu Kush, Himalaya, East Asia, eastern Africa, the European Alps, and the Carpathian region, with decreases in the Mediterranean and southern Andes (medium confidence). The frequency and intensity of extreme precipitation events will vary by season and region. For instance, in the Himalayan-Tibetan Plateau, extreme rainfall events are expected to increase throughout the 21st century, especially during the summer monsoon (Panday et al., 2015; Sanjay et al., 2017), indicating a shift towards more episodic and intense monsoonal precipitation, particularly in the eastern Himalayas (Palazzi et al., 2013).

3. Other Meteorological Variables

Atmospheric humidity, radiation, and wind speed significantly influence the high mountain cryosphere. Detecting their changes is challenging, so most studies focus on temperature and precipitation (Beniston et al., 2018). Wind affects snow deposition and glacier ablation. On the Tibetan Plateau, near-surface wind speed decreased from the 1970s to early 2000s, then stabilized or slightly increased (Yang et al., 2014a; Kuang and Jiao, 2016). This trend aligns with mid-latitude continental areas (Hartmann et al., 2013). However, research on wind patterns in mountain areas remains limited.

3.3.1.2 Snow Cover

Snow cover in the Tibetan Plateau and High Mountain Asia, which includes the Hindu Kush, Karakoram, and Himalayas, plays a crucial role in mountain ecosystems. It influences mass movements, such as landslides; contributes to floods; and nourishes glaciers, while also providing an insulating and reflective cover. This snow cover is particularly sensitive to climate change, especially in low-lying and mid-elevation areas.

The changes in snow cover in High Mountain Asia have significant implications for Cambodia. The region's snow and glacier melt contribute to the flow of major rivers, including the Mekong River, which is crucial for Cambodia's water supply, agriculture, and fisheries. Changes in snow cover and melt patterns can affect the timing and volume of river flows, impacting water availability and increasing the risk of floods and droughts in Cambodia (Chu et al., 2023).

Figure 3.8 provides projections of temperature and snow cover in mountain areas in Europe, High Mountain Asia (Hindu Kush, Karakoram and Himalaya), North America (Rocky Mountains) and South America (sub-tropical Central Andes), illustrating how changes vary with elevation, season, region, future time period and climate scenario.

3.3.1.3 Permafrost

Permafrost in high mountain Asia, including the Tibetan Plateau, has experienced significant warming in recent decades. This warming is attributed to increased air temperatures and changes in snow cover. Observations indicate that permafrost in this region warmed by an average of 0.19 ± 0.05°C per decade between 2007 and 2016 (Biskaborn et al., 2019). Over longer periods, observations in the European Alps, Scandinavia, Mongolia, the Tien Shan, and the Tibetan Plateau (Cao et al., 2018) show general warming and degradation of permafrost at individual sites (Phillips et al., 2009) (Table 3.4). The degradation of permafrost is evident through ground-ice loss and increased thickness of the active layer, which is the layer of ground above permafrost that thaws and freezes annually (Cao et al., 2018). The observed thickness of the active layer increased in the European Alps and Scandinavia (Christiansen et al., 2010) and on

the Tibetan Plateau during the past few decades, indicating permafrost degradation (Table 3.5).

The warming of permafrost in high mountain Asia has critical implications for the stability of mountain slopes and the integrity of infrastructure. As permafrost thaws, it can lead to increased landslides and other mass movements, posing risks to communities and ecosystems in the region (Phillips et al., 2009).

Table 3.4: Observed changes in permafrost Mean Annual Ground Temperature (MAGT) in mountain regions

Region	Elevation [m a.s.l.]	Surface Type	Period	MAGT [°C]	MAGT trend [°C per decade]	Reference
Global	>1,000	various (28)	2006–2017	not specified	0.2 ± 0.05	Biskaborn et al. (2019)
European Alps	2,500–3,000	debris or coarse blocks (>10)	1987–2005 2006–2017	>-3 >-3	0.0–0.2 0.0–0.6	PERMOS (2016) Noetzli et al. (2018)
	3,500–4,000	bedrock (4)	2008–2017	>-5.5	0.0–1.0	Pogliotti et al. (2015) Magnin et al. (2015) Noetzli et al. (2018)
Scandinavia	1,402–1,505	moraine (3)	1999–2009	0 to – 0.5	0.0–0.2	Isaksen et al. (2011)
	1,500–1,894	bedrock (2)	1999–2009	-2.7	0.5	Christiansen et al. (2010)
High Mountain Asia (Tien Shan)	~3,330	bare soil (2)	1974–2009	-0.5 to – 0.1	0.3–0.6	Zhao et al. (2010)
	3,500	meadow (1)	1992–2011	-1.1	0.4	Liu et al. (2017)
High Mountain Asia (Tibetan Plateau)	~4,650	meadow (6)	2002–2012	-1.52 to – 0.41	0.08–0.24	Wu et al. (2015)
	~4,650	steppe (3)	2002–2012	-0.79 to – 0.17		Wu et al. (2015)
	~4,650	bare soil (1)	2003–2012	-0.22	0.15	Wu et al. (2015)
	4,500–5,000	unknown (6)	2002–2011	-1.5 to – 0.16	0.08–0.24	Peng et al. (2015)
North Asia (Mongolia)	1,350–2,050	steppe (6)	2000–2009	-0.06 to – 1.54	0.2–0.3	Zhao et al. (2010)

Source: IPCC (2019)

Note: Values are based on individual boreholes or ensembles of several boreholes. The MAGT refers to the last year in a period and is taken from a depth of 10–20 m unless the borehole is shallower. Numbers in brackets indicate how many sites are summarized for a particular surface type and area; the underscored value is an average. Elevation is meters above sea level (m a.s.l.).

Table 3.5: Observed changes of active-layer thickness (ALT) in mountain regions.

Region	Elevation [m a.s.l.]	Surface Type	Period	ALT in last year [m]	ALT trend [cm per decade]	Reference
Scandinavia	353–507	peatland (9)	1978–2006 1997–2006	~0.65–0.85	7–13 13–20	Åkerman and Johansson (2008)
European Alps	2,500–2,910	bedrock (4)	2000–2014	4.2–5.2	10–100	PERMOS (2016)
High Mountain Asia (Tien Shan)	3,500	meadow (1)	1992–2011	1.70	19	Liu et al. (2017)
High Mountain Asia (Tibetan Plateau)	4,629–4,665	meadow (6)	2002–2012	2.11–2.3	34.8–45.7	Wu et al. (2015
	4,638–4,645	steppe (3)	2002–2012	2.54–3.03	39.6–67.2	Wu et al. (2015)
	4,635	bare soil (1)	2002–2012	3.38	18.9	Wu et al. (2015)
	4,848	meadow	2006–2014	1.92–2.72	15.2–54	Lin et al. (2016)

Source: IPCC (2019)

Note: Numbers in brackets indicate how many sites are summarized for a particular surface type and area. Elevation is meters above sea level (m a.s.l.)

3.3.1.4 Glaciers

Glaciers in High Mountain Asia, encompassing the Hindu Kush, Karakoram, and Himalayas, are vital for regional water resources and ecosystems. These glaciers have demonstrated the least negative mass budget compared to other regions, with an average loss of -150 ± 110 kg m² per year.

Figure 3.9 illustrates the spatial variability in glacier mass balance across High Mountain Asia. It highlights the regions with the most negative mass balances, such as the

Nyainqentanglha range, and those with nearly balanced or slightly positive mass balances, like the Kunlun Mountains. The figure provides a visual representation of the diverse climatic and glaciological conditions within High Mountain Asia, emphasizing the significant regional differences in glacier mass changes. This variability underscores the complexity of glacier dynamics in response to climate change and the importance of localized studies to understand and predict future changes in glacier behavior.

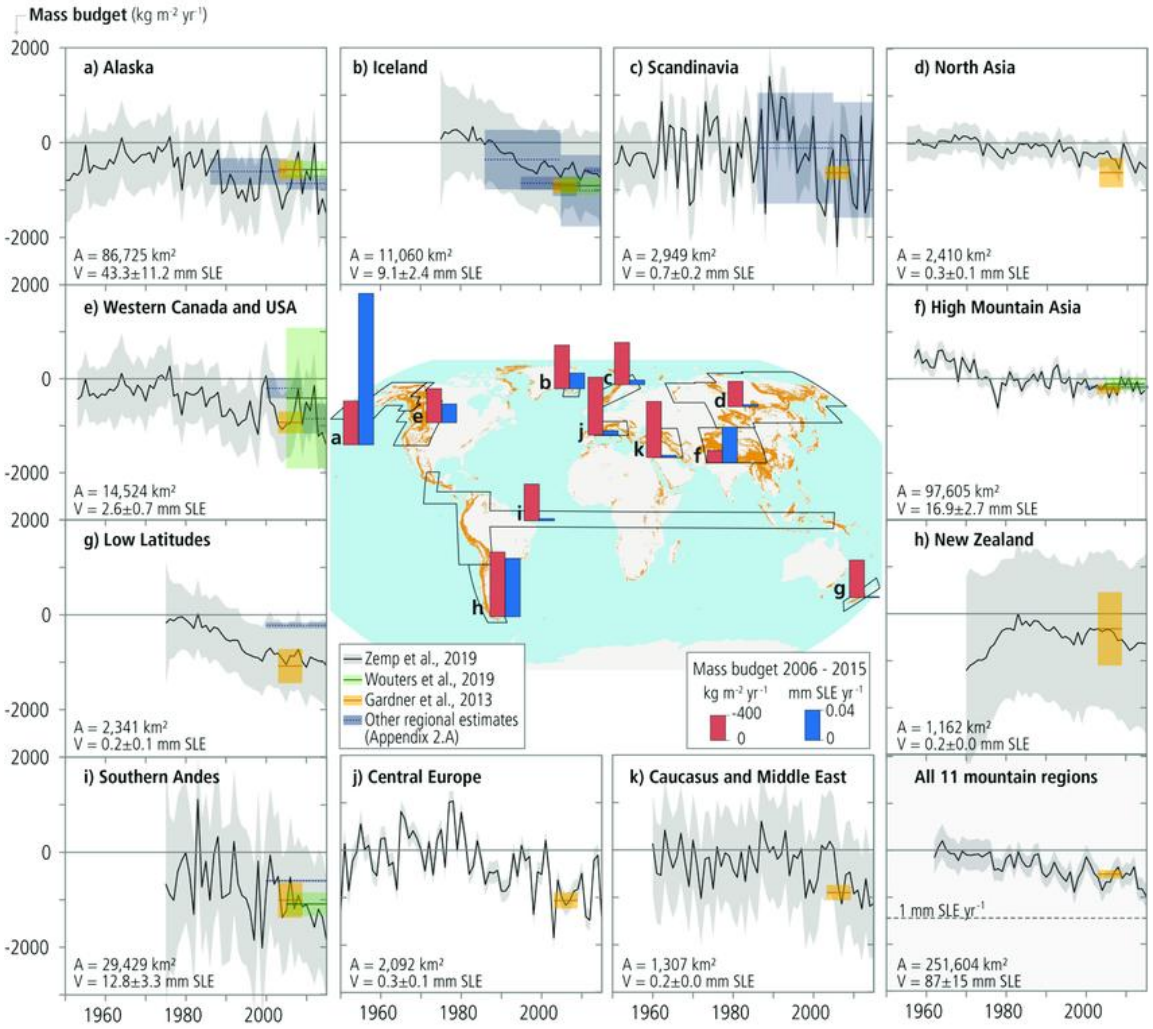

Figure 3.8: Glacier mass budgets for the eleven mountain regions
Source: IPCC (2019)

3.3.1.5 Lake and River Ice

Observations of lake and river ice in high mountain Asia, particularly on the Tibetan Plateau, show highly variable trends in ice cover duration over recent decades. Studies have reported both shorter and longer ice cover durations for different lakes in the region. For instance, Cai et al. (2019) found that between 2000 and 2017, 40 lakes on the Tibetan Plateau experienced shorter ice cover durations, while 18 lakes had longer durations. Similarly, Du et al. (2017) observed shorter ice cover durations for 43 out of 71 lakes larger than 50 km² during 2002–2015, although only five of these trends were statistically significant due to large interannual variability.

These variable trends in ice cover duration correspond to changes in surface water temperatures. Yang et al. (2014) reported that of 52 study lakes on the Tibetan Plateau, 31 showed a mean warming rate of 0.055 ± 0.033°C per year, while 21 lakes exhibited a mean cooling rate of -0.053 ± 0.038°C per year during 2001–2012.

The primary drivers of these changes in lake ice dynamics are air temperature and solar radiation. However, in mountainous regions like the Tibetan Plateau, additional factors such as lake morphometry, wind exposure, salinity, and hydrology, particularly processes driven by glaciers, also play significant roles (Kropácek et al., 2013; Song et al., 2014; Yao et al., 2016; Gou et al., 2017). Despite the high spatial and temporal variability, there is a general trend towards later freezing, earlier break-up, and shorter ice cover duration in the future as air temperatures continue to rise (Gebre et al., 2014; Du et al., 2017).

Changes in lake and river ice on the Tibetan Plateau significantly impact Cambodia's coastal and terrestrial cryosphere through the Mekong River, as detailed in Wangmo (2022). The altered ice dynamics, driven by rising temperatures, affect the hydrological cycle, leading to shifts in water flow timing and volume. This influences river discharge patterns, exacerbates sea level rise, and impacts aquatic ecosystems, agriculture, and socioeconomic conditions in Cambodia. Consequently, these changes pose challenges for water resource management, biodiversity, and community livelihoods, highlighting the interconnectedness of regional cryosphere changes and the far-reaching effects of changes.

3.3.2 Biodiversity Indices

3.3.2.1 Current State of Coastal and Marine Ecosystems

Cambodia comprises 25 municipalities and provinces, with four coastal provinces: Kep, Kampot, Preah Sihanouk, and Koh Kong, which feature a coastline stretching 440 km. The country is abundant in natural resources, particularly within its coastal and marine ecosystems, which include mangrove forests, coral reefs, seagrass beds, salt marshes, and estuaries. These ecosystems are crucial for Cambodia's economic development and the livelihoods of local communities. A study by the Asian Development Bank in 2000 estimated that coastal and marine biodiversity contributes approximately USD 12 million annually to local communities and the national economy. Cambodian coastal waters are among the richest in biodiversity globally, hosting significant aquatic resources and endangered marine species such as green turtles, dolphins, sharks, coral reefs, seagrasses, mangroves, groupers, shrimps, tortoises, and dugongs (UNEP, 2005).

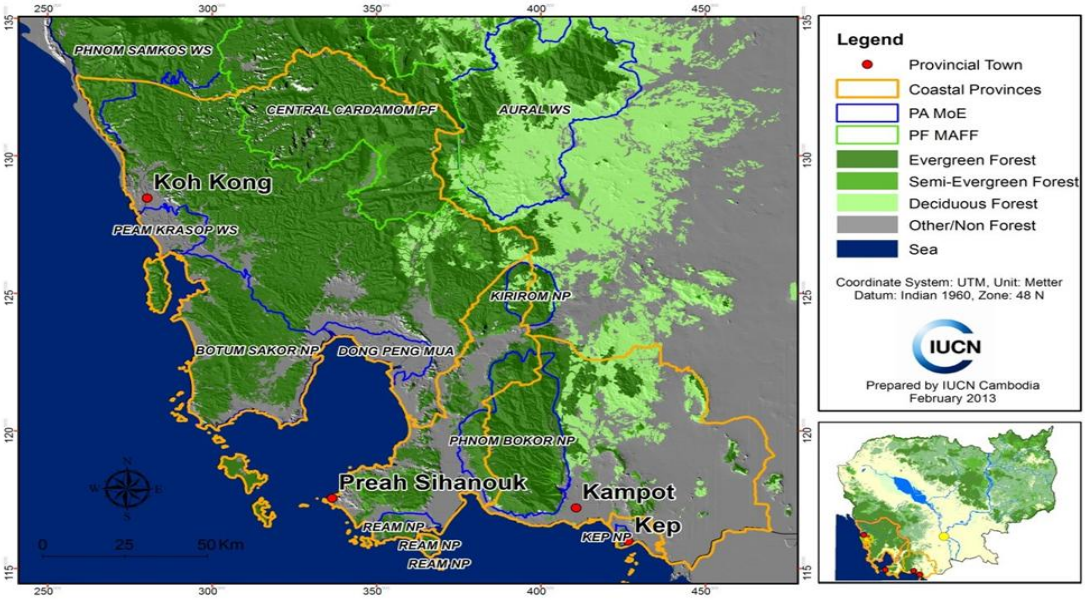

Figure 3.9: Coastal provinces of Cambodia
Source: IUCN (2013)

3.3.2.2 Current State of Mangrove Forest

Cambodia's wetlands, primarily dominated by mangrove forests, are crucial ecosystems. These mangroves, comprising 74 species, form relatively pristine forests that grow in four major zones from the shoreline to the landward edge (PEMSEA & MoE, 2019). In 1992, the total area of mangrove forests in Cambodia was 85,100 ha. IUCN (2013) indicated that the majority of these mangroves were located in Koh Kong province (63,200 ha), followed by Preah Sihanouk (13,200 ha), Kampot (7,300 ha), and Kep (1,400 ha).

The largest and most pristine mangrove forests are located in the estuary of Peam Krasob/Koh Sralao in Koh Kong province. Smaller mangrove areas can also be found in estuaries such as Koh Por, Koh Yor, Dong Tong, Andoung Tuk, and Sre Ambel. These mangroves are vital for biodiversity, providing habitats for various species and protecting coastal areas from erosion and natural disasters.

As Table 3.6 demonstrates, there was a significant reduction in mangrove areas, amounting to 4,835 ha, between 1993 and 1997. The most substantial losses occurred in the districts of Botum Sakor, Smach Meanchey, and Sre Ambel, with decreases ranging from 3 percent to 20 percent of their 1993 distribution. This decline was documented through various surveys, including the Forest Cover Monitoring Report in 1993 and 1997, JICA 1997 Land Use Data, and MoE interpretations from 2002, 2005, and 2011 (PEMSEA, 2019).

Between 1997 and 2002, Cambodia's coastal mangrove forests saw a reduction of 6,740 ha, with the most significant losses in Kampong Trach and Botum Sakor districts. From 1997 to 2005, approximately 7,759 ha were degraded, again primarily in Kampong Trach and Botum Sakor. By 2011, the total degraded area reached about 12,181 ha, as shown in Table 3.7, with major reductions in Botum Sakor, Koh Kong, and Kampong Trach districts (PEMSEA, 2019).

Table 3.6: Change in Mangrove Distribution from 1992 to 1997

District	1992/1993	1996/1997	Change	percent Change
Kampong Trach	1162	1162	0	0
Kampot	726	726	0	0
Kampong Bay	363	363	0	0
Botum Sakor	18520	16656	-1864	-10.1
Kiri Sakor	5741	5741	0	0
Koh Kong	13395	12971	-424	-3.2
Smach Meanchey	3133	2703	-430	-13.7
Modol Seima	10811	10811	0	0
Sre Ambel	10817	8700	-2117	-19.6
Prey Nob	586	586	0	0
Stung Hav	10518	10518	0	0
Damnak Chang'aeur	672	672	0	0
Kep	74	74	0	0
Total	76518	71683	-4835	-6.3

Source: PEMSEA (2019) (Data from the Department of Forestry and Wildlife, February 1999. Forest Cover Monitoring Book. This statistical information is supported by GTZ according to the Forest Cover Monitoring report).

Table 3.7: Change in Mangrove Distribution from 1997 to 2011

Districts	1997 (ha)	2002 (ha)	2005 (ha)	2011 (ha)	Change 1997-2002	Change 1997-2005	Change 1997-2011
Kampong Trach	3854	319	350	1191	-3535	-3504	-2663
Tuek Chhou	1179	660	667	759	-519	-512	-420
Kampot	585	408	431	365	-177	-154	-220
Damnak Chang'aeur	952	666	710	538	-286	-242	-414
Kaeb	130	165	154	132	35	24	2
Botum Sakor	12889	11216	11502	9127	-1673	-1387	-3762
Kiri Sakor	4360	4203	4421	2507	-157	61	-1853
Kaoh Kong	11150	11044	10388	8099	-106	-762	-3051
Khemarakphumint	2085	2265	2108	1628	180	23	-457
Mondol Seima	6027	6889	6137	6282	862	110	255
Srae Ambe	11112	10452	10234	9518	-660	-878	- 1594
Preah Sihanouk	146	45	45	115	-101	-101	-31
Prey Nob	7402	7479	7206	9351	77	-196	1949
Stueng Hav	352	490	929	769	138	577	417
Kampong Seila	818	0	0	55	-818	-818	-763
Coastal Zone	**63041**	**56301**	**55282**	**50860**	**-6740**	**- 7759**	**-12181**

Source: PEMSEA (2019) (Data from SOECCSR. 2013. JICA 1997 Land Use Data; MoE-CCU. 2002, 2005 and 2011 Interpretation)

3.3.2.3 Seagrass Beds

Seagrasses thrive in shallow, protected coastal waters, providing essential habitats for juvenile fish and serving as nurseries for various fish species. Cambodia has extensive seagrass beds. The most extensive seagrass beds are found in Kampot bay, followed by Koh Kong province. These seagrass beds also offer shelter and feeding grounds for numerous invertebrates and fish, many of which have significant economic value. Additionally, they serve as crucial feeding areas for endangered species such as dugongs and marine turtles. Nutrients produced by seagrass beds can also be transferred to nearby ecosystems, such as coral reefs (MoE, 2005).

In Cambodia, seagrasses are found in two main types: extensive meadows along the mainland and patches interlinked with coral reefs around islands. The total seagrass areas account for 33,814 ha. 3,831 ha are managed in Marine Protected Areas and Community Fisheries (Table 3.8). The largest seagrass beds in Southeast Asia, with a total area of 25,240 ha, are located in Kampot province. However, these beds face threats from water quality degradation and destructive fishing practices, such as the use of push nets and trawling. Water quality issues stem from siltation due to logging, increased use of fertilizers and pesticides in coastal agriculture, and the discharge of domestic and industrial wastewater (MoE, 2005). Increased water turbidity reduces sunlight penetration, affecting the photosynthetic capacity of seagrass plants (UNEP, 2008).

Table 3.8: Distribution and management status of seagrass beds of four coastal provinces

No	Province	Seagrass area (ha)	Area under management (ha)	Location of area under management
1	Kampot	25,240	1,500	Chang Houn-Trapeang Ropov

2	Koh Kong	3,993	1,000	Chroy Bros
3	Kep	3,095	731	Kep
4	Preah Sihanouk	1,486	600	Keo Phos
Total		**33,814**	**3,831**	

Source: MFF (2013) (data from DRF, 2013).

There are about 1,486 ha of seagrass beds situated in Preah Sihanouk province (Table 3.8). At present, 3,831 ha, accounting for approximately 11 percent of total seagrass beds, are under management for all coastal provinces of Cambodia. As indicated in the Strategic Planning Framework for Fisheries: 2010-2019, 9,000 ha, representing around 27 percent of total seagrass beds were put under management in 2019.

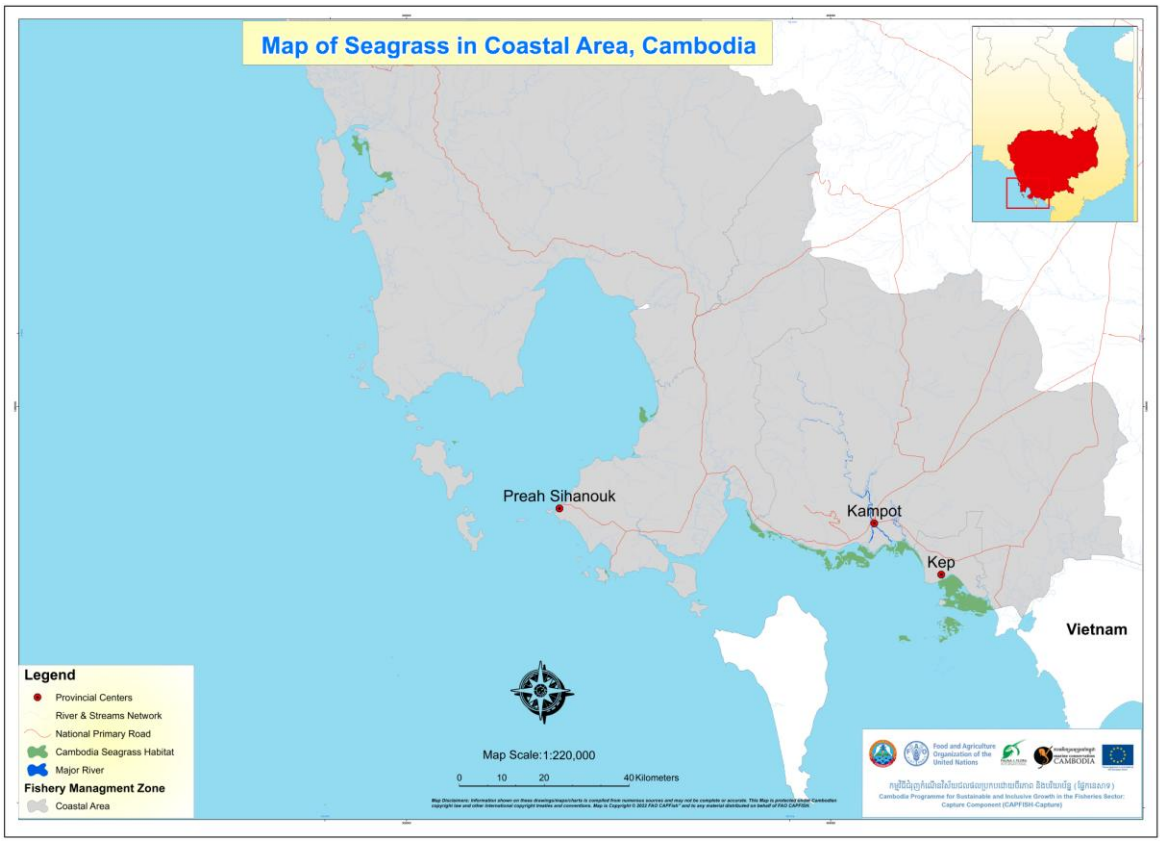

Figure 3.10: Location of Seagrass Distribution in Cambodia
Source: FAO CAPFish (2022)

3.3.2.4 Coral Reefs

Coral reefs are crucial coastal ecosystems that offer numerous social and economic benefits to local communities. Coral reefs, due to their physical structure, support a high diversity of invertebrates and fish, resulting in greater species abundance and diversity compared to open water (MoE, 1999). Cambodian waters host around 70 coral species, providing habitats for various fish species. The vast majority of coral reef habitat is classified as fringing reef, situated around Cambodia's 69 islands.

Surveys of coral reefs have been conducted by several projects funded by development partners and UN Agencies. These include Phase 2 of the Environmental Management in the Coastal Zone project by DANIDA, additional research and annual monitoring by the Fisheries Administration (FiA) funded by UNEP (MFF, 2013), and CAPFish funded by FAO (2022). However, information on the distribution of coral reefs in Cambodia is limited. Some offshore islands are known to have significant coral reefs, but the diversity of plant

and animal species in these areas is not well-documented. The DANIDA coastal zone management project has provided data on the location and extent of nearshore coral reefs (Figure 3.12). It was estimated that the Cambodian seascape contains approximately 2,700 ha of coral reef habitat located along the mainland coastline and fringing islands (Table 3.9). Of the 2,700 ha it is estimated the vast majority can be found in Koh Kong and Preah Sihanouk provinces (FiA, 2023). Local communities in Cambodia often engage in coral extraction and collection.

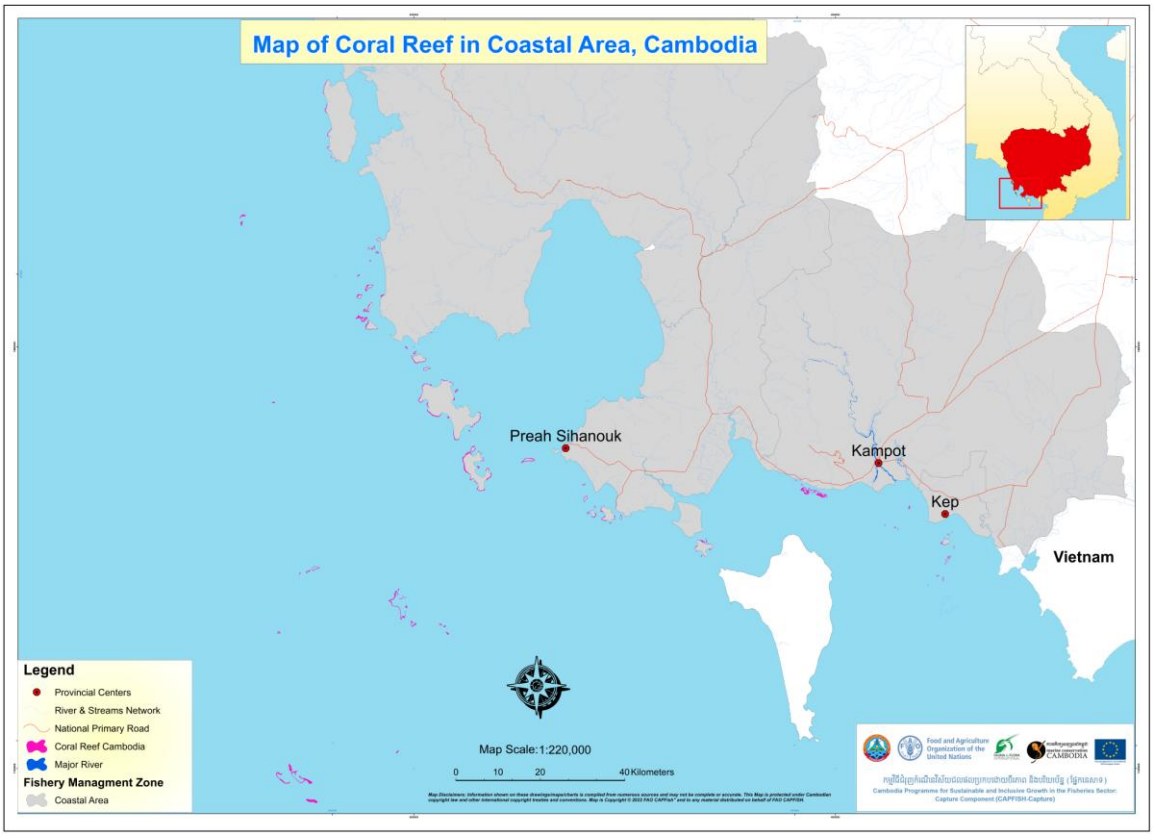

Figure 3.11: Location of coral reef distribution in Cambodia
Source: FAO CAPFish (2022)

Table 3.9: Distribution and management status of coral reefs of four coastal provinces

No	Province	Coral reefs (ha)	Area under management (ha)	Location of area under management	Type of Management
1	Kampot	953	-	-	-
2	Kep	52.5	-	-	-
3	Preah Sihanouk	1,198	468	Keo Phos	MFMA
4	Koh Kong	602	529	Chroy Bros	MFMA
Total		**2,805.5**			

Source: MFF (2013) (data from DRF, 2013).

3.3.3 Species Distribution and Abundance

3.3.3.1 Commercial Fish Abundance

Coral reefs, seagrass beds, and mangrove forests are interconnected habitats that play essential roles in supporting the abundance of commercial fish species. Coral reefs provide complex structures that offer shelter and breeding grounds, enhancing the

survival and growth of many fish species. Seagrass beds serve as critical feeding grounds and nurseries for juvenile fish, offering protection from predators and an abundant food supply (Honda et al., 2013; Serafy et al., 2015). Mangrove forests, with their intricate root systems, act as vital nursery habitats for many fish species, including those that later migrate to coral reefs and seagrass beds. Studies have shown that the presence of mangroves can significantly increase fish abundance on adjacent coral. The loss of any of these habitats can lead to a decline in fish diversity and abundance, emphasizing the need to conserve these interconnected ecosystems to sustain healthy fish populations (Whitfield, 2017).

The 2023 Fisheries Administration report classifies several taxonomic families of commercial fish species due to their significance in local fisheries. These families include grouper, parrotfish, barracuda, rabbitfish, bream, snapper, jack/trevally, and emperor. Condor Reef in Koh Kong Province exhibited the highest mean abundance of commercial fish species of the surveyed locations, with an average of 117 (±30.44 SE) individuals per 500 m^3 (Figure 3.13). FiA (2023) conducted a case study on the commercial fish abundance as shown in Figure 3.14: The isolated island of Koh Veal had the lowest mean abundance, with only 8.5 (±2.18 SE) individuals per 500 m^3. Notably, Koh Polou Wai recorded an exceptional outlier with a single observation of over 500 individuals per 500 m^3, attributed to a large school of parrotfish. Different locations showed varying dominant species. Snapper species were most frequently observed at Koh Sdach, Koh Rong MNP, Koh Ta Kiev, Condor Reef, and Shark Island. Rabbitfish dominated at Koh Kong Krao and Family Islands. Parrotfish were prevalent at Koh Tang and Koh Polou Wai. Grouper species were most common at Koh Veal. Barracuda were frequently observed at Koh Pring. These findings highlight the diversity and distribution of commercial fish species across different coastal habitats in Cambodia.

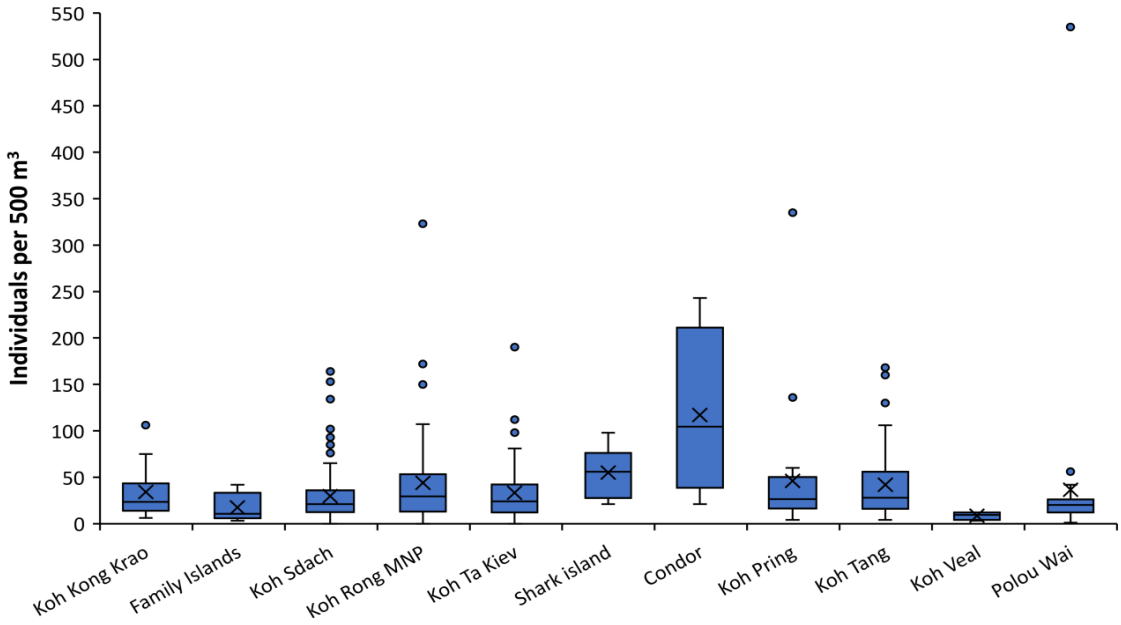

Figure 3.12: Abundance per 500 m^3 for all commercial fish families combined (Grouper, parrotfish, bream, barracuda, snapper, jack/trevally, emperors and rabbitfish)
Source: Fisheries Administration (2023)

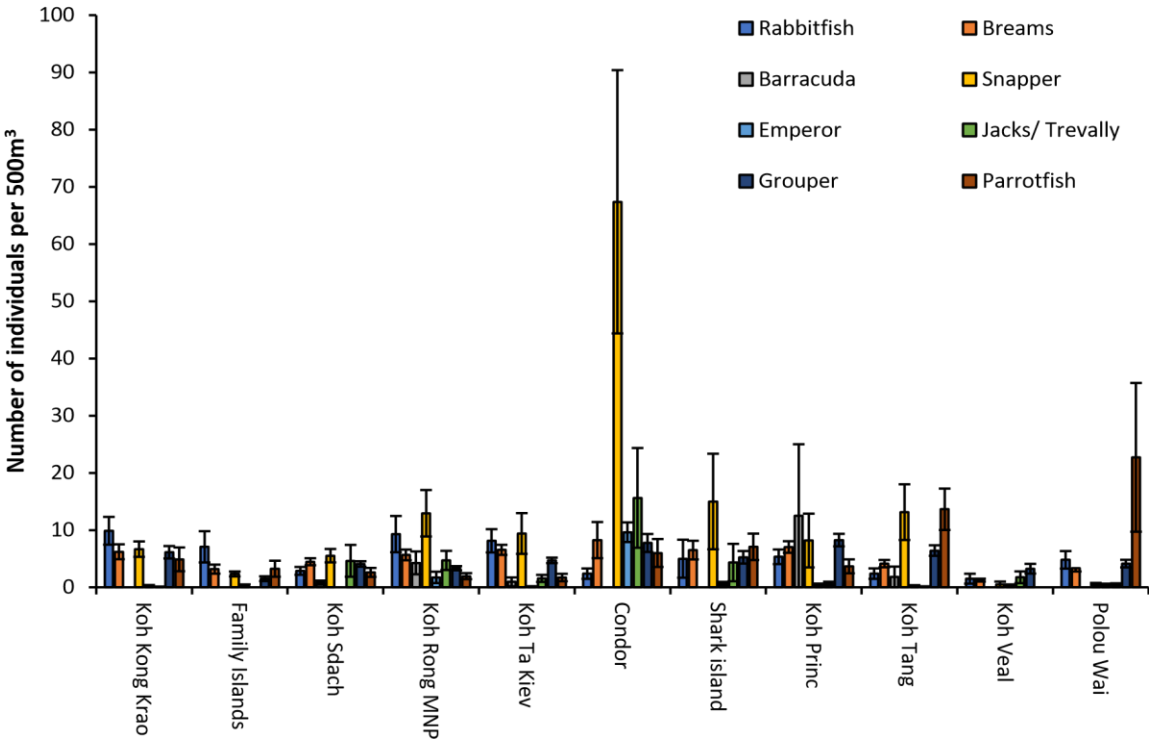

Figure 3.13: Commercial fish family abundance (indv/500m3) per survey location
Source: Fisheries Administration (FiA) (2023)

3.3.3.2 Invertebrate Abundance

According to the FiA (2023), Simpson's Index of Diversity was used to assess the species diversity of fish and invertebrate assemblages across different survey locations. This index quantifies diversity by considering the number of species present and their relative abundance. In the invertebrate survey, abundance was calculated for a 200 m² transect area (Figure 15). Species or families that appeared in unusually large numbers, such as fusiliers and long-spined urchins, were excluded to avoid skewing the results.

The mean abundance of long-spined urchins (Diadema spp.) was generally higher at outer island locations compared to nearshore locations. Koh Veal recorded the highest mean abundance of long-spined urchins at 1167 (±108.87 SE) individuals per 200 m², while Koh Kong Krao recorded the lowest at 0.041 (±0.041 SE) individuals per 200 m².

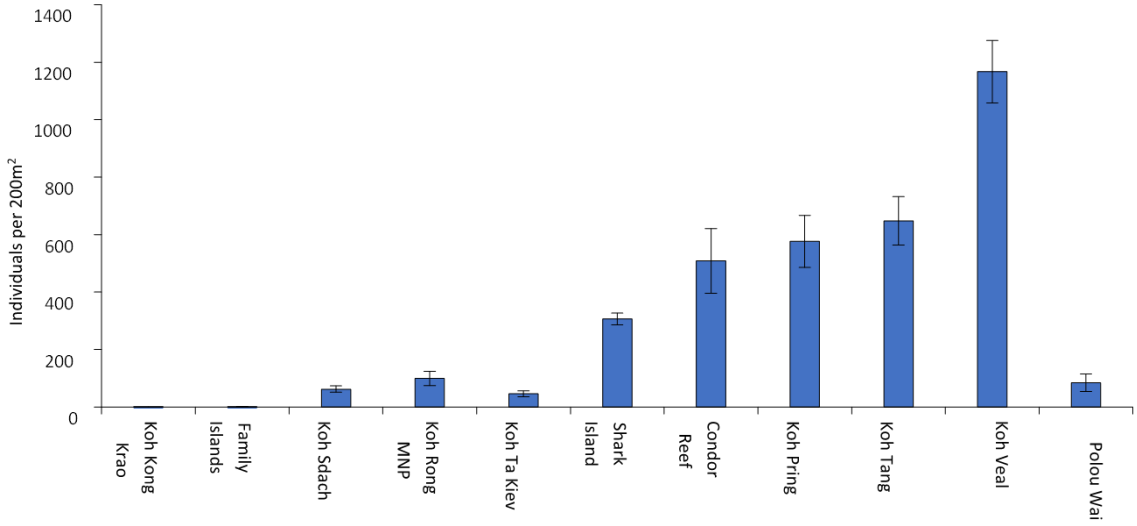

Figure 3.14: Long spined urchin (Diadema spp.) means abundance per 200m^2 for each survey location
Source: Fisheries Administration (2023)

The abundance of giant clams, which are key indicators of water quality and ecosystem health, was highest at Koh Tang and Shark Island, with both locations recording 1.75 individuals per 200 m² (Figure 3.16). The lowest abundance was observed at Koh Kong Krao with 0.125 individuals per 200 m². Giant clams were categorized by size, with the largest mean size class (31–40 cm) observed at Condor Reef and the smallest (0–10 cm) at Koh Polou Wai. These results underscore the importance of habitat-specific conservation efforts to maintain biodiversity and ecosystem health.

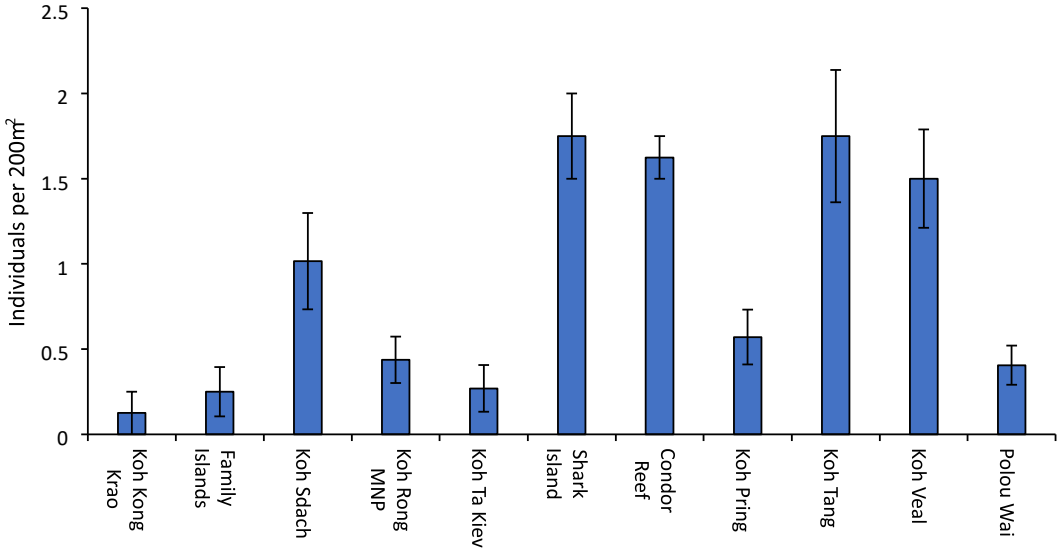

Figure 3.15: Mean abundance of Giant Clam (Tridacna spp.) observed at each survey location
Source: Fisheries Administration (2023)

3.3.4 Phenology Data

3.3.4.1 Phenology Data of Mangrove Forests in Cambodia

Mangrove forests in Cambodia are increasingly impacted by climate change and human activities (Table 3.10). Rising air temperatures threaten these ecosystems, affecting

species such as seabirds and marine turtles, which are sensitive to temperature extremes (Marshall & Johnson, 2007). Increased air temperatures lead to reduced water availability, range shifts (Hoegh-Guldberg et al., 2004), changes in the growing season, and ecosystem composition (Klein, 1999).

Species from plankton to corals and fish to seabirds are sensitive to water temperature changes (Marshall & Johnson, 2007). In mangrove systems, processes like respiration, photosynthesis, and productivity are influenced by temperature variations, resulting in reduced productivity at lower latitudes and increased winter productivity at higher latitudes as temperatures rise (Cheeseman et al., 1997; Clough & Sim, 1987).

Mangrove ecosystems are particularly vulnerable to rising sea levels, which significantly impact their distribution (Lovelock & Ellison, 2007). Sea level rise (SLR) in Cambodia leads to landward migration of mangroves, changes in vegetation structure, and reduced productivity, diminishing the ecosystem services provided by mangroves (Lovelock & Ellison, 2007). Human barriers preventing mangrove migration result in net losses, reducing coastal water quality, biodiversity, and fish nursery habitats, and negatively affecting adjacent coastal habitats (Ellison & Stoddart, 1991).

Fisheries are highly vulnerable to sea level rise (SLR), particularly in nursery grounds like mangroves and seagrass systems (Munday et al., 2008). SLR impacts connectivity among habitats, including estuaries and freshwater areas (Sheaves et al., 2006). Topographical changes caused by SLR affect organisms with specific spawning sites (Kingsford & Welch, 2007). Flood events and coastal inundation further impact fish species that rely on mangrove systems as nursery grounds (Lovelock & Ellison, 2007; Munday et al., 2007). Additionally, reduced rainfall adversely affects mangroves (Lovelock & Ellison, 2007).

Table 3.10: Impacts of Climate Change on Mangrove Ecosystems in Cambodia

Impact Factor	Description	References
Air Temperature	Sensitivity of species such as seabirds and marine turtles to temperature extremes	Marshall & Johnson, 2007
Water Temperature	Effects on respiration, photosynthesis, and productivity; reduced productivity at low latitudes	Cheeseman et al., 1997; Clough & Sim, 1987
Sea Level Rise (SLR)	Landward migration of mangroves, changes in vegetation structure, reduced ecosystem services	Lovelock & Ellison, 2007
Fisheries Vulnerability	Impact on nursery grounds, connectivity among habitats, and spawning sites	Munday et al., 2008; Sheaves et al., 2006; Kingsford & Welch, 2007
Rainfall Reduction	Adverse effects on mangrove health and productivity	Lovelock & Ellison, 2007

Source: Bezuijen et al. (2011)

3.3.4.2 Phenology Data of Coral Reef Systems

Coral reef systems in tropical regions are significantly impacted by climate change, particularly through increased water temperatures, which lead to coral bleaching. This occurs when corals expel their symbiotic dinoflagellate zooxanthellae due to stress from elevated sea temperatures (Veron et al., 2009). Even small increases in sea temperature

(1-2°C) above the long-term summer maxima can destabilize the relationship between corals and their symbiotic algae, essential for their energy and growth.

Increased water temperatures affect the reproductive output of coral colonies and the success of early life stages, leading to incomplete fertilization and decreased symbiont density in larvae (Bassim et al., 2002). Tropical cyclones cause physical damage to coral structures, resulting in flattened reefs and displaced coral skeletons, which are unsuitable for new coral settlement until natural consolidation occurs (Fabricius et al., 2007). Corals are also affected by changes in light regimes, with more intense storms and flood events leading to increased mortality and altered community composition due to nutrient and sediment influx (Hoegh-Guldberg et al., 2007). Ocean acidification further impacts corals' ability to accrete calcium carbonate, essential for their skeletal structure (Hoegh-Guldberg, 2007).

3.3.4.3 Phenology Data of Seagrass

Seagrass species must adapt to a wide range of conditions brought about by climate variability, including increased temperature, decreased light availability, physical disturbances from cyclone and storm activity, and potential exposure to nutrients and toxins. Flooding from severe storm events reduces salinity and increases turbidity, creating challenging and often fatal conditions for seagrasses (Waycott et al., 2007). Storms and floods create highly turbid conditions that limit light availability for seagrasses, leading to declines in seagrass populations in other tropical regions (Waycott et al., 2007). Seagrasses are particularly vulnerable to these changes, with physical disturbances likely from sediment movement, turbulent water motion, and storm surges (Waycott et al., 2007). Sea level rise, however, does not pose as significant a threat to seagrasses as it does to some other ecosystems, such as coral reefs. Seagrasses are well adapted to growing both vertically and horizontally, allowing them to grow upslope as sea levels rise (Waycott et al., 2007). The potential rate of vertical growth for most seagrasses is expected to be greater than the predicted rate of sea level rise (Waycott et al., 2007).

3.4 Water Cycle Changes in Coastal Cambodia

3.4.1 Observations, Models, Methods, and Their Reliability

As the world warms, atmospheric system changes have sped up the water cycle's temporal and spatial dynamics (Milly et al., 2005; Taylor et al., 2013). Rising temperatures and frequent extreme events like heatwaves, heavy rains, floods, and both sudden and prolonged droughts have become significant concerns for scientists, governments, and the public (IPCC, 2014; Hao et al., 2018). Climate warming has led to the retreat of glaciers, reduction in snow cover, and permafrost thawing, all of which impact the water cycle (Ding et al., 2020). These effects are compounded by human activities (Vörösmarty et al., 2000; Wang et al., 2010).

Analyzing long-term historical data helps understand changes in the frequency, duration, and intensity of hydrometeorological extreme events, crucial for assessing climate change's impacts on hydrology. Evidence shows that climate change has already significantly altered the water cycle (Gudmundsson et al., 2021). In recent decades, the field of attribution analysis has grown, using long-term observations and model simulations like the CMIP climate model to evaluate the likelihood of extreme events with and without climate change (Yang et al., 2020).

Using original, coarse-resolution climate models is insufficient for understanding detailed local climate changes over small regions. Thus, downscaling these models is essential for producing more accurate future climate projections. This refinement process adjusts global climate model outputs by integrating local characteristics, such as topography, vegetation, and land use, thereby improving the relevance and precision of regional climate projections (Cooney, 2012). Two main techniques are employed for downscaling: statistical and dynamical (Tang et al., 2016; Fowler et al., 2017). Statistical downscaling leverages the statistical correlations between large-scale climate variables and local weather patterns to project regional climate changes, making it a less computationally demanding method. On the other hand, dynamical downscaling uses outputs from Global Climate Models (GCMs) as inputs for regional climate models to provide more detailed information, though it is more resource-intensive and requires greater technical expertise (Anuchaivong et al., 2017).

In Cambodia, limited research has addressed climate change projections. Some studies have analyzed future temperature and rainfall using the CMIP3 climate model under two emission scenarios (Thoeun, 2014). Additionally, the World Bank has forecasted future climate scenarios in Cambodia using CMIP5 models under four different scenarios (World Bank, 2021). Climate change impacts on one of Cambodia's provinces have also been examined, employing CMIP5 climate models and downscaling methods across three Representative Concentration Pathways (RCPs) for precipitation and temperature projections (Chim et al., 2021).

However, climate projections using the updated CMIP6 climate models specifically for Cambodia have not yet been extensively conducted. Furthermore, most previous research has focused on average precipitation changes, with few studies examining shifts in extreme precipitation patterns, which are increasingly important under climate change impacts. Addressing this gap, Duong et al. (2023) utilized CMIP6 models to project climate changes for the near future (2015–2045) and the long term (2070–2100). The study examined changes in average precipitation and extreme events, such as consecutive dry days (CDD), consecutive wet days (CWD), and maximum 1-day precipitation (rx1day). Given the CMIP6 model's coarse resolution, applying it to smaller regions like Cambodia can result in substantial biases. To improve accuracy, the study applied the Bias-Corrected Spatial Downscaling (BCSD) method, which refines CMIP6 projections for Cambodia. This method is efficient and less resource-intensive, requiring only a personal computer and climate data, making it essential for research.

3.4.2 Past, Present, and Projected Changes in the Physical Components of the Water Cycle

3.4.2.1 Moisture and Precipitation Patterns, Including Extremes

The Extreme Rainfall Detection Monitoring and Indices (ETCCDMI) team provides crucial data on various extreme rainfall indicators, including types, frequency, intensity, and extremes (Zhang & Yang, 2004). Below table (Table 3.11) describes the analyzing of the time series slope trends of 11 extreme precipitation indices over the period from 1991 to 2021 at 17 rainfall stations in the coastal area of Cambodia. Cambodia is divided into four main regions: coastal, Mekong Delta, Tonle Sap, and Upper Mekong. Eleven rainfall indices were divided into three groups: the first group was CDDs, CWDs, RX1day, and RX5day; for the second group of indices, R10, R20, Rnn, and PRCPTOT; and for the third group of indices, R95p, R99p, and SDII. These parameters were classified into three

groups according to the nature of the parameters to facilitate the discussion. The spatial interpolation of rainfall indices was examined using data collected from various stations between 1991 and 2021. Negative values are represented by red triangles, while positive values are shown with blue triangles.

Pen et al (2024) indicated that from 1991 to 2021, the coastal region of Cambodia exhibited mostly increasing trends in rainfall indices (Figures 3.21 and 3.22). Notable increases were seen in the total annual precipitation (PRCPTOT) at 0.022 and consecutive wet days (CWDs) at 0.0405 (Figure 3.21a, b). Indices for heavy rainfall days (R10 and R20) also rose with rates of 0.0183 and 0.0108, respectively (Figure 3.21c, d). Extreme rainfall indices like R99p and R95p showed upward trends of 0.0142 and 0.0149, respectively, while RX1day and RX5day increased by 0.0111 and 0.0151. Conversely, consecutive dry days (CDDs) and the simple daily intensity index (SDII) decreased, with change rates of -0.0101 and -0.0216, respectively.

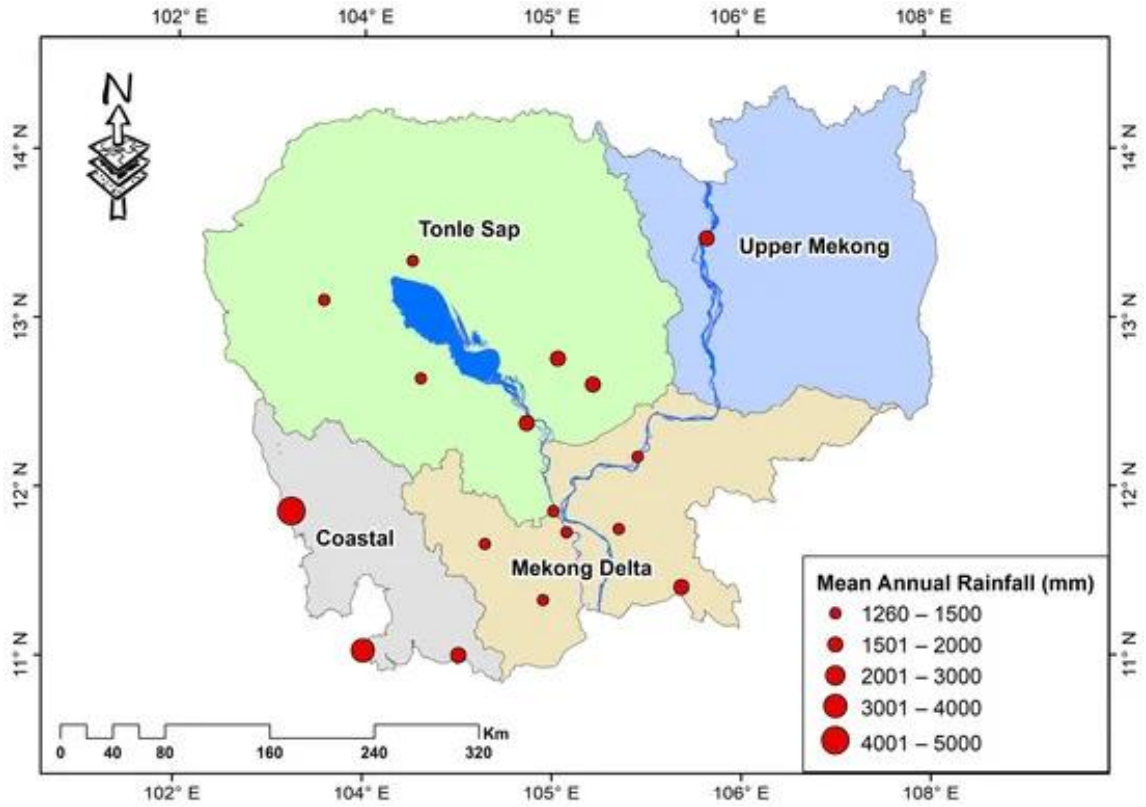

Figure 3.16: Mean annual rainfall data at each station in Cambodia (1991–2021)
Source: Pen et al. (2024)

Table 3.11: The trends of extreme rainfall indices at different stations in coastal area of Cambodia

No	Station Name	Group 1				Group 2				Group 3		
		CDDs	CWDs	RX1day	RX5day	R10	R20	Rnn	PRCPTOT	R95p	R99p	SDII
1	Kampot	−0.286	0.188	−0.359	−0.377	0.115	−0.008	0	3.334	−2.765	−0.86	−0.111
2	Takeo (Donkeo)	−0.849	0.141	−0.006	0.094	0.179	0.049	0	7.833	0.396	−2.725	−0.234
3	Takhmao—Ta Kdol	−1.549	0.037	−0.837	−1.451	0.2	−0.059	−0.004	2.769	−4.814	−3.972	−0.304
4	Phnom Srouch	0.239	−0.186	−0.409	−1.126	0.177	0.205	−0.004	−0.777	−1.101	−1.842	0.048
5	Pochentong	−0.456	−0.076	−0.693	0.34	0.331	0.197	−0.002	8.17	0.482	−0.737	0.066
6	Svay Rieng	−0.173	0.116	−0.078	−0.002	−0.023	0.021	0	0.138	−1.189	−2.791	−0.058
7	Prey Veng Town	−4.892	0.151	1.259	2.982	0.826	0.522	0	32.50	10.10	1.225	−0.094
8	Pursat	0.352	−0.045	−0.436	−1.188	−0.193	−0.112	0	−6.656	−3.612	−2.781	−0.043
9	Kampong Chhnang (Sre Pring)	−0.068	0.011	−1.612	−4.227	−0.174	−0.061	−0.011	−14.402	−18.176	−9.501	−0.172
10	Kampong Thom	−0.589	−0.031	−0.215	−0.869	−0.19	−0.092	0	−8.768	−6.752	−2.756	−0.07
11	Kampong Thmar	0.193	−0.199	−0.988	−1.369	−0.172	−0.061	−0.016	−5.695	−1.012	−1.338	0.119
12	Kampong Cham (Chhroy Thmar)	−0.294	0.031	−0.381	−0.95	−0.103	−0.042	0.004	−4.201	−3.158	−3.629	−0.047
13	Battambang	0.435	−0.009	0.113	−0.248	−0.31	−0.185	0.006	−6.762	−2.518	−0.14	−0.083
14	Siem Reap Koktatry	−0.112	−0.014	0.796	1.252	0.269	0.213	0.07	7.127	0.401	0.206	0.044
15	Stung Treng	−1.183	−0.143	0.14	0.099	0.181	0.217	−0.011	7.53	1.577	2.305	0.045
16	Krong Khemarak Phummin	−0.612	0.78	5.032	6.854	0.995	1.04	0.008	89.94	46.884	24.785	0.107
17	Sihanouk Ville	−0.093	0.284	0.569	0.803	0.019	−0.166	0	2.448	4.296	2.516	−0.112

Source: Pen et al. (2024)

Note: CDD-Consecutive dry day, CWD-Consecutive wet day, RX1day-maximum 1-day precipitation, RX5day- maximum 5-day precipitation

The coastal region, located southwest of the Gulf of Thailand, experiences increasing wet periods, whereas lower values were noted in other parts of Cambodia, such as the Tonle Sap region and the northeast. Krong Khemarak Phoumin in Koh Kong Province leads with an impressive 4180 mm/year, followed by Preah Sihanouk with 3032 mm/year, and Kampot with 1887 mm/year (see figure 3.17). Similarly, the maximum 1-day precipitation (RX1day) and maximum 5-day precipitation (RX5day) indices displayed a notable increase at Krong Khemarak Phoumin. This station recorded the most significant rise, with values increasing by 5.032 mm/year for RX1day and 6.854 mm/year for RX5day (Figures 3.18c and 3.18d) (Pen et al., 2024). Furthermore, at the Krong Khemarak Phoumin station, an upward trend was observed in the number of heavy rainfall days (R10) and very heavy rainfall days (R20) (Figures 3.18 and 3.19). Additionally, the total annual precipitation (PRCPTOT) increased by 89.94 mm/year at this station. These trends highlight intensified rainfall events in Cambodia's coastal zone.

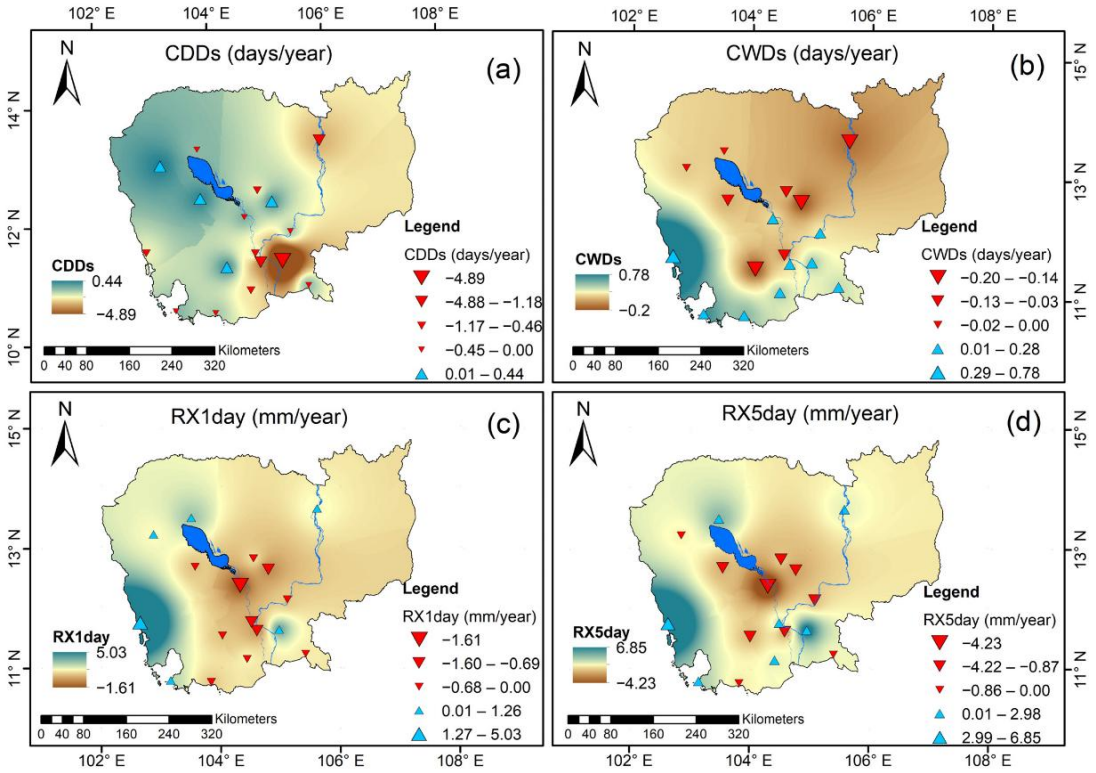

Figure 3.17: The spatial interpolation of the trends of the extreme rainfall indices in Cambodia: (a) CDDs, (b) CWDs, (c) RX1day, and (d) RX5day. The filled red downward and filled blue inverted triangles indicate decreasing and increasing trends, respectively

Source: Pen et al. (2024)

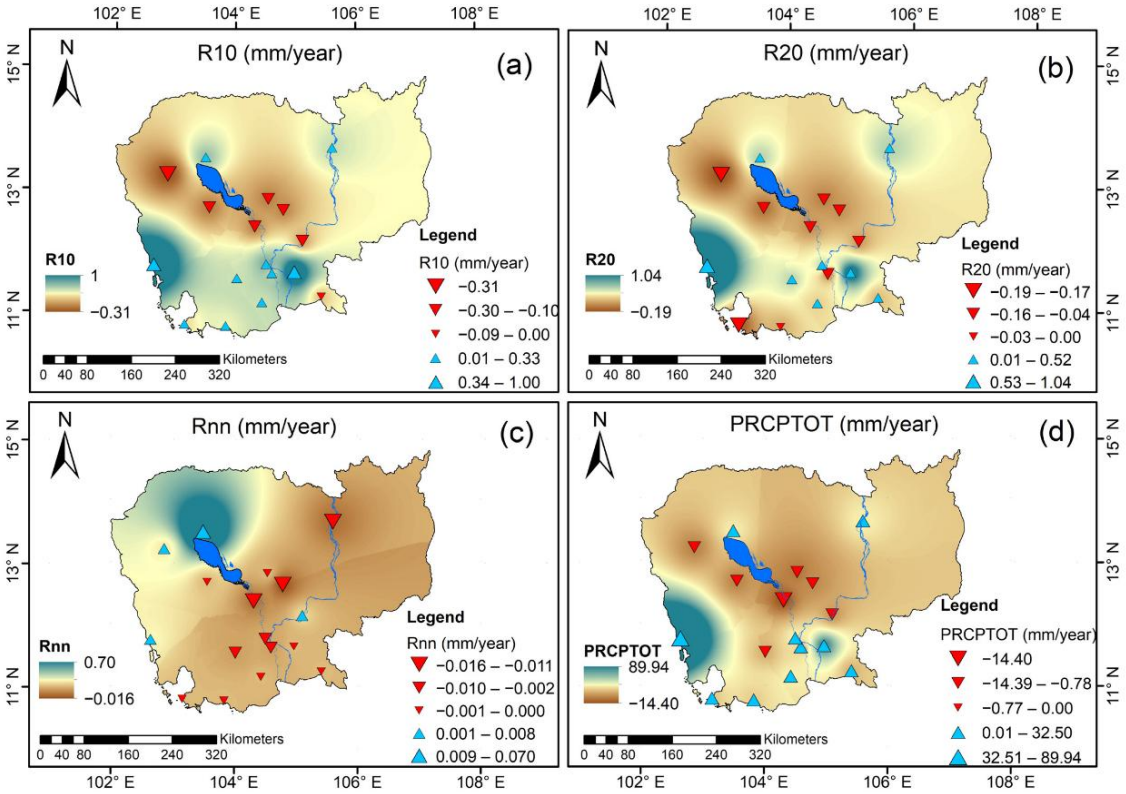

Figure 3.18: The spatial interpolation of the trends of the extreme rainfall indices in Cambodia: (a) R10, (b) R20, (c) Rnn, and (d) PRCPTOT. The filled red downward and filled blue inverted triangles indicate decreasing and increasing trends, respectively

Source: Pen et al. (2024)

The third group of indices, R95p, R99p, and SDII, showed varying trends. At the Krong Khemarak Phoumin station, there was a notable increase for R95p and R99p, with annual rates of 46.884 mm/year and 24.785 mm/year, respectively. While most stations exhibited a decline in SDII, significant increases were observed at the Krong Khemarak Phoumin station (Figure 3.20).

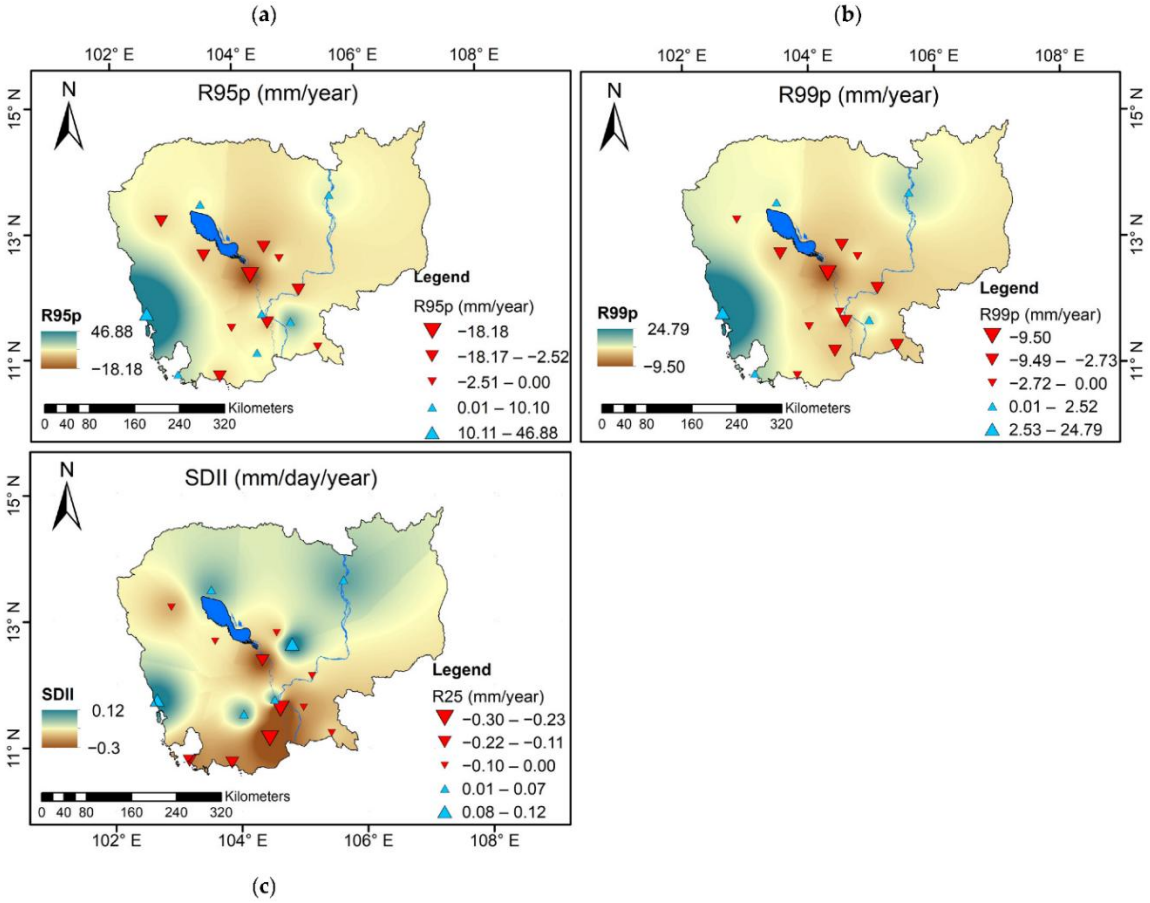

Figure 3.19: The spatial interpolation of the trends of the extreme rainfall indices in Cambodia: (a) R95p, (b) R99p, and (c) SDII. The filled red downward and filled blue inverted triangles indicate decreasing and increasing trends, respectively

Source: Pen et al. (2024)

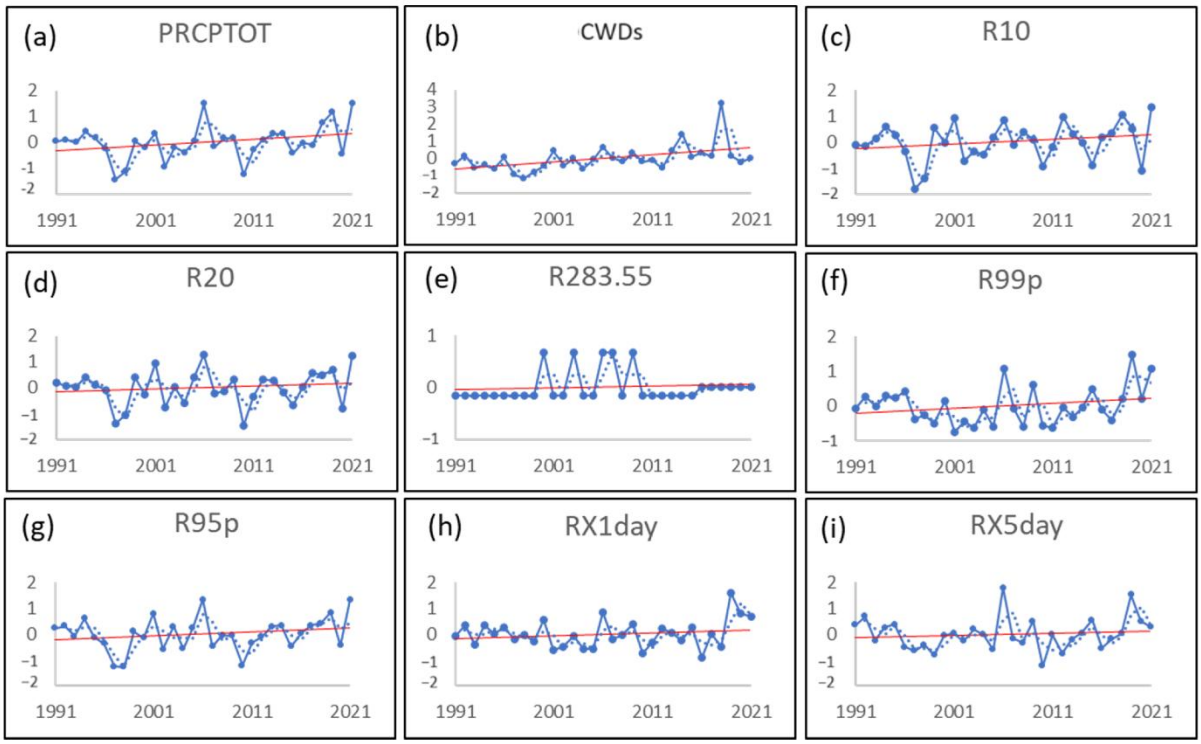

Figure 3.20: The temporal variation of the increasing trends for the coastal region of extreme rainfall indices: (a) PRCPTOT, (b) CWDs, (c) R10, (d) R20, (e) R283.55, (f) R99p, (g) R95p, (h) RX1day, and (i) RX5day. The solid red line is the linear trend, the solid blue line is the annual variations, and the dotted blue line is the ten-year smoothing average
Source: Pen et al., (2024)

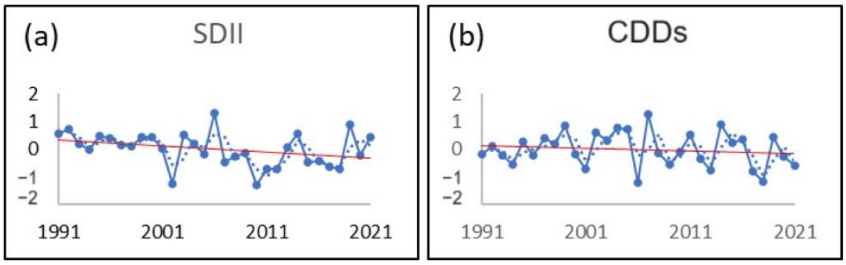

Figure 3. 21: The temporal variation of the decreasing trends for the coastal region of extreme rainfall indices: (a) SDII, and (b) CDDs. The solid red line is the linear trend, the solid blue line is the annual variations, and the dotted blue line is the ten-year smoothing average
Source: Pen et al., (2024)

In addition, Pen et al. (2024) conducted an analysis of dryness using the Consecutive Dry Day (CDD) Index (Figure 3.23). The findings indicate that during the wet season, Kampot station showed an increase of approximately 44 CDDs per year, highlighting more frequent dry periods in this coastal area. Conversely, at the Krong Khemarak Phoumin station, the wet season saw a reduction in dry days by about 18 days per year. During the dry season, a significant rise in CDDs was observed at the Kampot station, peaking at 152 days per year, while the Krong Khemarak Phoumin station experienced a decrease to 108 days per year. These variations in dry days provide valuable insights into seasonal trends in precipitation and dryness.

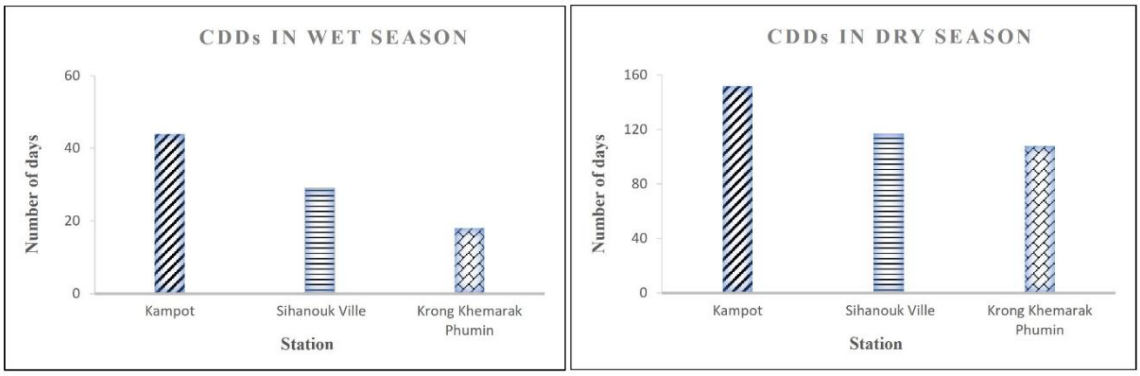

Figure 3.22: Number of consecutive dry days (CDDs) in both seasons: wet and dry seasons in the coastal region
Source: Pen et al. (2024)

These results indicate that the Krong Khemarak Phoumin station is experiencing a rise in the total amount of precipitation occurring on extremely wet days, driven by the region's frequent tropical storms, which lead to higher rainfall and flooding. Conversely, the Kampot station, despite having the lowest annual rainfall in the coastal region, shows a significant increase in CDDs, indicating a heightened risk of drought. This thorough analysis underscores the complex nature of climate impacts on Cambodia's coastal regions, highlighting the dual challenges of increased flooding and drought risks.

There is a notable scarcity of studies specifically focusing on precipitation projections in the coastal zones of Cambodia. However, the research by Duong et al. (2023) addressed this gap by using the Bias-Corrected Spatial Disaggregation (BCSD) method to downscale CMIP6 climate models. Their study projected future precipitation patterns and extreme events across Cambodia, focusing on four key indicators: mean precipitation changes, consecutive dry days (CDD), consecutive wet days (CWD), and maximum one-day precipitation (RX1day) under SSP2-4.5 and SSP5-8.5 scenarios. The results suggest that the coastal regions will experience significant changes, with the wet season becoming wetter and the dry season becoming drier, potentially leading to increased risks of both floods and droughts.

The analysis of downscaled CMIP6 models shows that the projected changes in mean precipitation under the SSP2-4.5 scenario for the far future period exhibit varying trends across different climate models, with most models showing a significant increase in future rainfall (Figure 3.24). However, the MRI-ESM2-0 model suggests a considerable decrease in rainfall for three out of four months, with reductions of up to 40 percent, except August. The multi-model ensemble calculations reveal a range from -20 percent to +40 percent in rainfall changes, aligning with trends observed in models like CMCC-CM2-SR5, MRI-ESM2-0, and NUIST-NESM3, with the northwestern part of Cambodia facing the most drastic changes. Annual rainfall is projected to increase across all climate models, except for MRI-ESM2-0, which shows a 10 percent decrease in most parts of the country. The multi-model ensemble aligns with these trends, suggesting that the dry season will become drier and the wet season wetter, potentially leading to increased occurrences of droughts and floods.

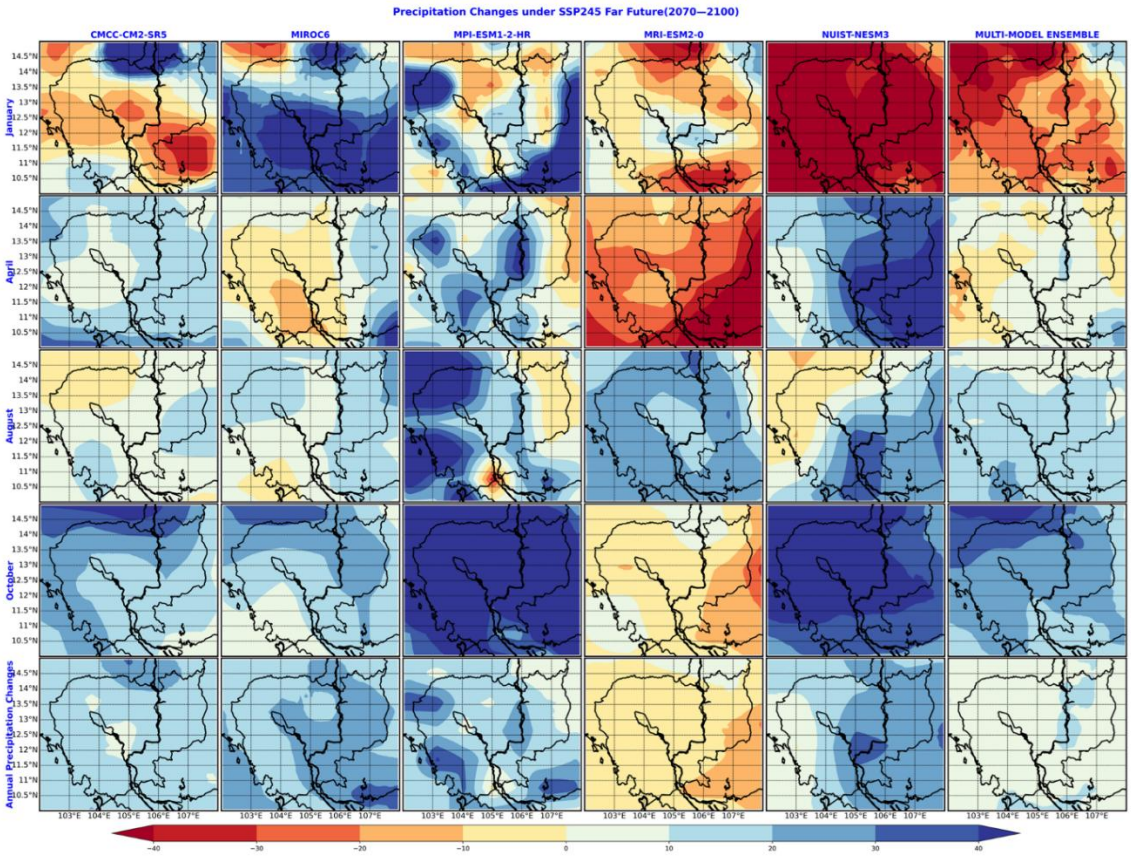

Figure 3.23: Percentage changes in climatological monthly precipitation for far future period (2070–2100) under SSP2-45. scenario. First-row panels for January, second-row panels for April, third row panels for August, and forth row panels for October. Note that the multi-model ensemble is the median among five models.
Source: Doung et al., (2023)

Figure 3.25 illustrates projected changes in mean precipitation under the SSP5-8.5 scenario for the far future period (2070–2100). The projections indicate that Consecutive Dry Days (CDD) will likely increase under both the SSP2-4.5 and SSP5-8.5 scenarios, posing a potential threat of dry spells or drought events in Cambodia. Conversely, Consecutive Wet Days (CWD) are expected to increase under SSP2-4.5 but decrease significantly in the eastern part under SSP5-8.5, suggesting more wet spells with moderate climate change but fewer under severe scenarios. Additionally, Maximum 1-day Precipitation (RX1day) is projected to increase, especially under SSP5-8.5, indicating a higher risk of extreme rainfall and potential flooding due to climate change (Doung et al., 2023).

The trend shows a significant increase in rainfall compared to SSP2-4.5. Most climate models project a substantial decline in January rainfall, notably with MRI-ESM2-0 showing around a 40 percent decrease, while MIROC6 predicts an increase of over 40 percent. April shows mixed results, with some models indicating decreased rainfall (CMCC-CM2-SR5 and MRI-ESM2-0), while others show an increase. In August and October, most models consistently project an increase in rainfall across Cambodia. The multi-model ensemble highlights a strong decrease in January (+10 percent to +40 percent) and mixed signals in April (−10 percent to +10 percent). Annually, rainfall changes follow the SSP2-4.5 projection trend but differ in percentage. CMCC-CM2-SR5 shows a minor decrease in southern rainfall. Overall, Duong et al. (2023) projects a slight increase in annual rainfall across the country, with rainfall likely decreasing during the dry season and increasing during the wet season.

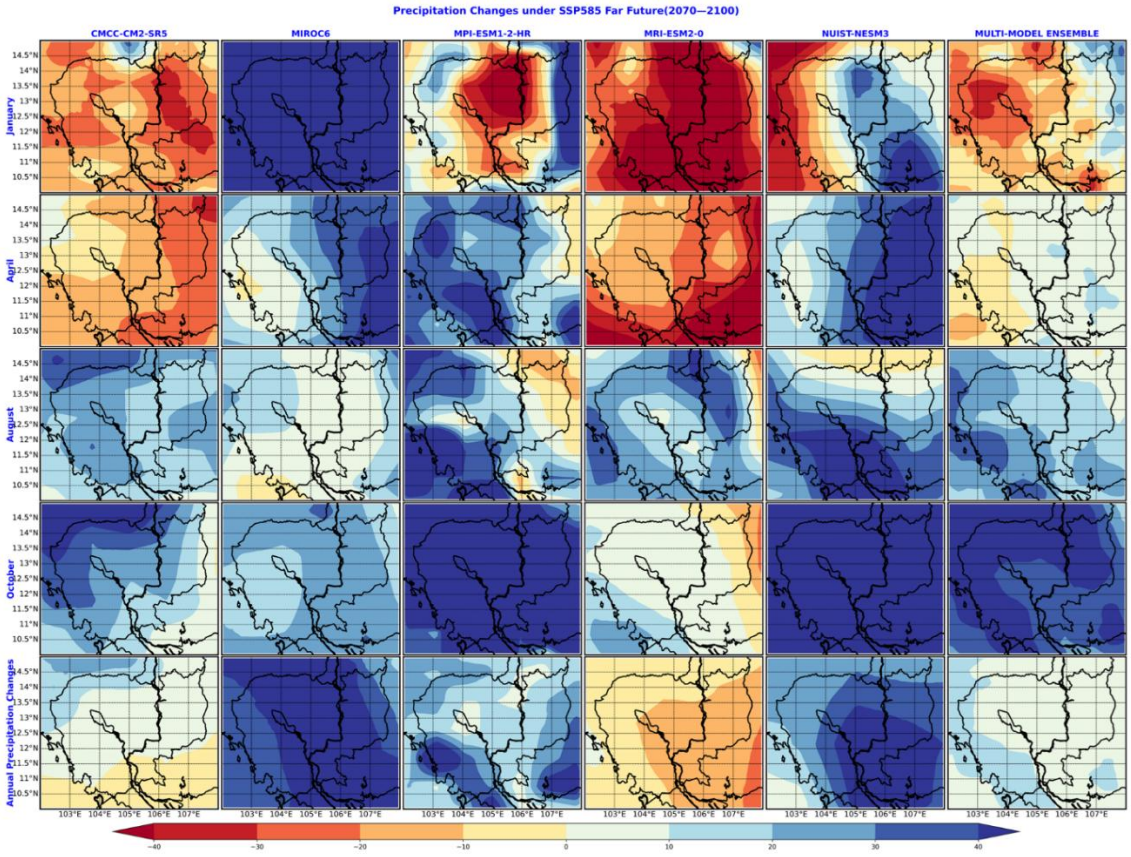

Figure 3.24: Projected changes in mean precipitation under the SSP585 scenario for the far future period (2070–2100)

Source: Doung et al., (2023)

3.4.2.2 Cloud-Aerosol Processes Affecting the Water Cycle

Aerosols can suppress rain formation, causing moisture to remain in the atmosphere and be transported downwind, potentially enhancing precipitation later (Bell et al., 2008). Additionally, aerosols reduce solar radiation heating at the Earth's surface, affecting thermal convection and influencing large-scale circulation patterns, such as monsoons (Koren et al., 2004; Bell, 2008). However, Cambodia lacks comprehensive studies and measurements on cloud-aerosol processes affecting the water cycle for past, present, and future projections.

3.4.2.3 Seasonality of Natural Water Storage and Availability

Sea level rise (SLR) is expected to increase ocean waves and sea tides, causing coastal erosion and flooding in low-lying coastal areas. Additionally, SLR combined with rising sea surface temperatures, can create major climate-related disasters, impacting coastal ecosystems. Popular beaches may see reduced tourist attraction due to coastal erosion, and increased saltwater intrusion will affect the quality of surface and groundwater. This saline intrusion in groundwater aquifers will impact many agricultural and lowland areas, particularly those relying on groundwater for drinking and farming (PEMSEA, 2019).

Socio-economic developments and global climate change directly affect wetlands and their habitats. Communities in Koh Kapik Ramsar Site (KKRS) in Koh Kong Province, one of the coastal provinces in Cambodia, have noted several threats impacting their livelihoods. According to Sorn and Veth (2019), freshwater bodies in KKRS have lower baseline conservation scores and are vulnerable to climate change impacts. There are four freshwater bodies in KKRS, which represent only 1 percent of the area but are crucial

sources of freshwater. Aquifers for fresh water are particularly vulnerable to climate change. These freshwater bodies are likely to be directly affected by higher temperatures and droughts, as well as by floods and sedimentation, although they are protected by surrounding mangrove forests and flora. The greatest impacts are expected from higher high tides during the dry season and storms, which produce saltwater intrusion. These habitats, though somewhat resilient to brackish conditions, may reach a tipping point with extreme water level changes, higher temperatures, and saltwater intrusion, making them vulnerable to climate change impacts.

Changes in rainfall patterns and prolonged droughts have led to an insufficient freshwater supply. In recent years, lack of usable water in ponds, wells, and channels during the dry season has forced families without nearby freshwater access to collect or buy water from other villages. Poor institutional planning exacerbates this issue, limiting the availability of drinking water throughout the year. Freshwater availability may be further stressed as climate change impacts increase (MoE, 2018). Long-term droughts (exceeding 12 months) are expected to have the most significant impact on Koh Kong Province over the next 20 years, potentially reducing groundwater levels due to less recharge and greater extraction. Longer droughts could also worsen existing saltwater intrusion in the province (MoE, 2018).

3.4.3 Impacts on Coastal Water Resources

Cambodia grapples with excess water during the wet season, insufficient water during the dry season, and increasing pollution, particularly in populated cities. These freshwater-related issues are pivotal among key regional vulnerabilities (NCSD, 2019). The relationship between climate change and freshwater resources is crucial. Climate change trends impacting groundwater and surface water quality and quantity include increased air temperatures, sea level rise, changes in precipitation patterns, and the frequency and intensity of weather events (Figure 3.26). Higher air temperatures result in increased temperatures of freshwater bodies, including lakes, seas, and oceans, leading to increased evapotranspiration (IPCC, 2022).

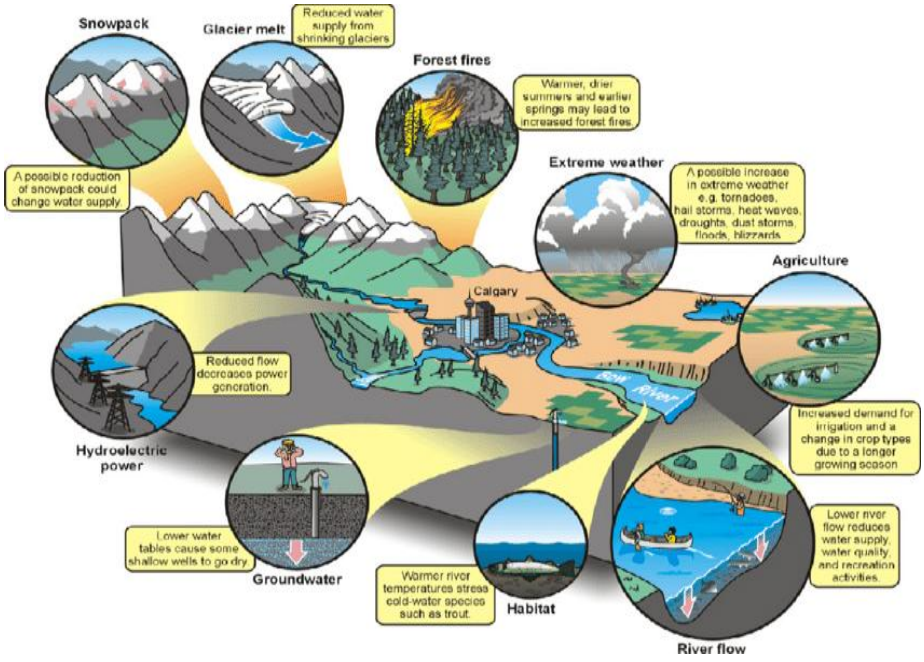

Figure 3.25: Impact of climate change on water resource
Source: National Resources Canada (2008)

In Cambodia, rising sea levels increase the risk of floods and saltwater intrusion, obstructing drainage in river deltas and coastal provinces such as Koh Kong, Preah Sihanouk, Kampot, and Kep (NCSD, 2019). Sea level rise, exacerbated by global warming, threatens to inundate low-lying areas and disrupt freshwater supplies. According to the Intergovernmental Panel on Climate Change (2022), the global mean sea level has risen significantly, with further increases projected (NASA, n.d.; MOE, 2015).

A study by Phan et al. (2021) on groundwater quality in the Koh Kong coastal area found that approximately 85 percent of tube wells and 76 percent of dug wells had a pH level below 6.5, lower than the Cambodian Drinking Water Quality Standard (CDWQS) range of 6.5 to 8.5 (MIME, 2004). Additionally, 37.5 percent of tube wells and 58.4 percent of dug wells contained arsenic (As) levels exceeding 10 µg/L, surpassing the WHO's Drinking Water Quality Guideline. The high levels of dissolved iron (Fe) and manganese (Mn) suggest that reductive processes are responsible for dissolving geogenic arsenic from sediments, a phenomenon observed globally and in other parts of Cambodia. Consequently, water treatment is necessary to make this water suitable for drinking and irrigation. Sem et al. (2021) reported that almost all water samples from Preah Sihanouk and Kampot were unsuitable for drinking purposes in terms of pH, turbidity, alkalinity, total dissolved solids (TDS), oxidation-reduction potential (ORP), and manganese (Mn). A summary of the water quality of tube wells and dug wells in the Koh Kong coastal area is presented in Table 3.12.

Table 3.12: Summary of water quality of tube well and dug well in Koh Kong province

	Mean	Median	SD	Min	Max	Mean	Median	SD	Min	Max	CDWQS
Depth (m)	43.57	45	22.84	7	68	4.44	4	1.76	2	10	
pH	5.84	5.88	0.62	4.7	6.56	6.13	6.1	0.55	5.36	7.7	6.50–8.50
Tem (°C)	26.54	26.2	3.14	22.4	31	26.85	25.4	3.84	21.8	34.9	
ORP (mV)	177.60	162.7	103.32	48.1	395.9	209.00	209.3	62.24	97.9	333.2	
Turb (NTU)	23.63	16.5	26.41	0	76	22.04	11	28.22	0	111	5
EC (µS cm−1)	709.46	233.435	1298.41	22.03	3855.67	524.08	225.67	765.36	28.1	3444.67	
TDS (mg L−1)	354.95	116.75	651.61	11.08	1935	262.42	113	382.87	14.09	1723.67	800
Salinity (g L−1)	0.21	0.025	0.47	0	1.35	0.14	0.01	0.29	0	1.3	
DO (mg L−1)	6.35	6.35	0.68	5.37	7.4	6.46	6.57	0.67	4.97	7.73	
As (µg L−1)	6.25	0	10.61	0	30	6.67	10	7.02	0	30	50
Ba (mg L−1)	6.00	6.5	3.21	1	11	5.83	6	2.16	3	10	0.7
Cu (µg L−1)	140.67	34.165	311.53	2	910	105.53	23	224.89	0	820	1000
F (mg L−1)	0.31	0.315	0.12	0.17	0.43	0.23	0.22	0.22	0	1.03	1.5
Fe (mg L−1)	0.78	0.685	0.74	0.06	2.18	1.02	0.65	1.22	0.19	6.17	0.3
Mn (mg L−1)	0.25	0.1	0.43	0	1.3	0.24	0.1	0.49	0	2.4	0.1
NO3-N (mg L−1)	0.51	0.35	0.40	0.1	1.3	0.67	0.4	0.65	0.1	2.1	11.29

	Mean	Median	SD	Min	Max	Mean	Median	SD	Min	Max	CDWQS
NO2− (mg L−1)	0.02	0.006	0.02	0	0.053	0.02	0.005	0.03	0	0.127	3
Zn (mg L−1)	0.04	0.03	0.03	0	0.08	0.04	0.03	0.04	0	0.17	3

Source: Phan et al. (2021)

Reduced freshwater availability has profound socio-economic impacts. Local communities, such as in the Koh Kapik Ramsar Site, face significant threats to their livelihoods. Agriculture, which is heavily reliant on stable water supplies, is particularly vulnerable. Poor institutional planning exacerbates these issues, limiting water availability throughout the year (MoE, 2018; Sorn & Veth, 2019). Higher temperatures and prolonged droughts also impact coastal ecosystems. Freshwater bodies, such as in the Koh Kapik Ramsar Site, are highly vulnerable to saltwater intrusion and sedimentation. These changes threaten the ecological balance and biodiversity of these critical habitats (Sorn and Veth, 2019).

3.4.4 Water Resource Change in the Coastal Basin of Cambodia/ Changes in Coastal Freshwater Availability

The coastal zone of Cambodia has several river basins, covering the land area of Kep, Kampot, Preah Sihanouk, and Koh Kong provinces. This section presents a case study of water resource changes in Kampong Bay River Basin, located within Cambodia's coastal basin of Kampot province. The Kampong Bay River Basin plays a vital role in supporting the water needs, agriculture, tourism, and hydropower generation for Kampot province. However, the region is facing significant challenges due to declining water quality from upstream pollution, population growth, and inadequate waste management. These issues are exacerbated by the growing urban population and rising water demands, which put additional pressure on the already strained water supply infrastructure.

Kampot relies on the Teuk Chhou River, which is part of the Kampong Bay River Basin, for its water needs and recharges the underground aquifers to sustain the domestic water use by the coastal communities (UNDP, 2020). The basin covers an area of 3,018 square kilometers and stretches 12 kilometers in length. Originating from Kamchay Mountain, the Teuk Chhou River flows through Teuk Chhou district and Kampot City, eventually reaching the Gulf of Thailand, a marine ecosystem shared with Thailand and Vietnam (PEMSEA, 2023).

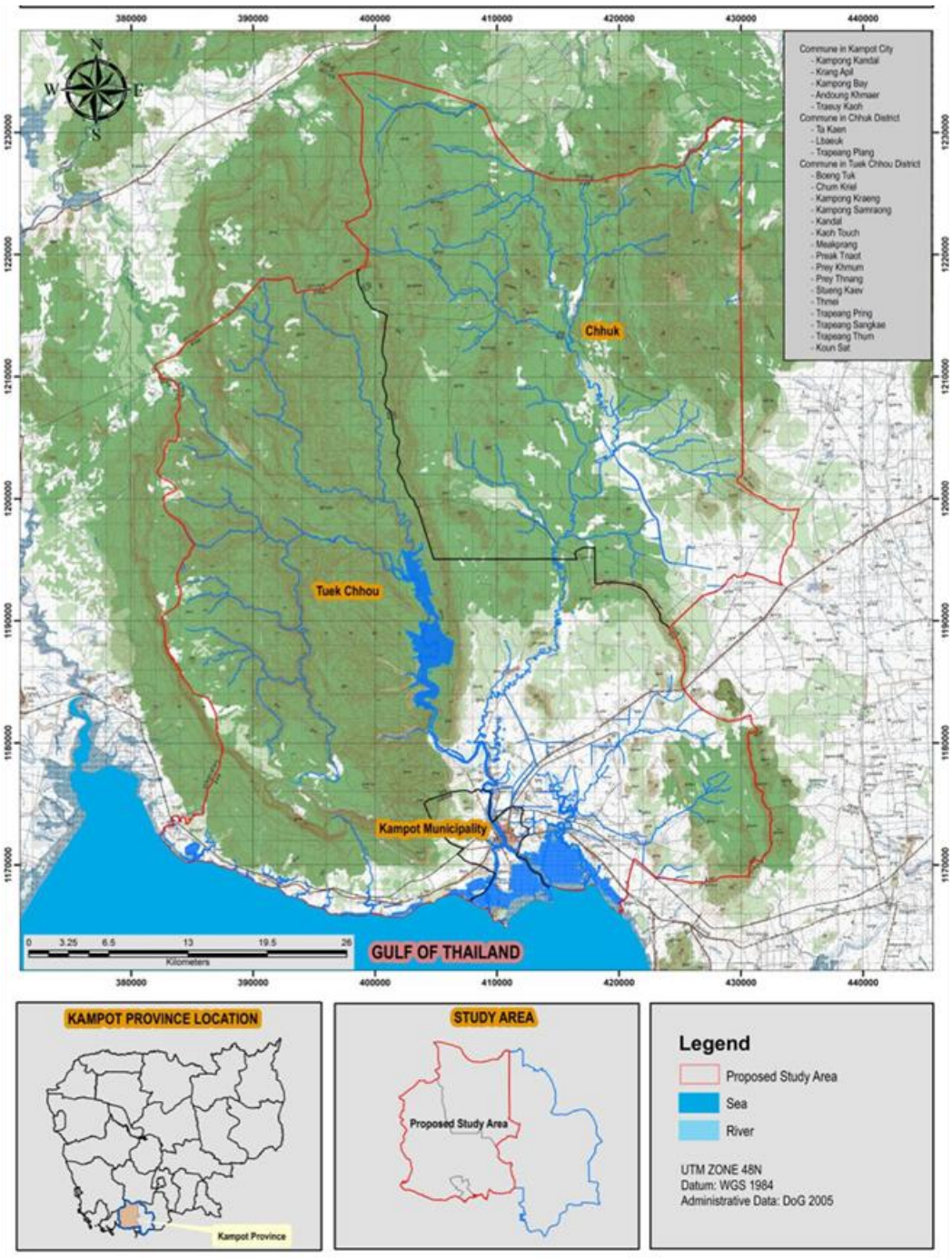

Figure 3.26: Location map of Kampong Bay relative to Kampot Province and Cambodia
Source: PEMSEA (2023)

This river basin is crucial for providing water to Kampot communities, supporting agriculture, local tourism, water supplies, and generating hydropower. The basin is essential for maintaining diverse freshwater and marine ecosystems (PEMSEA, 2023). The details of Kampot's water supply sources are summarized in Table 3.13.

Table 3.13: Existing Water Supply Sources

Source name	Capacity (m^3/day)	Annual Production Potential (1) (MCM)
Tek Chou River	5,875	1.93

Note: (1) Based on 90 percent capacity factor for the raw water pump station (10 percent allowance for down time)
Source: JICA (2010)

However, the region faces challenges due to declining water quality, driven by upstream pollution, population growth, and inadequate waste management. These issues threaten the river's ability to provide clean water, impacting agriculture, transportation, tourism, and power generation (PEMSEA, 2023). The growing urban population in Kampot province, which is projected to reach 57,200 by 2030, combined with limited water infrastructure and rising water demands, exacerbates the pressures on existing water supplies (JICA, 2010) (Table 3.14).

Table 3.14: Population History and Projections

Year	Urban Population
1998	45,240 a
2008	48,310 a/ 32,300 b
2020	43,700 b
2030	57,200 b

Note. a: Census for whole of Kampot Province, b: JICA study team estimates, October 2009
Source: JICA (2010)

Demand for water resources in Kampot Province is projected to increase from 1.2 million m^3 in 2008 to 4.1 million m^3 in 2030. This increased demand, along with high rates of leakage and inadequate waste management, further degrades water quality and availability, impacting essential services and economic activities in the region (JICA, 2010). Water demands for existing and future conditions can be found in Table 3.15 below.

Table 3.15: Water demands for existing and future conditions in urban Kampot Province of Cambodia

Parameter	**Units**	**2008**	**2020**	**2030**
Urban Population	Person	32,300	43,700	57,200
Domestic Demand	lpcd	121	140	150
	m3/day	2,224	4,336	7,747
	m3/hour	93	181	323
Tourism/commercial demand	multiplier	0.15	0.15	0.15
	m3/day	Included in domestic demand-	650	1,162
	m3/hour		27	48
Leakage	ratio	31 percent	20 percent	20 percent
	m3/day	684	997	1,782
	m3/hour	29	42	74
Average Day Demand	m3/day	3,213	5,983	10,690
	m3/hour	134	249	445
Maximum Day Demand	multiplier	1.25	1.25	1.25
	m3/day	4,404	7,479	13,363
	m3/hour	184	312	557
Maximum Hour Demand	multiplier	1.80	1.80	1.80
	m3/hour	330	561	1,002
	liter/sec	92	156	278

Parameter	Units	2008	2020	2030
Total Annual Demand	million m3	1.2	2.3	4.1

Note: Projection was made by JICA studies
Source: JICA (2010)

The ongoing decline in water quality presents serious threats to both the environment and the communities that rely on this essential resource. To ensure the long-term sustainability of the Kampong Bay River Basin, it is crucial to implement improved water management and conservation practices. These measures will help protect the ecosystem and support the well-being of local populations (JICA, 2010).

CHAPTER 4
DRIVERS OF CLIMATE CHANGE IN CAMBODIA

4.1 Chapter Summary

Anthropogenic activities are significantly altering the Earth's climate. The physical processes that drive climate change are intrinsically tied to the root causes of climate shifts throughout history and in the present day. Emissions of CO_2 and other GHGs are the primary drivers of the global rise in temperatures (IPCC, 2021b). GHGs cause global warming by trapping heat. Over the past 150 years, almost all of the increase in GHGs in the atmosphere has been caused by human activities (Stocker et al., 2013). Cambodia's GHG emissions are low compared to other countries; however, rapid economic growth has made the country increasingly carbon-intensive. The 2019 Edition of the Kingdom of Cambodia's Greenhouse Gas (GHG) Inventory covers emissions from 1994 to 2016, encompassing carbon dioxide (CO_2), methane (CH_4), nitrous oxide (N_2O), and hydrofluorocarbons (HFCs). According to Cambodia's First Biennial Update Report to the UNFCCC in 2020, total estimated GHG emissions were 163,592 Gg CO2-eq in 2016, which is 285 percent higher than in 1994. The inventory spans key sectors, including Energy, Industrial Processes and Product Use (IPPU), Agriculture, Forestry and Other Land Use (AFOLU), and Waste (National Council for Sustainable Development).

AFOLU is the main driver of this increase in GHG emissions is deforestation, as reflected in the emissions. CO_2 is the primary gas emitted in Cambodia, due to the significant contribution of the FOLU sector, followed by CH_4, N_2O, and HFCs. The rate of land use change from 2010 to 2016 was significantly higher than that observed from 1994 to 2009. During the later period, forest cover loss was particularly substantial, averaging 579,280 ha per year, compared to an annual average of 132,733 ha in the earlier interval. This accelerated deforestation has resulted in substantially increased greenhouse gas emissions.

Food security, economic growth, sustainable urban development, and environmentally friendly development are essential elements for achieving the United Nations Sustainable Development Goals (SDGs). Changes in land use have a significant impact on food security, the carbon cycle, and the economy and affect progress toward the SDGs. Human land use and management significantly affect terrestrial ecosystems. More than 70 percent of anthropogenic greenhouse gas emissions come from cities, and global urbanization offsets 30 percent of the gain in terrestrial net primary output caused by climate change (UNFCCC, 2020).

Agriculture, a key economic pillar of Cambodia, is the second-largest emitting sector in the country. In 2022, agriculture contributed 22 percent to Cambodia's GDP and employed 2.6 million people, making it a major source of GHG emissions. This economic reliance is also reflected in the county's emission patterns. The primary driver of increase in GHG emissions in agriculture is the expansion of rice cultivation.

The energy and waste sectors are the third and fourth largest contributors to GHG emissions and both show an increasing trend. Energy demand has experienced a significant increase, the transport sector is expanding, while the population migrates to

cities. All these factors lead to increasing fuel consumption and higher GHG emissions in the energy sector. The transportation sector is growing, the population is moving into cities, and energy demand has increased significantly. These factors all contribute to rising fuel consumption and greenhouse gas emissions in the energy sector. Due to the increasing population, emissions from the waste sector are primarily caused by changes in sanitation and waste management. In 2015, 83.5 percent of Cambodian households depended on firewood as an energy source, especially for cooking, and more than 80 percent of their energy sources was for cooking (ADB, 2019)

Industrial Processes and Product Use (IPPU) is the fifth largest contributor to national total GHG emissions. Due to the expanding contribution of cement production and fluorinated gas consumption and the IPPU sector's emissions have increased in recent years.

On December 30, 2021, Cambodia submitted its Long-term Strategy for Carbon Neutrality (LTS4CN) to the Secretariat of the UNFCCC. Cambodia aims to achieve carbon neutrality by 2050. This goal will require a decoupling of GDP growth from emissions growth. The LTS4CN largely builds on existing commitments and proposes a trajectory considered to be consistent with the updated NDC 2020, which included the target to lower emissions 41.7 percent by 2030, relative to a BAU scenario.

Air pollution has a number of serious negative effects on the environment, public health, and economic growth. Most air pollutants, like nitrogen oxides, have a direct impact on air quality close to where they are emitted, but other pollutants, like sulfur dioxide, can travel great distances and have an impact on air quality hundreds or even thousands of kilometers away. Air pollution has no geographic limits, and people can be exposed to it over both short and long periods. Particles can enter the lungs and become lodged there. PM2.5 particles, which have a diameter of 2.5 μm or smaller, are the most harmful to health (US EPA, 2022). PM2.5, has been associated with increased risks of respiratory and cardiovascular diseases, diabetes, stroke, and lung cancer. Cambodia recently published its first action plan, the “Clean Air Plan of Cambodia”, in 2021 to reduce ambient air pollution.

Widespread biomass burning from two burning seasons each year contributes to unhealthy living conditions across Southeast Asia. These burning seasons coincide with dry conditions on the mainland in November–May and across the more equatorial maritime nations in June–October. The combustion of biomass, such as wood and charcoal, releases aerosols and other gases that can be harmful to human health and also have a significant impact on air quality and climate.

Aerosols also affect air quality as well as contributing to climate change. Aerosols are compounds of liquid, solid, or mixed particles having a very different size distribution and chemical composition in the atmosphere (Putaud et al., 2010). Aerosols caused by human activity play a profound and complex role in the climate system through radiative effects in the atmosphere. Aerosol particles are either emitted directly into the atmosphere (primary aerosols) or produced in the atmosphere from precursor gases (secondary aerosols). Globally, anthropogenic aerosols are estimated to produce a net cooling ~−1.3 ± 0.7 W/m^2 at the top of the atmosphere; −0.3 ± 0.3 W/m^2 is attributed to the aerosol–radiation interaction (ARI), −1.0 ± 0.7 W/m^2 to aerosol-cloud interactions, ~−1.15 W/m^2 to total forcing from scattering aerosols and ~+0.12 W/m^2 to BC (IPCC, 2021b).

4.2 Introduction

Globally, GHG emissions are a dominant anthropogenic influence on the climate. However, at the regional and local scales, human activities (e.g., land cover change, biomass burning, and urbanization) can also lead to changes in the local climate. This chapter identifies some of the key human-induced drivers on the Earth system that can affect the climate in Cambodia, along with natural factors.

The main driver of climate change in Cambodia is the global accumulation of GHGs in the atmosphere, which is caused by human activities and natural phenomena. Land use conversion, deforestation, forest degradation, forest fires, and peatland destruction are the second-largest contributors to climate change. The rapid growth of population, urbanization, industrial zones, energy produced from fossil fuels, excessive and inefficient use of wood and charcoal, and an increase in the number of vehicles all contribute to higher carbon dioxide and black carbon emissions. Forest degradation leads to loss of biodiversity and further accelerates climate change by increasing CO_2 emissions and reducing carbon sequestration. Similarly, the decline in water availability from forests due to deforestation results in more intense droughts and related GHG emissions due to forest-based soil erosion. The use of fire activity to clear land and for agricultural purposes exacerbates CO_2 emissions and becomes an additional problem at various levels as a result of intense pollution. Climate change can accelerate the rate and extent of these activities, releasing even more carbon into the atmosphere, as a consequence of improper land management and soil degradation caused by agricultural expansion in forest lands and upland watershed areas. While the removal or destruction of forested areas is a significant source of GHGs, re-establishing forests through spatial zoning can have positive effects on atmospheric composition by promoting carbon sequestration and mitigation some of the negative externalities.

Human activities represent the main factor contributing to climate change in Cambodia, although there is unlikely to be an accurate indication of the actual extent of the problem. Cambodia has already made significant steps in terms of preparation and implementation of policy and legal instruments to adapt and mitigate to climate change.

Natural activities are also driving climate change. For Cambodia, the main natural influences on its climate are global weather systems and climate factors like solar radiation, the moon's phase, and volcanic activity. These natural climate forces can affect the climate over periods ranging from a few years to millions of years. Research suggests that the climate-altering effects of volcanic activity are minor compared to those of solar activity. Sunspot activity, which causes variations in solar radiation and leads to both surface and lower-atmosphere temperature increases, can also cause climate change. Solar irradiance is now measured routinely by meteorological satellites. Ground-based instruments measure volcanic aerosols from different angles to capture various parts of the solar spectrum. This is crucial because clouds reflect both shortwave and longwave radiation, which plays a major role in controlling Earth's climate. The influence of the solar cycle on climate is a separate factor, which can be seen in its potential connection to lunar phases and monsoon rainfall. However, short, minute-to-hourly fluctuations in the climate are likely not caused by solar activity. After a volcanic eruption, the troposphere can cool down. The amount of cooling depends on the eruption's location and whether it is strong enough to influence the global climate.

4.2.1 Key Emissions: Global Overview, Natural, Anthropogenic, Historical and Scenarios

Atmospheric concentrations of GHGs have increased significantly since the eighteenth century which is extremely concerning for the environment, as rising GHGs concentrations in the atmosphere cause global warming. The two primary sources of GHGs are natural systems and human activity. Many nations have directed their attention on the human activity, as demonstrated by the national pledges made in the United Nations Framework Convention on Climate Change (UNFCCC) and its GHG emission inventories. Burning fossil fuels; manufacturing products like steel, cement, and plastics; and agricultural activities all release GHGs, including carbon dioxide and methane. Emissions are still rising in many parts of the world. However, several countries have managed to cut their emissions in recent decades. Natural systems affecting climate, including forest fires, oceans, permafrost, wetlands, volcanoes, and earthquakes, in contrast, have higher levels of uncertainty and must be scientifically investigated (Yue et al., 2018). Further, some of these natural systems also relate to human activity, such as melting permafrost caused by anthropogenic activities.

GHG Emissions from Anthropogenic Sources

Greenhouse gases (GHGs) cause global warming by trapping heat in the Earth's atmosphere. The majority of the rise in GHGs in the atmosphere during the past 150 years is attributable to human activity. The largest sources of GHG emissions from human activities include transportation, electricity, industry, agriculture, commercial and residential, and land use and forestry.

From 1970 to 2010, the total amount of GHG emissions caused by human activity increased, with greater absolute decadal increases observed towards the conclusion of this time frame (high confidence). In 2000–2010, total anthropogenic GHG emissions reached 49 (±4.5) GtCO2-eq/yr, the highest level in human history. Despite the increasing implementation of policies aimed at mitigating climate change, the average annual growth in GHG emissions was 1.0 GtCO2-eq (2.2 percent) between 2000 and 2010, as opposed to 0.4 GtCO2-eq (1.3 percent) per year between 1970 and 2000 (Edenhofer et al., 2014).

About 78 percent of the growth in GHG emissions between 1970 and 2010 came from the combustion of fossil fuels and industrial activities (high confidence), including energy supply (47 percent), industry (30 percent), transport (11 percent), and buildings (3 percent) (medium confidence). Agriculture, forestry, and other land use contributed 22 percent of 2010 global GHG emissions; GHG emissions from this sector come mostly from agriculture (cultivation of crops and livestock) and deforestation (Edenhofer et al., 2014; FAO, 2014).

In 2019, 34 percent (20 GtCO2-eq) of global GHG emissions came from the energy sector, 24 percent (14 GtCO2-eq) from industry, 22 percent (13 GtCO2-eq) from agriculture, forestry and other land use (AFOLU), 15 percent (8.7 GtCO2-eq) from transport and 5.6 percent (3.3 GtCO2-eq) from buildings (Lamb et al., 2021). Once indirect emissions from energy use are considered, the relative shares of industry and building emissions rise to 34 percent and 16 percent, respectively. Average annual GHG emissions growth from 2010 to 2019 slowed compared to the previous decade in energy supply (from 2.3 percent to 1.0 percent) and industry (from 3.4 percent to 1.4 percent, direct emissions only), but remained roughly constant at about 2 percent per year in the transport sector (high

confidence). Emission growth in the AFOLU sector is highly uncertain, mainly because of the significant and unpredictable amount of carbon dioxide released from land use and forestry changes (Figure 4.1)(Dhakal, 2022).

In 2021, the world's CO_2 emissions from industrial operations and the use of energy surged to an all-time high. Based on the IEA's comprehensive research, which examined each region and fuel separately and incorporated the most recent official national statistics as well as publicly available energy, economic, and meteorological data, estimated emissions in 2020 increased by 6 percent to 36.3 Gt (International Energy Agency, 2021). Total energy-related CO_2 emissions increased by 1.1 percent in 2023. Compared to the e global GDP growth rate, which was approximately 3 percent, the percentage rise of emissions was significantly slower. As a result, CO_2 growth has been slower than global economic activity, a trend that was maintained last year. The ten-year period ending in 2023 has seen a minor increase in global CO_2 emissions of 0.5 percent annually (International Energy Agency, 2023).

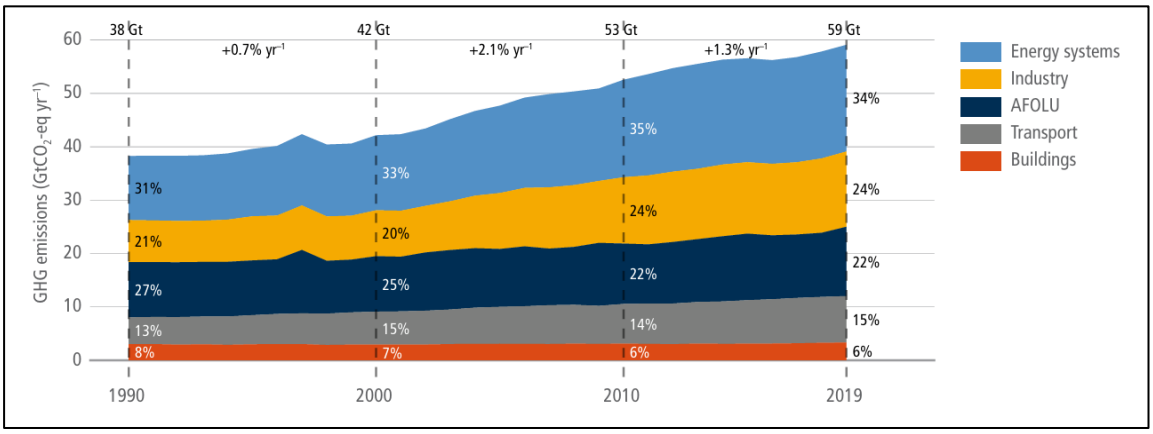

Figure 4.1 Trends in global GHG emissions by sector
Source: (Dhakal, 2022)

Anthropogenic CO_2 emissions are increasing, and this is one of the main causes of climate change. It affects the political, scientific, and public domains, among other spheres of society. It is ideal to use Earth system modeling and data assimilation to build a connection between the emission inventories and observed CO_2 concentrations to understand better the sources, patterns, and trends of CO_2 emissions. The Sixth Assessment Report of the Intergovernmental Panel on Climate Change (AR6 WGI) (Masson-Delmotte et al., 2021) shows that annual anthropogenic GHG emissions and atmospheric concentrations of GHGs are rising and have reached a record high, primarily due to the continued use of fossil fuels (Jackson et al., 2019).

Accurate assessment of anthropogenic CO_2 emissions is important to understand the global carbon cycle better. Janssens-Maenhout et al. (2020) describe how efforts to create a global capacity for anthropogenic CO_2 monitoring and verification support rely on atmospheric modeling and atmospheric observations, such as in situ (e.g. the Integrated Carbon Observation System, ICOS), airborne (such as aircraft campaigns), or spaceborne (e.g. the Orbiting Carbon Observatory, OCO-2, and the Greenhouse gases Observing Satellite, GOSAT) (Janssens-Maenhout et al., 2020). Scientists can estimate CO_2 emissions by using a "top-down" approach. This involves taking measurements of atmospheric CO_2 and other related pollutants and then using a mathematical process to figure out the original sources. For example, the European Centre for Medium-Range Weather Forecasts (ECMWF) is working to create an operational inversion system that

will use observed CO_2 and other key GHG concentrations in the atmosphere to estimate CO_2 fluxes (Choulga et al., 2021).

Figure 4.2 shows that the rate of emissions growth seen over the last decade is slower than that seen during the 1970s and 1980s, which saw major disruptions with the two energy shocks of 1973-4 and 1979-80, and a macroeconomic shock of global significance with the fall of the Soviet Union in 1989-90. When the last ten years are put in a broader historical context, a comparably slow rate of CO_2 emissions growth only occurred in the extremely disruptive decades of World War I and the Great Depression. Global CO_2 emissions are therefore undergoing a structural slowdown even as global prosperity grows.

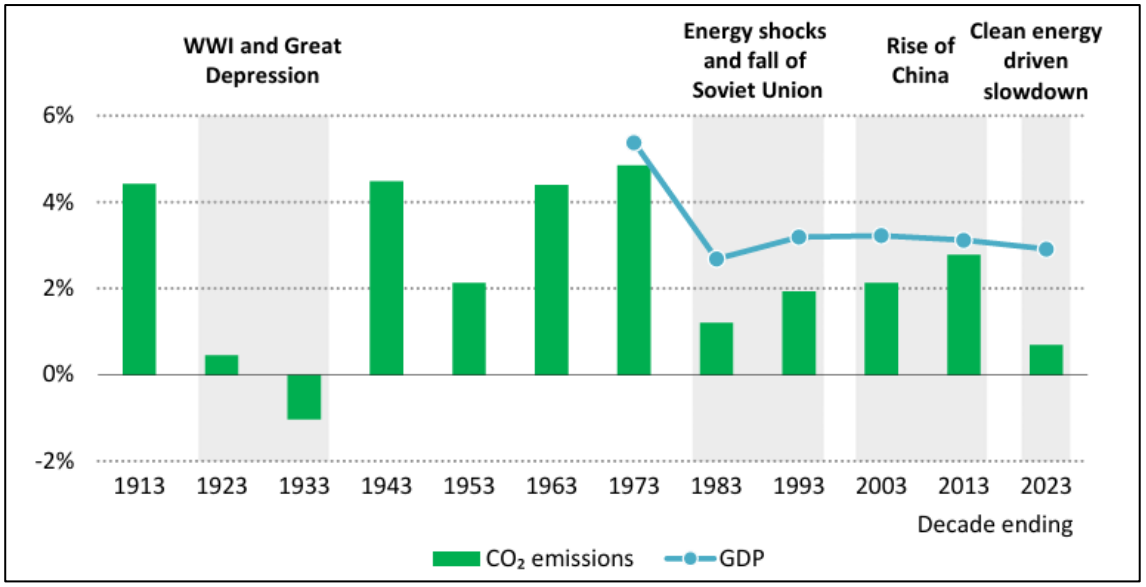

Figure 4.2 Annual average rate of global CO_2 emissions and GDP growth by decade, 1913-2023
Source: (International Energy Agency, 2023)

Natural-system GHG emissions

It is important to recognize that both GHG emissions and sinks from natural systems contribute to global changes. GHG emissions from natural sources include those from forest fires, oceans, wetlands, permafrost, volcanoes, mud volcanoes, and earthquakes. According to (Seiler et al., 1980), forest fires cause 2,200 Tg of annual carbon emissions globally. (Elliott et al. (1987) identified the equatorial sea area as the largest global source of CO_2 that delivers 1,000 Tg of carbon per year to the atmosphere, which accounts for 60 percent of the total CO_2 released by the oceans. In 2011, it was estimated that the annual global CH_4 released from freshwater ecosystems was approximately 103 Tg (Bastviken et al., 2011). Volcanic eruptions release copious amounts of volcanic gases, such as CH_4 and CO_2, which are carried straight into the atmosphere (Schmincke, 2004). Earthquakes also contribute to GHG emissions. The level of CO_2 emission after the Wenchuan earthquake was huge, almost equivalent to 2 percent of the global CO_2 emissions from fossil fuel combustion (Yue et al., 2018).

However, a comprehensive summary and discussion of the global balance of natural GHG emissions is still lacking, as are the contributions of both anthropogenic and natural GHG emissions. According to Yue et al., 2018, Global GHG emissions from natural systems are estimated to range approximately from 18.13 to 39.30 Gt CO2-eq per year, with a most likely value of 29.07 Gt CO2-eq. Emissions from forest fires account for the largest component of total emissions at 37.8 percent, followed by oceans, permafrost, and

wetlands at 21.05 percent, 20.64 percent, and 17.20 percent, respectively. Volcanoes and mud volcanoes contribute relatively low amounts of GHG emissions, i.e., approximately 1-3 percent of the total (Figure 4.3). It is also important to note that some natural sources of GHG emissions may have anthropogenic causes, such as forest fires accidentally started by humans.

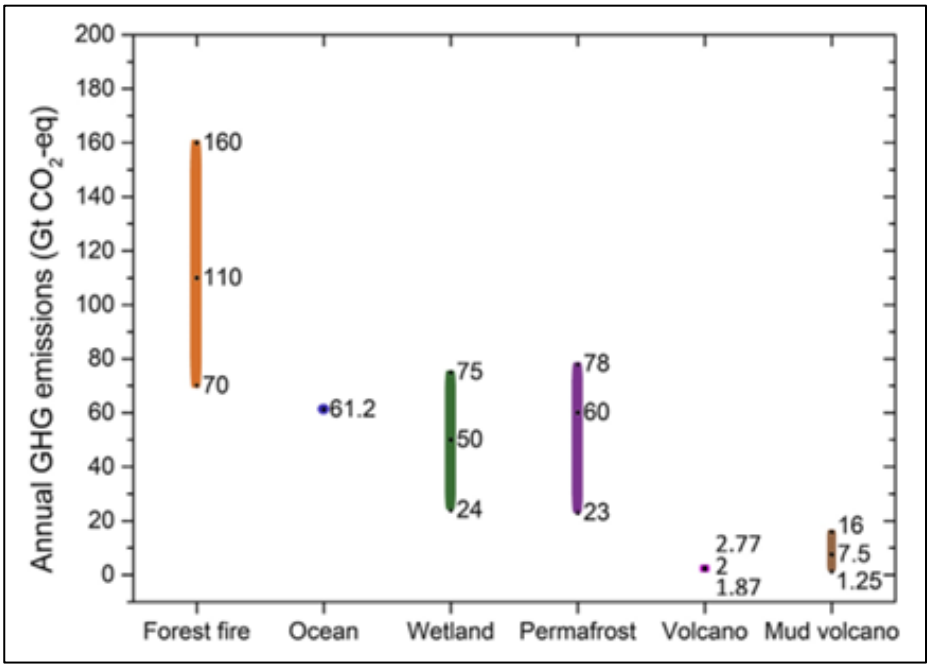

Figure 4.3 Global natural source GHG emissions; also shown are the maximum, minimum, and recommended (dark point) values
Source: (YUE et al., 2018).

Despite having the lowest absolute and per capita GHG emissions in Southeast Asia, Cambodia's economy is vulnerable to transition risks due to its fastest-growing emissions rate. In 2019, Cambodia's share of global greenhouse gas emissions was a mere 0.14 percent, with per capita emissions of 4.3 tCO2-eq, less than half of the OECD average of 10.8 tCO2-eq (World Bank, 2023). Estimates of greenhouse gas emissions and removals are categorized into the main categories of the 2006 IPCC Guidelines, which are sets of associated sources, sinks, and processes. The main processes for GHG emissions are energy; industrial processes and product use (IPPU); agriculture, forestry, and other land use (AFOLU); and waste.

The 2019 National GHG Emissions Inventory reported that the predicted greenhouse gas emissions for the entire inventory, which includes forestry and other land use (FOLU), were 163,882 Gg of CO2-eq. Change in carbon stocks due to deforestation and other changes in land use were the major contributors to the GHG emissions from 1994 to 2016. This was a 284 percent increase over the emissions in 1994 (Table 4.1). Without FOLU, the GHG emissions were 32,871 Gg of CO2-eq for year 2016, which is 110 percent higher than emissions in 1994 and the agriculture industry was the nation's second-biggest emitter. The agricultural sector's significant contribution to Cambodia's GDP is reflected in both the country's emission pattern and economy, which increased by a rate of ~2.5 in the period 1994-2016 (Figure 4.4).

Table 4.1: Trend of emissions (GHG, Gg CO2-eq)

Inventory Sector	1994	2000	2005	2010	2015	2016
Energy	2690.95	3102.73	3454.41	5306.37	8356.31	601.61

IPPU	3.81	6.04	12.73	492.84	1001.38	821.15
Waste	1756.18	2111.61	2415.89	2633.62	2974.53	050.67
Agriculture(3A + 3C)	11202.58	13032.31	15336.38	18136.08	18068.35	8397.67
Forest and Other Land Use (FOLU) (3B)	27018.62	27018.62	27018.62	131011.24	131011.24	31011.24
Total (without FOLU)	15653.52	18252.70	21219.42	26568.91	30400.57	32871.10
Total (with FOLU)	42672.14	45271.32	48238.04	157580.15	161411.82	163882.35

Source: (MoE, 2019b)

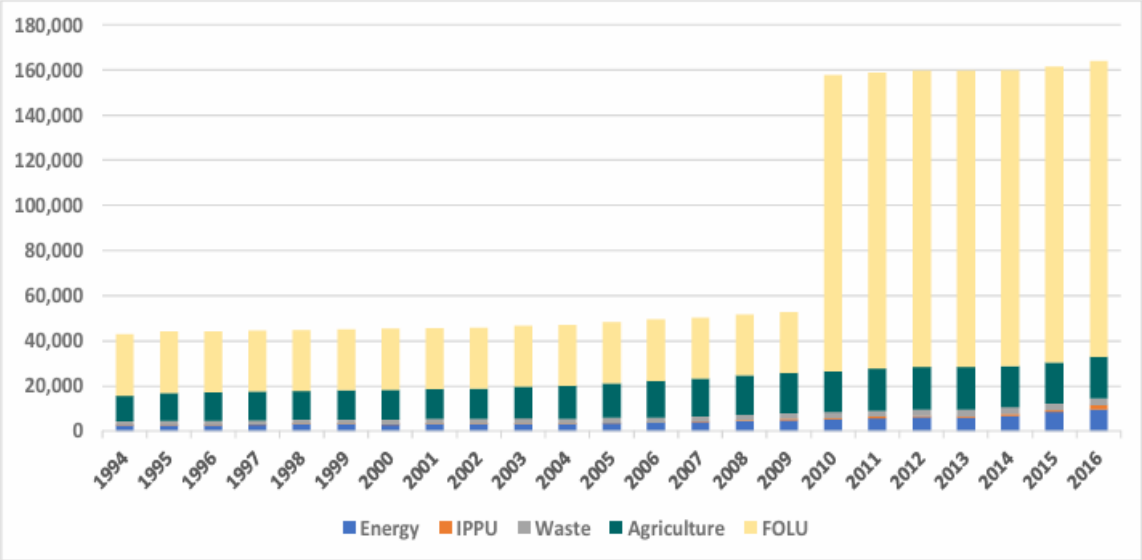

Figure 4.4 GHG emissions; Years 1994-2016 (Gg CO2-eq)
Source: (MoE, 2019b)

Deforestation is occurring at a rapid rate in Cambodia, which has increased physical climate risks and been a major source of emissions. According to satellite data from Global Forest Watch (2022), Cambodia has experienced one of the greatest rates of deforestation in the world, losing 30 percent of its forest cover in the last 20 years (World Bank, 2023). Based on the RGC's emissions inventories, data from the Climate Analysis Indicators Tool reveals that the land use, land-use change, and forestry (LULUCF) sector was the largest contributor to GHG emissions in 2019, making up 44 percent of total emissions. In 2019 the second largest source of GHG emissions was agriculture, contributing 30 percent of the gross total, followed by transport at 8 percent, industry at 8 percent, and electricity and heat at 7 percent (Figure 4.5).

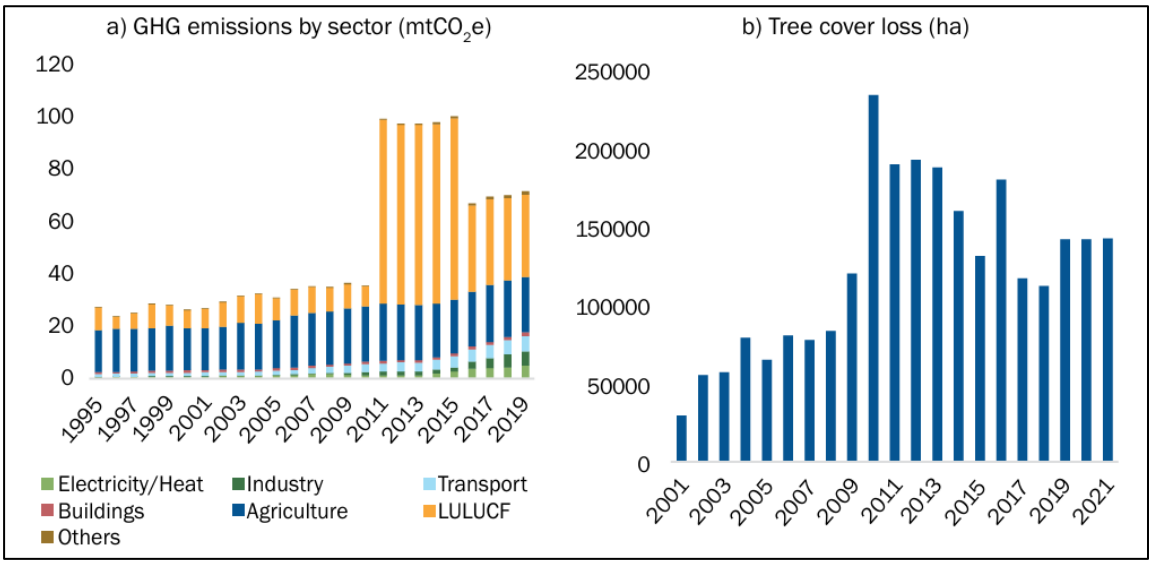

Figure 4.5 LULUCF is the largest contributor to Cambodia's gross GHG emissions (left), with the country experiencing significant tree cover loss over the past decade (right).
Source: (World Bank, 2023).
Note: Panel a) Climate Analysis Indicators Tool emissions data; Panel b): Global Forest Watch satellite data. The discrepancies between the satellite data and official emissions data reflect the fact that the emissions data is collated as part of a government-led inventory process that estimates potential forest loss, with estimates differing from satellite-based data. Government-led Forest cover inventories are published every five years, and GHG emissions are estimated by interpolations over those five-year periods and by projections.

Cambodia has pledged to achieve carbon neutrality by 2050. Achieving this goal will require a decoupling of GDP growth from emissions growth. On December 30, 2021, Cambodia submitted its LTS4CN to the UNFCCC. The LTS4CN largely builds on existing commitments and proposes a trajectory considered to be consistent with the updated NDC from 2020, which included the target to lower emissions by 41 percent by 2030, relative to a business-as-usual (BaU) scenario. Under a BaU scenario of current policies, emissions (excluding those from LULUCF) are projected to nearly triple between 2020 and 2050. With the exception of the LULUCF sector, this section models a low-carbon growth scenario that incorporates emission reduction strategies in accordance with Cambodia's NDC and LTS4CN climate pledges. The policies described in the LTS4CN are rigorously adhered to in the mitigation policy package, which contains measures to speed up transportation electrification, speed up the expansion of renewable energy in comparison to the BaU, implement a moderate carbon price, and encourage energy efficiency in accordance with the National Energy Efficiency Policy (NEEP). Figure 4.6, Panel b) summarizes the impacts of the low-carbon development scenario on emissions in the CGE model. This scenario results in non-LULUCF emissions that are 52 percent lower than the BAU by 2050. With the LTS4CN target of 50 million tCO_2-eq carbon sinks from the LULUCF sector, these policies are sufficient to achieve carbon neutrality by 2050. The lower emissions in this scenario stem particularly from lower power sector emissions and industrial emissions.

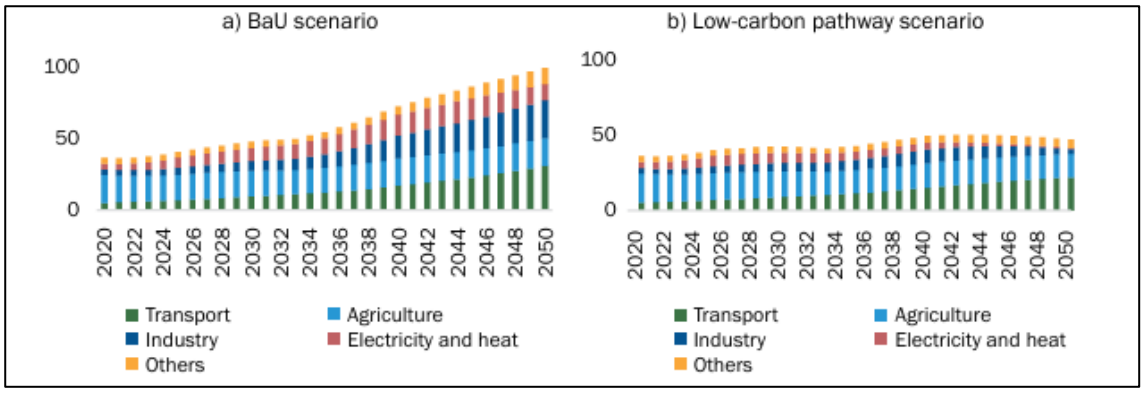

Figure 4.6 Under a BaU scenario, emissions (excluding LULUCF) are projected to nearly triple between 2020 and 2050 CGE model emissions (million tCO_2-eq), excluding LULUCF.
Source: (World Bank, 2023).

4.2.2 Connections to Air Quality and Atmospheric Composition

Over the last ten years, Cambodia has made a remarkable achievement of sustaining a robust and inclusive economic growth of around 7.9 percent per annum. Sustained rapid growth has played a significant role in raising living standards and drastically lowering poverty, which dropped from 13.5 percent in 2014 to about 10 percent in 2018. Based on this accomplishment, the RGC has established a long-term goal to make Cambodia an upper-middle-income nation by 2030 and a high-income country by 2050 (MEF & GSSD, 2019). With an average GDP growth of 6.98 percent between 2010 and 2015 and 7.1 percent between 2015 and 2019, the economy performed statistically (World Bank, 2019). GDP per capita was roughly USD 1,215 in 2016 (MEF, 2016) and USD 1,641 in 2019 (World Bank, 2019).

In 2022, Cambodia had an estimated population of 16.8 million with an annual population growth rate of 1.1 percent (World Bank, 2023). Even though 75 percent of the population currently reside in rural areas, the nation is becoming more urbanized at a rate of 2.9 percent each year, with almost half of the urban population living in the capital city. On the 2021 Human Development Index, which takes into account variables including life expectancy, education, and per capita income, Cambodia is ranked 146th out of 191 countries, representing a medium level of human development (UNDP, 2022).

With its rapidly growing economy, Cambodia is not immune to rapidly rising air pollution levels. Increasing industrial processes, a growing fuel-intensive vehicle fleet, wildfires, open field burning of solid waste, and construction sites are seen as the main contributors to this decline in air quality. Urban Cambodians, in particular, have observed a deterioration in the quality of the air they breathe and rural Cambodians are not immune to breathing high levels of air pollution. In 2015, 83.5 percent of Cambodian households depended on firewood as an energy source, primarily for cooking, and more than 80 percent (2018) of their energy use was for cooking (ADB, 2019).

Air pollution has a number of serious negative effects on the environment, public health, and economic growth (Table 4-2). Air pollution is a transboundary issue even though its effects are felt locally. For instance, most air pollutants, like nitrogen oxides, have a direct impact on air quality close to where they are emitted, but other pollutants, like sulfur dioxide, can travel great distances and have an impact on air quality hundreds or even thousands of kilometers away. Several studies have been undertaken on the health effects of air pollutants, including epidemiological, clinical, toxicological, and evidence-

based investigations on the relationship between pollutants and diseases. Table 4.2 summarizes some of the health impacts of air pollution.

Table 4.2: Pollutant exposure and health impact

Pollutants	Exposure	Impact
PM2.5	Short-term	mortality and morbidity
	Long-term	• Lung cancer • Mortality and morbidity • Cardiovascular mortality and morbidity, • Several health outcomes: atherosclerosis • Adverse birth outcomes and childhood respiratory disease
MP10		• Mortality, morbidity (both, short-term and long-term) • Cardiovascular diseases, including ischemic heart disease, cerebrovascular disease and heart failure associated
NO_2	Long-term	• Respiratory and cardiovascular mortality • Respiratory symptoms and lung function in children
	Short-term	• Respiratory outcome
SO_2		• Effect on heart rate variability • Asthma symptoms in children • Respiratory symptoms and lung function in children • Chronic obstructive pulmonary disease • Mortality and morbidity risk
O_3		• Premature mortality and non-fatal respiratory diseases

Source: (MoE, 2021)

In Cambodia, like in other countries, economic development is absolutely leading to an increase in the level of air pollution. The summary of PM2.5, SO_X, NO_X, CO, CO_2, O_3, TSP and other substances are emitted from various sources such as vehicles, motorbikes, factories, generators, etc. is shown in Figure 4.7.

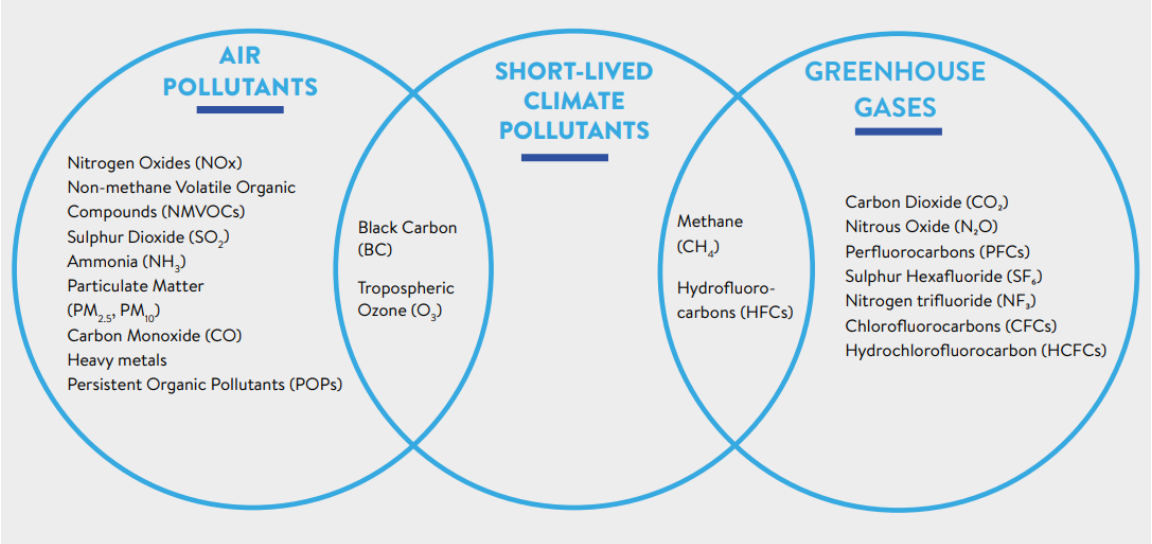

Figure 4.7 Summary of pollutants that are classified as air pollutants, short-lived climate pollutants and GHGs

Source: (CCAC SNAP, 2019)

4.2.2.1 Implications for GHG Lifespan

The upward trend of human population growth results in higher needs for energy. Currently, most of the energy demand is fulfilled by the burning of fossil fuels, which emit massive amounts of GHGs. CO_2 and other GHGs, such as CH_4 and N_2O, are emitted when

burning fossil fuels; producing materials such as steel, cement, and plastics; and agricultural activities. CO_2 is the biggest cause of human-made climate change, but other greenhouse gases are important too. They come from different sources, linger in the atmosphere for various amounts of time, and are more or less potent at trapping heat. Greenhouse gases are usually counted in "CO_2 equivalents" (CO_2-eq). One CO_2-eq is the amount of heat an equal amount of CO_2 would be expected to trap over the next 100 years. Emissions of CO_2 and other GHG are the primary drivers of the global rise in temperatures (IPCC, 2021b). GHGs cause global warming by trapping heat. Over the past 150 years, almost all of the increase in GHGs in the atmosphere has been caused by human activities (Hartman et al., 2013). On the global scale, the key GHGs emitted by human activities include the following:

- **Carbon dioxide (CO_2)**: CO_2 enters the atmosphere through burning fossil fuels (coal, natural gas, and oil), solid waste, trees, and other biological materials, and also as a result of certain chemical reactions (e.g., cement production).
- **Methane (CH_4):** The number-two cause of climate change is methane, the main component of natural gas. CH_4 reflects about 100 times as much heat as CO_2, but its lifetime in the atmosphere is much shorter: about 10 years. CH_4 is an especially hard GHG to measure because most emissions do not come from industrial plants. Instead, they come from livestock, other agricultural practices, changes in forests and wetlands, land use, decay of organic waste in municipal solid waste landfills, and leaks from gas wells and pipes.
- **Nitrous oxide (N_2O)**: N_2O is a powerful GHG that persists in the atmosphere for over 100 years. It is best known as laughing gas, but that kind of commercial use makes up only a tiny part of emissions. N_2O is emitted during agricultural, land use, and industrial activities; combustion of fossil fuels and solid waste; as well as during treatment of wastewater.
- **Fluorinated gases**: Fluorinated gases, primarily hydrofluorocarbons, or HFCs, are used in refrigerators, air conditioners, and a variety of industrial processes. Hydrofluorocarbons, perfluorocarbons, sulfur hexafluoride, and nitrogen trifluoride are synthetic, powerful greenhouse gases that are emitted from a variety of household, commercial, and industrial applications and processes (Climate Portal, 2023; US EPA, 2024).

The GHG inventory of Cambodia includes estimates of GHGs, including CO_2, CH_4, N_2O and HFC emissions, and includes the following sectors: energy; industrial processes and product use (IPPU); agriculture, forestry and other land use (AFOLU); and Waste. The inventory was developed following the 2006 IPCC Guidelines. Table 4.3 shows the emissions estimated by gas and sector for the years from 1994 through 2016. Due to limited information on their occurrence, the emissions of Perfluorocarbons (PFC), Sulphur hexafluoride (SF_6), and Nitrogen trifluoride (NF_3) have not been estimated. Gases considered ozone precursors: CO, NOx, non-methane volatile organic compounds (NMVOCs), and SO_2, have been estimated when the required data was available. In terms of the contribution of each GHG to national total emissions, CO_2 is the main gas emitted, driven by the large contribution of the FOLU sector to national total emissions, followed by CH_4, N_2O and HFC (Table 4.3).

Table 4.3: Emissions by category and gas in 2016

Inventory Sector	CO_2	CH_4	N_2O	HFC*	NO_X	CO	NMVOC	SOx
	(Gg)							
Energy	8845.29	23.04	0.61	NA	43.43	160.46	45.03	32.61
IPPU	1449.46	NA	NA	371.68	NE	NE	NE	NE
Waste	814.55	79.7	0.82	NA	NE	NE	NE	NE
Agriculture (3A + 3C)	17.42	645	7.56	NA	NE	NE	NE	
Forest and OtherLand Use (FOLU) (3B)	131011.24	NA	NA	NA	NA	NA	NA	NA
Total (without FOLU)	11127.73	747.87	8.98	371.68	43.43	160.46	45.03	32.61
Total (With FOLU)	142137.97	747.87	8.98	371.68	43.43	160.46	45.03	32.61

Source: (MoE, 2019b)

4.2.2.2 Aerosols

Aerosols in the atmosphere are compounds of liquid, solid, or mixed particles having a very different size distribution and chemical composition (Putaud et al., 2010). Their variability is due to the numerous sources and varying formation mechanisms. Aerosol particles are either emitted directly to the atmosphere (primary aerosols) or produced in the atmosphere from precursor gases (secondary aerosols). Globally, anthropogenic aerosols are estimated to produce a net cooling of ~-1.3 ± 0.7 W/m^2 at the top of the atmosphere; -0.3 ± 0.3 W/m^2 is attributed to the aerosol–radiation interaction (ARI), -1.0 ± 0.7 W/m^2 to aerosol-cloud interactions, ~-1.15 W/m^2 to total forcing from scattering aerosols and ~$+0.12$ W/m^2 to BC (IPCC, 2021). The combined aerosol forcing offsets roughly one-third of the warming from anthropogenic GHGs. However, the large spread in the estimated aerosol forcing leads to large discrepancies in climate sensitivity (Wang et al., 2021).

All atmospheric aerosols scatter incoming solar radiation, and a few aerosol types can also absorb solar radiation. Aerosols that mainly scatter solar radiation have a cooling effect, by enhancing the total reflected solar radiation from the Earth. Strongly absorbing aerosols have a warming effect. In the atmosphere, there is a mixture of scattering and absorbing aerosols, and their net effect on Earth's energy budget is dependent on surface and cloud characteristics. Scattering aerosols above a dark surface and absorbing aerosols above a bright surface are the most efficient. Scattering (absorbing) aerosols above a bright (dark) surface are less efficient because the solar radiation is reflected (absorbed) anyway. Absorbing aerosols are particularly efficient when positioned above clouds and are a main contributor to the total reflection of solar radiation back to space (Myhre, 2013).

The majority of aerosols can travel great distances even though they are only sustained in the atmosphere for brief periods of time, usually four days to a week. In a week, particles traveling at 5 meters per second through the atmosphere will cover thousands of kilometers. Dust plumes from the Sahara frequently cross the Atlantic and reach the Caribbean. Winds sweep a mixture of Asian aerosols, particularly dust from the Gobi

Desert and pollution from the east of China, over Japan and toward the central Pacific Ocean. Smoke from wildfires in Siberia and Canada can find its way to the Arctic ice cap (Chung et al., 2005).

Aerosols can have a more significant and widespread geographical impact on the energy balance and climate, even though their concentrations and instantaneous forcing are greatest close to their sources. Aerosol pollution frequently exceeds WHO standards in urban areas where industrialization, transportation emissions, and fast urbanization converge, posing serious threats to environmental integrity and human health(Khan et al., 2023). Aerosols makeup the majority of fine particulate matter (PM2.5), which causes respiratory illnesses cardiovascular conditions, and early death. This emphasizes the urgent need for pollution control and air quality management.

4.2.2.3 Biomass Burning

Biomass burning of both living and dead vegetation emits significant amounts of trace gases, GHG, and particulate matter into the atmosphere and surface albedo, which has significant implications for atmospheric chemistry and climatic change. Consequently, it leads to the rapid decomposition of organic-rich soil horizons (Chang and Song, 2010, Tylor, 2010). Between 2000 to 2006, average emissions from burning were estimated at 128 ± 51 Tg C year-1 in equatorial Asia (Van der Werf, 2008). In the Greater Mekong Subregion, the total biomass burnt area in 2015 was estimated to be approximately 33.3 million ha releasing 178 ± 42 Mt CO_2, while all biomass burning in the Asian continent released an estimated 1,100 Tg CO_2 (Agapol, 2020; Streets et al, 2003).

In Cambodia, biomass burning occurs in the agriculture sector for rice straw and sugar cane cultivation and burning grassland. Rice straw is typically left to be open-burned in the field. It is estimated that roughly 30 percent of the straw residue is burned in the field (Sokles, 2022). For sugar cane, burning before harvest is very common because harvesting is difficult without burning due to the lack of mechanization; it is estimated that 100 percent of the sugar cane area is burned. For grasslands, it is assumed that residues are burned yearly during the dry season; however, in the First and Second National Communication report, the estimates used 50 percent (IPCC 1996 guidelines) by the Ministry of Environment for emission calculation. Fires in deciduous forests also occur regularly and approximately 60 percent of deciduous forests are estimated to catch fire at least once a year, especially during the dry season (Maxwell, 2004). However, this has not been adequately studied (Halperin and Turner, 2013).

CH_4 emissions from crop residue burning and grassland burning was 2.72 Gg/year in 1994, 3.13 Gg/year in 2005, 6.96 Gg/year in 2016, and 9.93 Gg/year in 2005 (MoE, 2019), respectively. For NO_2 emission from crop residue and grassland burning, it accounts approximately 0.22 Gg/year, 0.27 Gg/year, 0.39 Gg/year, and 0.61 Gg/year in 1994, 2005, 2016, (MoE, 2019) and 2021 (ODC, 2024), respectively. However, the emission from deciduous forest burning is not properly recorded. Table 4.4 below illustrates the burning area and amount of estimating biomass burned in Cambodia from 1990 to 2021.

Table 4.4: Burning area and amount of estimating biomass burned in Cambodia from 1990-2021

	Area Burnt (ha)			Biomass Burnt (t)		
	Rice	**Sugar cane**	**Grassland**	**Rice**	**Sugar cane**	**Grassland**
1990	41,500	6,000	240,000	155,930	39,000	984,000
1991	500,700	6,000	240,000	145,822	39,000	984,000
1992	490,620	6,000	240,000	140,286	39,000	984,000
1993	532,088	6,473	240,000	151,752	42,075	984,000

	Area Burnt (ha)			Biomass Burnt (t)		
1994	431,880	7,000	240,000	128,453	45,500	984,000
1995	555,700	7,420	241,417	176,718	48,230	989,808
1996	541,840	7,022	242,833	173,029	45,643	995,617
1997	556,387	8,035	244,250	176,131	52,228	1,001,425
1998	566,190	6,933	245,667	179,917	45,065	1,007,233
1999	600,893	8,374	247,083	197,238	54,431	1,013,042
2000	547,648	7,480	248,500	186,141	48,620	1,018,850
2001	569,278	7,727	248,500	191,737	50,226	1,018,850
2002	572,072	9,395	248,500	186,738	61,068	1,018,850
2003	644,778	8,482	248,500	218,531	55,133	1,018,850
2004	603,372	6,739	248,500	199,442	43,804	1,018,850
2005	692,247	5,992	248,500	252,324	38,948	1,018,850
2006	722,156	8,296	248,500	263,714	53,924	1,018,850
2007	735,650	10,458	248,500	275,179	67,977	1,018,850
2008	747,946	13,297	248,500	286,103	86,431	1,018,850
2009	763,976	13,533	248,500	296,915	87,965	1,018,850
2010	798,126	17,072	248,500	317,423	110,968	1,018,850
2011	806,122	22,069	248,500	331,674	143,449	1,018,850
2012	787,528	27,859	248,500	321,047	181,084	1,018,850
2013	842,346	30,665	248,500	345,973	199,323	1,018,850
2014	859,565	25,503	248,500	187,061	165,770	1,018,850
2015	858,744	27,316	248,500	348,218	177,554	1,018,850
2016	878,079	28,972	248,500	191,052	188,318	1,018,850
2017	59,565	25,503	351,337	187,061	165,770	1,018,850
2018	858,744	27,316	351,337	348,218	177,554	1,018,850
2019	78,079	28,972	341,132	191,052	188,318	1,018,850
2020	56,700	28,950	341,132	520,670	188,175	1,398,641
2021	973,440	28,770	319,828	529,781	187,005	1,311,295

Source: (MoE, 2019; CAES-RUA, 2024)

4.2.2.4 Urban Air Pollution

Air pollution and climate change are closely interlinked with each other. Increasing concentrations of air pollution, such as particulate matter, ozone, and volatile organic compounds (VOCs), can influence trends in climatic parameters such as radiative forcing, temperature, and albedo (Algo, 2016). Increased exposure to air pollution, specifically PM2.5, has been associated with increased risks of respiratory and cardiovascular diseases, diabetes, stroke, and lung cancer (EEA, 2024). Besides PM2.5, the high concentration of ozone at ground level can be harmful to human health by affecting the respiratory and cardiovascular systems. NOx, SOx, CO_2, and volatile organic compounds are major pollutants that are harmful to humans (Ioannis, 2020). Urbanization is a main source of air pollution. As a result of more economic activities and increased consumption due to prosperity, urban areas emit higher amounts of air pollutants than non-urban areas (Molina, M. J., & Molina, L. T., 2004).

In Cambodia, as in other developing countries, economic development is leading to an increase in the level of air pollution. The concentration. PM2.5, SO_X, NO_X, CO, CO_2, O_3, TSP, and other substances are emitted from various sources, including vehicles, motorbikes, factories, generators, and other urbanization activities (MoE, Clean Air Plan of Cambodia, 2021). In the largest cities —Phnom Penh, Siem Reap, Battambang, and Preah Sihanouk —emissions from mobile sources, especially from vehicles, contribute to air pollution, including VOCs, CO_2, as well as PM2.5 and PM10, among others. According to a study by the Ministry of Environment in 2024, vehicle emissions are one of the major sources of air pollution in the transportation sector, accounting for 60.5 percent of CO_2

emissions. It is reported that around 70 percent of air pollution in Phnom Penh is caused by transportation, with diesel-fueled vehicles being the main contributor (MoE,2024).

In addition, open burning of waste, home cooking, and infrastructure construction is also considered key sources of air pollution in urban areas in Cambodia. Forest fires are also a source of urban air pollutants, particularly during the dry season (MoE, Clean Air Plan of Cambodia, 2021); about 60 percent of deciduous forests are estimated to catch fire at least once a year (Maxwell, 2004).

4.3 Implications of Different Socio-economic and Emission Pathways

A number of frameworks have been developed to comprehend the growing threats of socio-ecosystem collapse and degradation, ranging from the changes caused by humans in the last several centuries to the climate, marine, and terrestrial systems (Lade et al., 2019; Nash et al., 2017; Zommers et al., 2020). The IPCC estimates Global Climate Risk from anthropogenic climate change by the end of the twenty-first century. Global Climate Risk is defined as the globally aggregated risks related to climate change that affect terrestrial and ocean systems across ecological and human dimensions at all latitudes and levels of socioeconomic development in both developed and developing countries. A comprehensive understanding of climate risk on a global scale is essential for international decision-making (Agassiz, 2001; Zommers et al., 2020).

Based on macroeconomic modeling by the World Bank (2023) Click or tap here to enter text. climate change could reduce Cambodia's GDP by 3 to 9 percent by 2050. The estimates of the annual impacts of climate change on GDP from two macroeconomic models: CGE and MINDSET (Figure 4.9). Both models incorporate estimates of asset losses from floods and estimates of the impact of climate change on labor productivity, crop yields, and tourism. The one-year-only MINDSET model accounts for asset losses from a one-in-ten-years flood, of which three might be expected between 2020 and 2050. The CGE model averages annual asset losses from floods. Both models show similar aggregate impacts from climate change by 2050. In the CGE model, the impacts range from 3.0–9.4 percent in the low and high climate change scenarios, respectively. In the MINDSET model, impacts reach a similar 9.1 percent in the high scenario. In the MINDSET model, it is possible to disaggregate effects by impact channel. The results demonstrate that asset losses from floods have the greatest impact, accounting for 7.4 percent of the total 9.1 percent loss. A sensitivity analysis included in the Technical Appendix shows that this impact from floods would fall to 2.9 percent points for a one-in-a-two-years flood and therefore impacts in any given year depend on the magnitude of the floods that occur.

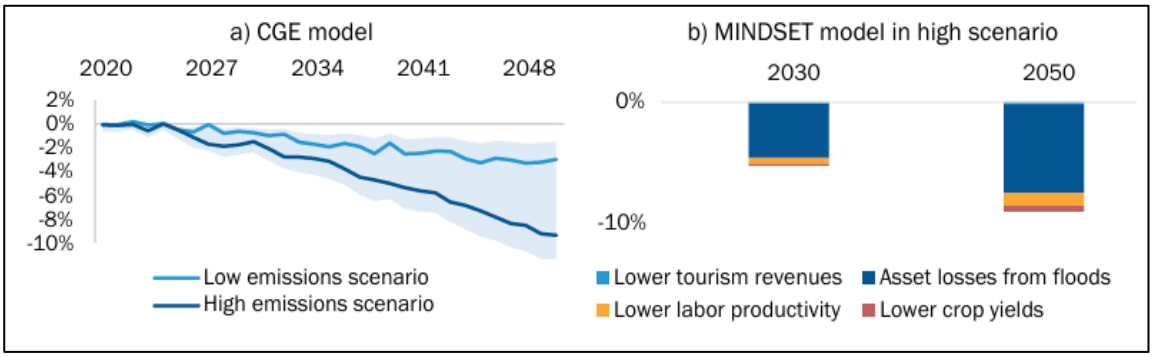

Figure 4.8 Climate change could lower GDP by 3.0–9.4 percent by 2050 (GDP impacts of climate change relative to a no-climate change baseline, without adaptation (percent)).
Source: (World Bank, 2023)
Notes: Panels a) and b) include asset losses from floods, impacts of heat on labor productivity, impacts of climate change on tourism, and impacts of climate change on agriculture crop yield losses, without adaptation measures. In panel a), asset losses are the average. In panel b), asset losses are based on losses from a 1 in 10-year flood, excluding supply chain effects. Panel c) includes the direct effects of the floods, knock-on supply chain effects, and demand-side multiplier effects, with limited adaptation possibilities. Supply chain flexibility is the length of time that companies can continue producing without receiving new inputs, for example by holding reserve stocks; the maximum on the x-axis is six weeks.

The impact of flooding could be considerably greater in a year with a high-impact flood, but it would mostly depend on how businesses plan and prepare for floods. The MINDSET model is also used to estimate the effects of floods of different return periods, including their demand-side multiplier effects and knock-on supply chain effects, in order to better understand the possible macroeconomic implications of high-impact floods and how they differ based on how businesses prepare. The impacts of smaller floods can be mostly offset by businesses preparing adequately. However, even for floods that occur once every ten years, losses could reach up to 7–11 percent of GDP, with lower impacts where businesses are more prepared. A one-in-83-years flood could knock off 20–23 percent of GDP in one year. In the 30 years between 2020 and 2050, there is a 33 percent chance of such an event occurring. These results highlight the macro-criticality of adaptation measures and disaster risk financing (DRF).

Without adaptation measures, Cambodia's physical assets in manufacturing, services, and housing are highly vulnerable to flood damage, with potential losses modeled by the World Bank ranging from an optimistic low scenario (20th percentile of SSP1-RCP2.6) to a pessimistic high scenario (80th percentile of SSP5-RCP8.5) based on various climate change projections (World Bank, 2023). Probabilistic modeling for this CCDR shows that the estimated asset losses from a 1-in-25-years flood in 2020 totaled USD 412 million in manufacturing, USD 344 million for services, and USD 108 million for housing (Figure 4.10). Annual average losses in 2020 were estimated to be approximately USD 530 million. Climate change is projected to increase the frequency of high-impact floods, resulting in higher average losses. By 2050, annual average losses are projected to increase to USD 3.3 billion under an optimistic climate change scenario. Under a pessimistic climate change scenario, annual average losses stand at around USD 10.6 billion. This is assuming a worst-case scenario with no risk-informed land-use planning and thus high construction levels in flood risk areas.

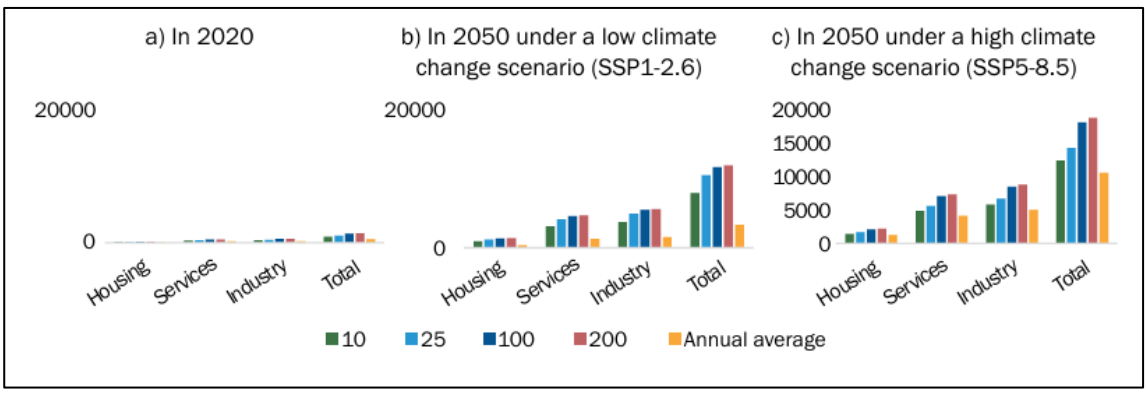

Figure 4.9 Cambodia Climate change is projected to substantially increase asset losses from floods of different return periods (USD, millions).
Source: (World Bank, 2023)

The Climate Economic Growth Impact Model (CEGIM) project, a collaborative study done by the Ministry of Economy and Finance (MEF), the Ministry of Environment, and the National Council for Sustainable Development (NCSD) with financial and technical support from the United Nations Development Program (UNDP), reports that real GDP will grow at an average of 6.9 percent per year from 2017 to 2050, leading to Cambodia achieving upper middle-income country (UMIC) status in 2035. Climate change is predicted to reduce average GDP growth to 6.6 percent and absolute GDP by 0.4 percent in 2020, 2.5 percent in 2030, and 9.8 percent in 2050, resulting in UMIC status being delayed by one year. Figure 18 presents the GDP growth paths without climate change and with climate change, including 3 levels of adaptation (Figure 4.11).

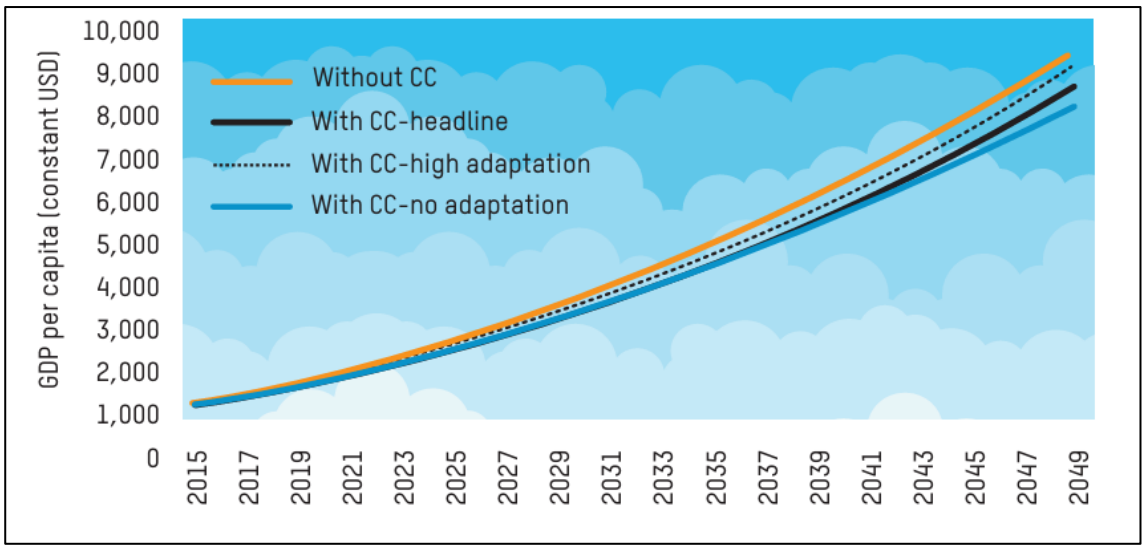

Figure 4.10 Impact of CC on economic growth paths – 3 Scenarios.
Source: (MEF and NCSD, 2019)

Figure 4.11 shows how sectors are affected by climate change and whether the impact comes through loss of income, labor productivity, or damage to assets. In 2050, reduced labor productivity accounts for 57 percent of all loss and damage. It affects all sectors but is particularly high in manufacturing and construction. Loss of income accounts for 17 percent of all loss and damage and is concentrated in the four agricultural sectors. Damage to assets accounts for 26 percent of loss and damage and is spread across all sectors, being especially significant for service sectors, which are affected by damage to roads.

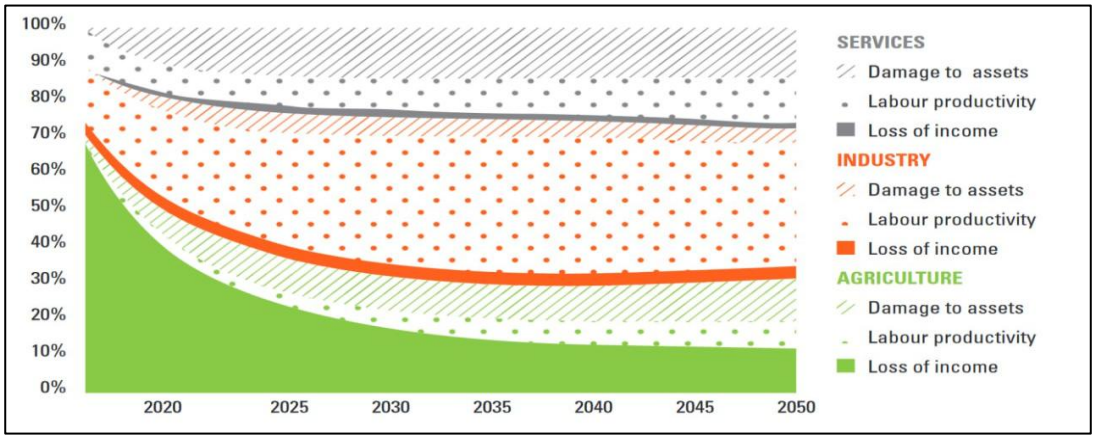

Figure 4.11 Economic impact of CC by sector and type of impact (percent drop in absolute GDP 2050)
Source: (MEF and NCSD, 2019)

4.3.1 Terrestrial Ecosystems and Climate Change

The effects of climate change are already being felt globally, endangering cities, communities, crops, water, and wildlife through more frequent and severe storms, floods, droughts, and wildfires. Nature, wildlife, and humans are all fundamentally threatened by climate change. Climate change has already altered marine, terrestrial, and freshwater ecosystems, caused species losses and declines in key ecosystem services by altering (1) geographic ranges and habitats; (2) survival, growth, and development; (3) reproduction and replication; (4) transmission and exposure; (5) behavior; and (6) access to immunologically native animals and people who lack resistance to infection.

Terrestrial ecosystem function is largely governed by the composition and physical structure of vegetation, and the effects of climate change on vegetation may disrupt ecosystem services and reduce biodiversity (Cardinale et al., 2012). Human land usage and management have a significant impact on terrestrial ecosystems (Yue et al., 2020).

Anticipated climatic changes are expected to force both continuous and abrupt changes in the distribution of ecosystems and species (Nolan et al., 2018). As global GHG emissions rise, it is crucial to estimate the expected degree of ecosystem modification and understand the full potential magnitude of impacts if current GHG emission rates continue unabated. Ecosystem transition typically occurs through the replacement of dominant plant species or functional types by others, whether recruited locally or migrating from afar. Mass mortality of incumbent dominants accelerates ecosystem change, and many forests and woodlands are currently experiencing extensive dieback events and other significant disturbances (Allen et al., 2015), with further mortality events predicted under increasing temperatures and drought (Asner et al., 2016). Furthermore, there is mounting evidence of individual species' shifting geographic ranges, and in many areas, vegetation changes are being driven by the interaction of climate change with invasive species, fire regimes, land use, and rising CO_2 levels (Parmesan et al., 2015).

In Cambodia, climate change is causing a variety of natural disturbances such as increased extreme droughts, floods, tropical cyclones, more frequent wildfires, rising sea levels which has been largely induced through land-use changes, deforestation and reductions in soil organic matter levels related to soil tillage. To counter reductions in agricultural yields, communities rely on illegal logging in protected forests to supplement food and income, including collecting fuelwood or charcoal (MoE, 2019a). This affects forests' ability to provide both climate and soil water regulation in the agriculturally vital Mekong River Basin. The sectors most affected by climate change are agriculture, infrastructure, forestry, human health, and coastal zone areas which are particularly vulnerable to sea level rises and intrusion (MoE, 2020b). Existing temperature rise is already affecting the development and behavior of many organisms in terrestrial ecosystems. The effects of climate change extend beyond direct impacts on ecosystems and species; they also interact with other human stressors, such as development. Although some stressors cause only minor impacts when acting alone, their cumulative impact may lead to dramatic ecological changes (IPCC, 2014). Figure 4.13 shows how ecological systems are impacted by the interaction of climate change and non-climate stresses at various scales.

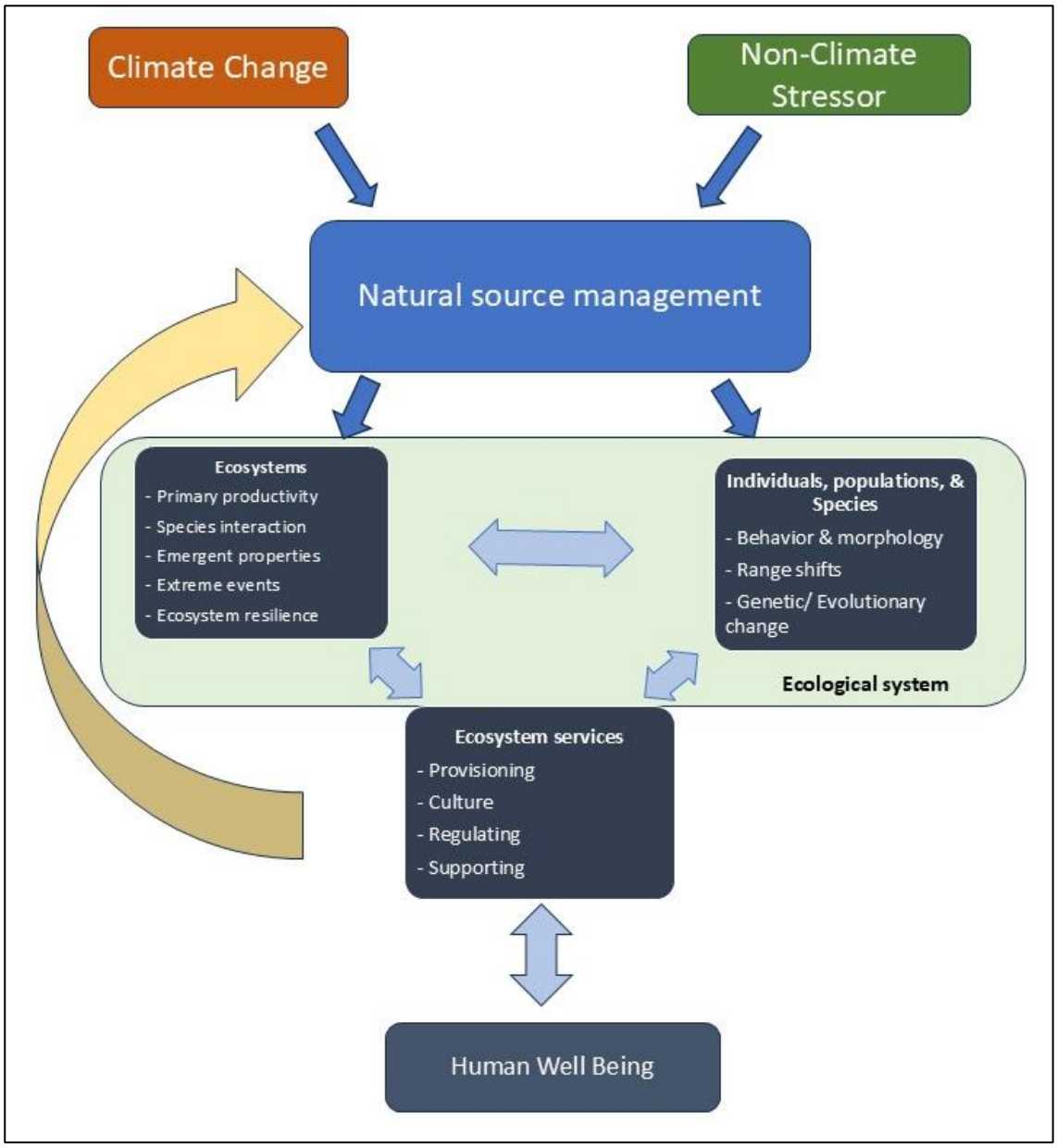

Figure 4.12 Ecological systems are impacted by the interaction of climate change and non-climate stresses at various scales

Source: Adapted from (Weiskopf et al., 2020).

Note: These stressors have an impact on ecological processes and characteristics as well as individuals, populations, and species. Depending on the species or environment, different stressors have different relative effects from climate change. Maintaining the ecosystem services requires diverse biological communities and healthy ecosystems(Finlayson et al., 2005) that support human well-being. Natural resource management affects biodiversity, ecosystems and their services and can moderate or exacerbate climate change and non-climate stressors

4.3.2 Land Use/ Land Cover Change

The rapid growth of economic development, infrastructure development, urban expansion, and changes in the legal framework or policy, particularly regarding land tenure security and the expansion of agricultural land to respond to the increasing human population, have influenced natural land cover (Toure, Stow, Shih, Weeks, & Lopez-Carr, 2018; Velastegui-Montoya, de Lima, & Adami, 2020). Changes in land use and land cover due to deforestation, afforestation, agricultural conversions, and urbanization, can affect temperature, precipitation, winds, and soil moisture (Sleeter, 2018; Pitman, 2012). In

addition, mining and infrastructure development are also significant drivers contributing to land use and land cover changes that lead to deforestation and habitat loss, and impacting ecosystems and local communities (Nut et al., 2021). Land cover change, particularly due to development purposes such as new settlements, often results in the permanent loss of natural resources. Change over large areas can potentially influence the Earth's climate by altering regional and global circulation patterns, changing the albedo of Earth's surface, and altering the amount of carbon dioxide in the atmosphere. In addition, land cover can be affected by climate change, leading to a loss of forest cover from climate-related disturbances, increasing degradation of vegetation into grasslands, and the loss of beaches due to coastal erosion and rising sea levels (Algo, 2016).

Over the last three decades, population and economic growth, market demand, major political change and property rights development, climate change, and human migration have significantly influenced Cambodia's LULU and landscape (Upham, 2014; Sochanny Hak, 2018). After the civil war, Cambodia was transitioning to a market-oriented democratic state. During that time, large-scale forest concessions were promoted under the 1992 Land Law and were provided to private companies, resulting in agricultural land at the expense of forest loss (Upham, 2014; Sochanny Hak, 2018). However, after the 2001 Land Law was enacted, the new property rights were named in different categories, namely: State Public Land, State Private Land, Economic Land Concessions (ELCs) and Communal Land Titles. These caused confusion over property rights on communal land of indigenous communities and economic land concessions (Sochanny Hak, 2018). Much of the communal land overlapped with the ELCs, which were previously categorized as State Public Land and reassigned as State Private Land for investment by foreign and domestic investors through the ELC process (Upham, 2014; Sochanny Hak, 2018).

Forest cover in Cambodia has decrease dramatically from year to year, with the deforestation rate increasing from 1.1 percent before 2000 to 1.3 percent up to 2010 (FAO, 2010). Between 1990 and 2010, forest cover in Cambodia fell from 12.94 to 10.09 million ha, 73 percent to 57 percent of the total land area, respectively. Over the same period, the area of forest designated for conservation increased from 2.77 to 3.98 million ha, which is equivalent to 23 percent of the total land area and 39 percent of the forest area (Izquierdo, 2010). In 2018, the forest cover remains only approximately 8.51 million ha, equal to 46.86 percent. Between 2014 and 2018, the forest land has decreased from 9.03 to 8.51million ha. Deciduous forest lost approximately 0.27 million ha, followed by approximately 0.17 million ha of evergreen forest as illustrated in Table 12 and Figure 4.14 and Figure 4.15 (MoE, 2020a).

Deforestation drivers in Cambodia include illegal logging, expansion of settlements and agriculture, infrastructure development, climate change and forest fire, and timber and wood fuel demand. One of the key drivers is agricultural expansion, both through small-scale clearing for farms and plantations, as well as through the granting of forestland for large-scale agro-industrial development through ELCs. In effort to combat illegal logging, the government has introduced a moratorium on timber harvesting of natural forests and has allowed for community forest practices since 2003 (FAO, 2010). The direct and indirect drivers of land cover change are listed in Table 4.10 below. FOLU is the major contributor of GHGs, followed by the agriculture sector in Cambodia. A total of 27,018 Gg CO_2 was released in 1994, dramatically increased to 131,011 Gg CO_2 in 2010, and significantly decreased to 31,011 Gg CO_2 in 2016, respectively, while the agriculture sector emitted 11,202 Gg CO_2 in 1994, 18,138 Gg CO_2 in 2010, and decreased to 8,397 Gg CO_2 in 2016 (MoE, 2019).

Table 4.5: Drivers of land use land cover change in Cambodia

	Within the forest sector	Outside the forest sector
Direct	High impact and illegal logging.	• Agricultural expansion; • Low agricultural yields; • Expansion of settlements; • Infrastructure development; • Forest fire; • Timber demand; • Wood fuel demand.
indirect	• Low institutional capacity and weak policy implementation; • Weak forest sector governance - Weak enforcement and control; - Low levels of stakeholder participation and involvement; - Corruption, clientelism and nepotism; - Lack of transparency and accountability; - Lack of assessment of social and environmental impacts. • Lack of demarcation of forest areas; • Low awareness of forestland management rights and responsibilities	• Population increases; • Rising incomes and demands for resources; • Increasing accessibility of forest areas; • Low agricultural yields; • Migration into forest areas; • Military activity; • Large scale agri-industrial development (ELCs and SLCs); • Lack of information on national land use and land use plans; • Governance - Overlapping/unclear jurisdictions; - Weak land tenure – tenure is weakest in forests and other areas outside residential or farming zones; - Weak enforcement of the law; - Lack of a fair and transparent conflict resolution - mechanism; - Chronic incidence of high-level interministerial and interagency disputes. • Social norms (claiming land through utilization); • Low awareness of environmental roles of forests.

Source: (FAO, 2010)

Table 4.6: Cambodia's land use and land cover change between 2014 to 2018

IPCC	Land Cover	MoE 2014	MoE 2016	MoE 2018	2014-2016	2016-2018	Average
Forest	Evergreen forest	2,973,903	2,861,233	2,799,032	-112,670	-62,201	-87,436
	Semi-evergreen forest	1,108,320	1,071,947	1,038,969	-36,373	-32,978	-34,676
	Deciduous forest	3,480,532	3,336,349	3,205,830	-144,183	-130,519	-137,351
	Flooded forest	481,078	477,813	471,599	-3,265	-6,214	-4,740
	Regrowth forest	228,560	196,842	176,088	-31,718	-20,754	-26,236
	Bamboo	130,678	125,398	122,397	-5,280	-3,001	-4,141
	Mangrove	33,002	31,226	31,298	-1,776	72	-852
	Rear Mangrove	25,906	25,906	25,755	0	-151	-76
	Pine forest	8,196	8,195	8,186	-1	-9	-5
	Pine Plantation	3,709	3,870	3,872	161	2	82
	Tree Plantation	44,289	43,122	39,254	-1,167	-3,868	-2,518
	Oil Paim Plantation	36,311	51,276	51,792	14,965	516	7,741
	Rubber Plantation	484,316	509,224	536,735	24,908	27,511	26,210
Cropland	Crop land	1,987,413	2,217,435	2,438,627	230,022	221,192	225,607
	Paddy Field	3,333,474	3,421,407	3,486,026	87,933	64,619	76,276

IPCC	Land Cover	MoE 2014	MoE 2016	MoE 2018	2014-2016	2016-2018	Average
	Degraded Land	1,600,000	1,600,000	1,600,000	0	0	0
Grassland	Grassland	351,337	341,132	319,828	-10,205	-21,304	-15,755
	wood Shrub	622,190	616,177	593,556	-6,013	-22,621	-14,317
Other land	Rock	2,054	1,100	2,341	-954	1,241	144
	Sand	40,581	41,245	41,564	664	319	492
Settlement	Village	328,820	352,987	365,709	24,167	12,722	18,445
	Build up Area	42,166	42,930	43,943	764	1,013	889
Wetland	Water	813,839	783,860	758,273	-29,979	-25,587	-27,783
Total Land (ha)		**18,160,674**	**18,160,674**	**18,160,674**			

Source: (MoE, 2020a)

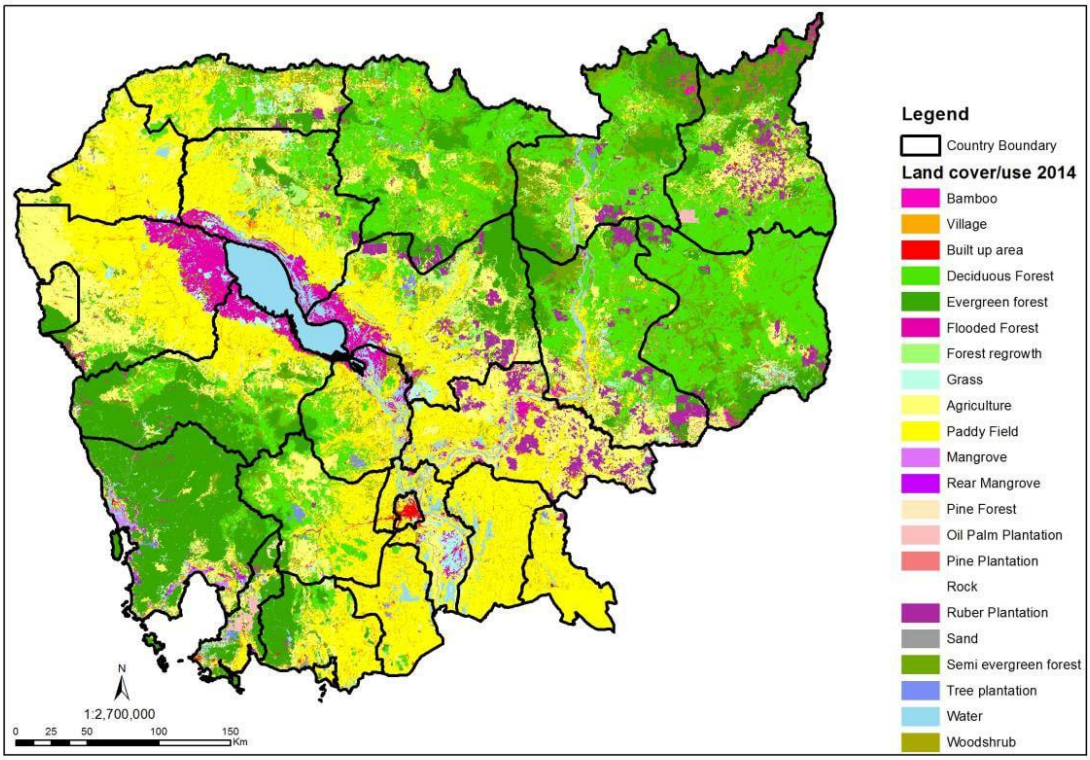

Figure 4.13 Land use land cover map 2014
Source: (MoE, 2015)

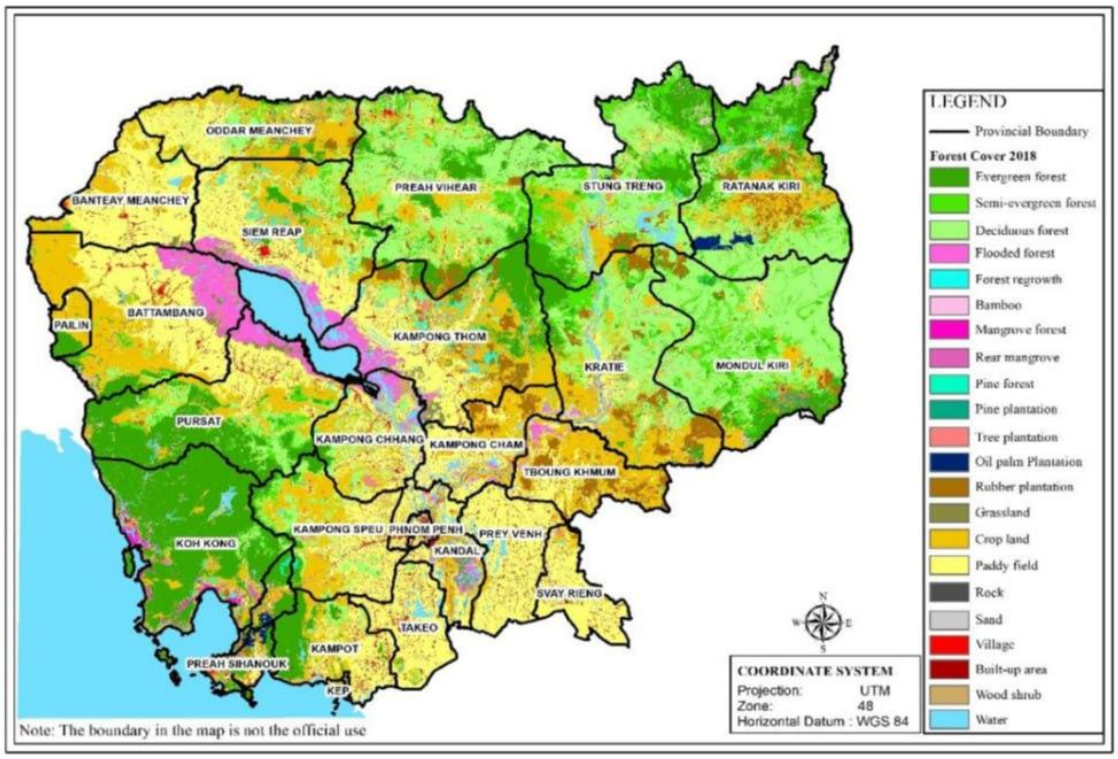

Figure 4.14 Land use land cover 2018
Source: (MoE, 2020a)

4.3.3 Urbanization

Globally, approximately 4.4 billion people, equivalent to 56 percent of the world's population, dwell in urban areas. The urban population is predicted to more than double in current size by 2050. By 2030, the expansion of urban land consumption is projected to surpasses population growth by approximately 50 percent, adding an estimated 1.2 million km² of new urban built-up areas worldwide (World Bank, 2023). Urbanization typically offers significant employment opportunities to citizens. Booming urban population growth is expected to meet the demand for labor in urban-based industries, including garment sectors, construction, manufacturing, agriculture, tourism, services, and trade (Lay and Neang, 2021).

In 2023, the population in Cambodia is 17.09 million, and it is projected with significant growth to 18.2 million by 2028, 19.3 million by 2033, and 21.7 million by 2050, respectively, with an average annual increase of 1.27 percent from 2019 to 2030 and 0.76 percent from 2019 to 2050 (MoP, 2023). Alongside this population growth, urbanization rates in Cambodia are also on the rise from year to year. In 2015, the urban population accounted for only 22.19 percent, 24.23 percent in 2020, and 25.11 percent in 2023, respectively (Statista, 2024). However, this percentage is projected to reach 30.6 percent by 2030 and 36 percent by 2050 (World Bank, 2017). Population growth, economic development, and rapid rural-urban migration have accelerated urbanization processes in major cities across the country. Cambodia is expected to continue to urbanize at an average annual rate of approximately 2.5 in the next 35 years.

Given Cambodia's relatively early stage of urbanization, there is still an important opportunity to shape the future direction of urbanization. To positively shape the future of urbanization, strong institutions for future urban planning and management, collaboration across agencies, and a sustained commitment to sustainability and

inclusion will be needed. Urbanization in Cambodia is closely bound with urban-rural development challenges and inequalities (Lay and Neang, 2021). Urbanization reflects the quality of living, living standards, income distribution, and social service provision in urban areas; however, it presents many challenges, particularly the impacts of climate change-related hazards, and exacerbates rural-urban divides. The impacts of climate change-related hazards on urban areas, including heat stress, extreme and excessive precipitation, flash floods, flooding, water scarcity, drought, and air pollution, are highlighted in the IPCC Fifth Assessment Report. Moreover, urbanization in major cities and regions changes the physical characteristics of the surface, resulting in significant impacts on the local climate and surface hydrology, including urban temperature variation, drought and water scarcity, flooding, and geo-hydrological hazard (Revi, 2014).

4.3.4 Urban Heat Island Effect and Heat Stress

Numerous urban environmental issues frequently arise as a result of rapid urban transition (Akyüz, 2021). Urban heat islands (UHI) are parts of a metropolitan area that are much warmer than their surroundings (Marko et al., 2016). A UHI effect tends to make cities warmer than their rural surroundings because of surfaces and structures, such as roads and buildings, that absorb and retain heat. Together with a relative lack of vegetation, and hence evaporative cooling, this causes a city to be hotter than its rural surroundings(Lee et al., 2024). The UHI phenomenon is strongly correlated with large dark surface areas, the increase in air temperature, and the constant increase of buildings and paved roads that result from urbanization (Zhao et al., 2016).

Urban surfaces have distinct thermal characteristics than rural vegetated regions, including lower albedo, less water available for evaporative cooling, and a greater capacity for heat storage(Taha, 1997). The effects of temperature rise and heat stress in urban areas are increasingly compounded by the urban heat island phenomenon. Dark surfaces, residential and industrial sources of heat, an absence of vegetation, and air pollution can push temperatures higher than those of the rural surroundings, commonly anywhere in the range of 0.1°C to 3°C for global megacities. Excess anthropogenic heat emission (AHE) caused by human activity, such as fuel combustion, e.g. from transport and air conditioning, is also an important contribution to UHI (Dong et al., 2017). Urban heat islands form as a result of altered landscapes in cities. Some of the main contributing factors are:

- **Urban surfaces**: Compared to natural surfaces, human-made building materials like concrete and pavement absorb more heat and reflect less sunlight. These urban surfaces contribute to the constant rise in city temperatures by rapidly heating up during the day and releasing heat gradually at night. In contrast, natural landscapes such as trees, vegetation, and water bodies help cool the air by providing shade, transpiring water from plant leaves, and evaporating surface water.
- **Urban geometries**: Tall buildings have the potential to produce an urban canyon effect, which traps heat close to the surface where people may feel it and restricts wind flow.
- **Anthropogenic heat**: People in cities operate buildings and industrial operations in close proximity to one another, drive cars, and run air conditioners—activities that produce waste heat that raises local temperatures. When these heat-generating activities are concentrated over limited areas, they can have major impacts on the microclimate.

- **Urban greenhouse effect**: Pollutant concentrations and water vapor content are typically higher in urban atmospheres. These elements can trap and intensify heat above cities when combined with warmer air.

UHIs cause issues such as increased energy consumption for cooling and increased thermal stress. UHIs can create dangerous conditions when they exacerbate extreme temperatures in cities. The negative effects of excessive heat on people and the economy are well known. Extreme heat has been associated in numerous studies with disease and mortality in susceptible groups, including the elderly, very young children, and those suffering from respiratory conditions. Severe heat can also lower productivity and harm vital services like energy and transportation networks (Venter et al., 2021). UHI produced by large urban areas can impact precipitation by enhancing low-level convergence due to both an increase in surface roughness and destabilization of the boundary layer (Thielen et al., 2000). The combination of increasing heat island intensity and more frequent and severe heat waves has the potential to drastically increase harm to communities. The problem stems from the fact that temperature-related damages tend to be nonlinear, with larger marginal increases in negative impacts on human well-being at high temperatures. Climate change and land use changes have similar effects on society's health and living conditions. Both modifications concentrate on the deterioration of ecosystem dynamics and their stability.

Heat stress affects human populations in several ways. Heat stress caused by heatwaves may result in more serious conditions like heat stroke. Elevated temperatures have the potential to exacerbate air pollution levels, which can result in the development of severe cardiorespiratory allergies. The urbans climate is influenced by pollution as well. Pollution particles reflect solar radiation, reducing the amount of solar energy that reaches the surface. Urbanization has been shown to have significant effects on heat islands (Sumanta Das, 2022).

Cambodia is among the top 23 countries with acute exposure to extreme heat, with an average of 64 days annually when the maximum temperature surpasses 35°C. The country also experiences some of the highest temperatures in the globe. In 2020, the mean urban temperatures in four Cambodian cities—Poipet, Siem Reap, Phnom Penh, and Battambang—were 36.7, 35.5, 35.2, and 35.2°C, respectively. In comparison, a sample of 100 East Asian and Pacific cities saw temperatures of 31.9°C. UHI effects are particularly noticeable in Phnom Penh and Siem Reap, where urban regions were 1.16 and 1.19°C hotter than non-urban areas in 2020 (World Bank, 2023). Urban temperatures have risen rapidly in Phnom Penh (Figure 4.16) where the construction of roads and buildings increases the heat island effect as these infrastructure types absorb and re-emit the sun’s heat more than natural landscapes (EPA, 2023). The urban poor are particularly susceptible to the negative effects of heat stress on their health and productivity because they frequently work outdoors and typically reside in overcrowded housing without adequate ventilation or cooling.

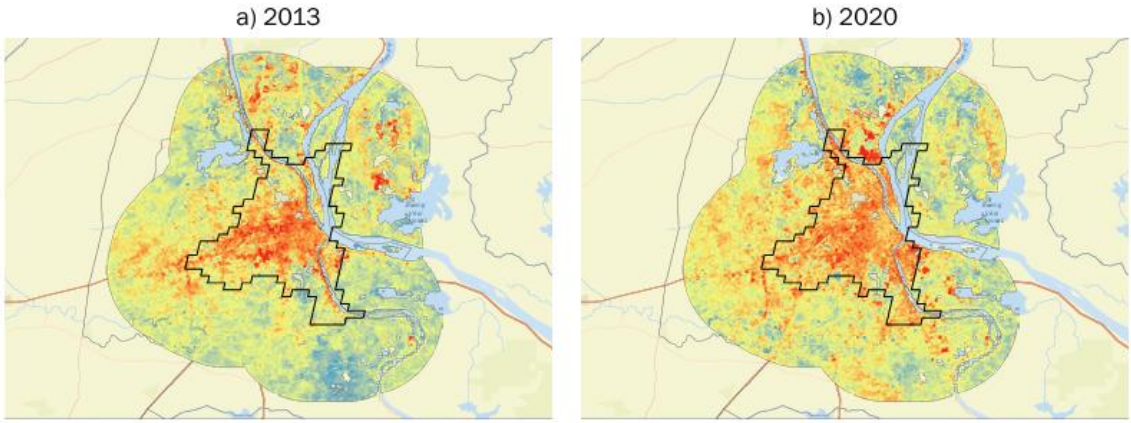

Figure 4.15 Phnom Penh suffers from the greatest urban heat island effect, with central urban temperatures 1.16°C higher than those on the outskirts of the city Urban heat index (red = hotter, blue = cooler).
Source: (EPA, 2023)
Note: These figures display the spatially disaggregated heat index for Phnom Penh overtime. The black line denotes the city boundary. The urban heat island effect refers to the difference in temperature between the central urban area and the temperature 5 km outside the center.

UHIs in cities of developing countries, such as Cambodia, have become areas of increasing research and government policy discussion. The influence of infrastructure, human activities, and environmental changes leads to the intensification of UHI, resulting in significant implications for natural climate variability, public health, and overall climate change. The factors contributing to the formation of urban heat islands in Cambodian cities are varied, including urbanization, the removal of trees and vegetation, the replacement of vegetative surfaces with impervious ones, and the heating of bodies of water due to urbanization. The rise in extreme heat poses a serious risk to public health, particularly for urban residents and outdoor workers, for whom heat increases are exacerbated by UHI effects. Particularly high urban heat island levels have been reported in Cambodia's capital Phnom Penh, with the temperature differential between rural and urban areas reaching as high as 4°C during the daytime. Beyond the impacts on human health, the temperature peaks resulting from the combined effects of urban heat island, climate change, and future urban expansion are likely to damage the productivity of the service sector economy. These may occur both through direct impacts on labor productivity, but also through the additional costs of adaptation such as cooling measures (World Bank, 2023).

4.3.5 Feedbacks of LULCC and GHGs

Changes in how we use land can alter the Earth's surface and how we manage it (Pongratz et al., 2018). On the global scale, impacts of LULCC include GHG fluxes and emissions of aerosol precursors (biogeochemical effects), mostly of CO_2, N_2O, and CH_4 (Hong et al., 2021a). Understanding the causes of climate change and determining the magnitude of the underlying human impact need quantifying the effects of LULCC on the local to global climate. LULCC's climatic effects can also provide a practical means of mitigating global warming or adapting to local climate changes that lessen their influence on living conditions. Emissions of CO_2 into the atmosphere are mainly due to the clearing of forests and other natural vegetation for conversion to agricultural land, forest and land degradation, wood harvesting and related product decay, peat drainage, and peat burning. Removals of CO_2 from the atmosphere by LULCC are mainly due to reforestation

and recovery of non-forest vegetation following agricultural abandonment, afforestation, and regrowth of forests following wood harvest (Friedlingstein et al., 2020). The majority of N_2O emissions stems from the application of nitrogen fertilizers, manure management, and biomass burning (Tian et al., 2020) and CH_4 emissions are mainly caused by enteric livestock fermentation, biomass burning under incomplete combustion, and rice cultivation (Saunois et al., 2020). LULCC alters the surface energy balance (biogeophysical impacts) and changes the land surface's physical characteristics, including albedo, leaf area, and roughness, which affect evapotranspiration efficiency. These affect the climate both locally at the site of LULCC, e.g., through evaporative cooling, and also in remote areas through advection of heat and moisture and by altering atmospheric circulation, or "non-local effects"(Winckler et al., 2017). LULCC alters local surface properties, which affect latent and sensible heat fluxes, the surface radiation balance, and greenhouse gas fluxes. Effects depend on vegetation types and location, in particular strong zonal differences exist. Effects of global LULCC are routinely assessed by IPCC, including in the Sixth Assessment Report and the Special Report on Climate Change and Land.

In Cambodia, LULCC has dramatically changed over the last three decades following major political change, population and economic growth, market demand for food crops, climate change, and human migration (Diepart et al., 2015). According to the MAFF 2018, deforestation in Cambodia caused a notable loss of forest cover, from 10.83 million ha (59.64 percent) in 2006 to 8.52 million ha (46.90 percent) in 2014, and to 8.22 million ha (45.26 percent) in 2016 (MAFF, 2018). During this period, the area of arable land (e.g., fields, crops, gardening) and plantations of rubber (*Hevea brasiliensis*) and oil palm (*Elaeis guineensis*) increased by about 2.69 million ha. The MoE (2016) reported that, based on the forest assessment in 2016, Cambodia's forest cover has decreased from 73.04 percent in 1965 to 48.14 percent in 2016. However, about 13 percent of the dense forest area was transformed to degraded forestland. Forest cover was reduced dramatically during the following 20 years from 1997 to 2016, and only 25 percent remained in 2016, especially along the main roads. Approximately 65 percent of the forest cover loss primarily occurred between 2006 and 2016 (Kong et al., 2019).

In Cambodia, LULCC is one of the significant drivers of GHG emissions, as it not only converts carbon sinks to a source of GHS emission, but also changes the biophysical properties of land cover that govern surface energy budgets. However, the feedback of LULCC-induced GHG emissions on the land surface processes has rarely been explored in Cambodia. Previously exogenous consideration of LULCC-induced GHG emissions results in a severe underestimation of the spatial and temporal variation in the net carbon exchange. In turn, the consideration of GHG emissions-induced LULCC feedbacks dampens the growth of vegetation and enhances the land cover conversion to crops, and thus could mitigate local warming over the affected areas (Dieye, 2016)

In last 10 years, the land category of FOLU in Cambodia significantly impacted the country's GHG emissions. Based on the National GHG emissions inventory 2019, the large emission of 131,011 Gg CO_2-eq/yr was estimated due to change measures between 2010 and 2014. Indeed, emissions largely exceed removals for this category. In agriculture, rice cultivation and enteric fermentation are the main sources, at 9,856 Gg CO_2-eq/yr and 3,554 Gg CO_2-eq/yr. The inventory's baseline data included all areas that are not forests, so the emissions of this sub-sector have not been broken down into more specific categories. All of the GHG estimates in the present inventory have to do with forests; they could be about afforestation, deforestation, or forest changes. However, deforestation should be documented under the final use category, which is unknown, rather than the

forest category. Table 4.12 and Table 4.13 illustrates carbon stock change and CO_2 emission estimation in land from 2000-2016.

Table 4.7: Carbon Stock changes in land

AGB + BGB Fluxes(tC/yr)	2000	2005	2010	2015	2016
Forest becoming otherland*	-9165575	-9165575	-40230160	-40230160	-40230160
Other land* becoming forest	1933497	1933497	5339125	5339125	5339125
Forest remainingforest	-136636	-136636	-839303	-839303	-839303
Other land* remaining other land*	0	0	0	0	0
Total forest	1796860	1796860	4499822	4499822	4499822
Total other land*	-9165575	-9165575	-40230160	-40230160	-40230160
Total (tC/yr)	-7368715	-7368715	-35730339	-35730339	-35730339

*Other lands encompass all lands which are not forests (croplands, grasslands, etc.).
Source: (MoE, 2019b)

Table 4.8: CO2 emissions for Land (Gg)

AGB + BGB Fluxes	1994	2000	2005	2010	2015	2016
Emissions (Gg CO_2/yr)	34 149	34 149	34 149	151 274	151 274	151 274
Removals (Gg CO_2/yr)	-7 130	-7 130	-7 130	-20 263	-20 263	-20 263
Emissions/Removals (Gg CO_2/yr)	27 019	27 019	27 019	131 011	131 011	131 011

Source: (MoE, 2019b)

Because of the increased production efficiency of land area, total LULCC emissions (CO_2, CH_4, N_2O) stayed relatively constant at about 11 Pg CO_2-eq (CO_2-equivalent using 100-year Global Warming Potential) during the second half of the last century, despite increases in population and production per person. However, the last two decades saw a surge in emissions per land area and across the globe due to cropland clearing in carbon-dense tropical forests. LULCC is thus responsible for 25 percent of anthropogenic (LULCC + fossil) emissions (Hong et al., 2021b). Net CO_2 emissions related to LULCC conversions and forestry represent about half (39–61 percent) of all LULCC-related GHG emissions from 1961–2017 or about 10–15 percent of total (land use plus fossil) anthropogenic CO_2 emissions for the last decade (Friedlingstein et al., 2020), while CH_4 and N_2O emissions from agricultural management make up the rest.

There are already observed increases in all the above emission sources. The resulting impacts includes temperature increases, rainfall changes, greater occurrences of extreme weather, and increased flooding and its associated impacts. An increase in temperature and potential exacerbation of rainfall reduction could create a classic case of “the dry getting drier”. Meanwhile, the rise in extreme weather events and flooding could further worsen the adverse impacts already observed on agriculture, health, infrastructure, and livelihood. Sea Level Rise (SLR) would increase death rates, as projected for 2030. If current development pathways continue without change, accompanying feedbacks are likely to occur, further hindering development and efforts to alleviate poverty.

Targeted measures and mitigation efforts could be implemented now to reduce many of the impacts noted above. Such interventions could involve climate-proofing development through low, medium, and high-cost options. Efforts would also include addressing agroclimatic zone considerations and combating sea level rise (SLR) using both soft and

hard solutions. In-depth consideration of agriculture and water management is also necessary. Finally, climate change is likely to exacerbate problems in the growth areas mentioned above, which may necessitate a rethinking of development planning.

4.4 Directions for Future Studies

Future study on the drivers of climate change in Cambodia should emphasize a more detailed and granular analysis of both external and internal factors. Although Cambodia is currently a low emitter of GHG, rapid economic growth and deforestation are increasing its contribution to global warming. Further studies should explore these interlinked issues, particularly the ways in which economic development and climate vulnerability shape and reinforce each other.

4.4.1 Challenges: Data Availability and Variability

One of the challenges in determining the drivers of climate change in Cambodia is the difficulty in collecting historical data and utilizing this data to understand the drivers of climate change. These challenges result from a lack of high-quality, long-term, and spatially disaggregated data, making it difficult to accurately model and project climate impacts. The issue is especially pronounced in areas like land use and land cover change, urbanization, ecosystems, climate change, and air quality, etc.

4.4.2 Research Gaps and Directions for Future Studies

Major research gaps remain in understanding the drivers of climate change in Cambodia, especially regarding the complex interactions between human activities and the environment. Key areas that are likely to be prioritized in future climate studies for Cambodia include:

- Carbon stock assessment;
- Climate impact by land use and land cover change;
- Urbanization and climate resilience;
- Climate change and ecosystem services impact;
- Clean technology, policy, governance, and international cooperation;
- Climate impacts and urban vulnerability risk assessment; and
- Climate technologies and innovation (e.g. climate-resilient technologies).

4.4.3 Ways Forward

- Improving the availability and accessibility of data and information

Future studies on the qualitative and quantitative assessment of drivers of climate change in Cambodia require improved data availability and quality, as well as stronger integration and sharing of information among stakeholders.

- Enriching knowledge of the driver of climate change

It is important to acknowledge the existing knowledge gaps in determining the drivers of climate change that impact both natural and human systems. Enriching our knowledge of climate change drivers for future studies requires a comprehensive approach that extends beyond the well-established role of GHG. The research on the driver of climate change should be focused on participatory approaches, strengthened by social sciences, and guided by a transdisciplinary framework to ensure its findings remain relevant across diverse decision-making contexts.

CHAPTER 5
PROJECTIONS OF CAMBODIA FUTURE CLIMATE CHANGE

5.1 Chapter Summary

Preparing an adaptation and mitigation plan for climate change is a long-term task that requires involvement from many stakeholders. Predicting future climate is essential since it provides information about the pattern of climate that helps make the strategic plan more precise in responding to future climate scenarios. In this chapter, the projection of the future climate change in Cambodia is provided based on state-of-the-art climate simulation combined with post-processing techniques by local experts in Cambodia.

The temperature in Cambodia is projected to increase around 2°C (1.5 to 2.5 °C) under the moderate climate change scenario (SSP2-4.5), and around 4°C (3.5 to 5 °C) under the worst climate change scenario (SSP5-8.5) by the end of the century (2071-2100). The hottest months in the country (March to May) would experience a stronger increase in temperature compared to the other months. As a result of climate change, Cambodia is highly at risk of increased drought events and flood events. For flood events, there is an indication of more frequent occurrence under the strong increase of global mean temperature up to 4°C under the SSP5-8.5 scenario. The future climate of Cambodia would likely be getting drier during the dry season and wetter during the rainy season. The report also suggests the potential threats of dry spell events related to drought and more heavy rainfall events related to floods in most parts of Cambodia because of the impact of climate change. Thus, an effective climate change adaptation policy is strongly required for the whole of Cambodia.

There is evidence of climate change effects already impacting Cambodia and other countries globally. It is recommended to increase investment in climate change adaptation and enable climate change response in all related sectors that are potentially affected by the fast pace of climate change, as indicated in this report. Hotter temperatures, more frequent heat waves, dry spell events related to drought, and more heavy rainfall events related to floods are the key indicators of the impact of climate change in Cambodia.

5.2 Introduction

The escalating crisis of climate change has emerged as one of the most pressing challenges confronting the world today. A resounding endorsement of this critical situation has come from over 11,000 scientists worldwide, who have collectively embraced the terms "Climate Crisis" or "Climate Emergency" as a reflection of the grave threat posed by climate change (Ripple et al., 2020). These scientific experts have unequivocally declared that the climate crisis has reached a critical juncture, emphasizing the urgent need for a substantial increase in efforts to protect our planet's biosphere. This declaration underscores the imperative for global unity and immediate action to address the pressing challenges posed by climate change. The climate system, intricately interconnected with Earth's other systems, is experiencing profound transformations that have far-reaching implications (Carrington, 2019). The immediate need for global

cooperation to address pressing issues is evident. The Earth's systems, including the climate, are interdependent. Recent scientific research has demonstrated that human actions are the primary contributors to climate change and global warming (IPCC, 2021). Climate change, fueled by human activities, poses significant risks to socioeconomic development and environmental sustainability. Southeast Asia is increasingly vulnerable to these impacts, experiencing rising human casualties, economic losses, and damage to natural resources. The region has witnessed a disturbing trend of more frequent and severe floods, droughts, saltwater intrusion, and extreme weather events in recent years.

Cambodia's vulnerability to climate change within Southeast Asia stems from its heavy reliance on agriculture, water resources, infrastructure, forest ecosystem, human health, coastal zone and fisheries, coupled with limited capacity to adapt due to shortages in technical expertise, institutional resources, and climate adaptation funding (Yusuf & Herminia, 2009). Cambodia is vulnerable to a range of climate hazards, including frequent floods, periods of drought, extreme heat waves, and cyclones. These events pose significant risks to the country's population, infrastructure, and economy (World Bank & Asian Development Bank, 2021). Coastal regions in Cambodia face challenges such as saltwater contamination of groundwater and seawater intrusion. Rising sea levels, driven by melting glaciers and the expansion of ocean water, pose a significant threat to these areas. Climate change has emerged as a critical global issue, demanding immediate attention. Cambodia, like other countries worldwide, must prioritize the development and implementation of comprehensive and effective climate change policies, strategies, and actions. Cambodia has already developed a number of policy instrument related to climate change, notable the Circular Strategy on Environment (2024-2028), Pentagon Strategy Phase 1 (2024-2028), NDC updated (2020-2030), and the update CCCSP (2024-2033). These initiatives should be implemented at all levels, from international cooperation to local and individual actions, to address the pressing challenges posed by climate change.

Developing an effective climate change adaptation and mitigation plan is a long-term endeavor that requires the collaboration of various stakeholders. Accurate climate predictions are crucial for informing these plans, as they provide insights into future climate patterns and aid in developing targeted strategies. Socioeconomic development is a primary driver of climate change, with higher levels of carbon emissions linked to increased economic activity. Scientists have developed various climate change scenarios by modeling different carbon emission levels and creating climate models to simulate future climate conditions under these scenarios. These models provide valuable data for research and help researchers predict future climate trends.

5.2.1 Development of Projections

Climate Change scenarios are projections about how Earth’s weather patterns might evolve. These predictions are created using computer simulations that consider factors like greenhouse gases, population increase, and changes in land use. According to the IPCC, there are various scenarios, each with its own set of assumptions, ranging from moderate to extreme temperature increase. The approach for calculating and determining the extreme phenomena is detailed in Annex A6: Approach for making projections of Cambodia future climate change.

Reports from the IPCC, used two SSP scenarios to predict future climate change in Cambodia. Currently, the world is approaching SSP2-, while SSP5- represents the worst-

case scenario. SSP2-4.5 and SSP5-8.5 scenarios will be applied to Cambodia's domain. SSP2-4.2 denotes the climate change scenario SSP2 while the number 45 means that the radiative forcing is 4.5 W/m² by the year 2100. SSP5-8.5 denotes the climate change scenario SSP5 while the number 85 represents the radiative forcing of 8.5W/m² by 2100.

The study domain over Cambodia is relatively small compared to the global climate model produced by IPCC. To project future climate change with less bias and accurate output, appropriate climate models must be selected and evaluated using statistical indicators to filter for the climate models that have the highest statistical relation with observation data. Once the suitable models are chosen, another challenge arises because the resolution of the global climate model is 1° latitude X 1° longitude which cannot be applied to small domain studies like Cambodia. Thus, downscaling global climate models should be an effective way to tackle the coarse resolution of global climate models. Downscaling is a method used to refine low-resolution data to high-resolution data.

Cambodia's geographical characteristics are complex, consisting of coastal areas, mountainous regions, and a central plain with scattered high-elevation areas. Therefore, it is necessary to carefully choose climate models that apply to Cambodia's geography. This section of the report considers various models and their appropriateness for Cambodia.

5.2.2 Climate Models

General Circulation Models (GCMs) are a de facto standard for future climate change projection, climate change adaptation, and mitigation planning. However, these climate datasets are not yet ready to use for climate change impact studies. Post-processing and climate downscaling steps are required for more reliable climate change information for a local area. In this report, a statistical downscaling technique was applied to downscale both temperature and precipitation to obtain finer-scale data for the analysis of climate change projection in Cambodia.

The projection of future climate change mainly consists of two types of datasets which are historical observed data and climate model data. These two datasets will be used as input to reproduce a finer scale of climate data to apply for a small domain study. For the downscaling of precipitation, Multi-Source Weighted-Ensemble Precipitation (MSWEP) was selected as observed data in Cambodia since it has high resolution, 0.1° latitude X 0.1° longitude and stored in daily time series (Beck, et al., 2019). The available period of the dataset is from 1979 to the present; however, only data from 1980 to 2014 are used in this study. The selected domain of the dataset is 10°-15° latitude and 102°-108° longitude which covers the entire area of Cambodia.

Precipitation data generated from climate models are downloaded from the CMIP6 data portal (Eyring, et al., 2016). The data is then divided into historical and future periods. Historical data is from 1980 to 2014, which is mainly used for evaluating performance of the statistical downscaling method. The future data is from 2015 to 2100. The domain of these datasets is selected within the 10°-15° latitude and 102°-108° longitude which fully covers the area of Cambodia. There are five CMIP6 GCM datasets from different climate modeling centers used in this study (Table 5.1). We selected five climate models from CMIP6 by choosing one model or one ensemble from each institution to ensure that they are independent from each other (avoid inter-model dependency).

Table 5.1: The Five Data Datasets of CMIP6 models used in this study

Dataset	Model Acronym	Resolution	Frequency	Available Period
Euro-Mediterranean Centre for Climate Change (CMCC)	CMCC-CM2-SR5	1.25°	daily	1850-2100
Model for Interdisciplinary Research on Climate (MIROC)	MIROC6	1.4°	daily	1850-2100
Max Planck Institute for Meteorology (MPI)	MPI-ESM1-2-HR	0.94°	daily	1850-2100
Meteorological Research Institute (MRI)	MRI-ESM2-0	1.13°	daily	1850-2100
Nanjing University of Information Science and Technology (NUIST)	NUIST-NESM3	1.88°	daily	1850-2100

Regarding temperature projection, the NASA Earth Exchange Global Daily Downscaled Projections (NEX-GDDP-CMIP6) dataset was also used with the same downscaling method as what was applied for precipitation above. The details of the downscaling method are provided in Section 5.2.3 below. The same global climate models as in Table 5.1 above are applied for temperature projection.

5.2.3 Downscaling

Bias-corrected spatial disaggregation (BCSD) is a statistical downscaling method first introduced by Wood et al. (2024). . BCSD was applied to downscale the model data from coarse resolution to a finer resolution of around 10km in Cambodia (Duong, Song, & Chhin, 2023). The process consists of three main steps which are detailed in Wang and Chen (2014). Step 1 is to upscale the observation data to the same scale as the model; Step 2 is to bias-correct the model data by using quantile mapping; and Step 3 is to downscale the bias-corrected to a finer resolution (See in Annex A6). Importantly, this downscaling method is applied to downscale precipitation data in Cambodia to be used in this report (Duong, Song, & Chhin, 2023).

5.2.4 Model Evaluation and Dealing with Uncertainties

Before downscaling the climate models, performance evaluation is needed to check the consistency of the outputs. The downscaling method is evaluated using two statistical indicators: correlation coefficient and root mean square error (See details in Annex A6). The BCSD method was applied to historical data from CMIP6 to check the suitability for application over Cambodia (Duong, Song, & Chhin, 2023). The period of the dataset is from 1980 to 2014 and is divided into two periods: calibration (1980-2004) and validation (2005-2014). The calibration period was set as a baseline while the validation period is considered as a future period. Therefore, we give more weight to the validation period results. After checking the results showing that the statistical indicators are acceptable (See in Annex A6), BCSD is then applied to future data.

5.3 Cambodia Climate Projections

5.3.1 Observation for Weather and Climate Extreme Events in a Changing Climate

5.3.1.1 Seasonal Temperature Change

☀ Annual Mean Temperature Change

Figure 5.1 illustrates the area average timeseries of surface temperature change within the Cambodian territory relative to the mean value during the baseline period (1950-1979). Until 1990-2014, the temperature in Cambodia was estimated to increase by around 0.5 to 1 °C. It is projected to increase by around 1 to 1.5 °C during the near future period (2015-2044) and by around 1.5 to 2.5 °C during the far future period (2071-2100) under the SSP2-4.5 scenario. The projection under the SSP5-8.5 scenario indicates a similar temperature change to that of the SSP2-4.5 scenario during the near future period. However, from the mid-century onward, the temperature in Cambodia increased significantly, rising from around 2°C to 4.5°C by the end of the century (2100), with an uncertainty range between 3.5°C to 5°C. Thus, significant temperature increases are projected for Cambodia under the scenario SSP5-8.5, which aligns with the global mean temperature projection reported by the IPCC.

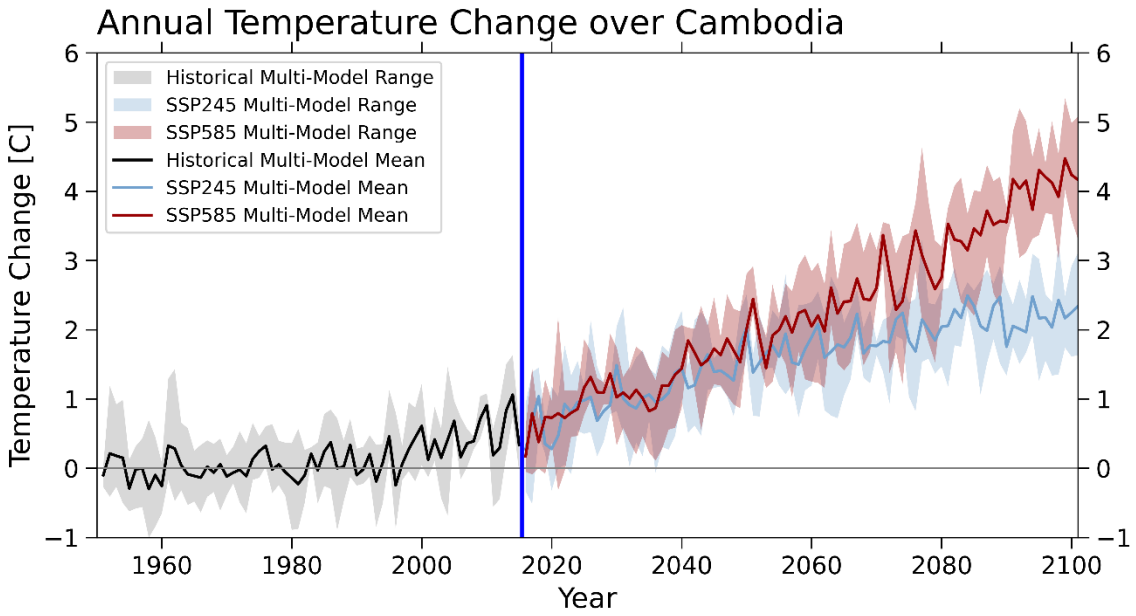

Figure 5.1: Annual temperature change over Cambodia from historical to the future based on two scenarios: SSP2-4.5 and SSP5-8.5. The timeseries was obtained by averaging the temperature data within the territory of Cambodia for multi-model listed in Table 5.1. The average temperature within the period 1950-1979 was set as the baseline to calculate the temperature change.

Under the SSP2-4.5 scenario, the temperature in Cambodia is projected to increase by around 1 °C on average during the near future period (2015-2044) (Figure 5.2a). The temperature increases of more than 1 °C is mainly detected over the following regions in Cambodia: Kampong Speu, Kampot in the western highlands and coastal plains; Kampong Cham, Kampong Chhnang, Kampong Thom, Kandal, Phnom Penh, Takeo, Tboung Khmum in the central Cambodia plains; and Kratie, Mondulkiri, Ratanakiri, and Stung Treng in the eastern highlands and plains.

Under the same scenario as above, the temperature in Cambodia is projected to increase

by around 2.13 °C on average during the far future period (2071-2100) (Figure 5.2b). Most provinces in Cambodia are expected to see a significant temperature increase of more than 2 °C. The exceptions are some parts of a few provinces in the western highlands and coastal plains and the central Cambodia plains, where the temperature change is less than 2 °C. This indicates a significant increase in temperature across most provinces in Cambodia by the end of the century under the moderate climate change scenario (SSP2-4.5).

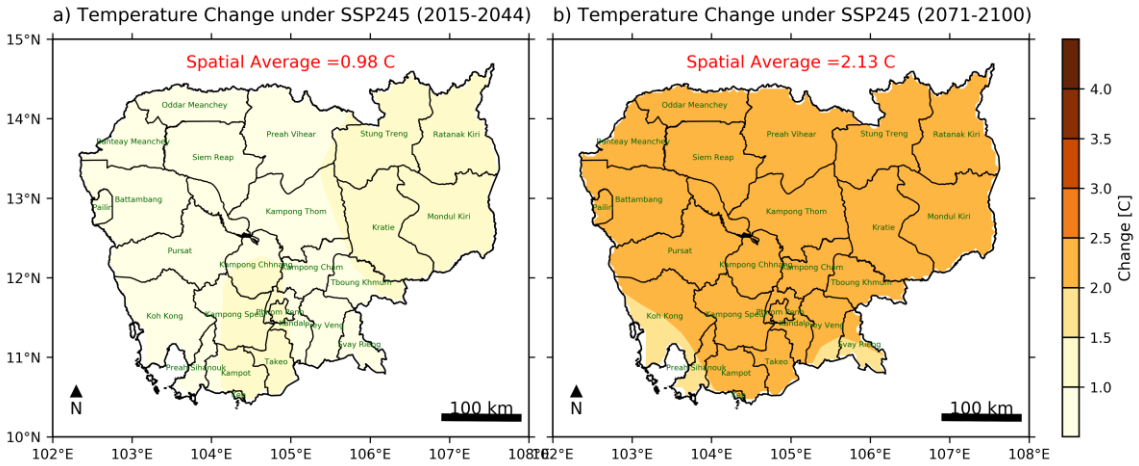

Figure 5.2: Spatial temperature change in Cambodia based on multi-model mean for (a) near future period (2015-2044) and (b) far future period (2071-2100) under SSP2-4.5 scenario. The average temperature within the period 1950-1979 was set as the baseline to calculate the temperature change.

Under the SSP5-8.5 scenario, the temperature change in Cambodia indicates a similar average value to the SSP2-4.5 scenario in the near future period (1.08°C during 2015-2044) (Figure 5.3a). This is consistent with the average time series of annual temperature changes (Figure 5.1), indicating that the two scenarios projected similar temperature changes in the near future period (2015-2044). In the far future period (2071-2100), Cambodia is expected to experience substantial temperature changes under the SSP5-8.5 scenario (Figure 5.3b). On average, the temperature in Cambodia would increase by up to 3.5°C. The provinces around Tonle Sap Lake and in the northern part of the country would experience even greater temperature changes, up to around a 4°C increase. This substantial temperature increase due to climate change could result in more frequent heat waves, leading to health problems and other issues, especially under the extreme scenario of IPCC (SSP5-8.5).

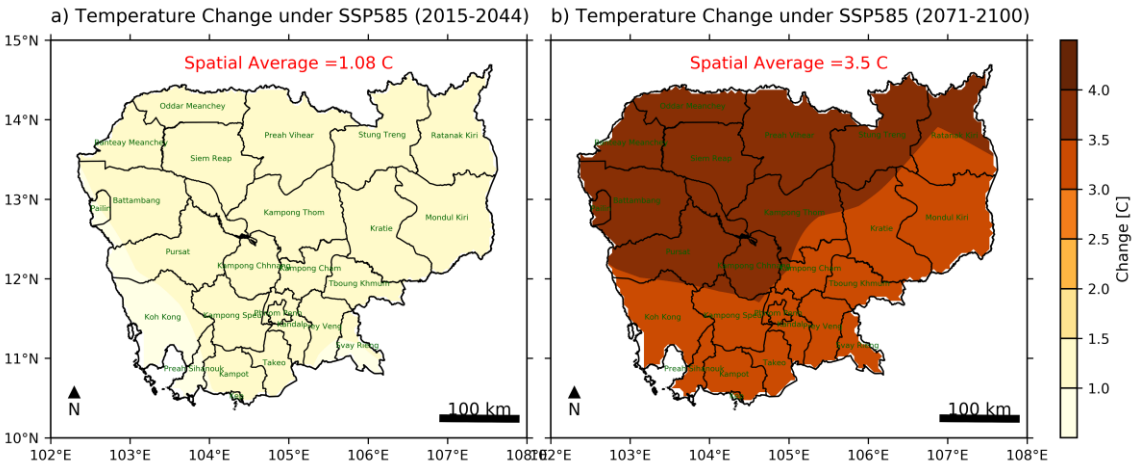

Figure 5.3: Spatial temperature change in Cambodia based on multi-model mean for (a) near future period (2015-2044) and (b) far future period (2071-2100) under SSP5-8.5 scenario. The average temperature within the period 1950-1979 was set as the baseline to calculate the temperature change

☀ Seasonal Temperature Change

The temperature changes in Cambodia were analyzed based on four seasons of the year, i.e., periods from December to February (DJF), March to May (MAM), June to August (JJA), and September to November (SON), to investigate seasonal patterns. Generally, Cambodia experiences the coldest temperatures in DJF and the hottest temperatures in MAM. In JJA and SON, Cambodia experiences moderate temperatures because of the rainy season linked to the southwest monsoon and tropical cyclone activities in the region. The cloudy conditions and rainfall make the surface temperature in the country drop to moderate levels even during JJA. The temperature changes in each season in the near future period (2015-2044) under the SSP2-4.5 scenario are illustrated in Figure 5.4. On average, the temperature in Cambodia is projected to increase by around 0.96°C in DJF, 1.11°C in MAM, 0.93°C in JJA, and 0.9°C in SON. In the hottest months (MAM), Cambodia would experience the most significant increase in surface temperature. This trend is likely to be observed across most provinces, except those in coastal areas.

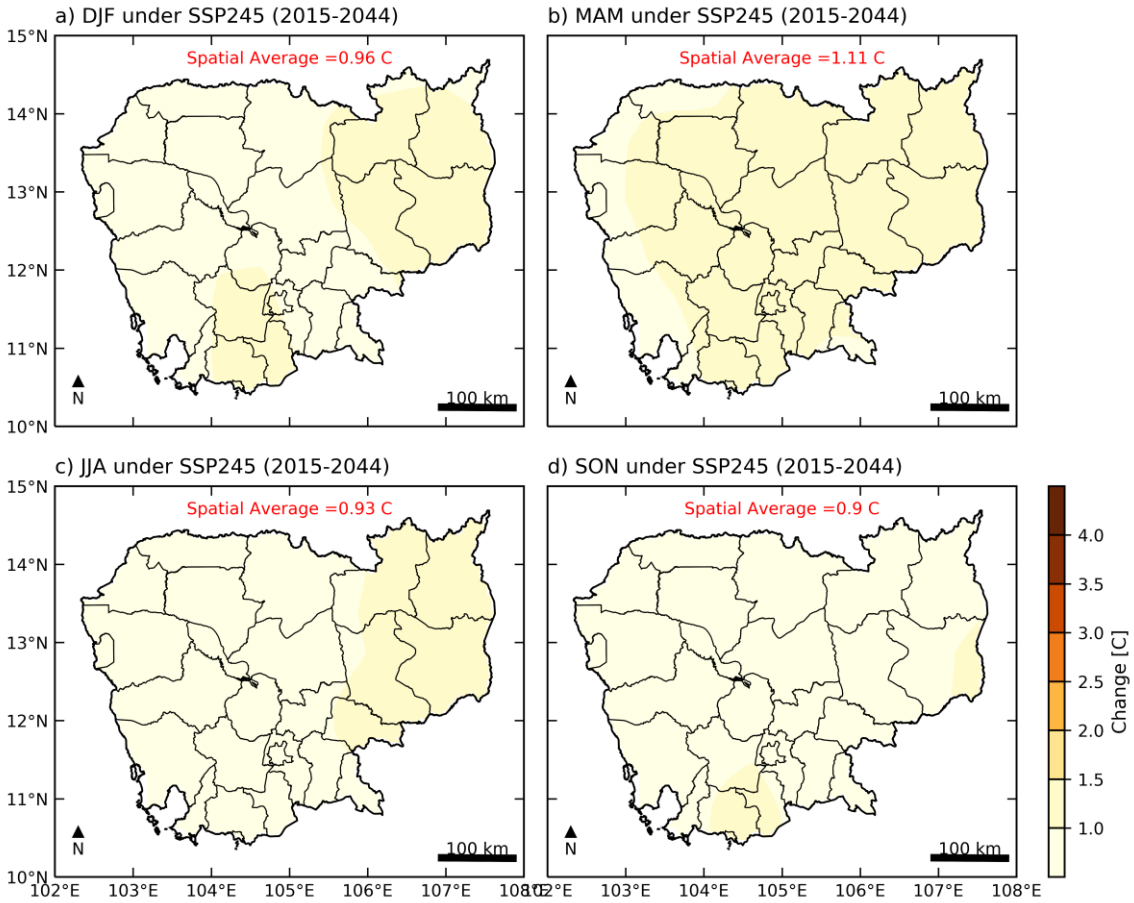

Figure 5.4: Spatial temperature change in Cambodia based on multi-model mean for each season (a) December-January-February (DJF), (b) March-April-May (MAM), (c) June-July-August (JJA), and September-October-November (SON) in near future period (2015-2044) under SSP2-4.5 scenario. The average temperature within the period 1950-1979 was set as the baseline to calculate the temperature change

The temperature changes in each season in the far future period (2071-2100) under the SSP2-4.5 scenario are illustrated in Figure 5.5. On average, the temperature in Cambodia is projected to increase by around 2.13 °C in DJF, 2.42 °C in MAM, 1.9 °C in JJA, and 2.06 °C in SON. In the near future period, Cambodia will experience a stronger increase in surface temperature in the hottest month (MAM) compared to other periods. The strongest temperature increase occurs in Kampong Thom, Preah Vihear, Stung Treng, Ratanakiri, Mondulkiri, and Kratie (Figure 5.5b). Temperature increase in JJA is the lowest compared to the other periods. This indicates a potential risk of hotter temperatures in MAM even under the moderate climate change scenario (SSP2-4.5).

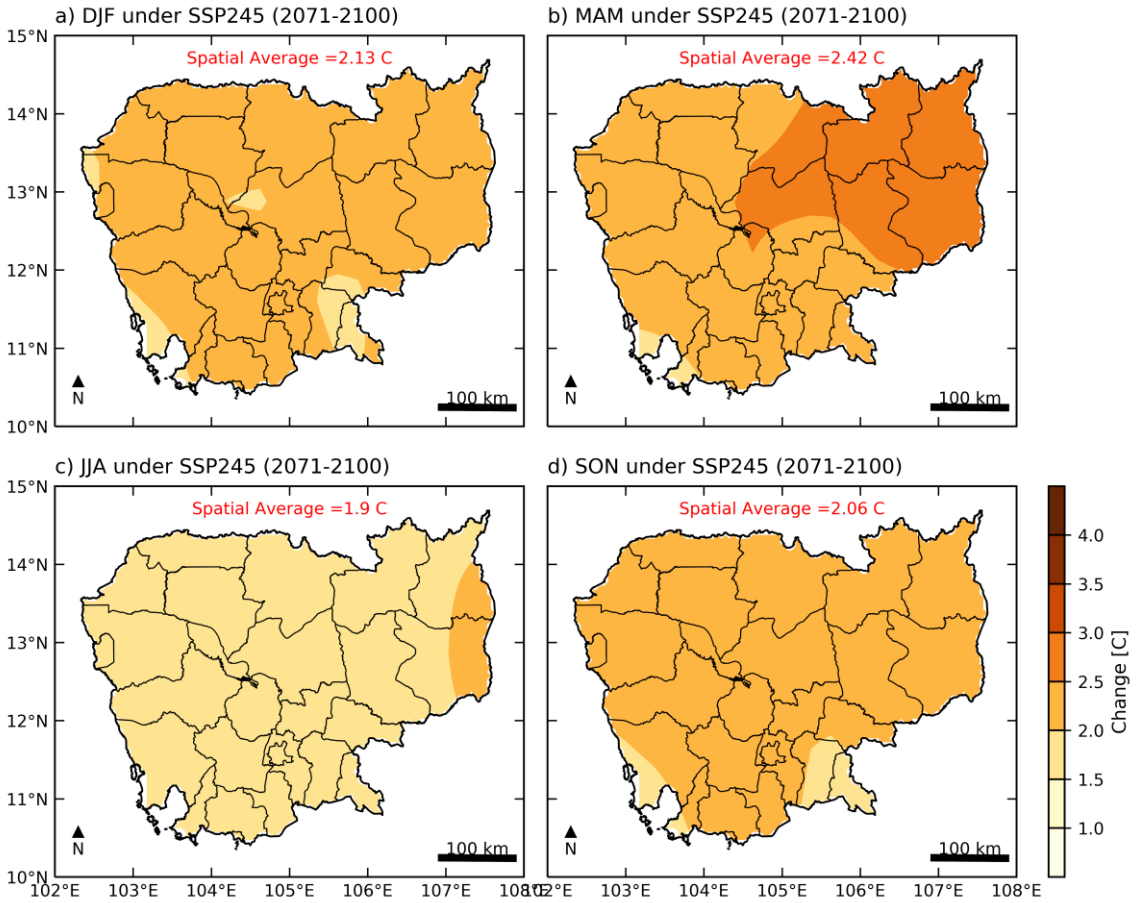

Figure 5.5: The same as Figure 5.4, for far future period (2015-2044)

The temperature changes in each season in the near future period (2015-2044) under the SSP5-8.5 scenario is illustrated in Figure 5.6. On average, the temperature in Cambodia is projected to increase by around 1.07 °C in DJF, 1.24 °C in MAM, 0.98 °C in JJA, and 1.04 °C in SON. The temperature changes under this scenario follow a similar pattern to that of the SSP2-4.5 scenario in the near future period (2015-2044), which is consistent with the temperature trend shown in Figure 5.1. The strongest temperature increase is projected for MAM. Almost all provinces are likely to experience similar temperature changes based on this scenario in the near future.

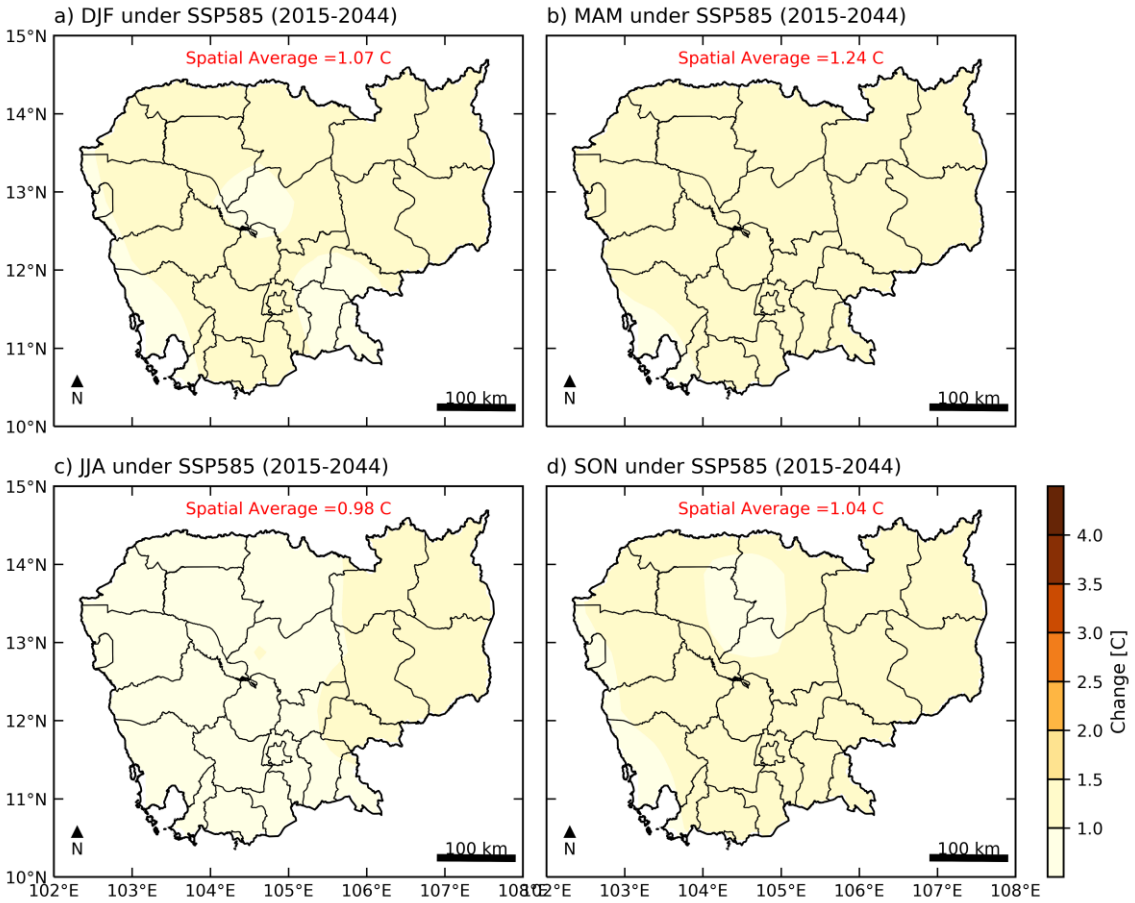

Figure 5.6: The same as Figure 5.4, for SSP5-8.5 scenario

The temperature changes in each season in the near future period (2071-2100) under the SSP5-8.5 scenario is illustrated in Figure 5.7. On average, the temperature in Cambodia is projected to increase by around 3.68 °C in DJF, 3.83 °C in MAM, 3.17 °C in JJA, and 3.33 °C in SON. The temperature in Cambodia is expected to increase substantially under this scenario by the end of the century. Specifically, the temperature in MAM is projected to experience the most substantial increase compared to other periods. This indicates the potential risk of more frequent heatwave occurrences with extremely hot temperatures in the country under the worst climate change scenario.

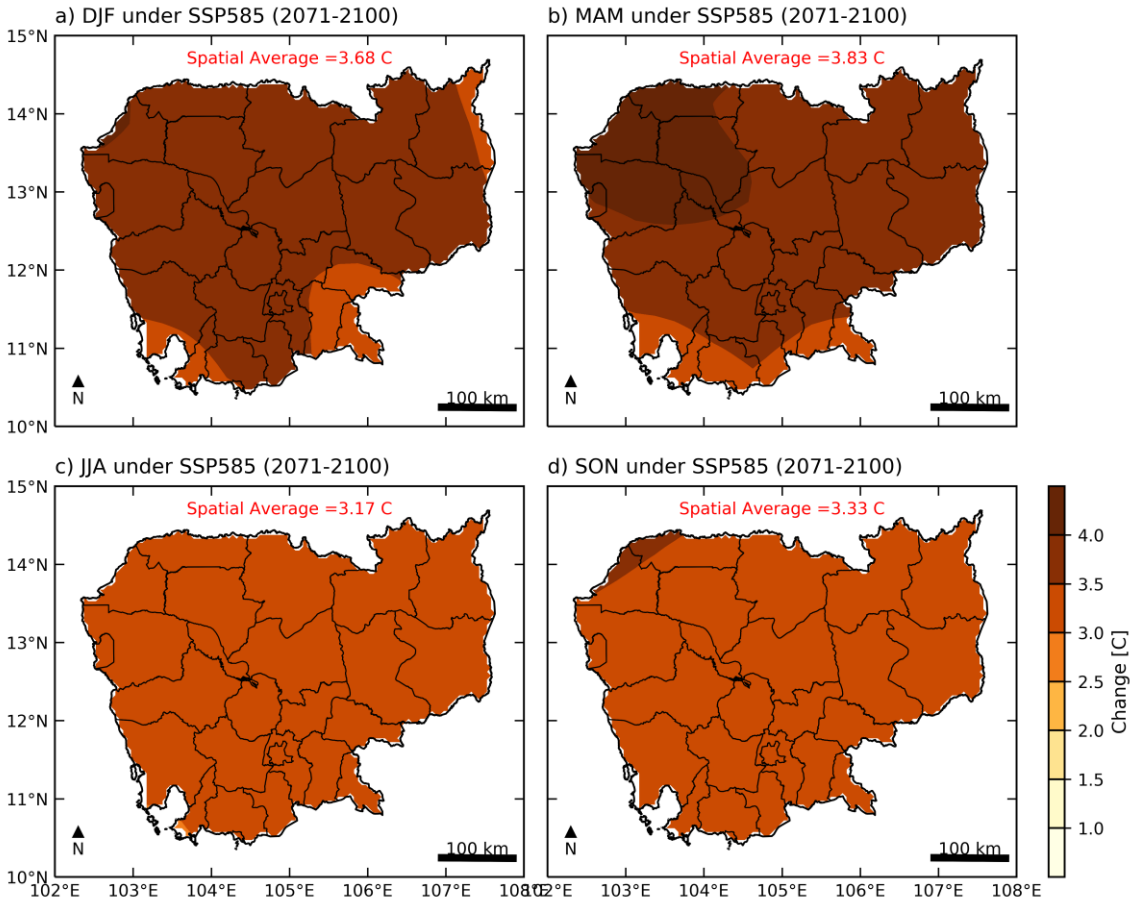

Figure 5.7: The same as Figure 5.5, for SSP5-8.5 scenario

The compact summary of temperature changes for each season, each time horizon, and each scenario is provided in Table 5.2. The values listed in the table is based on the area-average across Cambodian territory, and multi-model mean.

Table 5.2: Summary table of temperature changes by multi-model mean

Timeline	Season	SSP2-4.5	SSP5-8.5
Near future	DJF	0.96 °C	1.07 °C
	MAM	1.11 **°C**	1.24 **°C**
	JJA	0.93 °C	0.98 °C
	SON	0.9 **°C**	1.04 **°C**
	Annual	0.98 °C	1.08 °C
Far future	DJF	2.13 **°C**	3.68 **°C**
	MAM	2.42 °C	3.83 °C
	JJA	1.9 **°C**	3.17 **°C**
	SON	2.06 °C	3.33 °C
	Annual	2.13 **°C**	3.5 **°C**

5.3.1.2 Seasonal Rainfall Change

Seasonal rainfall is calculated to identify the rainfall pattern for each season of the year for both climate change scenarios, SSP2-4.5 and SSP5-8.5. As Cambodia is highly influenced by the monsoon circulation, the seasonal match of rainfall pattern in the country is divided into dry season, pre-monsoon, full monsoon, and post-monsoon (Chhin, Shwe, & Yoden, 2020; Matsumoto, 1997). In this report, the seasonal rainfall change is classified into four seasons, which are dry season in December-January-February (DJF), pre-monsoon in March-April-May (MAM), full monsoon in June-July-August (JJA) and post-monsoon in September-October-November (SON). Below, the data are analyzed in greater detail by 3-month period.

Figure 5.8 illustrates the projected changes of seasonal rainfall under scenario SSP2-4.5 for the near future period (2015-2044). For DJF, CMCC-CM2-SR5 indicates a drastic decrease in rainfall with a spatial average (mean value across Cambodia) of -15.492 percent, ranging between negative 10 percent to 30 percent spread diagonally from the northwest to the southeast of the country, with a slight increase of rainfall at the coast. MIROC6 and MPI-ESM1-2-HR depicted a decrease in rainfall in the eastern region, with the highest percentage of negative 20 percent; however, the spatial average is from -3.97 percent and 1.66 percent respectively. MRI-ESM2-0 shows that rainfall tends to increase in most of the country with a spatial average of 17.32 percent. NUIST-NESM3 shows less consistent outcomes: rainfall is sparsely decreased and increased across the country with a spatial average of 13.09 percent. However, the multi-model-mean shows that the spatial average has a very tiny increase of only 1.59 percent which indicates that future rainfall will increase for the winter season.

Furthermore, seasonal rainfall changes in MAM for both CMCC-CM2-SR5 and MRI-ESM2-0 show that rainfall would likely decrease all over the country with a spatial average of -5.88 percent and -20.53 percent respectively. Other models show a slight increase of rainfall scatter across the country in MAM, with a spatial average of 9.2 percent for MIROC6, 14.82 percent for MPI-ESM1-2-HR and 13.65 percent for NUIST-NESM3. The multi-model-mean concludes that the overall change in MAM will be on the increasing trend with a spatial average of 2.16 percent.

In JJA, CMCC-CM2-SR5 stands out the most as the decrease of rainfall spread over the domain, with a flat percentage of around 10 percent. Additionally, the MRI-ESM2-0 and NUIST-NESM3 show that one-third portion of the country will experience a decrease in rainfall, however, the spatial average remains positive for both models. So far, MIROC6 and MPI-ESM1-2-HR only contain a few spots of decreasing trend with spatial averages of 7.42 percent and 8.08 percent respectively. The multi-model-mean shows a flat trend of increasing below 10 percent over the entire domain which is the opposite of the CMCC-CM2-SR5 output.

Lastly, all of the output from each model indicates an increase in rainfall percentage in SON except CMCC-CM2-SR5 and MRI-ESM2-0 which indicated a few spots of rainfall decrease on the edge of the domain. The multi-model-mean showed that the percentage of rainfall will be increased in SON, with a spatial average of 9.07 percent, the highest percentage among the four seasons.

To sum up, the decreasing rainfall tends to occur in the drier season like DJF and MAM while the wet season like JJA and SON indicates no sign of rainfall decline. To wrap up the output, there might be less daily rainfall and rising rainfall intensity during the wet season

that would trigger flash floods and impact flood-prone areas like the Tonle Sap Lake region.

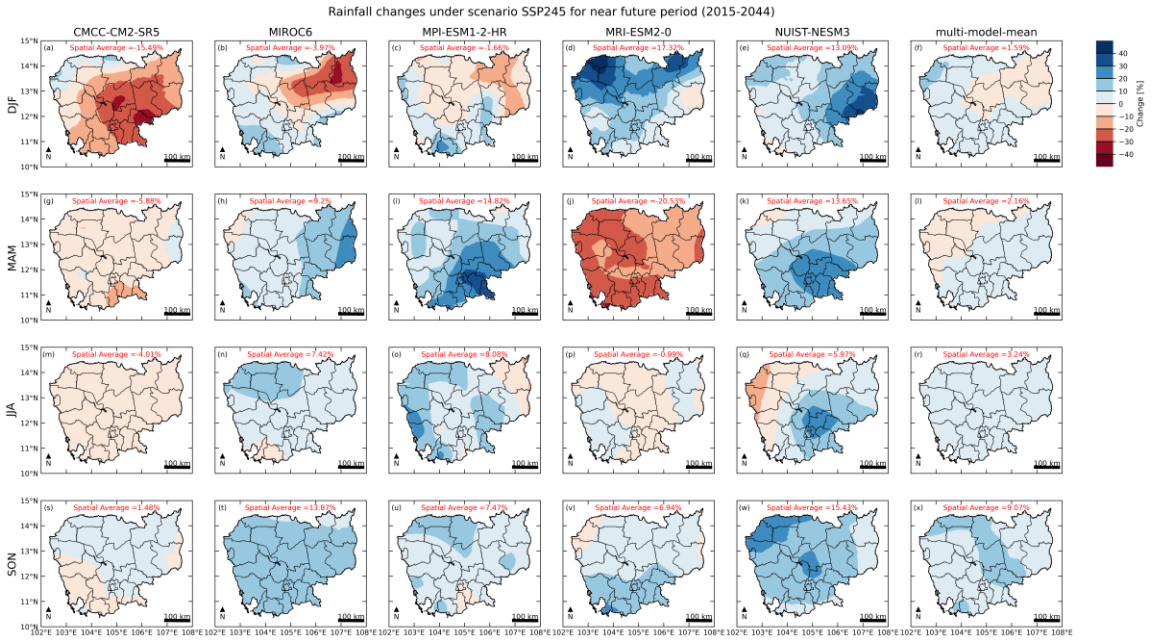

Figure 5.8: Percentage changes in seasonal precipitation for near future period (2015-2044) under SSP2-4.5 scenario. First-row panels for Winter, second-row panels for Spring, third-row panels for Summer and fourth-row panels for Autumn. Note that the multi-model-mean is the mean among five models

Figure 5.9 illustrates the projected changes in seasonal rainfall under scenario SSP2-4.5 for far future period (2071-2100). DJF, MPI-ESM1-2-HR and MRI-ESM2-0 shows the most significant change, with a decreasing percentage of almost two-thirds over the country, ranging from 10 percent to 30 percent. Moreover, the spatial average is negative for both models. In MIROC6, the increasing percentage forms a gradient pattern, from southwest to northeast, with an overall increasing trend. The spatial average is 32.03 percent, which is the highest among the models. In CMCC-CM2-SR5, a decrease of below negative 20 percent. would likely occur in the southeast part of the country. Interestingly, in NUIST-NESM3, the pattern shows that a decreasing trend steadily gains until an increasing trend of more than 40 percent spread diagonally from southwest to northeast. The spatial average is the second highest percentage with 35.37 percent. In conclusion, the multi-model-mean shows that DJF would likely undergo rainfall increase with a moderate percentage of 12 percent.

In MAM, CMCC-CM2-SR5, MPI-ESM1-2-HR and NUIST-NESM3 are on the same trend, which increases from 10 percent to more than 30 percent, with a spatial average of 7.79 percent, 19.54 percent and 25.75 percent, respectively. MIROC6 indicates a one-third decrease in the west and an increase from below 10 percent to below 30 percent in the east. MRI-ESM2-0 returns opposite results to other models; a decreasing percentage overall with a negative spatial average of 28.01 percent. However, the multi-model-mean remains positive for rainfall changes, with only 5.76 percent of spatial average, possibly as a result of the strong increasing percentage of MRI-ESM2-0 and NUIST-NESM3 output.

For JJA, the results of each model contain both decrease and increase, but the rainfall changes seem to be tilted on the increasing trend for all models. The multi-model-mean increases, with a spatial average of 12.58 percent, a similar percentage to DJF. In SON, NUIST-NESM3 is the only model that contains a decreasing percentage of rainfall, however, the spatial average is still positive. Notably, MPI-ESM1-2-HR displays a sharp

increase in rainfall in SON compared to all outputs, with the highest spatial average of 40.72 percent. Finally, the multi-model-mean shows that SON would likely face a significant increase in rainfall, with the highest spatial average (22.31 percent) compared to other seasons.

In summary, the consequences of high rainfall intensity in the far future period might be worse in the near future period, as only the multi-model-mean in the MAM contains a small decrease in rainfall. This may lead to more frequent flood events and droughts, since the spatial average percentage is much higher than in the near future period.

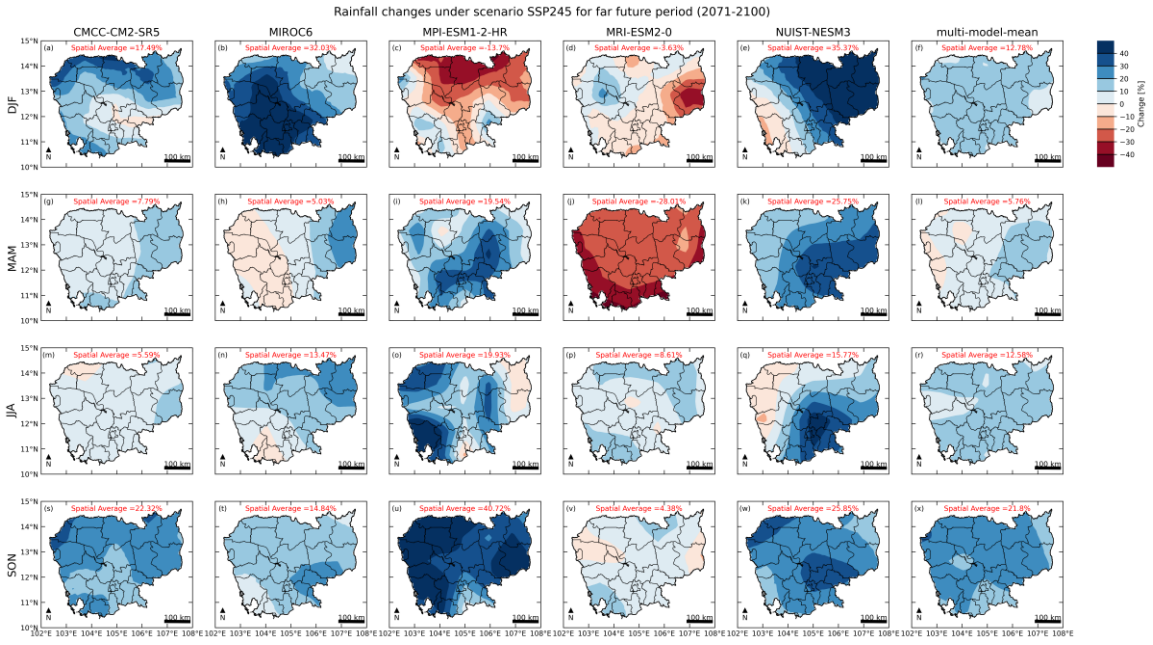

Figure 5.9: The same as Figure 5-8, for far future period (2071-2100) under scenario SSP2-4.5.

Figure 5.10 illustrates the projected changes of seasonal rainfall under scenario SSP5-8.5 for the near future period (2015-2044). In DJF, MIROC6 is the only model that does not contain any decreasing trend of rainfall; the highest increase in rainfall tends to occur in the middle part of the country which will increase over 30 percent, with aspatial average of 22.52 percent. MPI-ESM1-2-HR and MRI-ESM2-0 show a gradual rise from negative to positive percentage. MPI-ESM1-2-HR presents a steady decrease of rainfall from central to eastern regions of the country, while MRI-ESM2-0 show a decrease of rainfall aligning from central to southern and southeastern parts of the country. The other two models indicate mostly a decrease in rainfall in most regions of the country. The multi-model-mean indicates that the southeast of the country will experience rainfall decrease while the northwest experiences an increase, with a range between 10 percent to 20 percent. However, the spatial average still indicates a rainfall increase, though one-third of the country will face rainfall decline.

For MAM, MIROC6, MPI-ESM1-2-HR and NUIST-NESM3 each contain small spots that show rainfall decrease, while the results of spatial average show increases, with percentages of 1.95 percent, 8.23 percent and 7.53 percent. Others show an overall decrease, which is also reflected in the multi-model-mean spatial average of -1.28 percent, however, there is a portion of the north where a 10 percent increase of rainfall is indicated.

In JJA, CMCC-CM2-SR5 indicates that the rainfall will decrease all over the country except the central-east, which shows a rainfall increase; however, the spatial average remains

negative at -1.38 percent. Both MIROC6 and MPI-ESM1-2-HR illustrate a clear increase of rainfall over the entire country, with only a small decrease of rainfall on the eastern border. Both models indicate a 10 percent increase over the spatial average. MRI-ESM2-0 shows a mix of increasing and decreasing rainfall; however, the spatial average settled at -1.14 percent . NUIST-NESM3 illustrates a descending pattern from positive to negative from the southeast to the northwest, with a range of 30 percent to -20 percent, but the spatial average remains positive at 5.47 percent. Three of five models indicate that rainfall will likely increase; therefore, the multi-model-mean shows that JJA will undergo a slight increase in rainfall. For SON, only CMCC-CM2-SR5 shows a decrease in rainfall changes, with a spatial average -2.91 percent, while other models show an increase in rainfall. The multi-model-mean indicates an increase in rainfall over the country, with a spatial average of 10.84 percent.

In summary, rainfall will likely decrease only in MAM, potentially resulting in droughts during this season. For other seasons, rainfall will likely increase overall.

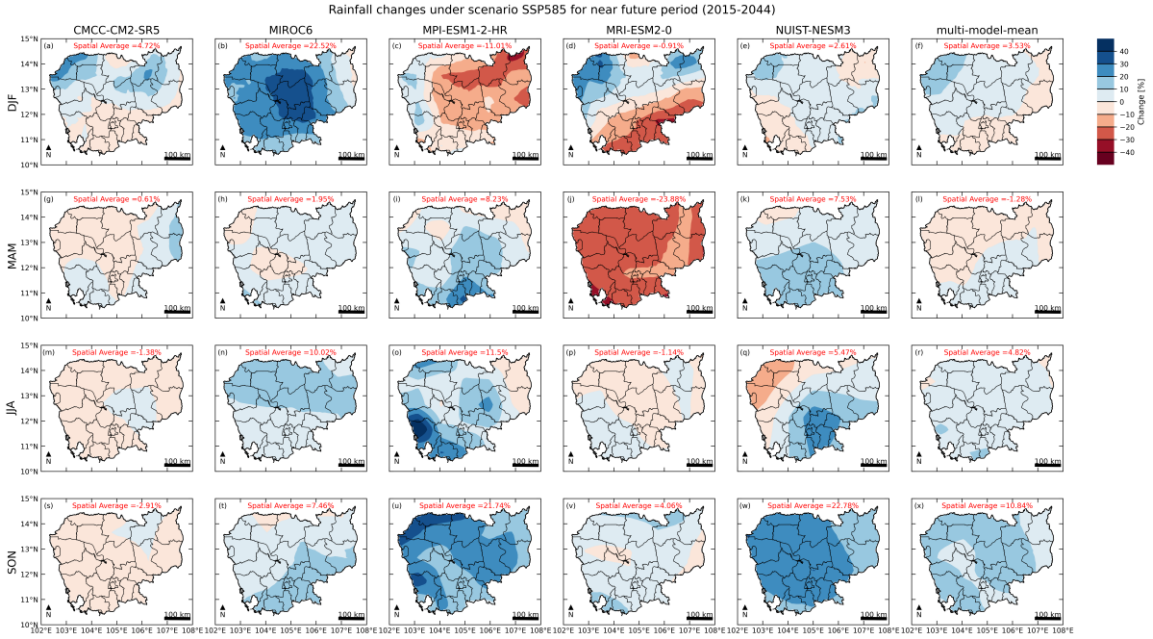

Figure 5.10: The same as Figure 5.8, for near future period (2015-2044) under scenario SSP5-8.5.

Figure 5.11 illustrates the projected changes of the seasonal rainfall change under scenario SSP5-8.5 for the far future period (2071-2100). In DJF, MIROC6 shows that rainfall would soar by more than 40 percent, spreading across the domain with a spatial average of 78.31 percent. Likewise, NUIST-NESM3 also shows a sharp increase in rainfall, except for a small portion on the western border, where there is a -10 percent to -20 percent decrease in rainfall. Other models indicate that rainfall will decrease overall, but MRI-ESM2-0 has the most drastic decrease, with a spatial average of -31.9 percent. However, the multi-model-mean shows a moderate rainfall increase only, with a spatial average of 17.19 percent.

For MAM, both CMCC-CM2-SR5 and MRI-ESM2-0 illustrate a strong decline in rainfall from -10 percent to more than -40 percent. While other models display moderate-to-significant increases in rainfall, NUIST-NESM3 is the most noticeable among all models. However, the multi-model-mean shows a lower increase in rainfall than the DJF season, with a spatial average of only 6.45 percent. In JJA and SON, all models produced a positive output of rainfall increase. For both JJA and SON the multi-model-mean shows a drastic

increase in rainfall. In short, all multi-model-means for all seasons indicate a significant increase in rainfall without any sign of decrease.

As rainfall would likely increase under the SSP5-8.5 scenario in the far future period for all seasons, formidable flooding may occur in this scenario more than in other scenarios. Hypothetically, scenario SSP5-8.5 is assumed to be the worst climate change scenario; thus, the results in this figure support the hypothesis.

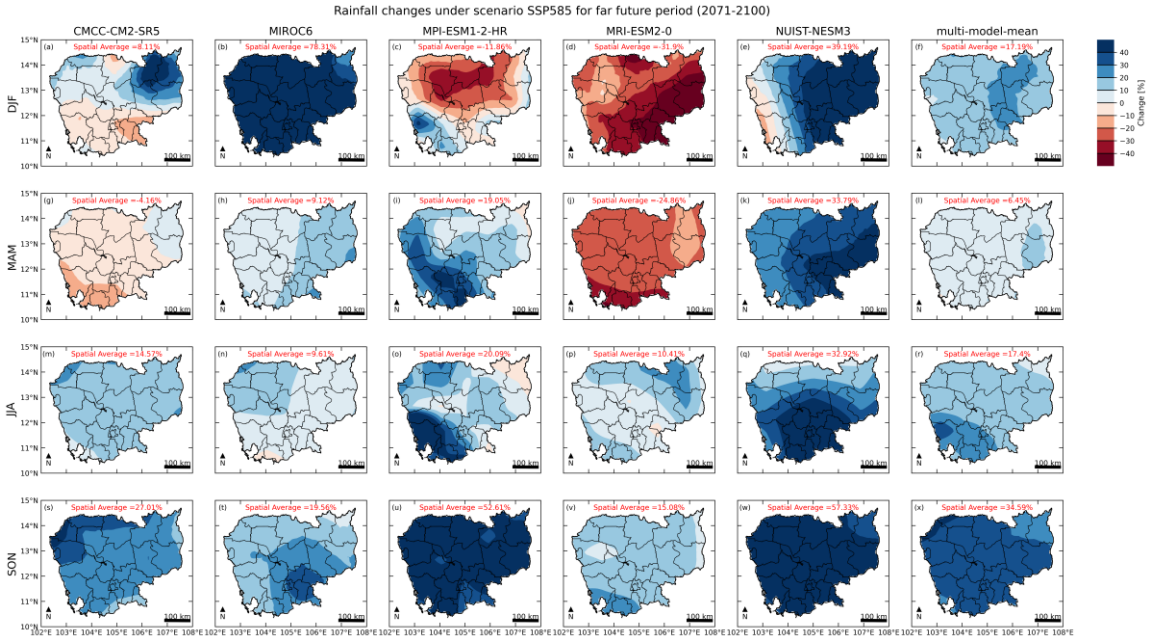

Figure 5.11: The same as Figure 5.8, for far future period (2071-2100) under scenario SSP5-8.5.

The compact summary of precipitation changes for each season, each time horizon, and each scenario is provided in Table 5.3. The values listed in the table is based on the area-average across Cambodian territory, and multi-model mean.

Table 5.3: Summary table of rainfall changes by multi-model-mean

Timeline	Season	SSP2-4.5	SSP8.5
Near future	DJF	1.22%	1.77%
	MAM	2.01%	-1.83%
	JJA	3.18%	4.33%
	SON	10.28%	11.08%
Far future	DJF	12%	16.39%
	MAM	5.51%	6.2%
	JJA	12.32%	17.12%
	SON	22.31%	35.16%

5.3.2 Extreme Events, Encompassing Weather and Climate Timescales

Accurate climate change projections over the long-term are crucial for national policy preparation. Therefore, several climate change indicators were calculated based on the output of the downscaled climate models. For precipitation, five climate indicators used are listed in Table 5.2 below. Each indicator is calculated under SSP2-4.5 and SSP5-8.5 scenarios for the near future period (2015-2044) and the far future period (2071-2100).

Table 5.4: Precipitation climate change indicators

Indicator	Definition
Consecutive dry day (CDD)	Consecutive Dry Day (CDD) index is an indication of dry spell conditions in an area that is linked to drought hazard information.
Consecutive wet day (CWD)	The Consecutive Wet Day (CWD) index indicates information of wet spell in an area.
Maximum 1 day precipitation	The maximum 1 Day Precipitation (RX1Day) index indicates the information about the magnitude of heavy rainfall in a single day that is linked to flood event.
Number of days rainfall more than 50mm	Number of Days rainfall more than 50 mm (nR50mm) is an index showing the frequency of moderate rainfall days.

- Consecutive dry days

Consecutive dry days (CDD) is a climate indicator used to assess the severity of dry spells that can lead to droughts. CDD is calculated by counting the number of consecutive days with less than a specific amount of precipitation (1mm in this calculation). To predict future CDD trends, we analyzed downscaled data from various climate models. Information on CDD can help identify drought-prone regions and inform the development of adaptation plans to address water scarcity.

Figure 5.12 shows the CDD projection under SSP2-4.5, which indicates a general trend of decreasing dry spells across most of the country. However, some models, such as CMCC-CM2-SR5 and MRI-EMS2-0, predict an increase in CDD in the southern and southeastern regions. While the individual models show varying levels of change, the multi-model-mean suggests a slight overall increase in CDD across a larger area, primarily due to the balancing effect of different model projections. However, in certain regions, particularly in the near future, there may be a slight decrease in CDD, though this effect is less pronounced in the far future.

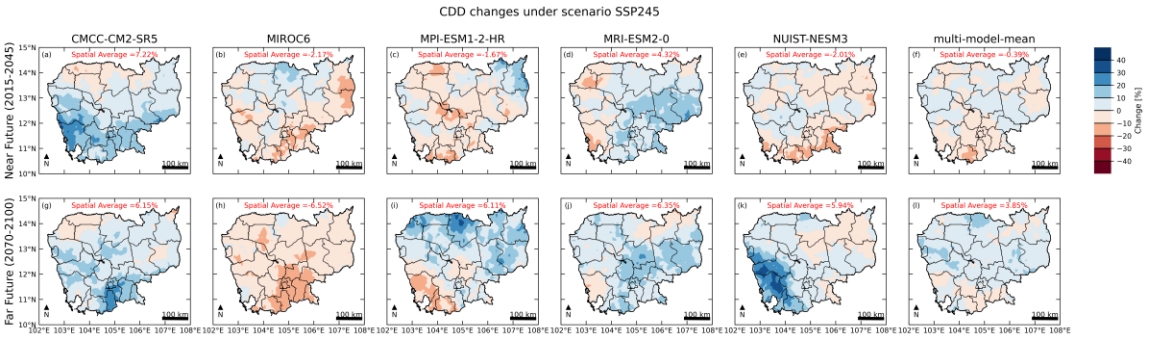

Figure 5.12: Percentage changes in consecutive dry days under scenario SSP2-4.5. First-row panels for near future (2015-2044), and second-row panels for far future (2071-2100).

Figure 5.13 depicts the anticipated changes in the CDD under scenario SSP5-8.5. In the near future period (first-row panels), nearly all climate models forecast a reduction in the percentage of CDD, except CMCC-CM2-SR5, which shows an upward trend. The multi-model-mean suggests that the CDDs are likely to decrease by up to 10 percent in most regions of Cambodia, while they may increase by approximately 10 percent in small areas in central parts of the country and near the borders with Thailand, Lao PDR, and Vietnam. In the far future period (second-row panels), MPI-ESM1-2-HR and NUIST-NESM3 predict both increases and decreases in the CDD percentages, ranging from -20 percent to +40 percent, whereas CMCC-CM2-SR and MRI-ESM2-0 show a more significant increase across all of Cambodia. Finally, the multi-model-mean indicates a slight increase in the CDD, around 20 percent, particularly in the coastal region (bottom right panel of Figure 5.13).

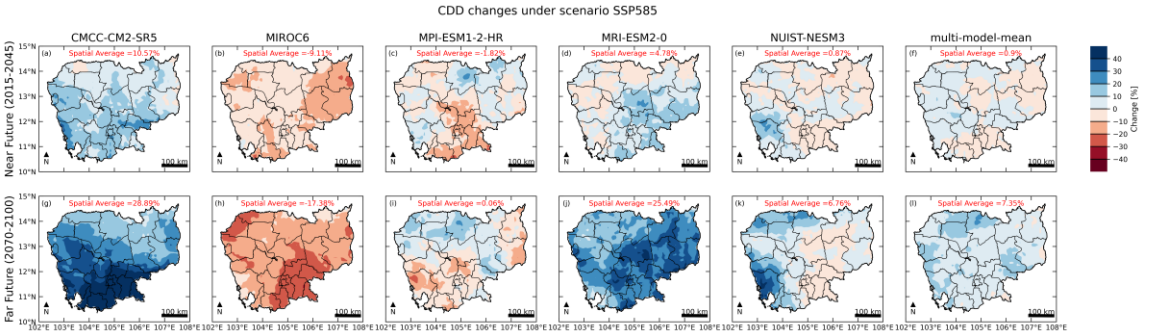

Figure 5.13: The same as Figure 5.12, for scenario SSP5-8.5.

In summary, the projections indicate an increase in CDD across most regions of Cambodia, particularly under the SSP5-8.5 scenario by the end of the century. This suggests a potential threat of dry spells and droughts in the country due to the impacts of climate change.

- Consecutive wet days

The Expert Team on Climate Change Detection and Indices (ETCCDI) defined the CWD the number of consecutive days with at least 1 mm of precipitation. CWD is determined by counting the number of consecutive days with rainfall exceeding a specified amount (1 mm in this case). Information on the CWD can be utilized to predict flooding or identify regions that may experience extended periods of rainfall. Additionally, a decrease in the projected CWD could indicate the potential for dry spells or drought.

Figure 5.14 presents the projection of CWD under the SSP2-4.5 scenario. For the near future (first-row panels), the CMCC-CM2-SR5 and NUIST-NESM3 models suggest a likely

decrease in CWD across the entire domain, while the other three models show a mix of increasing and decreasing CWD. The multi-model-mean indicates a combination of decreases (from the southwest to the northeast) and increases (in the northwest and southeast) in CWD in Cambodia. For the far future (second-row panels), most models predict an increase in CWD, except for NUIST-NESM3, which shows decrease. Consequently, the multi-model-mean projects an overall increase in CWD across Cambodia.

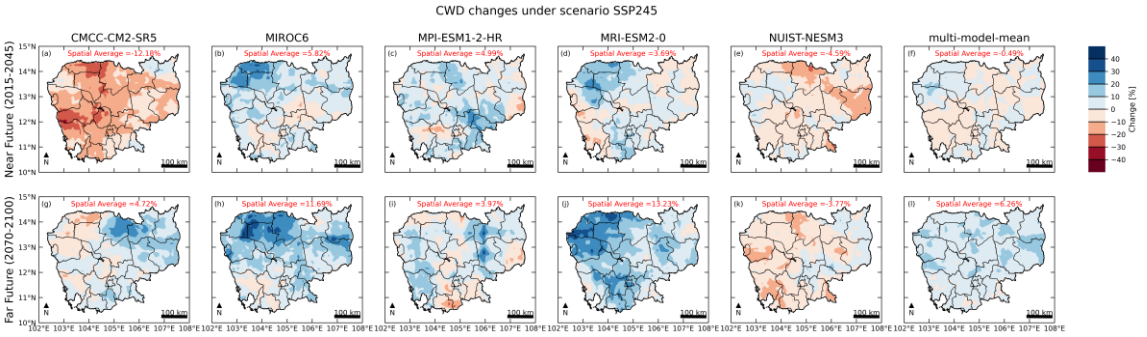

Figure 5.14: Percentage changes in the consecutive wet days under scenario SSP2-4.5. First-row panels for near future (2015-2044), second-row panels for far future (2017-2100)

Figure 5.15 shows the projection of CWD under the SSP5-8.5 scenario. In the near future (first-row panels), the CMCC-CM2-SR5 and NUIST-NESM3 models display nearly identical patterns of up to 20 percent decreases in CWD. Conversely, MIROC6 indicates a significant increase in CWD with a few areas of decline. Similarly, the MPI-ESM1-2-HR and MRI-ESM2-0 models show an increase in CWD in the western parts of the country and a decrease in the eastern parts. The multi-model-mean however, suggests an overall increase in CWD, with variations of ±10 percent across the domain. For the far future (second-row panels), all models except CMCC-CM2-SR5 predict a similar spatial pattern: an increase in the western part and a significant decrease in the eastern part. Consequently, the multi-model-mean also reflects this pattern, despite the large negative changes projected by CMCC-CM2-SR5.

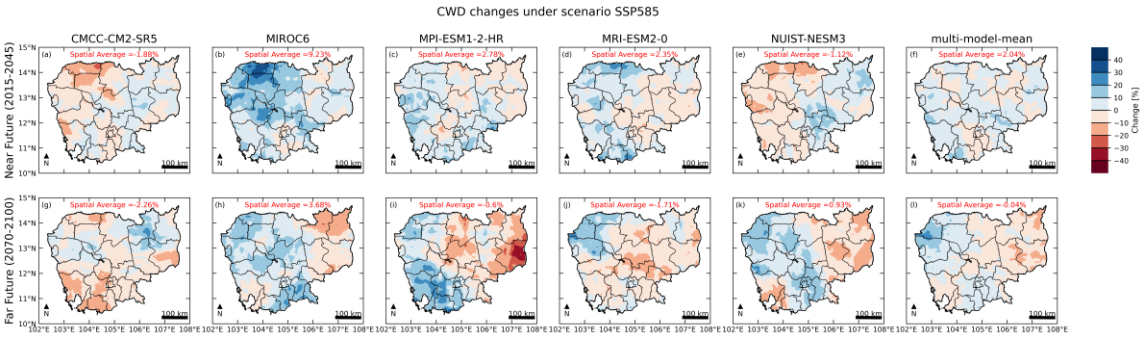

Figure 5.15: The same as Figure 5.14, for scenario SSP5-8.5.

Overall, the projection indicates an increase in CWD under the moderate SSP2-4.5 scenario, while a significant decrease is expected in the eastern part of the country under the unmitigated SSP5-8.5 scenario. This implies that wet spells are likely under the moderate climate change scenario, but the opposite is true for the unmitigated scenario, where the number of wet days would decrease, leading to dry spells consistent with the CDD projection.

☀ Maximum 1 day precipitation

The maximum 1-day precipitation (rx1day) is a climate index that measures the highest rainfall accumulated within a 24-hour period. Projecting rx1day is crucial for planning mitigation and adaptation strategies for flooding events, such as flash floods or riverine floods, in specific regions. However, information on rx1day is still limited. Therefore, users should be aware of model biases and utilize multi-model data before making any decisions.

Figure 5.16 illustrates the percentage changes in rx1day under the SSP2-4.5 scenario. In the near future (first-row panels), projections indicate that rx1day is likely to increase by 10 percent to over 40 percent, particularly in the MIROC6, MPI-ESM1-2-HR, and NUIST-NESM3 models, while the other two models show a slight decrease in northern Cambodia. Despite some models showing a decline in rx1day percentages, the multi-model ensemble indicates positive changes ranging from 10 percent to 30 percent, with a notable 20 percent increase spreading from the northwest to the southeast of the country. For the far future (second-row panels), all models project that rx1day will rise by 10 percent to over 40 percent, with the MPI-ESM1-2-HR model showing the most significant increase, exceeding 40 percent across Cambodia. However, the MRI-ESM2-0 model shows a decrease in rx1day for some regions, mainly in the north. Overall, the multi-model-mean projects an increase, with significant variability across Cambodia.

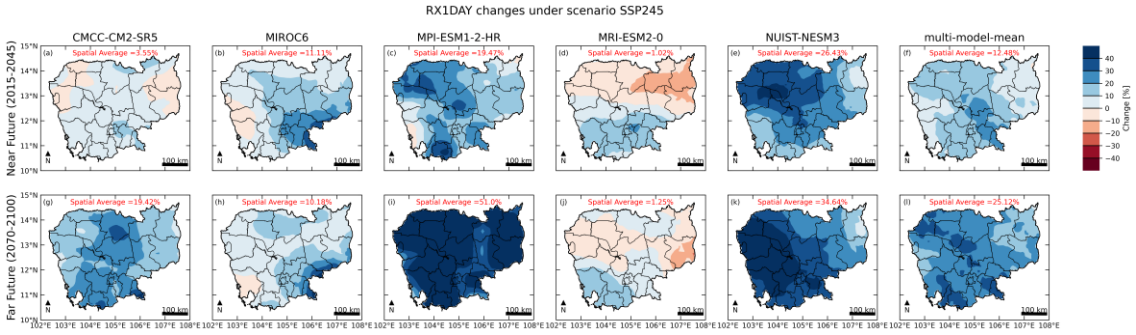

Figure 5.16: Percentage change in rx1day under scenario SSP2-4.5. First-row panels for near future (2015-2044), and second-row panels for far future (2071-2100).

Figure 5.17 shows the projection of rx1day under the SSP5-8.5 scenario. In the near future (first-row panels), the MPI-ESM1-2-HR and NUIST-NESM3 models project the most significant increases in rx1day across the entire country, while the other three models show a mix of increases and decreases. The multi-model-mean suggests that rx1day will likely increase by about 10-30 percent. For the far future (second-row panels), all models predict a similar trend of rising rx1day across the entire domain, except for some northern areas where the MIROC6 and MRI-ESM2-0 models show decreases of about 10-20 percent. Additionally, the CMCC-CM2-SR5, MPI-ESM1-2HR, and NUIST-NESM3 models indicate strong percentage increases in rx1day, exceeding 40 percent over Cambodia. Finally, the multi-model-mean projects an increase ranging from 30 percent to over 40 percent (bottom right panel of Figure 5.17).

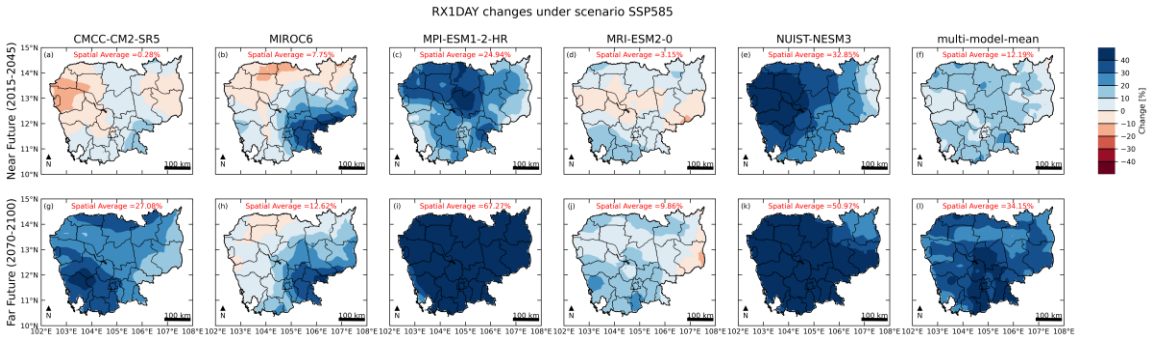

Figure 5.17: The same as Figure 5.16, for scenario SSP5-8.5.

In summary, the projection of rx1day indicates an increase across most parts of Cambodia, particularly under the SSP5-8.5 scenario by the end of the century. This suggests a potential threat of extreme rainfall leading to floods in the country due to climate change impacts.

- Number of days rainfall greater than 50mm

Another key indicator is extreme precipitation days, the number of days with rainfall more than 50mm, nR50mm. This indicator is connected to flood risk. The projection based on SSP2-4.5 shows an increase of nR50mm, except for coastal areas, which show minor decrease (Figure 5.18). Again, both scenarios show similar spatial features, only different in change magnitude.

Figure 5.18 shows the projection of the nR50mm under SSP2-4.5 scenario. In the near future period, all climate models indicate the percentage of nR50mm increasing in the central regions while decreasing in the northeast and southwest, except MRI-ESM2.0 which show the opposite. However, after calculation of the multi-model-mean, the result show that nR50mm will increase all over Cambodia, but with less percentage in elevated areas (top right of the map plot) and coastal areas (bottom left of the map plot). The far future period shows similar results as the near future period, however CMCC-CM2-SR5 shows a completely different result from the near future period, with every part of Cambodia increasing more than 40 percent. To summarize, the result of the multi-model-mean is the same in the near future period. However, nR50mm in far future period will increase across Cambodia by more than 40 percent.

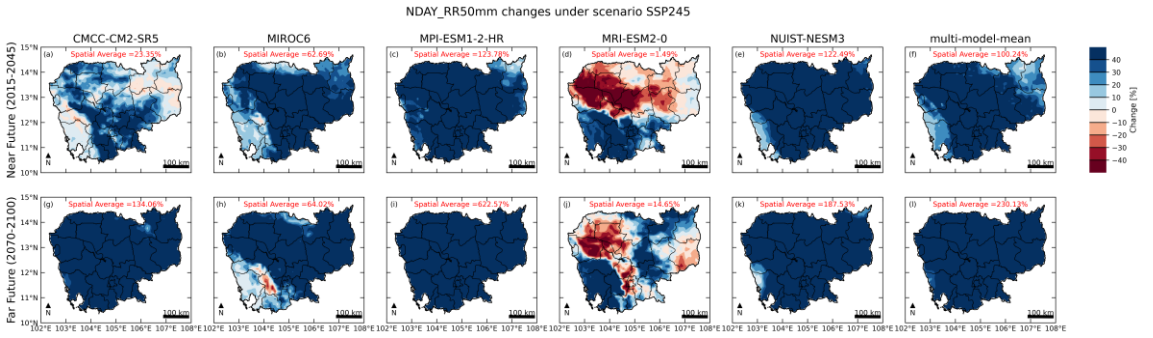

Figure 5.18: Percentage change in nR50mm under scenario SSP2-4.5. First-row panels for near future (2015-2044), and second-row panels for far future (2071-2100).

Figure 5.19 shows the prediction of nR50mm under scenario SSP5-8.5. For the near future period, MPI-ESM1-2-HR and NUSIT-NESM3 indicate an increase of more 40 percent over the entire region, while the other models show a mixture of increase and decrease. Noticeably, MRI-ESM2-0 show a sharp decrease of nR50mm, below -40 percent over the

Tonle Sap region. This result impacts the result of multi-model-mean, which show nR50mm increase all over the country except a small decrease near Tonle Sap Lake. For the far future period, each model shows a complete increase of nR50mm, except MIROC6, which shows a small decrease, ranging from -10 percent to -40 percent in the northwest, and MRI-ESM2-0, which shows a decrease of roughly -10 percent in the east. The multi-model-mean indicates a complete increase of over 40 percent in each region of Cambodia.

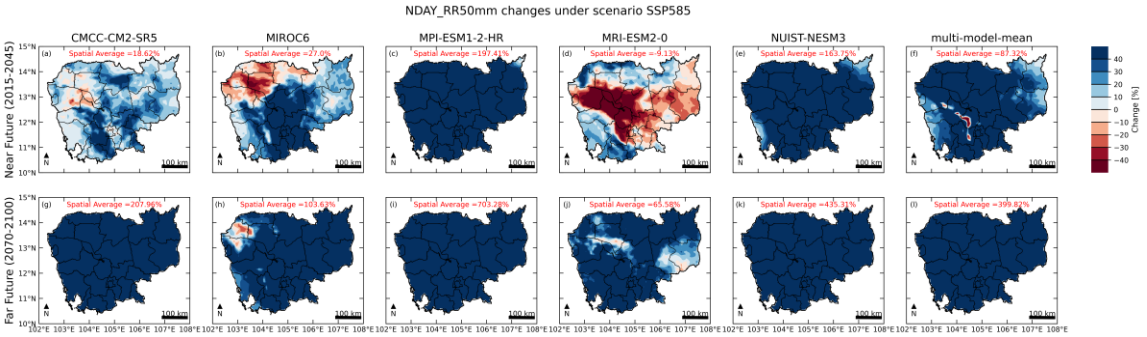

Figure 5.19: The same as Figure 5.18, for scenario SSP5-8.5.

In conclusion, the models show that Cambodia will face a dramatic increase of nR50mm in the future for both climate change scenarios, which means more days of the year with higher rainfall intensity, which increases the risk of floods, especially in already flood-prone area in Cambodia. Importantly, the result from each climate model indicated that the central plain area will have a higher percentage of nR50mm increase. The compact summary of the changes of extreme climate indices for each time horizon and each scenario is provided in Table 5.5. The values listed in the table are based on the area-average across Cambodian territory and the multi-model-mean.

Table 5.5: Summary table of extreme indicator changes by multi-model-mean

Timeline	Season	SSP2-4.5	SSP5-8.5
Near future	CDD	-0.39%	-0.39%
	CWD	-0.49%	2.04%
	rx1day	12.48%	12.19%
	nR50mm	100.24%	87.32%
Far future	CDD	3.85%	7.35%
	CWD	6.26%	-0.04%
	rx1day	25.12%	34.15%
	nR50mm	230.13%	399.82%

5.3.3 Assessment of Projected Changes of Extremes and Potential Surprises

The results of the projection of the mean precipitation change, CDD, CWD, rx1day, and nR50mm based on the finer-scale downscaling data in the current report conclude that the future climate of Cambodia would likely be getting drier during the dry season and wetter during the rainy season. The results also suggest the potential threats of more dry spell events related to drought and more heavy rainfall events related to floods in most parts of Cambodia as a result of climate change. This is consistent with the law of atmospheric physics that warm air can store more water vapor for a longer time (causing dry spells). However, when those large amounts of water vapor become rain droplets, it results in stronger rainfall intensity, triggering floods. Moreover, several previous research studies indicate the same trend as these results. Climate projection over Southeast Asia using the regional climate model by Chotamonsak et al (2011) showed that the studied area would be experiencing drier conditions with more heavy rainfall events (Chotamonsak, Salathé, Kreasuwan, Chantara, & Siriwitayakorn, 2011). Additionally, the current report shows that future climate change aligns with the IPCC predictions, with a rise in rainfall in the rainy season and a decline in rainfall in the dry season. Our projection on extreme events also indicates that Cambodia is vulnerable to drought and flooding. Another study also shows that the flow in several streams and rivers in Cambodia is predicted to decrease in the future compared to the baseline period due to the lack of rainfall in the dry season (Oeurng, et al., 2019). Likewise, the projection of precipitation in the Siem Reap province of Cambodia also suggested that rainfall will be decrease in the dry season. The results of this report could increase confidence in projections of future change in rainfall patterns in Cambodia based on the newly updated climate modeling activity, in CMIP6.

5.4 Case Studies Across Timescales

The boxes below present case studies on climate change impacts across key sectors in Cambodia, including water resources, agriculture, biodiversity, the economy, and society. They demonstrate how climate change makes existing vulnerabilities worse and creates systemic risks that cut across environmental, social, and economic domains. These cases were selected to provide an evidence-based overview of sectoral challenges and to emphasize the importance of integrated and adaptive responses in policy and practice.

BOX 1

Examples of Climate Change Impacts on Water Resources in Cambodia

REDUCTION IN WATER AVAILABILITY

Climate change projections indicate that Cambodia will face increased water scarcity by 2030 and 2050. Climate-induced shifts in river basin hydrology are likely to bring more intense monsoon rainfall but also higher temperatures and prolonged droughts, leading to increased evapotranspiration and reduced surface water availability (USAID, 2019). This dynamic has already driven higher groundwater extraction and overexploitation, further stressing water systems.

Projections suggest that by 2050, Cambodia could experience severe water scarcity due to prolonged droughts and altered precipitation regimes (UNEP, 2019). The central and

northern regions are particularly vulnerable. According to the Asian Development Bank (2017), droughts may affect up to 2 million people by 2050, sharply reducing water supplies for agriculture and domestic use. Water demand for irrigation in the Tonle Sap Basin is projected to rise by 22-36 percent in the dry season for the future period of 2051–2071 (Touch et al., 2020), indicating major challenges for climate-resilient agriculture.

Coastal areas are further at risk from sea-level rise and saline intrusion, which threaten access to safe drinking water and the viability of inland waterways crucial to rice and freshwater fish production.

DEGRADATION IN WATER QUALITY

Poor water quality, driven primarily by eutrophication linked to inadequate sanitation and nutrient management, is already one of the most widespread problems affecting Cambodia's available water supply, fisheries, and recreational water use. Climate change is expected to worsen this degradation. Higher water temperatures reduce dissolved oxygen and lower the self-purifying capacity of freshwater systems. Increased flooding can introduce pollutants and pathogens into water sources, while prolonged droughts concentrate contaminants, heightening the risks to human and ecological health.

Additionally, deforestation and flood events may cause increased sedimentation, introducing harmful pollutants and bacteria into rivers and lakes. These pollutants can degrade fish habitats and compromise food security for vulnerable populations that depend on aquatic resources.

BOX 2

Examples of Climate Change Impacts on Agricultural and Aquatic Productivity in Cambodia

DECLINING AGRICULTURAL PRODUCTIVITY

Climate change is expected to significantly impact Cambodia's agricultural productivity, especially in rainfed systems. Under optimistic climate change scenarios, rice yield losses could reach 21 percent between 2030 and 2060. Under pessimistic scenarios, losses may rise to 30 percent (World Bank, 2023). Yield reductions are not limited to rice: rainfed maize yields are projected to decline by 6–9 percent, and cassava yields by 5–11 percent, potentially disrupting food supply chains and rural incomes.

Rice, as Cambodia's staple crop, is particularly sensitive to climate change. Research from the International Rice Research Institute (IRRI) suggests that every 1°C increase in temperature may result in a 10 percent decline in rice yields, increasing vulnerability among smallholder farmers. With growing population pressure, Cambodia may become increasingly reliant on rice imports to maintain national food security by 2030 (Trisurat et al., 2018).

BOX 3

Examples of Climate Change Impacts on Biodiversity and Ecosystems in Cambodia

LOSS OF BIODIVERSITY AND ECOSYSTEM DEGRADATION

Climate change poses a major threat to Cambodia's biodiversity and ecosystems, with projections indicating substantial and potentially irreversible losses. Key drivers include water depletion, pollution, and increasing climate extremes, which reduce the resilience of vital ecosystems.

Healthy soils—rich in microbial life—are critical for sustainable agriculture. However, climate change, particularly extreme heat and shifting rainfall patterns, threatens soil quality. Under moderate climate scenarios, soil erosion is projected to increase by 16.9 percent by 2060, undermining agricultural productivity and natural vegetation cover (Mekong River Commission, n.d.).

AQUATIC ECOSYSTEM STRESS: TONLE SAP LAKE

The Tonle Sap, Southeast Asia's largest freshwater lake, is under severe stress due to prolonged droughts, drastically impacting water levels and leading to significant declines in fish stocks (USAID, 2019). These changes threaten food security and livelihoods for millions who depend on the lake's ecosystem services.

TERRESTRIAL ECOSYSTEM VULNERABILITY

In Cambodia's eastern plains and Prey Lang landscape, rising temperatures—projected to increase by 4 to 6°C by 2050—could trigger tropical forest dieback, increased wildfires, and outbreaks of pests. These impacts jeopardize non-timber forest products (NTFPs) and the economic stability of forest-dependent communities.

COASTAL AND MARINE ECOSYSTEM THREATS

Cambodia's southern mangroves, essential for coastal protection and marine biodiversity, face threats from sea-level rise, industrial dredging, and flooding. These pressures undermine ecosystem integrity and compromise marine resources critical to local economies and coastal resilience.

BOX 4

Examples of Climate Change Impacts on Economy in Cambodia

GDP LOSSES FROM CLIMATE CHANGE

Macroeconomic modeling suggests that without targeted interventions, Cambodia's GDP could decline by 3 to 9 percent by 2050 due to climate change (World Bank, 2023; MEF & GSSD, 2019). In a baseline scenario without climate change, GDP is projected to grow steadily—reaching 9.75 times the 2016 level by 2050. However, under a mid-level scenario (RCP4.5), GDP could be:

- 2.5 percent lower by 2030
- 6.0 percent lower by 2040

- 9.8 percent lower by 2050

These reductions delay economic progress. While Cambodia could reach upper-middle-income country (UMIC) status by 2035 under normal conditions, climate change may push that milestone to 2036. By 2050, the country could fall USD 4,227 short, per capita, of high-income Country (HIC) status without climate impacts, and USD 5,094 short with them.

INCREASED COSTS FROM CLIMATE-RELATED DISASTERS

The frequency and severity of climate-induced extreme events—including floods, storms, and heatwaves—pose mounting economic risks. Without adaptation, annual average losses in key sectors (manufacturing, services, and housing) could rise from USD 530 million in 2020 to USD 3.3 billion by 2050 (World Bank, 2023).

Historical damages underline the urgency:

- USD 132 million (2009)
- USD 625 million (2011)
- USD 357 million (2014)

The average annual loss is estimated at USD 54 million, about 0.7 percent of GDP. Modeling suggests that a 1-in-25-year flood in 2020 could cause asset losses of:

- USD 412 million in manufacturing
- USD 344 million in services
- USD 108 million in housing

By 2050, these losses could climb to USD 10.6 billion under pessimistic climate scenarios, threatening both economic stability and human wellbeing.

BOX 5

Examples of Climate Change Impacts Social in Cambodia

FOOD INSECURITY

Climate change is projected to severely impact Cambodia's agricultural production and fisheries, threatening food availability, increasing malnutrition, and raising food prices. This undermines progress toward SDG targets 2.1 and 2.2 on eliminating hunger and malnutrition. The World Bank notes that climate-related price volatility could intensify food insecurity, particularly for vulnerable populations (World Bank, 2020). Pests and diseases, exacerbated by climate change, may also degrade food safety and reduce crop and livestock yields (FAO, 2018).

WATER SECURITY

Access to safe and reliable water is already a concern in Cambodia, and climate change will further compromise water, sanitation, and hygiene (WASH) services. As of 2023, 43 percent of communes are highly vulnerable to climate impacts on water access (UNICEF, 2023). These service gaps heighten exposure to waterborne diseases and reduce community resilience.

POVERTY AND INEQUALITY

By 2030, climate-related agricultural losses and disasters could push 1 million additional Cambodians into poverty (World Bank, 2016). The impacts will hit rural and agricultural communities hardest, widening the urban-rural divide and exacerbating existing inequalities (UNDP, 2019; ADB, 2019).

HEALTH AND LABOR PRODUCTIVITY

Climate change is linked to increased incidence of diseases, including diarrhea, respiratory illnesses, and heat-related conditions. Studies suggest childhood diarrhea could increase by 19 percent by 2040 due to environmental stressors (Aguilar Gomez et al., 2024). Poor health lowers productivity and raises healthcare costs. Under high warming (RCP8.5), Cambodia could lose up to 6.54 percent of labor productivity by 2055 (UNDP, 2016).

TOURISM IMPACTS

Climate change is projected to reduce tourism revenue by 8–17 percent by 2050, depending on the scenario. International tourism may decline by 12–33 percent, while domestic tourism could drop by 4–11 percent between 2041–2050 (World Bank, 2023), threatening a key sector for job creation and national revenue.

BOX 6

Practices for Adaptive Climate Actions in Cambodia

Cambodia's approach to climate change adaptation recognizes the importance of integrating social, economic, environmental, and cultural factors into planning and implementation. Adaptive actions must be tailored to local risk profiles, with a tiered structure where national-level policies enable subnational implementation.

In agriculture, practices such as adjusting harvesting windows and cropping calendars, selecting flood- and drought-tolerant plant varieties, improving irrigation efficiency, reducing soil erosion, and applying nitrogen to enhance low-fertility soils are key to maintaining productivity under changing climate conditions.

Given projections of increased rainfall intensity during the wet season, effective water resource planning and flood control infrastructure are critical. Priority actions include:

- Constructing multipurpose dams for flood and drought management;
- Enhancing water allocation systems for domestic use, agriculture, and hydropower; and
- Engaging stakeholders in climate-related decision-making to improve policy alignment and resilience.

These practices not only reduce vulnerability and economic losses, but also contribute to more inclusive and sustainable adaptation pathways, especially for marginalized rural communities.

BOX 7

Priorities for Climate-Resilient Agriculture and Water in Cambodia

Cambodia is advancing climate-resilient strategies in the agriculture and water sectors, focusing on improved risk management, data integration, and institutional coordination.

Improved Climate Information Use

Climate data should inform decisions such expanding irrigation in drought-prone areas, shifting agriculture to safer zones, and designing climate insurance. Key actions include:

- Establishing climate information forums for stakeholder exchange and engagement;
- Strengthening agro-meteorological networks in high-variability areas to provide accurate information for farmers; and
- Developing a centralized climate database to support cross-sectoral planning.

Institutional Integration

Agriculture and water sectors require integrated governance. Strengthening institutional frameworks enables:

- Climate-informed decision-making tools
- Coordinated data-sharing across ministries
- Promotion of low-risk planning for improved resilience

Research and Development

Building research capacity is essential to address climate risks in agriculture, health, forestry, and coastal zones. Key priorities include:

- Launching pilot projects linking science and community action;
- Enhancing climate awareness and food security planning;
- Supporting interdisciplinary research partnerships.

This approach helps Cambodia transition toward evidence-based, adaptive agriculture and water systems, protecting livelihoods under a changing climate.

Adapted from Turap, Merupakan, Lebih, & Turap, 2024

5.5 Directions for Future Studies

5.5.1 Improving the Process of Gathering and Tracking Data

5.5.1.1 Enhancing Meteorological Networks

It is crucial to establish a more comprehensive and denser network of meteorological stations in Cambodia. These strategically positioned stations will collect crucial ground-truth data necessary for validating models and will cover different ecological zones and elevational gradients. In addition, climate timescale requires rather long data record for capturing the status of the climate. This requires data rescue efforts, to gather and preserve existing historical data from specialized centers and research institutions. This increase, which will provide extensive and thorough data coverage, will greatly enhance the precision and dependability of climate models.

5.5.1.2 Integrating Satellite and Remote Sensing Data

Utilizing satellite remote sensing data can augment understanding of more extensive environmental alterations. These devices provide uninterrupted monitoring capabilities, enabling scientists to observe weather patterns, land surface temperatures, and precipitation cycles. Through the integration of terrestrial and satellite data, scientists can generate a comprehensive dataset that effectively captures the intricacies of both local and regional climate processes.

5.5.2 Refining Climate Modeling Techniques

5.5.2.1 Advancing the Creation of Climate Models with Enhanced Precision

The prioritization of refining statistical downscaling techniques remains crucial. As noted, many existing models do not have the granularity needed for small and geographically varied regions like Cambodia. The goal is to create detailed models that can accurately represent the small-scale variations in climate that are unique to the different habitats found in Cambodia. These changes are caused by factors such as the topography, land use, and weather patterns in the area. These factors make the forecasts accurate and relevant to the specific region and community.

5.5.2.2 Exploring Multiple Climate Scenarios

In order to account for the inherent uncertainties in climate modeling, it is crucial to explore a range of scenarios using data rescue efforts IPCC's various climate change projections. This technique offers a comprehensive perspective by considering both the most favorable and the most unfavorable situations in terms of greenhouse gas emissions. Such an extensive and diverse investigation will provide policymakers with the necessary information to develop flexible and robust plans.

5.5.3 Enhancing Bias Correction Techniques

5.5.3.1 Dynamic Adjustment Algorithms

Integrating dynamic adjustment techniques can enhance the accuracy and precision of model outputs. These algorithms consistently revise bias corrections using up-to-date data. These strategies enhance the model's capacity to consider changes in seasonal and yearly variations by adjusting corrections gradually, guaranteeing continuous precision as environmental conditions change.

5.5.3.2 Local calibration of models for climatic zoning

Geographically sensitive bias correction is necessary to consider the varied climatic conditions present in different regions of Cambodia. Methods such as linear scaling and variance scaling are frequently employed to rectify systematic biases, but it is necessary to calibrate them using localized datasets in order to more accurately represent area climate characteristics. This requires the customization of correction factors for various climatic regions in Cambodia to properly address the geographically diverse biases.

5.5.3.3 Expand the Climate Model Ensembles

Ensemble modeling approaches, which combine results of multiple models, can improve bias correction. Ensemble averaging and Bayesian model averaging are techniques that can be employed to combine data from several models. This synthesis of results enhances

the accuracy of forecasts by considering various uncertainties associated with different models.

5.5.3.4 Integration of Machine Learning and Artificial Intelligence

Utilizing machine learning techniques to dynamically adapt bias correction provides an innovative solution. AI algorithms may utilize extensive datasets to find and analyze systematic flaws, enabling the identification and application of corrective strategies. These techniques, such as neural networks or support vector machines, enhance bias correction by identifying intricate patterns and relationships from climate data.

5.5.3.5 Assessing and Validating Corrections

Regular validation of bias correction approaches is essential for preserving their credibility. This involves comparing adjusted model outputs with independent observational datasets that were not utilized during the correction procedure. To accurately measure enhancements and verify the effectiveness of adjustments in reducing disparities between observed and modeled data, it is recommended to use metrics such as root mean square error (RMSE) and mean bias error (MBE).

5.5.3.6 Enhancing Climate Indices for Policy and Sectoral Insights

- Further development of Climate Indices Development

Creating comprehensive metrics for precipitation and temperature will offer crucial understanding of climatic fluctuations and shifts. These indices can indicate trends such as a rising occurrence of severe weather events or changes in seasonal patterns, which are essential for informing policy decisions.

- Supportive indices for Sector-specific Decisions

Customizing climate indices to meet the specific needs of different sectors ensures that industries such as agriculture, water resources, and health can access relevant information. For example, understanding temperature extremes can help the agricultural sector develop more effective strategies for selecting crops and improving their resilience to challenging conditions. These indices can serve as essential tools in formulating policies for climate adaptation and mitigation. Policymakers can create strategic plans to address climate-related challenges by using clear and comprehensive indicators of climate change impacts.

5.5.3.7 Incorporating Socio-economic and Land-Use Mode

- Analyzing the Effects of Human Activities on the Environment

Incorporating socio-economic scenarios and land-use changes into climate projections is essential for comprehensive modeling. These models account for human-driven factors, such as deforestation, urban expansion, and agricultural practices, which significantly impact climatic patterns.

5.5.3.8 Harnessing Technological Innovations

- Utilizing Machine Learning

Applying machine learning and artificial intelligence technology can greatly improve the capabilities of climate models. These techniques enable the more effective processing of intricate datasets, hence permitting enhanced forecasts and scenario assessments.

- Allocating resources to support computational infrastructure

Developing Cambodia's computing infrastructure is crucial for effectively managing large-scale datasets and complex models. A resilient infrastructure framework will facilitate the ongoing advancement of state-of-the-art climate modeling approaches.

5.5.3.9 Recommendations

The nation’s climate change research enterprise should integrate both disciplinary and interdisciplinary research across the physical, social, biological, health, and engineering sciences. Efforts should focus on fundamental, use-inspired research that contributes to both improved understanding and more effective decision-making. Research must also be flexible in identifying and addressing emerging research challenges. A single entity should be granted the authority and resources to coordinate and implement an integrated research efforts that support both improving the understanding of and responding to climate change.

The climate change research program should be formally linked with action-oriented response programs focused on limiting the magnitude of future climate change, adapting to the impacts of climate change, and informing climate-related actions and decisions. The climate change research program should collaborate with other relevant partners, including universities, national and local governments, the international research community, the business sector, and relevant nongovernmental organizations to expand and engage the human capital needed to carry out climate change research and response programs.

REFERENCES

Abdul Azim Amirudin, E. S. (2020). Differential influences of teleconnections from the Indian and Pacific Oceans on rainfall variability in Southeast Asia. Atmosphere.

Abhijeet Abhishek, N. N. (2021). Evaluating the impacts of drought on rice productivity over Cambodia in the Lower Mekong Basin. *Hydrology*.

ADB. (2000). Cambodia demonstration project: Coastal and marine environmental management in South China Sea, Phase 2 (ADB-5712). Kingdom of Cambodia.

ADB. (2012). *Flood Damage Emergency Reconstruction: Preliminary Damage and Loss Assessment; Asian Development Bank: Mandaluyong, Philippines.*

ADB. (2019). *Completion Report of the Rural Energy Project of the Asian Development Bank.* Manilla.

ADB. (2017). *Climate Change Assessment in the Greater Mekong Subregion.*

ADB. (2019). *Addressing Climate Change and Its Impacts on Poverty in Cambodia.*

ADB. (2023). Building disaster-resilient infrastructure through enhanced knowledge (Technical Assistance Consultant's Report No. 52251-001).

ADB. (2023). Framework for Integrating Gender Equality and Social Inclusion in the Asian Development Bank's South Asia Operations.

Adom, P. K. (2024). The socioeconomic impact of climate change in developing countries over the next decades: A literature survey. *Heliyon*, 10(15), e35134. doi:https://doi.org/10.1016/j.heliyon.2024.e35134

Agapol. J, et al. (2020). Spatial and Temporal Distribution of Biomass Open Burning Emissions in the Greater Mekong Subregion. *Climate*, 1-27. doi:10.3390/cli8080090

Aguilar Gomez, S., Baquie, S., & Robyn, P. J. (2024). Environmental Hazards, Climate, and Health in Cambodia: The Shield of Sanitation. Environmental Hazards, Climate, and Health in Cambodia: The Shield of Sanitation, March. *Environmental Hazards, Climate, and Health in Cambodia: The Shield of Sanitation*, https://doi.org/10.1596/1813-9450-10715.

Akarath Soukhaphon, I. G. (2021). The Impacts of Hydropower Dams in the Mekong River Basin: A Reviw. *Water*.

Algo, J. L. (2016). *Philippine Climate Change Assessment.* The Oscar M. Lopez Center for Climate Change Adaptation.

Akyüz, E. (2021). The Development of Environmental Human Rights. *International Journal of Environment and Geoinformatics , 8(2) , 218-225. DOI: 10.30897/ijegeo.839725*.

Allen, J. T., & Allen, E. R. (2016). A review of severe thunderstorms in Australia. Atmospheric research. *178*, 347-366. doi:https://doi.org/10.1016/j.atmosres.2016.03.011

Alvar-Beltrán, J. S. (2022). Modelling climate change impacts on wet and dry season rice in Cambodia. *Agronomy and Crop Science*.

Andreae, M. O., et al. (2004). Smoking rain clouds over the Amazon. *Science, 303*(5662), 1337-1342.

Andreae, M. O. (2007). *Aerosols before pollution.*

Anuchaivong, P., Sukawat, D., & Luadsong, A. (2017). Statistical downscaling for rainfall forecasts using modified constructed analog method in Thailand. The Scientific World Journal, 2017, Article 1075868. https://doi.org/10.1155/2017/1075868

Arnfield, A. (2003). Two decades of urban climate research: a review of turbulence, exchanges of energy and water, and the urban heat island. . *International journal of climatology, 23 (1), 1-26.*

Ashfaq, M., Shi, Y., Tung, W., T. R., Gao, X., Pal, J. S., & Diffenbaugh, N. S. (2009). Suppression of south Asian summer monsoon precipitation in the 21st century. *36(1)*.

Attavanich, W., Musumba, M., E. Mu, J., & Aisabokhae, R. (2011). Land Use and Climate Change.

Australian Broadcasting Corporation, A. (1997). *83 survivors of typhoon Linda rescued in Cambodia.* Retrieved from https://reliefweb.int/report/cambodia/83-survivors-typhoon-linda-rescued-cambodia

Avijit, G. (2022). *Larger Rivers: Geomorphology and Management.*

Baird, I. and Thorne, M. (2023). The downstream impacts of dams on the seasonally flooded riverine forests of the Mekong River in northeastern Cambodia. South East Asia Research, 377-399.

Bassim, K., Sammarco, P., & Snell, T. (2002). Effects of temperature on success of (self and non-self) fertilization and embryogenesis in Diploria strigosa (Cnidaria, Scleractinia). Marine Biology, 140, 479-488.

Bates, B.C., Z.W. Kundzewicz, S. Wu and J.P. Palutikof, Eds., (2008):: Climate Change and Water. Technical Paper of the Intergovernmental Panel on Climate Change, IPCC Secretariat, Geneva

Beck, H., Wood, E., Pan, M., Fisher, C., Miralles, D., Van Dijk, A., Adler, R. (2019). MSWep v2 Global 3-hourly 0.1° precipitation: Methodology and quantitative assessment. *Bull. Am. Meteorol. Soc.*, 100, 473–500. doi:https://doi.org/10.1175/BAMS-D-17-0138.1

Beckley, B.; Zelensky, N.P.; Holmes, S.A.; Lemoine, F.G.; Ray, R.D.; Mitchum, G.T.; Desai, S.; Brown, S.T. (2024). Integrated Multi-Mission Ocean Altimeter Data for Climate Research Version 5.2. Ver. 5.2. PO.DAAC, CA, USA. Retrieved from: https://doi.org/10.5067/ALTCY-TJA52.

Bell, T. L., et al. (2008). Midweek increase in U.S. summer rain and storm heights suggests air pollution invigorates rainstorms. *Journal of Geophysical Research, 113*, D02209. https://doi.org/10.1029/2007JD008623

Beniston, M., et al. (2018). The European mountain cryosphere: A review of its current state, trends, and future challenges. The Cryosphere, 12(2), 759–794. https://doi.org/10.5194/tc-12-759-2018

Bezuijen, M. R., Morgan, C., & Mather, R. (2011). A rapid vulnerability assessment of coastal habitats and selected species to climate risks in Chanthaburi and Trat (Thailand), Koh Kong and Kampot (Cambodia), and Kien Giang, Ben Tre, Soc Trang and Can Gio (Vietnam). IUCN.

Biskaborn, B. K., et al. (2019). Permafrost is warming at a global scale. Nature Communications, 10(1), 264. https://doi.org/10.1038/s41467-018-08240-

Boysen, L., Brovkin, V., Arora, V., Cadule, P., de Noblet-Ducoudré, N., Kato, E., Pongratz, J., & Gayler, V. (2014). Global and regional effects of land-use change on climate in 21st century simulations with interactive carbon cycle. *Earth Syst. Dynam., 5, 309–319, 2014*.

Brun, F., et al. (2017). A spatially resolved estimate of High Mountain Asia glacier mass balances, 2000–2016. Nature Geoscience, 10(9), 668–673.

Buckley, R. (2001). Environmental impacts. *In The encyclopedia of ecotourism*.

Bunleng, S. E., Nyda, C., Janalisa, H., Net, Y., Sebastian, K., Chandary, R., & Lutz, K. (2024). The Effects of Urban Heat Island in Phnom Penh: A Case Study of Khan Boeung Keng Kang and Khan Pou Senchey. *Cambodia Journal of Basic and Applied Research*, 6(1), 8-22.

Cai, Y., et al. (2019). Variations of lake ice phenology on the Tibetan Plateau from 2001 to 2017 based on MODIS data. Journal of Geophysical Research: Atmospheres, 124(2), 825–843. https://doi.org/10.1029/2018JD028993

Calculation of the Standardized Precipitation-Evapotranspiration. Link: https://cran.r-project.org/web/packages/SPEI/SPEI.pdf

Cao, B., et al. (2018). Thermal characteristics and recent changes of permafrost in the upper reaches of the Heihe River Basin, Western China. Journal of Geophysical Research: Atmospheres, 123(15), 7935–7949.

Cao, J. (2017). *The importance of aerosols in the earth system: science and engineering perspectives.*

Carrington, D. (2019). Climate crisis: 11,000 scientists warn of untold suffering. *The Guardian*, ISSN 0261-3077.

Chadwick, A. (2023). Shallow-water wave theory. Coastal Wiki. Flanders Marine Institute. Retrieved from https://www.coastalwiki.org/wiki/Shallow-water_wave_theory

Chadwick, D. S. (2011). *Manure management: Implications for greenhouse gas emissions.*

Chang. D., & Song. Y. (2010, March 01). Estimates of biomass burning emissions in tropical Asia based on. *Atmospheric Chemistry and Physics*, 2335–2351.

Chen, A., Ho, C. H., Chen, D., & Azorin-Molina, C. (2019). Tropical cyclone rainfall in the Mekong River Basin for 1983–2016. *Atmospheric Research*, 226, 66-75.

Cheeseman, J. M., Herendeen, L. B., Cheeseman, A. T., & Clough, B. F. (1997). Photosynthesis and photoprotection in mangroves under field conditions. Plant, Cell & Environment, 20(5), 579-588.

Chhin, R., Shwe, M., & Yoden, S. (2020). Time-lagged correlations associated with interannual variations of pre-monsoon and post-monsoon precipitation in Myanmar and the Indochina Peninsula. *Int. J. Climatol.*, 40, 3792–3812. doi:https://doi.org/10.1002/joc.6428

Chhinh, N., & Millington, A. (2015). Drought Monitoring for Rice Production in Cambodia. *Climate, 3*(4), 792-811. doi:https://doi.org/10.3390/cli3040792

Chim, K., Tunnicliffe, J., Shamseldin, A., & Chan, K. (2021). Identifying future climate change and drought detection using CanESM2 in the upper Siem Reap River, Cambodia. Dynamics of Atmospheres and Oceans, 94, Article 101182. https://doi.org/10.1016/j.dynatmoce.2021.101182

Chotamonsak, C., Salathé, E., Kreasuwan, J., Chantara, S., & Siriwitayakorn, K. (2011). Projected climate change over Southeast Asia simulated using a WRF regional climate model. *Atmos. Sci. Lett.*, 12, 213–219. doi:https://doi.org/10.1002/asl.313

Christiansen, H. H., et al. (2010). The thermal state of permafrost in the Nordic area during the International Polar Year 2007–2009. Permafrost and Periglacial Processes, 21(2), 156–181. https://doi.org/10.1002/ppp.687

Chu, D., Liu, L., & Wang, Z. (2023). Snow Cover on the Tibetan Plateau and Topographic Controls. *Remote Sensing*, *15*(16), 4044.

Climate-Data.org. (n.d.). Climate: Kampot. Climate-Data.org. Retrieved September 13, 2024, from https://en.climate-data.org/asia/cambodia/kampot/kampot-26390/

Climate Change Institute and University of Maine. (2024). Daily Sea Surface Temperature. Retrieved March 27, 2025, from https://climatereanalyzer.org/clim/sst_daily/?dm_id=world2.

Climate Engine, C. (2023). Desert Research Institute and University of California, Merced. Accessed on (7/9/2023). http://climateengine.org, version 2.1.

Clough, B., & Sim, R. G. (1989). Changes in gas exchange characteristics and water use efficiency of mangroves in response to salinity and vapour pressure deficit. Oecologia, 79, 38-44.

Cooney, C. M. (2012). Downscaling climate models: Sharpening the focus on local-level changes. Environmental Health Perspectives, 120(1), a22–a28. https://doi.org/10.1289/ehp.120-a22

Cosslett, T. L., Cosslett, P. D., Cosslett, T. I., & Cosslett, P. D. (2018). The lower Mekong basin: rice production, climate change, ENSO, and Mekong dams. *Sustainable Development of Rice and Water Resources in Mainland Southeast Asia and Mekong River Basin*, 85-114.

Dadashazar, H. P. (2021). Cloud drop number concentrations over the western North Atlantic Ocean: seasonal cycle, aerosol interrelationships, and other influential factors. *Atmospheric Chemistry and Physics*, 10499-10526.

Dai, A. (2001). Global precipitation and thunderstorm frequencies. Part II: Diurnal variations. *Journal of Climate, 14*(6), 1112-1128. doi: https://doi.org/10.1175/1520-0442(2001)014%3C1112:GPATFP%3E2.0.CO;2

Daniel T. C. Cox, I. M. (2020). Global variation in diurnal asymmetry in temperature, cloud cover, specific humidity and precipitation and its association with leaf area index. *Global Change Biology*, 7099-7111.

Das, S. (2022). *International Journal of Environment and Geoinformatics (IJEGEO), 9(1): 064-073. doi. 10.30897/ijegeo.938231*, 66.

Das, S. (2022). A Review of UHI formation over changing climate and its impacts on Urban Land . *International Journal of Environment and Geoinformatics (IJEGEO), 9(1): 064-073. doi. 10.30897/ijegeo.938231*, 66.

Das, S. (2022). A Review of UHI formation over changing climate and its impacts on Urban Land Use and Environments. *International Journal of Environment and Geoinformatics (IJEGEO), 9(1): 064-073. doi. 10.30897/ijegeo.938231*, 66.

Das, S. (2022). A Review of UHI formation over changing climate and its impacts on Urban Land Use and Environments and Adaptation Measures. *International Journal of Environment and Geoinformatics (IJEGEO), 9(1): 064-073. doi. 10.30897/ijegeo.938231*, 65-66.

Da Silva, N. A. J. (2021). Impact of the Madden–Julian Oscillation on extreme precipitation over the western Maritime Continent and Southeast Asia. *Quarterly Journal of the Royal Meteorological Society*, 3434-3453.

Deems, J. S., et al. (2013). Combined impacts of current and future dust deposition and regional warming on Colorado River Basin snow dynamics and hydrology. Hydrology and Earth System Sciences, 17(11), 4401–4413. https://doi.org/10.5194/hess-17-4401-2013

Dehecq, A., et al. (2019). Twenty-first century glacier slowdown driven by mass loss in High Mountain Asia. Nature Geoscience, 12, 22–27.

Deutsche Welle, D. (2013). *Asian storm claims dozens. https://www.dw.com/en/deadly-storm-sweeps-vietnam-cambodia/a-17128997.*

Diehl, K., Simmel, M., & Wurzler, S. (2007). Effects of drop freezing on microphysics of an ascending cloud parcel under biomass burning conditions. *Atmospheric Environment, 41*(2), 303-314.

Dieye, A. (2016). *Land Cover Land Use Change and Soil Organic Carbon Under Climate Variability in the Semi-Arid West African Sahel (1960-2050).* South Dakota State University.

Ding, Y., Chang, S., & Cheng, R. (2020). Cryospheric hydrology: Decode the largest freshwater reservoir on earth. Bulletin of the Chinese Academy of Sciences, 4, 414–424. (in Chinese).

Du, J., et al. (2017). Satellite microwave assessment of Northern Hemisphere lake ice phenology from 2002 to 2015. The Cryosphere, 11(1), 47–63. https://doi.org/10.5194/tc-11-47-2017

Duong, S., Song, L., & Chhin, R. (2023). Precipitation Projection in Cambodia Using Statistically Downscaled CMIP6 Models. *Climate*, 11, no. 12: 245.

Douville, H., K. Raghavan, J. Renwick, R.P. Allan, P.A. Arias, M. Barlow, R. Cerezo-Mota, A. Cherchi, T.Y. Gan, J. Gergis, D. Jiang, A. Khan, W. Pokam Mba, D. Rosenfeld, J. Tierney, and O. Zolina,. (2021). Water Cycle Changes. In Climate Change 2021: The Physical Science Basis. Contribution of Working Group I to the Sixth Assessment Report of the Intergovernmental Panel on Climate Change (pp. 1055-1210). Cambridge: Cambridge University Press

EEA. (2024, November 20). *European Environmental Agency*. Retrieved from European Environmental Agency: https://www.eea.europa.eu/en/topics/in-depth/air-pollution/eow-it-affects-our-health

Ellison, J. C., & Stoddart, D. R. (1991). Mangrove ecosystem collapse during predicted sea-level rise: Holocene analogues and implications. Journal of Coastal research, 151-165.

European Commission, E. (2023). *INFORM Index for Risk Management. Cambodia Country Profile.* Retrieved from https://drmkc.jrc.ec.europa.eu/inform-index/INFORM-Risk/Country-Risk-Profile

Eyring, V., Bony, S., Meehl, G., Senior, C., Stevens, B., Stouffer, R., & Taylor, K. (2016). Overview of the Coupled Model Inter-comparison Project Phase 6 (CMIP6) experimental design and organization. *Geosci. Model Dev.*, 9, 1937–1958. doi:https://doi.org/10.5194/gmd-9-1937-2016

Fabian, P. S., Kwon, H. H., Vithanage, M., & Lee, J. H. (2023). Modeling, challenges, and strategies for understanding impacts of climate extremes (droughts and floods) on water quality in Asia: A review. *Environmental Research*, 225(February), 115617. https://doi.org/10.1016/j.envres.2023.115617.

Fabricius, K. E., Golbuu, Y., & Victor, S. (2007). Selective mortality in coastal reef organisms from an acute sedimentation event. *Coral Reefs*, *26*(1), 69-69.

FAO. (2010). *Global forest resources assessment 2010.* Phnom Penh, Cambodia: FAO, Rome.

Feng Chen, W. M. (2023). Southeast Asian ecological dependency on Tibetan Plateau streamflow over the last millennium. *Nature Geoscience*, 1151-1158.

Fisheries Administration (FiA). (2023). Seagrass and Coral Reef distribution and monitoring in Cambodia. Phnom Penh, Cambodia.

FloodList. (2013). *39 Dead in Cambodia Floods. https://floodlist.com/asia/39-dead-cambodia-floods.*

Flower, B., & Fortnam, M. (2015). *Urbanising disaster risk: vulnerability of the urban poor in Cambodia to flooding and other hazards. People in Need, Phnom Penh, Cambodia.*

Food and Agriculture Organization, F. (2018). *The State of Food Security and Nutrition in the World.*

Fowler, H. J., Blenkinsop, S., & Tebaldi, C. (2007). Linking climate change modelling to impacts studies: Recent advances in downscaling techniques for hydrological modelling. International Journal of Climatology, 27(12), 1547–1578. https://doi.org/10.1002/joc.1556

Fox-Kemper, B., H. T. Hewitt, C. Xiao, G. Aðalgeirsdóttir, S. S. Drijfhout, T. L. Edwards, N. R. Golledge, M. Hemer, R. E. Kopp, G. Krinner, A. Mix, D. Notz, S. Nowicki, I. S. Nurhati, L. Ruiz, J-B. Sallée, A. B. A. Slangen, Y. Yu. (2021). Ocean, Cryosphere and Sea Level Change. In: Climate Change 2021: The Physical Science Basis. Contribution of Working Group I to the Sixth Assessment Report of the Intergovernmental Panel on Climate Change [Masson-Delmotte, V., P. Zhai, A. Pirani, S. L. Connors, C. Péan, S. Berger, N. Caud, Y. Chen, L. Goldfarb, M. I. Gomis, M. Huang, K. Leitzell, E. Lonnoy, J. B. R. Matthews, T. K. Maycock, T. Waterfield, O. Yelekçi, R. Yu and B. Zhou (eds.)]. Cambridge University Press. In press.

Gao, Y., et al. (2018). Does elevation-dependent warming hold true above 5000 m elevation? Lessons from the Tibetan Plateau. *npj Climate and Atmospheric Science, 1*(19). https://doi.org/10.1038/s41612-018-0030-z

Gebre, S., Boissy, T., & Alfredsen, K. (2014). Sensitivity of lake ice regimes to climate change in the Nordic region. The Cryosphere, 8(4), 1589–1605. https://doi.org/10.5194/tc-8-1589-2014

Gen Li, C. G. (2021). Inter-annual variability of spring precipitation over the Indo-China Peninsula and its asymmetric relationship with El Niño-Southern Oscillation. *Climate Dynamics*.

Glover, P. B. (2004). *Southeast Asia: From Prehistory to History (1st ed.).* London: Routledge. https://doi.org/10.4324/9781003416609.

Gou, P., et al. (2017). Lake ice phenology of Nam Co, Central Tibetan Plateau, China, derived from multiple MODIS data products. Journal of Great Lakes Research, 43(6), 989–998. https://doi.org/10.1016/j.jglr.2017.08.011

Gudmundsson, L., Boulange, J., Do, H. X., Gosling, S. N., Grillakis, M. G., Koutroulis, A. G., Leonard, M., Liu, J., Schmied, H. M., Papadimitriou, L., & Pokhrel, Y. (2021). Globally observed trends in mean and extreme river flow attributed to climate change. Science, 371(6534), 1159–1162.

Halperin, J. and Turner, L. (2013). *Forest Degradation in Cambodia: An Assessment of Monitoring Options in the Central Cardamom Protected Forest.* Phnom Penh, Cambodia.

Hanieh Saeedi, D. W. (2022). The Environmental Drivers of Benthic Fauna Diversity and Community Composition. *Marine Evolutionary Biology, Biogeography and Species Diversity*.

Hao, Z., Singh, V. P., & Hao, F. (2018). Compound extremes in hydroclimatology: A review. *Water, 10*(6), Article 718. https://doi.org/10.3390/w10060718

Hartmann, D. L., et al. (2013). Observations: Atmosphere and surface. In T. F. Stocker, D. Qin, G.-K. Plattner, M. Tignor, S. K. Allen, J. Boschung, A. Nauels, Y. Xia, V. Bex, & P. M. Midgley (Eds.), Climate change 2013: The physical science basis. Contribution of Working Group I to the Fifth Assessment Report of the Intergovernmental Panel on Climate Change (pp. 159–254). Cambridge University Press.

Hartmann, H., & Andresky, L. (2013). Flooding in the Indus River basin: A spatiotemporal analysis of precipitation records. Global and Planetary Change, 107, 25–35. https://doi.org/10.1016/j.gloplacha.2013.04.002

Hasselmann, K., Barnett, T. P., Bouws, E., Carlson, H., Cartwright, D. E., Enke, K., ... & Walden, H. (1973). Measurements of wind-wave growth and swell decay during the Joint North Sea Wave Project (JONSWAP). Deutsche Hydrographische Zeitschrift, Ergänzungsheft, Reihe A, Nr. 12, 1-95.

Haszpra, M. H. (2020). Investigating ENSO and its teleconnections under climate change in an ensemble view – a new perspective. *Earth System Dynamics*.

Hersbach, H., Bell, B., Berrisford, P., Biavati, G., Horányi, A., Muñoz Sabater, J., & ... & Thépaut, J. N. (2023). ERA5 hourly data on single levels from 1940 to present. *Copernicus Climate Change Service (C3S) Climate Data Store (CDS).*

HKO, H. K. (1998). *Tropical Cyclones in 1997.*

Ho, T. N., Wang, S. Y., & Yoon, J. H. (2024). Trends and variations of tropical cyclone precipitation contributions in the Indochina Peninsula. *Theoretical and Applied Climatology*, 155(8), 7433-7445.

Hock, R., et al. (2019). GlacierMIP: A model intercomparison of global-scale glacier mass-balance models and projections. *Journal of Glaciology, 65*(251), 453–467. https://doi.org/10.1017/jog.2019.22

Hoegh-Guldberg, H., & Hoegh-Guldberg, O. (2004). Implications of Climate Change for Australia's Great Barrier Reef. WWF Australia and Queensland Tourism Industry Council.

Hoegh-Guldberg, O., Mumby, P. J., Hooten, A. J., Steneck, R. S., Greenfield, P., Gomez, E., & Hatziolos, M. (2007). Coral reefs under rapid climate change and ocean acidification. *science*, *318*(5857), 1737-1742.

Honda, K., Nakamura, Y., Nakaoka, M., Uy, W. H., & Fortes, M. D. (2013). Habitat use by fishes in coral reefs, seagrass beds and mangrove habitats in the Philippines. *Plos one*, *8*(8), e65735.

Huang, W., Park, E., Wang, J., & Sophal, T. (2024). The changing rainfall patterns drive the growing flood occurrence in Phnom Penh, Cambodia. *Journal of Hydrology: Regional Studies, 55*, 101945. doi:https://doi.org/10.1016/j.ejrh.2024.101945

Hue Nguyen Thanh, T. N.-D. (2023). The distinct impacts of the two types of ENSO on rainfall variability over Southeast Asia. *Climate Dynamics*.

Humanitarian Response Forum. (2020). *Floods Response Plan Cambodia. Issued 4.*

Humanitarian Response Forum. (2024). *Floods in Cambodia-Situation Report (SitRep) No. 2.*

IFRC. (2002). *Cambodia floods 2000.* https://www.ifrc.org/docs/appeals/00/220000FR.pdf.

Ioannis. M, E. S. (2020). *Environmental and Health Impacts of Air Pollution: A Review.* doi:10.3389/fpubh.2020.00014

IPCC. (2014). Climate change 2013: The physical science basis. Contribution of Working Group I to the Fifth Assessment Report of the Intergovernmental Panel on Climate Change. Cambridge University Press.

IPCC. (2018). *Summary for policymakers*. In V. Masson-Delmotte, P. Zhai, H. Pörtner, D. Roberts, J. Skea, P. Shukla, A. Pirani, W. Moufouma-Okia, C. Péan, R. Pidcock, S. Connors, J. B. R. Matthews, Y. Chen, X. Zhou, M. I. Gomis, E. Lonnoy, M. Tignor, & T. Waterfield (Eds.), *Global warming of 1.5°C: An IPCC special report on the impacts of global warming of 1.5°C above pre-industrial levels and related global greenhouse gas emission pathways in the context of strengthening the global response to the threat of climate change, sustainable development, and efforts to eradicate poverty* (pp. 1-32). World Meteorological Organization.

IPCC. (2019). The Ocean and Cryosphere in a Changing Climate: A Special Report of the Intergovernmental Panel on Climate Change (Figure 2.2). In H.-O. Pörtner, D. C. Roberts, V. Masson-Delmotte, et al. (Eds.). Cambridge University Press. https://www.ipcc.ch/srocc/

IPCC. (2021). Climate Change 2021: The Physical Science Basis. Contribution of Working Group I to the Sixth Assessment Report of the Intergovernmental Panel on Climate Change. *Cambridge University Press, Cambridge, United Kingdom and New York, NY, USA, In press*. doi:doi:10.1017/9781009157896

IPCC. (2022). Chapter 3: Oceans and coastal ecosystems and their services. In Climate change 2022: Impacts, adaptation and vulnerability.

IPCC. (2022b). Climate Change 2022: Impacts, Adaptation and Vulnerability. Sixth Assessment Report of IPCC.

Ishaq Ali Shah, H. K.-A. (2024). Evaluation of climate change impact on plants and hydrology. *Frontiers in Environmental Science*.

IUCN. (2013). The Mangroves of Cambodia: An Overview of Cambodia's Mangrove Forests and Conservation Initiatives. Phnom Penh, Cambodia.

Izquierdo, J. B. (2010). *Assessment of land use, forest policy and.* FAO, Regional Office for Asia and the Pacific Country Representation, Cambodia.

James, R. K., Lynch, A., Herman, P. M., Van Katwijk, M. M., Van Tussenbroek, B. I., Dijkstra, H. A., ... & Bouma, T. J. (2021). Tropical biogeomorphic seagrass landscapes for coastal protection: Persistence and wave attenuation during major storms events.

Jeffry, L. O. (2021). *Greenhouse gases utilization.*

JICA. (2010). *The study on national integrated strategy of coastal area and master plan of Sihanouk-ville for sustainable development: Final report (Book II)*

JICA. (2015). *Country Report Cambodia: Natural Disaster Risk Assessment and Area Business Continuity Plan Formulation for Industrial Agglomerated Areas in the ASEAN Region; Japan International Cooperation Agency: Tokyo, Japan.*

Johnson, J. E., & Marshall, P. A. (2007). The Great Barrier Reef and climate change: vulnerability and management implications.

Jorge Alvar-Beltrán, R. S. (2022). Climate Change Impacts on Irrigated Crops in Cambodia. *Agricultural and Forest Meteorology*, 324, 109105.

José López, D. A. (2021). Systemic effects of rising atmospheric vapor pressure deficit on plant physiology and productivity. *Global Change Biology*.

Jung, C., & Schindler, D. (2018). On the inter-annual variability of wind energy generation–A case study from Germany. *Applied Energy*, 230, 845-854.

Jung, C., & Schindler, D. (2020). Integration of small-scale surface properties in a new high resolution global wind speed model. *Energy Conversion and Management*, 210, 112733.

Kaloustian, N., & Diab, Y. (2015). Effects of urbanization on the urban heat island in Beirut. *Urban Climate, 14*, 154–165. doi:https://doi.org/10.1016/j.uclim.2015.06.004

Kalsher, M. J. (1998). Hazard level perceptions of warning components and configurations. *International Journal of Cognitive Ergonomics*, 2(1-2), 123-143.

Kautz, L. (2021). Atmospheric blocking and weather extremes over the Euro-Atlantic sector–a review. *Weather and Climate Dynamics Discussions*, 1-43.

Keir Chapman. (2024, May 22). *Earth Site Education*. Retrieved from https://www.earth-site.co.uk/Education/terrain-and-topography-of-cambodia-mountains-valleys-and-plains/

Khain, A., Rosenfeld, D., & Pokrovsky, A. (2005). Aerosol impact on the dynamics and microphysics of deep convective clouds. *Quarterly Journal of the Royal Meteorological Society, 131*(611), 2639-2663.

Khmer Times (2024). *Cambodia pursues passive cooling strategies in buildings*. Retrieved from https://www.khmertimeskh.com/501554215/cambodia-pursues-passive-cooling-strategies-in-buildings/

Khorsro Morovati, F. T. (2023). Contributions from Climate Variation and Human Activities to Flow Regime Change of Tonle Sap Lake from 2001-2020. *Hydrology*, 128800.

Kingsford, M. J., & Welch, D. J. (2007). Vulnerability of pelagic systems of the Great Barrier Reef to climate change.

Klein, R. J., Nicholls, R. J., & Mimura, N. (1999). Coastal adaptation to climate change: can the IPCC Technical Guidelines be applied?. Mitigation and adaptation strategies for global change, 4, 239-252.

Koren, I., Kaufman, Y. J., Remer, L. A., & Martins, J. V. (2004). Measurement of the effect of Amazon smoke on inhibition of cloud formation. *Science, 303*(5662), 1342-1345.

Kosal Chim, J. T. (2021). Identifying future climate change and drought detection using CanESM2 in the upper Siem Reap River, Cambodia. *Dynamics of Atmospheres and Oceans*.

Kropáček, J., Maussion, F., Chen, F., Hoerz, S., & Hochschild, V. (2013). Analysis of ice phenology of lakes on the Tibetan Plateau from MODIS data. *The Cryosphere*, 7(1), 287-301.

Kuang, X., & Jiao, J. J. (2016). Review on climate change on the Tibetan Plateau during the last half century. *Journal of Geophysical Research: Atmospheres, 121*(8), 3979–4007. https://doi.org/10.1002/2015JD024728

LaDochy, S., & Witiw, M. (2023). Thunderstorms and Thunderstorm-Associated Severe Weather. In Fire and Rain: California's Changing Weather and Climate. *Cham: Springer Nature Switzerland*, pp. 143-162. doi:https://doi.org/10.1007/978-3-031-32273-0_10

Lay, S. & Neang, P. (2021, November 21). Urbanization in Cambodia: Development and disparity. *Cambodian Education Forum*.

Lee, K., Kim, H. S., & Choi, Y. S. (2019). Effects of high-resolution geostationary satellite imagery on the predictability of tropical thunderstorms over Southeast Asia. Natural Hazards and Earth System Sciences. *19*(10), 2241-2248. doi:https://doi.org/10.519

Lee, S., & Sambath, T. (2006). Landslide susceptibility mapping in the Damrei Romel area, Cambodia using frequency ratio and logistic regression models. *Environmental Geology, 50*, 847-855. doi:https://doi.org/10.1007/s00254-006-0256-7

Leng, H. (2014). *Country report of Cambodia disaster management* .

Li, J., Zhang, R., Ling, Z., Bo, W., & Liu, Y. (2014). Effects of Cardamom Mountains on the formation of the winter warm pool in the Gulf of Thailand. Continental Shelf Research, 91, 211-219. https://doi.org/10.1016/j.csr.2014.08.013

Licheng Wang, X. G. (2022). Phase Shifts of the PDO and AMO Alter the Translation Distance of Global Tropical Cyclones. *Earth's Future*.

Limsakul, A., Limjirakan, S., & Sriburi, T. (2010). Observed Changes in Daily Rainfall Extreme Along Thailand's Coastal Zones. Applied Environmental Research, 32(1), 49-68

Lorn, S. K. (2022). Health impact assessment from rice straw production in Cambodia. *Applied Sciences*, 12(20), 10276.

Lovelock, C. E., & Ellison, J. (2007). Vulnerability of mangroves and tidal wetlands of the Great Barrier Reef to climate change.

MAFF. (2016). *Climate change priorities action plan for agriculture, forestry, and fisheries sector 2016-2020. Technical Working Group for Policy and Strategy to Respond to Climate Change of the Ministry of Agriculture, Forestry and Fisheries (TWG-CCAFF).*

Mak, S. (2021). Downstream State and Water Security in the Mekong Region. *Water*.

Mangroves for the Future. (2013). Cambodia National Strategy and Action Plan 2014-2016.

Mantua, N.J. 1999: The Pacific Decadal Oscillation. A brief overview for non-specialists, Encyclopedia of Environmental Change.

Marko, K., Zulkarnain, F., and Kusratmoko, E. (2016). Coupling of Markov chains and cellular automata spatial models to predict land cover changes (case study: upper CiLeungsi catchment area). *IOP Conf. Ser.: Earth Environ. Sci., 47, 012032*.

Martin, F. (2021). Madden-Julian Oscillation (MJO). Retrieved on 14 January 2025 from NOAA climate.gov: https://www.climate.gov/media/13488.

Marvin, M. R. (2023). Uncertainties from biomass burning aerosols in air quality models obscure public health impacts in Southeast Asia. *EGUsphere*, 1-23.

Matsumoto, J. (1997). Seasonal transition of summer rainy season over indo-china and adjacent monsoon region. *Adv. Atmos. Sci.*, 14, 231–245. doi:https://doi.org/10.1007/s00376-997-0022-0

Maxwell, A. (2004). Fire regimes in north-eastern Cambodian monsoonal forests, with a 9300-year sediment charcoal record. *Journal of Biogeography*, pages 225–239.

Maurer, E. P. and Hidalgo, H. G., 2008: Utility of daily vs. monthly large-scale climate data: an intercomparison of two statistical downscaling methods, Hydrology and Earth System Sciences,12, 551-563.

McCarl, B., Attavanich, W., Musumba, M., E. Mu, J., & Aisabokhae, R. (2011). Land Use and Climate Change.

McField, M. (2017). Impacts of climate change on coral in the coastal and marine environments of Caribbean Small Island Developing States (SIDS). Caribbean marine climate change report card: Science Review, 2017, 52-59.

McKee, T. B., Doesken, N. J., & Kleist, J. (1993). The relationship of drought frequency and duration to time scales. In Proceedings of the 8th Conference on Applied Climatology (Vol. 17, No. 22, pp. 179-183). Link: https://climate.colostate.edu/pdfs/relationshipofdroughtfrequency.pdf

McMurry, P. H. (2000). *A review of atmospheric aerosol measurements.*

McVicar, T. R., Roderick, M. L., Donohue, R. J., Li, L. T., Van Niel, T. G., Thomas, A., & ..... Dinpashoh, Y. (2012). Global review and synthesis of trends in observed terrestrial near-surface wind speeds: Implications for evaporation. *Journal of Hydrology*, 416, 182-205.

MEF, & GSSD. (2019). *Addressing climate change impacts on economic growth in Cambodia. https://ncsd.moe.gov.kh/resources/document/addressing-climate-change-impacts-economic-growth.*

Mekong River Commission. (2012). *Working Paper 2011–2015: The Impact & Management of Floods & Droughts in the Lower Mekong Basin & the Implications of Possible Climate Change. Mekong River Commission, Vientiane, Lao PDR.*

Mekong River Commission. (n.d.). *Climate Change*. Retrieved from https://www.mrcmekong.org/climate-change/
Mey, S. Y. (2024). Assessment of updalnd forest in Mondulkiri. ICERD, 20-70.
MFF (2013). National Situation Analysis: Cambodia. Mangroves for the Future, Phnom Penh, Cambodia.
Milly, P. C. D., Dunne, K. A., & Vecchia, A. V. (2005). Global pattern of trends in streamflow and water availability in a changing climate. *Nature, 438*(7066), 347–350. https://doi.org/10.1038/nature04312
MIME. (2004). *Drinking water quality standards*. Phnom Penh, Cambodia.
Mishra, A.K., Singh, V.P. & Desai, V.R. (2009). Drought characterization: a probabilistic approach. Stoch Environ Res Risk Assess 23, 41–55. https://doi.org/10.1007/s00477-007-0194-2
MoE. (1999). Cambodian national wetland action plan for Kingdom of Cambodia 1999-2003. Funded by Wetlands International-Lower Mekong River Program.
MoE. (2005). *State of the coastal environment and socio-economy in Cambodia*. Phnom Penh, Cambodia
MoE. (2007). Coastal environmental management action plan 2007-2011. National Coastal Steering Committee.
MoE. (2015). Second national communication to the United Nations Framework Convention on Climate Change. UNFCCC.
MoE. (2018). Peam Krasop Wildlife Sanctuary Management Plan (2018-2022). Koh Kong.
MoE. (2019). *National GHG Emission Inventory Report.* Phnom Penh, Cambodia: Ministry of Environment.
MoE. (2019). *National GHG Emissions Inventory Report: Prepare for submission to GSSD.* Phnom Penh, Cambodia: GDANCP.
MoE. (2020). *Cambodia Forest Cover 2018.* Phnom Penh, Cambodia: Ministry of Environment.
MoE. (2021). *Clean Air Plan of Cambodia.* Phnom Penh, Cambodia: Ministry of Environment.
MoE. (2021). *Clean Air Plan of Cambodia.*
MoE. (2022). Third national communication to the United Nations Framework Convention on Climate Change. UNFCCC.
MoE. (2024). Cambodia's Initial Biennial Transparency Report (BTR1).
Molina, M. J., & Molina, L. T. (2004). Megacities and At
mospheric Pollution. *Journal of the Air & Waste Management Association*, 54(6), 644–680. doi:http://doi.org/10.1080/10473289.2004.10470936
Monin, N. (2021). *The Impacts of Climate Change on Agriculture and Water Resources in Cambodia: From Local Communities' Perspectives.* Phnom Penh, Cambodia: CDRI(Cambodia Development Resource Institute).
MoP. (2023). *Population Projection 2020-2033.* Phnom Penh: RGC.
MoP. (2023). *Population Projection 2020-2033 Based on Age Restructure of National Population Projection 2019-2050 and CDHS 2021-22.* Phnom Penh, Cambodia: National Institute of Statistics, Ministry of Planning.
MoWRAM. (2009). Country Assessment Report for Cambodia of the Ministry of Water Resources and Meteorology. Phnom Penh, Cambodia.
MRC. (2018). *Annual Mekong Hydrology, Flood, and Drought Report 2018.* Mekong River Commission.
MRC. (2023). *Climate Change*. Retrieved from https://www.mrcmekong.org/climate-change/

Munday, P. L., Jones, G. P., Pratchett, M. S., & Williams, A. J. (2008). Climate change and the future for coral reef fishes. Fish and Fisheries, 9(3), 261-285.

Munday, P. L., Jones, G. P., Sheaves, M., Williams, A. J., & Goby, G. (2007). Vulnerability of fishes of the Great Barrier Reef to climate change.

Mushtaq, Z. S. (2022). *Aerosol Science and Engineering.*

NAPA. (2016). *NAPA 2006.*

National Aeronautics and Space Administration. (n.d.). IPCC AR6 sea level projection tool. NASA Sea Level Change Portal. Retrieved September 12, 2024, from https://sealevel.nasa.gov/ipcc-ar6-sea-level-projection-tool?lat=10&lon=103&data_layer=scenario&boxinfo=true

National Council for Sustainable Development (NCSD), Ministry of Environment. (2019). *Working paper*. Kingdom of Cambodia. Nation Religion King.

National Council for Sustainable Development (2020). "First Biennial Update Report of Cambodia to the United Nations Framework Convention On Climate Change". Retrieved from https://unfccc.int/sites/default/files/resource/FBUR_Cambodia.pdf

Natural Resources Canada. (2008). *Bow River Basin*. http://www.nrcan.gc.ca/earth-sciences/products-services/mapping-product/geoscape/waterscape/bow-river-basin/60

NBC News, N. (2009). *Tropical storm death toll in Vietnam now 99. https://www.nbcnews.com/id/wbna33600749.*

Nepal, S. (2016). Impacts of climate change on the hydrological regime of the Koshi River basin in the Himalayan region. *Journal of Hydro-Environment Research, 10*, 76–89. https://doi.org/10.1016/j.jher.2015.12.001

NRDC (Natural Resource Defense Council). (2024). Sea Level Rise 101: The causes and effects of this undeniable consequence of climate change—and how communities can respond. Retrieved on November 15, 2024 from website: https://www.nrdc.org/stories/sea-level-rise-101#effects.

ODC. (2019, October 09). *Open Development Cambodia*. Retrieved from https://data.opendevelopmentcambodia.net/dataset/geographical-relief-of-cambodia

Oeurng, C., Cochrane, T., Chung, S., Kondolf, M., Piman, T., & Arias, M. (2019). Assessing climate change impacts on river flows in the Tonle Sap Lake Basin, Cambodia. *Water* , 11, 618. doi:https://doi.org/10.3390/w11030618

Oke, T. R. (1973). City size and the urban heat island. . *Atmospheric Environment, 7 (8), 769-779.*

Oke, T.R. and Maxwell, G.B. (1975). Urban heat island dynamics in Montreal and Vancouver. *Atmospheric Environment, 9 (2), 191-200.*

O'Rourke, J. (2023). Venus, the planet: introduction to the evolution of Earth's sister planet. *Space Science Reviews*

Oudry, G., Pak, K., & Chea, C. (2016). Assessing vulnerabilities and responses to environmental changes in Cambodia. *International Organization for Migration, Phnom Penh.*

Palazzi, E., von Hardenberg, J., & Provenzale, A. (2013). Precipitation in the Hindu-Kush Karakoram Himalaya: Observations and future scenarios. Journal of Geophysical Research: Atmospheres, 118(1), 85–100. https://doi.org/10.1029/2012JD018697

Panday, P. K., Thibeault, J., & Frey, K. E. (2015). Changing temperature and precipitation extremes in the Hindu Kush-Himalayan region: An analysis of CMIP3 and CMIP5

simulations and projections. International Journal of Climatology, 35(10), 3058–3077. https://doi.org/10.1002/joc.4192

Partnerships in Environmental Management for the Seas of East Asia (PEMSEA). (2023). *IRBM stories - Kampong Bay River Basin: The lifeline of Kampot Province*.

Patnaik, M. M. (2021). Vulnerability of marine fisheries to sea surface temperature and cyclonic events: Evidences across coastal India. *ScienceDirect*.

PEMSEA, & Ministry of Environment (Cambodia). (2019). *National state of oceans and coasts 2018: Blue economy growth of Cambodia*. Partnerships in Environmental Management for the Seas of East Asia (PEMSEA), Quezon City, Philippines.

Pen, S., Rad, S., Ban, L., Brang, S., Nuth, P., & Liao, L. (2024). An Analysis of Extreme Rainfall Events in Cambodia. Atmosphere, 15(8), 1017.

Phan, K., Chek, S., Eav, C., Sieng, H., & Kim, K. W. (2021). Assessing salinization and water quality in Koh Kong Coastal areas of Cambodia: potential impacts of climate change. *Water, Air, & Soil Pollution*, *232*(12), 510.

Phillips, M., Mutter, E. Z., Kern-Luetschg, M., & Lehning, M. (2009). Rapid degradation of ground ice in a ventilated talus slope: Flüela Pass, Swiss Alps. Permafrost and Periglacial Processes, 20(1), 1–14. https://doi.org/10.1002/ppp.638

Phnom Penh Post. (2020). *Ministry says La Nina will bring heavy rain, flooding*. Retrieved from https://www.phnompenhpost.com/national/ministry-says-la-nina-will-bring-heavy-rain-flooding

Phy, S. R., Sok, T., Try, S., Chan, R., Uk, S., Hen, C., & Oeurng, C. (2022). Flood hazard and management in Cambodia: A review of activities, knowledge gaps, and research direction. *Climate, 10*(11), 162. doi:https://www.mdpi.com/2225-1154/10/11/162

Phys Org. (2024, March). *Cambodia's famed Kampot pepper withers in scorching heat wave*. Retrieved from https://phys.org/news/2024-05-cambodia-famed-kampot-pepper-withers.html

Pitman, A. J.-D.-P. (2012). Effects of land cover change on temperature and rainfall extremes in multi-model ensemble simulations. *Earth System Dynamics*, 3(2), 213–231. doi:http://doi.org/10.5194/esd-3-213-2012

Pornampai Narenpitak, S. K. (2024). *Regional impacts of solar radiation modification on surface temperature and precipitation in Mainland Southeast Asia and the adjacent oceans.* Scientific Reports.

Ratanak, N., & Dong, H. (2018). Public Knowledge, Concern and Engagement of Climate Change in Cambodia-A Perspective of Residents in Phnom Penh. Phnom Penh, Cambodia

RCRC. (2014). *Cambodia Disaster Management Reference Handbook.* Retrieved from https://www.rcrc-resilience-southeastasia.org/wp-content/uploads/2017/12/2014_disaster_management_reference_handbook_cambodia.pdf

Regional Integrated Multi-Hazard Early Warning System, R. (2011). Regional Integrated Multi-Hazard Early Warning System (RIMES). Managing Climate Change Risks for Food Security in Cambodia.

Reliefweb. (1997). Typhoon Linda - Nov 1997. https://reliefweb.int/disaster/st-1997-000267-vnm#overview.

Reliefweb. (2013). 25 Sep 2013: SE ASIA – Floods and Severe Weather. https://reliefweb.int/map/china/25-sep-2013-se-asia-%E2%80%93-floods-and-severe-weather.

Reliefweb. (2013). Typhoon Usagi - Sep 2013. https://reliefweb.int/disaster/tc-2013-000120-phl.

Reliefweb. (2020). Typhoon Molave - Oct 2020. https://reliefweb.int/disaster/fl-2020-000211-vnm.

Reliefweb. (2022). Cambodia, Flooding, Landslide, Storms, and Wind in Northern Province (TC NORU) (29 Sep 2022). https://reliefweb.int/report/cambodia/cambodia-flooding-landslide-storms-and-wind-northern-province-tc-noru-29-sep-2022.

Reliefweb. (2023). *Cambodia, Flooding and Landslides in Pursat (27 Sep 2023)*. Retrieved from https://reliefweb.int/report/cambodia/cambodia-flooding-and-landslides-pursat-27-sep-2023

Revi, A. D.-D.-M. (2014). Urban areas. In *Climate Change 2014: Impacts, Adaptation, and Vulnerability. Part A: Global and Sectoral Aspects.* Contribution of Working Group II to the Fifth Assessment Report of the Intergovernmental Panel on Climate Change.

RGC. (2023). Pentagon Strategy-Phase I: Growth, Employment, Equity, Efficiency and Sustainability: Building the Foundation Towards Realizing the Cambodia Vision 2050. The Royal Government of the Seventh Legislature of the National Assembly. Phnom Penh, August 2023

Rohrer, M., Salzmann, N., Stoffel, M., & Kulkarni, A. V. (2013). Missing (in-situ) snow cover data hampers climate change and runoff studies in the Greater Himalayas. Science of the Total Environment, 468–469, S60–70. https://doi.org/10.1016/j.scitotenv.2013.09.056

Ros, B., Nang, P., & Chhim, C. (2021). *Agricultural Development and Climate Change: The Case of Cambodia (Vol. 65). Phnom Penh: CDRI.*

Rosenfeld, D. (2006). Aerosol–cloud interactions control of earth radiation and latent heat release budgets. Space Science Reviews, 125(1-4), 149-157. https://doi.org/10.1007/s11214-006-9053-6

Rosenfeld, D., Andreae, M. O., Asmi, A., Chin, M., de Leeuw, G., Donovan, D. P., ... & Quaas, J. (2014). Global observations of aerosol-cloud-precipitation-climate interactions. *Reviews of Geophysics*, *52*(4), 750-808.

Rosenfeld, D., et al. (2007). Inverse relations between amounts of air pollution and orographic precipitation. *Science, 315*(5817), 1396-1398.

Royal Government of Cambodia, R. (2010). *Cambodia–Post Ketsana Disaster Needs Assessment; National Committee for Disaster Management: Phnom Penh, Cambodia.*

Sanjay, J., et al. (2017). Downscaled climate change projections for the Hindu Kush Himalayan region using CORDEX South Asia regional climate models. Advances in Climate Change Research, 8(3), 185–198.

Santamouris, M. (2014). On the energy impact of urban heat island and global warming on buildings. *Energy and buildings*, 82, 100-113.

Sapana Lohani, T. E. (2020). Rapidly Accelerating Deforestation in Cambodia's Mekong River Basin: A Comparative Analysis of Spatial Patterns and Drivers. *Water*.

Schaffelke, B., Mellors, J., & Duke, N. C. (2005). Water quality in the Great Barrier Reef region: responses of mangrove, seagrass and macroalgal communities. *Marine pollution bulletin*, *51*(1-4), 279-296.

Schefczyk, L., & Heinemann, G. (2017). Climate change impact on Thunderstorms: Analysis of thunderstorm indices using high resolution COSMO-CLM simulations. Met. Z,. *Meteorologische Zeitschrift, 26*. doi:https://doi.org/10.1127/metz/2017/0749

SeaTemperature.net. (n.d.). Current sea water temperature in Cambodia. Retrieved September 12, 2024, from https://seatemperature.net/country/cambodia

Sem, S., Chin, E., Khoeun, T., Doung, R., Chhuon, K., Lun, S., ... & Eang, K. E. (2021). Groundwater Quality Assessment in the Coastal Area of Preah Sihanouk and Kampot Province, Cambodia.

Serafy, J. E., Shideler, G. S., Araújo, R. J., & Nagelkerken, I. (2015). Mangroves enhance reef fish abundance at the Caribbean regional scale. *PloS one*, *10*(11), e0142022.

Siguang Zhu, H. C. (2021). Distinct impacts of spring soil moisture over the Indo-China Peninsula on summer precipitation in the Yangtze River basin under different SST backgrounds. *Climate Dynamics*.

Sheaves, M., Collins, J., Houston, W., Dale, P., Revill, A., Johnston, R., & Abrantes, K. (2006). Contribution of floodplain wetland pools to the ecological functioning of the Fitzroy River Estuary.

Sheposh, R. (2024, August 25). *Low-pressure area (weather system)*. Retrieved from https://www.ebsco.com/research-starters/earth-and-atmospheric-sciences/low-pressure-area-weather-system

Sleeter, B. T. (2018). Land Cover and Land-Use Change. In Impacts, Risks, and Adaptation in the United States: Fourth National Climate Assessment. Washington, DC, USA: U.S. Global Change Research Program,. doi:doi: 10.7930/NCA4.2018.CH5

Smirnov, M. B. (2020). Atmospheric processes involving condensed water. *Physics of the Solid State*.

Sochanny Hak, J. M. (2018). Impact of government policies and corporate land grabs on indigenous people's access to common lands and livelihood resilience in northeast Cambodia. *Land 2018*. doi:https://doi.org/10.3390/land7040122

Sokles. L, et al. (2022). Health Impact Assessment from Rice Straw Production. *Applied Science*. doi:10.3390/app122010276

Son, N. T., Chen, C. F., & Chen, C. R. (2021). Flood assessment using multi-temporal remotely sensed data in Cambodia. *Geocarto International, 36*(9), 1044-1059. Retrieved from https://doi.org/10.1080/10106049.2019.1633420

Song, C., Huang, B., Ke, L., & Richards, K. S. (2014). Remote sensing of alpine lake water environment changes on the Tibetan Plateau and surroundings: A review. ISPRS Journal of Photogrammetry and Remote Sensing, 92, 26–37.

Sorn, P., & Veth, S. (2019). Climate change vulnerability assessment: Koh Kapik Ramsar Site, Cambodia. Bangkok, Thailand: IUCN. X + 36pp.

Soulard, C.E. (2020). Implementation of a Surface Water Extent Model in Cambodia using Cloud-Based Remote Sensing. *Remote sensing*.

Srinivasan, G., Agarwal, A., & Bandara, U. (2024). Climate change impacts on water resources and agriculture in Southeast Asia with a focus on Thailand, Myanmar, and Cambodia. *In The Role of Tropics in Climate Change.* , (pp. 17-32).

Statista. (2024, November 04). *Urbanization in Cambodia 2023*. Retrieved from Aaron O'Neill: https://www.statista.com/statistics/455789/urbanization-in-cambodia/

Streets, D. G. (2003). Biomass burning in Asia: Annual and seasonal estimates and atmospheric emissions. *Global Biogeochemical Cycles*, 17(4).

Streets, D. G., Yarber, K. F., Woo, J.-H., & Carmichael, G. R. (2003). Biomass burning in Asia: Annual and seasonal. *Global Biogeochemical Cycles*, 17(4), n/a–n/a. doi:10.1029/2003GB002040

Suddhiyam, N. W. (2013). *Vulnerability to climate change: Adaptation strategies and layers of resilience.* Patancheru 502 324, Andhra Pradesh, India: International Crops Research Institute for the Semi-Arid Tropics.

Sumanta Das. (2022). A Review of UHI formation over changing climate and its impacts on Urban Land Use and Environments and Adaptation Measures. *International Journal of Environment and Geoinformatics (IJEGEO), 9(1): 064-073. doi. 10.30897/ijegeo.938231*.

Sutton, W. R., P, J., Srivastava, Koo, J., Vasileiou, I., & Pradesh, A. (2019). *Striking a Balance: Managing El Niño and La Niña in Cambodia's Agriculture. RepNo 132065. World Bank, Washington, DC. License: Creative Commons Attribution C.*

Sytharith Pen, Saeed Rad, Liheang Ban, Sokhorng Brang, Panha Nuth and Lin Liao. (2024). An Analysis of Extreme Rainfall Events in Cambodia. *Atmosphere*.

Tang, J., Niu, X., Wang, S., Gao, H., Wang, X., & Wu, J. (2016). Statistical downscaling and dynamical downscaling of regional climate in China: Present climate evaluations and future climate projections. *Journal of Geophysical Research, 121*(5), 2110–2129. https://doi.org/10.1002/2015JD024141

Taylor, R. G., Todd, M. C., Kongola, L., Maurice, L., Nahozya, E., Sanga, H., & MacDonald, A. M. (2013). Evidence of the dependence of groundwater resources on extreme rainfall in East Africa. *Nature Climate Change, 3*(4), 374–378. https://doi.org/10.1038/nclimate1731

Tebaldi, C., Debeire, K., Eyring, V., Fischer, E., Fyfe, J., Friedlingstein, P., . . . Ziehn, T. (2021). Climate model projections from the Scenario Model Intercomparison Project (ScenarioMIP) of CMIP6. Earth Syst. Dynam., 12(1), 253-293. doi:10.5194/esd-12-253-2021

Tetsuya, W. (2022). Seasonal and Diurnal Variations of Meteorological Elements in a Tropical Deforested Area in Cambodia. 1-10.

Thanh Duc Dang, A. F. (2020). On the representation of water reservoir storage and operations in large-scale hydrological models: implications on model parameterization and climate change impact assessments. *Hydrology and Earth System Sciences*.

The International Charter: Space And Major Disasters, I. (2013). *Flood in Cambodia. https://disasterscharter.org/web/guest/activations/-/article/flood-in-cambod-4 .*

Thoeun, H. C. (2015). Observed and projected changes in temperature and rainfall in Cambodia. *Weather and Climate Extremes*, 7, 61-71.

Thrasher, B., Maurer, E. P., McKellar, C., & Duffy, P. B., 2012: Technical Note: Bias correcting climate model simulated daily temperature extremes with quantile mapping. Hydrology and Earth System Sciences, 16 (9), 3309-3314, https://doi.org/10.5194/hess-16-3309-2012.

Timmermans, M. L. (2020). Understanding Arctic Ocean circulation: A review of ocean dynamics in a changing climate. *Geophysical Research*.

Touch, T., Oeurng, C., Jiang, Y., & Monkhtar, A. (2020). Integrated Modeling of Water Supply and Demand Under Climate Change Impacts and Management Options in Tributary Basin of Tonle Sap Lake. *Water*.

Toure, S., Stow, D., Shih, H., Weeks, J., & Lopez-Carr, D. (2018). Land cover and land use change analysis using multi-spatial resolution. *Remote Sen. Environ.*, 210, 259–268.

Tran Canh. (2000). *Land of Cambodia.* Department of Natural Resource Assessment and Environmental Data Management, Ministry of Environment.

Tran, T. L., Ritchie, E. A., & Perkins-Kirkpatrick, S. E. (2022). A 50-year tropical cyclone exposure climatology in southeast Asia. *Journal of Geophysical Research: Atmospheres*, 127(4), e2021JD036301.

Trisurat, Y., Aekakkararungroj, A., Ma, H. o., & Johnston, J. M. (2018). Basin-wide impacts of climate change on ecosystem services in the Lower Mekong Basin. *Ecological Research*, 33(1), 73–86. doi:https://doi.org/10.1007/s11284-017-1510-z

Tsujimoto, K., Ohta, T., Aida, K., Tamakawa, K., & So Im, M. (2018). Diurnal pattern of rainfall in Cambodia: its regional characteristics and local circulation. *Progress in Earth and Planetary Science, 5*, 1-18. doi:https://doi.org/10.1186/s40645-018-0192-7

Tudoroiu, M., et al. (2016). Negative elevation-dependent warming trend in the Eastern Alps. Environmental Research Letters, 11(4), 044021. https://doi.org/10.1088/1748-9326/11/4/044021

Turap, T., Merupakan, T. B., Lebih, T. B., & Turap, T. D. (2024). The Role of Tropics in Climate Change.

Tylor, D. (2010). Burning, humans and climate change in Southeast Asia. *Biodiversity and Conservation*, 1025-1042.

UN Environment Programme. (2019). *Global Environment Outlook – GEO-6: Healthy Planet, Healthy People.*

United Nations Environment Programme. (2005). Sixth meeting of the regional working group for the wetlands sub-component of the UNEP/GEF project: "Reversing environmental degradation trends in the South China Sea and Gulf of Thailand". Sihanoukville, Cambodia, 12th – 15th September 2005.

United Nations Environment Programme. (2007). *Procedure for determination of national and regional economic values for ecotone goods and services, and total economic values of coastal habitats in the context of the UNEP/GEF project entitled: "Reversing environmental degradation trends in the South China Sea and Gulf of Thailand"* (South China Sea Knowledge Document No. 3, UNEP/GEF/SCS/Inf.3).

United Nations Environment Programme. (2008). Strategic action programme for the South China Sea (UNEP/GEF/SCS Technical Publication No. 16).

UNCCD. (2019). *Drought Initiative-Cambodia. https://www.unccd.int/sites/default/files/country_profile_documents/1%2520FINAL_NDP_Cambodia%255B1157%255D.pdf.*

UNDP. (2016). *Climate Change and Labour: Impacts of Heat in the Workplace. In Climate Vulnerable Forum Secretariat. https: //www.ilo.org/wcmsp5/groups/public/---ed_emp/---.*

UNDP. (2022). *Human Development Report 2021/2022.* Retrieved from https://hdr.undp.org/system/files/documents/global-report-document/

UNESCO, & UN-Water. (2020). *United Nations World Water Development Report 2020: Water and Climate Change, Paris, UNESCO.*

UNFCCC. (2020, October 5). Urban Climate Action Is Crucial to Bend the Emissions Curve. Retrieved from https://unfccc.int/news/urban-climate-action-is-crucial-to-bend-the-emissions-curve

UNICEF. (2023). United Nations Children's Fund, Climate rationale for water, sanitation and hygiene services in Cambodia, UNICEF, New York, 2023.

United Nations Development Programme, U. (2019). *Climate Change Adaptation in Cambodia: A Pathway to Sustainable Development.*

Upham, L. M. (2014). Creating Law from the Ground Up: Land Law in Post-Conflict Cambodia. *Asian Journal of Law and Society , Volume 1 , Issue 1 , May 2014 ,* , pp. 55 - 77.

Upreti, M. S. (2024). Major challenges in the urbanizing world and role of earth observations for livable cities. *In Earth observation in urban monitoring*.

USAID. (2019). *Climate Risk Profile-Cambodia. In USAID-Fact Sheet (Issue February). https://doi.org/10.1007/978-3-531-18950-5_17.*

Van der Werf, G. R. et al. (2008). Climate regulation of fire emissions and deforestation in equatorial Asia. *Proceedings of the National Academy*, 105(51), 20350–20355. doi:10.1073/pnas.0803375105

Velastegui-Montoya, A., de Lima, A., & Adami, M. (2020). Multitemporal analysis of deforestation in response to the construction of the Tucurui Dam. *Geo-Inf.*, 583.

Veron, J. E., Hoegh-Guldberg, O., Lenton, T. M., Lough, J. M., Obura, D. O., Pearce-Kelly, P. A. U. L., ... & Rogers, A. D. (2009). The coral reef crisis: The critical importance of< 350 ppm CO2. Marine pollution bulletin, 58(10), 1428-1436.

Vinayachandran, P. N., Seng, D. C., & Schmid, F. A. (2022). Climate change and coastal systems. In Blue economy (pp. 341–377). Springer. https://doi.org/10.1007/978-981-19-5065-0_12

Vörösmarty, C. J., & Dork, S. (2000). Anthropogenic disturbance of the terrestrial water cycle. BioScience, 50(9), 753–765. https://doi.org/10.1641/0006-3568(2000)050[0753:ADOTTW]2.0.CO;2

Wang, J., Hong, Y., Gourley, J., Adhikari, P., Li, L., & Su, F. (2010). Quantitative assessment of climate change and human impacts on long-term hydrologic response: A case study in a sub-basin of the Yellow River, China. International Journal of Climatology, 30(14), 2130–2137. https://doi.org/10.1002/joc.2032

Wang, L., & Chen, W. A. (2014). CMIP5 multimodel projection of future temperature, precipitation, and climatological drought in China. *Int. J. Climatol.*, 34, 2059–2078. doi:https://doi.org/10.1002/joc.3822

Wangmo, D. (2022). The Climate Change Impacts on Tibet: An Analysis of Key Research Findings on the Cryosphere. Tibet Policy Journal, 65.

Warner, J. A. (1968). A reduction in rainfall associated with smoke from sugarcane fires—An inadvertent weather modification? *Journal of Applied Meteorology*, 7(2), 247-251.

Watson, R. T. (1990). *Greenhouse gases and aerosols.* Cambridge University Press.

Waycott, M., Collier, C., McMahon, K., Ralph, P., McKenzie, L., Udy, J., & Grech, A. (2007). Vulnerability of seagrasses in the Great Barrier Reef to climate change. Great Barrier Reef Marine Park Authority and Australian Greenhouse Office.

Weng, Q. (2009). Thermal infrared remote sensing for urban climate and environmental studies: Methods, applications, and trends. *ISPRS Journal of photogrammetry and remote sensing, 64*(4), 335-344.

Wenjia Hu, Y. W. (2020). Predicting potential mangrove distributions at the global northern distribution margin using an ecological niche model: Determining conservation and reforestation involvement. *Forest Ecology and Management*.

Whitfield, A. K. (2017). The role of seagrass meadows, mangrove forests, salt marshes and reed beds as nursery areas and food sources for fishes in estuaries. *Reviews in Fish Biology and Fisheries*, *27*(1), 75-110.

WHO, C. O. (2020). World health organization. *Air Quality Guidelines for Europe*, 91.

William, S. R., Jitendra, S. P., Jawoo, K., Loannis, V., & Angga, P. (2019). Striking a Balance Managing El Niño and La Niña in Cambodia's Agriculture. Washington, DC: The World Bank.

Wood, A., Leung, L., Sridhar, V., & Lettenmaier, D. (2004). Hydrologic Implications of Dynamical and Statistical Approaches to Downscaling Climate Model Outputs. *Clim. Change*, 62, 189-216.

Wood, A.W., E.P. Maurer, A. Kumar, and D.P. Lettenmaier, 2002: Long-range experimental hydrologic forecasting for the eastern United States. J. Geophysical Research-Atmospheres,107, 4429, https://doi.org/10.1029/2001JD000659.

World Atlas (2025). "What Kind of Climate Does Cambodia Have?". Retrieved from https://www.worldatlas.com/articles/what-type-of-climate-does-cambodia-have.html

World Bank, W. (2016). *Cambodia: Climate Change Impacts on Agriculture and Food Security.*

World Bank. (2017, December 20). *Urban Development in Phnom Penh*. Retrieved from World Bank Group: https://www.worldbank.org/en/country/cambodia/publication/urban-development-in-phnom-penh

World Bank. (2020). *Food Price Volatility: Causes and Consequences.*

World Bank. (2021). *Climate Change Knowledge Portal for Development Practitioners and Policy Makers: Historical Hazards.* Retrieved from https://climateknowledgeportal.worldbank.org/country/cambodia/vulnerability

World Bank. (2021). *Climate Change Knowledge Portal for Development Practitioners and Policy Makers: Historical Hazards*. Retrieved from https://climateknowledgeportal.worldbank.org/country/cambodia/heat-risk

World Bank. (2019). Retrieved October 2019, from https://data.worldbank.org/country/cambodia

World Bank. (2021). *Climate Change Knowledge Portal for Development Practitioners and Policy Makers: Historical Hazards.* Retrieved from https://climateknowledgeportal.worldbank.org/country/cambodia/vulnerability

World Bank. (2021). *Climate Change Knowledge Portal for Development Practitioners and Policy Makers: Historical Hazards*. Retrieved from https://climateknowledgeportal.worldbank.org/country/cambodia/heat-risk

World Bank. (2021). *Cambodia climate risk country profile*. Retrieved November 9, 2023, from https://www.worldbank.org

World Bank. (2021). Climate data: Historical - Cambodia. Climate Change Knowledge Portal. Retrieved September 13, 2024, from https://climateknowledgeportal.worldbank.org/country/cambodia/climate-data-historical

World Bank. (2023). *Cambodia Country Climate and Development Report.* Retrieved from https://documents1.worldbank.org/curated/en/099092823045083987/pdf/P17887106c6c2d0e909aa1090f3e10505c1.pdf

World Bank. (2023, April 03). *Urban Development*. Retrieved from https://www.worldbank.org/en/topic/urbandevelopment/overview

World Bank. (2023). *Cambodia Country Climate and Development Report.* Retrieved from https://documents1.worldbank.org/curated/en/099092823045083987/pdf/P17887106c6c2d0e909aa1090f3e10505c1.pdf

World Bank. (2024). *Climate Risk Profile: Cambodia. The World Bank Group.* Retrieved from https://climateknowledgeportal.worldbank.org/sites/default/files/country-profiles/16814-WB_Cambodia%20Country%20Profile-WEB.pdf

World Bank, W., & Asian Development Bank, A. (2021). *Climate Risk Profile: Cambodia.* Retrieved from https://www.adb.org/publications/climate-risk-country-profile-cambodia

World Health Organization, W. (2018). *Climate Change and Health in Cambodia.*

Xianan Jiang, Á. F. (2020). Fifty Years of Research on the Madden-Julian Oscillation: Recent Progress, Challenges, and Perspectives. *Geophysical Research: Atmospheres*.

Yadav, I. C. (2019). Biomass burning, regional air quality, and climate change. *Encyclopedia of Environmental Health*, 2.

Yadav, I. C. (2019). Yadav, I. C., & Devi, N. L. (2019). Biomass burning, regional air quality, and climate change. Encyclopedia of Environmental Health, 2. *Encyclopedia of Environmental Health*, 2.

Yang, K., et al. (2014). Recent climate changes over the Tibetan Plateau and their impacts on the energy and water cycle: A review. Global and Planetary Change, 112, 79–91. https://doi.org/10.1016/j.gloplacha.2013.12.001

Yang, L. (2014). Green Building Design: Wind Environment of Building. Shanghai: Tongji University Press. *Atmospheric Environment, 7 (8), 769-779.*

Yang, Y., Keating, A., & Sourn, C. (2024). Measuring community disaster resilience for sustainable climate change adaptation: Lessons from time-series findings in rural Cambodia. *Disasters*, e12647. doi:https://doi.org/10.1111/disa.12647

Yang, Y., Zhang, S., Roderick, M. L., McVicar, T. R., Yang, D., Liu, W., & Li, X. (2020). Comparing Palmer Drought Severity Index drought assessments using the traditional offline approach with direct climate model outputs. Hydrology and Earth System Sciences, 24(6), 2921–2930. https://doi.org/10.5194/hess-24-2921-2020

Yao, X., et al. (2016). Spatial-temporal variations of lake ice phenology in the Hoh Xil region from 2000 to 2011. Journal of Geographical Sciences, 26(1), 70–82. https://doi.org/10.1007/s11442-016-1255-6

Yeh, S. W., Cai, W., Min, S. K., McPhaden, M. J., Dommenget, D., Dewitte, B., & Kug, J. S. (2018). ENSO atmospheric teleconnections

Yi Lin, Y. R. (2023). Spatiotemporal impacts of climate change and human activities on water resources and ecological sensitivity in the Mekong subregion in Cambodia. *Environmental Science and Pollution Research*, 4023-4043.

Yoichi Fujihara, K. O. (2021). Characteristics of the annual maximum and minimum water temperatures in Tonle Sap Lake, Cambodia from 2000 to 2019. *Remote Sensing*.

Yokelson, R. J. (2009). Emissions from biomass burning in the Yucatan. *Atmospheric Chemistry and Physics, 9(15), 5785-5812.*, (15).

Yokoi, R. W. (2022). *Future greenhouse gas emissions from metal production: gaps and opportunities towards climate goals.*

Yusuf, A. A., & Herminia, F. (2009). Climate Change Vulnerability Mapping for Southeast Asia Vulnerability Mapping for Southeast Asia. *Singapore*. doi:http://www.eepsea.org

Zemp, M., et al. (2019). Global glacier mass changes and their contributions to sea-level rise from 1961 to 2016. Nature, 568(7752), 382–386. https://doi.org/10.1038/s41586-019-1071-0

Zhang, G., et al. (2014). Estimating surface temperature changes of lakes in the Tibetan Plateau using MODIS LST data. Journal of Geophysical Research, 119(14), 8552–8567. https://doi.org/10.1002/2014JD021615

Zhang, X., & Yang, F. (2004). RClimDex (1.0) user manual. Climate Research Branch Environment Canada, 22, 13-14. Link: https://rcc.acmad.org/procedure/RClimDexUserManual.pdf

Zhao, W., Abhishek, & Kinouchi, T. (2022). Uncertainty quantification in intensity-duration-frequency curves under climate change: Implications for flood-prone tropical cities. *Atmospheric Research*, 270. https://doi.org/10.1016/j.atmosres.2022.106070.

Zhao, X., Heidinger, A. K., & Walther, A. (2016). Climatology analysis of aerosol effect on marine water cloud from long-term satellite climate data records. Remote Sensing, 8(4), 300.

Annex A1: Method for calculating the Temperature Indices and Detecting Changes in Temperature

1. **Maximum Temperature (TXx)**

TXx is the annual value of daily maximum temperature.

- step1: Collect daily maximum temperatures (TXx): gather daily maximum temperature values for each day in the period of interest.
- step 2: Identify the highest value: from the collected TXx values, find the single highest temperature.

TXx =max (Tmax1, Tmax2, …,Tmaxn)

where:

Tmax1, Tmax2, ……, Tmaxn are the daily maximum temperature over n days.

2. **Minimum Temperature (TXn)**

TXn is the annual minimum value of daily minimum of temperature

- step1: Collect daily minimum temperatures (TXn): gather daily minimum temperature values for each day in the period of interest.
- step 2: Identify the lowest value from the collected TXn values, find the single lowest temperature as E.q.1 below:

TXn =min (Tmin1, Tmin2,…,Tminn) E.q.1

where:

Tmin1, Tmin2, ……, Tminn are the daily minimum temperatures over n days.

3. **Hot Days Maximum (TX90p) and Warm Night Minimum (TN90p)**

TX90p is the day that the daily maximum temperature exceeds the 90th percentile of a reference period. TN90p is the nights that the daily minimum temperature exceeds the 90th percentile of a reference period.

- step1: gather daily maximum/minimum temperature data for each year
- step2: sort the daily maximum/minimum temperature for the year in ascending order from lowest to highest.
- step3: calculate the 90th percentile by using formula E.q.2. Then the 90th percentile of maximum/minimum temperature is found in the sorted list.

$$\mathbf{P90} = \frac{\mathbf{90}}{\mathbf{100}} \times (\mathbf{N} + \mathbf{1}) \qquad \textbf{E.q.2}$$

Where:

N is the total number of maximum/minimum temperature data points for the year.

- step4: find the threshold maximum/minimum temperature corresponding to the 90th percentile sorted list (P90). Let's assume it is 32.8 ^{o}C.

- step5: count any day in the sorted list that is above 32.8 ^{o}C in the sorted list (P90).

*Note: TX90p uses the maximum temperature data and TN90p uses the minimum temperature data.

4. **Cool Day Maximum (TX10p) and Cold Night Minimum (TN10p)**

TX10p is days that the daily maximum temperature falls below the 10th percentile of a reference period. TN10p i nights that minimum temperature falls below the 10th percentile of a reference period.

- step1: gather daily maximum/ minimum temperature data for each year
- step2: sort the daily maximum/minimum temperature for the year in ascending order from lowest to highest.
- step3: calculate the 10th percentile by using formula E.q.3. Then the 10th percentile of maximum/minimum temperature is found in the sorted list.

$$\mathbf{P10} = \frac{\mathbf{10}}{\mathbf{100}} \times (\mathbf{N} + \mathbf{1}) \qquad \textbf{E.q.3}$$

Where:

N is the total number of maximum/minimum temperature data points for the year.

- step4: find the threshold maximum/minimum temperature corresponding to the 10th percentile sorted list (P10). Let's assume it is 32.8 ^{o}C
- step5: count any day in the sorted list that is below 32.8 ^{o}C in the sorted list (P10)

*Note: TX10p uses the maximum temperature data and TN10p uses the minimum temperature data.

Annex A2: Method for Calculating the Trend of Annual Rainfall and the Magnitude of the Trend

1. Mann-Kendall test and Sen's Slope method

The Mann-Kendall test is a non-parametric test for identifying the increasing or decreasing trend in a long-time series dataset and is used in various studies such as hydrology, meteorology, environment, and climate. This method is based on two hypotheses. The first is the null hypothesis, which indicates no significant trend in a time series dataset. Second is the alternative hypothesis, which indicates a significant increasing or decreasing trend in a time series dataset over time (Kendall, 1948; Mann, 1945). The Mann- Kendall Test- statistic S is given as:

$$S = \sum_{k=1}^{n-1} \sum_{j=k+1}^{n} \operatorname{sgn}(\chi_j - \chi_k) \qquad \textbf{(Eq. 4)}$$

$$S = sgn(x_j - x_k) = \begin{cases} 1 \text{ if } (x_j - x_k) > 0 \\ 0 \text{ if } (x_j - x_k) = 0 \\ -1 \text{ if } (x_j - x_k) < 0 \end{cases} \qquad \textbf{(Eq. 5)}$$

The variance of S denoted by σ_s^2 is computed as:

$$\sigma_s^2 = \frac{n(n-1)(2n+1) - \sum_{j=1}^{q} t_j(t_j-1)(2t_j+5)}{18} \qquad \textbf{(Eq. 6)}$$

where *n* is the number of data points, *q* is the number of tied groups in the data set, and t_j is the number of data points in the j_{th} tied group. The slope of the trend in a time series dataset can be calculated using new non-parametric methods (Sen, 1968). Then *S* and σ_s^2 were used to compute the test statistic Z_s as:

$$\begin{aligned} Z_s &= \frac{S-1}{\sigma} \quad if\, S > 0 \\ Z_s &= 0 \qquad if\, S = 0 \\ Z_s &= \frac{S+1}{\sigma} \quad if\, S < 0 \end{aligned} \qquad \textbf{(Eq. 7)}$$

A positive value of *S* indicates that there is an increasing trend and a negative value indicates a decreasing trend. The null hypothesis H_0 that there is no trend in the data is either accepted or rejected depending if the computed Z_S statistics is less than or more than the critical value of Z-statistics obtained from the normal distribution table at 5% significance level.

2. Trends of annual rainfall

Trend analyses were conducted using the Mann-Kendall (MK) test, and the magnitude of trends was assessed using the Sen Slope method, as previously described. The results are summarized in Table 1. No significant trends in annual rainfall were detected at the 0.05 significance level for any of the individual stations, as the computed Z statistics were all below the critical value of 1.96. Although these trends are not statistically significant, a

general decreasing in rainfall is evident, as indicated by the negative values of the Mann-Kendall statistic (S).

Annex A3: Method for Calculating Rainfall Indices

1. Determination of Extreme Rainfall Indices

Extreme rainfall indices are measures used to quantify and analyze heavy precipitation events. These indices can help understand the intensity, duration, and frequency of extreme rainfall events, which is vital for flood forecasting, water management, and assessing the impacts of climate change. The analysis in this report covers a period of 34 years (1990 – 2023) and includes the following extreme rainfall indices: RX1day, R50, and R100 (which capture intense rainfall events), CDD, and CWD (which reflect periods of drought and rainfall). RClimDex 1.0 was used to assist in the computation of these indices (Zhang and Yang, 2004). The trends identified in these indices help reveal whether extreme weather events are becoming more frequent or severe. The determination and calculation of these indices are described as follows.

Rx1day (Annual maximum 1-day precipitation): The highest daily rainfall amount recorded within a year.

R50mm (Annual count of days with daily precipitation ≥ 50 mm): Count of the number of days in a year where the daily rainfall was 50 mm or more.

R100mm (Annual count of days with daily precipitation ≥ 100 mm): Similar to R50mm, count of the days with daily rainfall of 100 mm or more.

CDD (Consecutive Dry Days):

- Identify a sequence of days with no rainfall.
- Count the number of days in the longest such sequence within a year.

CWD (Consecutive Wet Days):

- Identify a sequence of days with rainfall on each day.
- Count the number of days in the longest such sequence within a year.

2. Trend analysis using Mann Kandell Test and Sen's Slope

A non-parametric Mann-Kendall test was employed to assess trends in extreme rainfall indices and SPI, determining whether these indices exhibit significant increasing, decreasing, or stationary patterns. Estimating the magnitude of trend using the Sen's slope estimator. R package (trend) was used to assist in the Mann Kandell test and estimation of Sen's slope (see Annex A2 for more on the Man

The Mann-Kendall test is a non-parametric test for identifying the increasing or decreasing trend in a long-time series dataset and is used in various studies such as hydrology, meteorology, environment, and climate. This method is based on two hypotheses. The first is the null hypothesis, which indicates no significant trend in a time series dataset. Second is the alternative hypothesis, which indicates a significant increasing or decreasing trend in a time series dataset over time (Kendall, 1948; Mann, 1945). The Mann- Kendall Test- statistic S is given as:

$$S = \sum_{k=1}^{n-1} \sum_{j=k+1}^{n} \operatorname{sgn}(x_j - x_k)$$

$$S = sgn(x_j - x_k) = \begin{cases} 1 \text{ if } (x_j - x_k) > 0 \\ 0 \text{ if } (x_j - x_k) = 0 \\ -1 \text{ if } (x_j - x_k) < 0 \end{cases}$$

The variance of S denoted by σ_s^2 is computed as:

$$\sigma_s^2 = \frac{n(n-1)(2n+1) - \sum_{j=1}^{q} t_j (t_j - 1)(2t_j + 5)}{18}$$

where *n* is the number of data points, *q* is the number of tied groups in the data set, and t_j is the number of data points in the j_{th} tied group. The slope of the trend in a time series dataset can be calculated using new non-parametric methods (Sen, 1968). Then *S* and σ_s^2 were used to compute the test statistic Z_s as:

$$Z_S = \frac{S-1}{\sigma} \quad if\, S > 0$$
$$Z_S = 0 \quad if\, S = 0$$
$$Z_S = \frac{S+1}{\sigma} \quad if\, S < 0$$

A positive value of *S* indicates that there is an increasing trend and a negative value indicates a decreasing trend. The null hypothesis H_0 that there is no trend in the data is either accepted or rejected depending if the computed Z_S statistics is less than or more than the critical value of Z-statistics obtained from the normal distribution table at 5% significance level.

Annex A4: Method for Flood and Drought Assessment at the Country Scale

1. Calculation of Standardized Precipitation Index (SPI)

McKee and his colleagues introduced the Standardized Precipitation Index (SPI) at Colorado State University to systematically evaluate droughts over time. SPI is simply the difference of precipitation from the mean for a specified period divided by the standard deviation where the mean and standard deviation are determined from past records.

Calculating SPI requires at least 30 years of monthly precipitation data for a specific location. This method standardizes precipitation time series data into a normal distribution (Z-distribution). Criteria were defined for identifying drought events based on SPI values. A drought begins when the SPI consistently remains negative and ends when it turns positive. Initially, SPI was calculated for periods of 3, 6, 9, 12, and 24 months. However, research by Mishra et al. (2009) showed that the choice of time interval significantly impacts the statistical properties of droughts. The SPI is computed by fitting a gamma probability density function to the observed precipitation frequency distribution. SPEI, an R package, was used to assist in the computation of SPI.

The calculation in this report was based on three timescales: 3-, 6-, and 12-month SPI. Hence, the data were aggregated as follows:

- 3-month SPI: Sum of the precipitation for the current month and the previous two months.
- 6-month SPI: Sum of the precipitation for the current month and the previous five months.
- 12-month SPI: Sum of the precipitation for the current month and the previous eleven months.

Probability Distribution Fitting:

- For each time scale, fit a probability distribution to the aggregated precipitation data. A common choice is the Gamma distribution.
- The parameters of the fitted distribution characterize the long-term behavior of precipitation for that time scale.

Probability Calculation: Calculate the probability of the observed aggregated precipitation occurring based on the fitted probability distribution. This gives the cumulative probability.

The Gamma distribution is provided as follows:

$$g(x) = \frac{1}{\beta^{\alpha}\Gamma(\alpha)} x^{\alpha-1} e^{-\frac{x}{\beta}} \text{ for } \alpha>0;\ \beta>0;\ x>0$$

where α being the shape parameter, β being the scale parameter and x being the precipitation.

$$\alpha = \frac{1}{4A}\left(1 + \sqrt{1 + \frac{4A}{3}}\right)$$

and

$$\beta = \frac{\bar{x}}{\alpha}$$

For n observations, the parameter A is computed as:

$$A = ln\bar{x} - \frac{\sum lnx}{n}$$

The equation for the cumulative probability G(x) of an actual amount of rainfall occurring for a certain month and time scale may now be generated by integrating the probability density function relating to x and inserting the estimations of and:

$$G(x) = \int_0^x g(x)dx = \frac{1}{\beta^{\alpha}\Gamma(\alpha)} x^{\alpha-1} e^{-\frac{x}{\beta}} dx$$

The rainfall event could have a value of 0. However, x = 0 fails to establish the gamma function. The cumulative distribution is then changed as follows:

$$H(x) = q + (1 - q)G(x)$$

where q, is the probability of no rainfall on a specified time scale. H(x) is then transformed into standardized normal distribution Z at mean = 0 and Standard deviation = 1.

SPI Calculation:

The following formula is used to calculate the standard deviation:

$$\sigma = \sqrt{\frac{1}{N}\sum_{i=1}^{N}(x_i - \bar{x})^2}$$

where N is the number of years (in a given period), x_i is the annual precipitation, and $\bar{x}$ is the average precipitation.

Then SPI is calculated using the formula (Z-score):

$$SPI = z = \frac{x_i - \bar{x}}{\sigma}$$

The resulting z-score from the normalization step is the SPI value for that time scale.

2. Classification and Interpretation:

Drought and wetness conditions are interpreted based on SPI values classified in Table A4.1:

Table A4.1: SPI classification

SPI Values	Drought/Wetness Condition
SPI ≥ 2	Extremely wet

1.5 ≤ SPI < 2	Very wet
1 ≤ SPI < 1.5	Moderately wet
-1 < SPI < 1	Near normal
-1 ≥ SPI > -1.5	Moderately dry
-1.5 ≥ SPI > -2	Severely dry
SPI ≤ -2	Extremely dry

Positive SPI indicates wetter-than-average conditions whereas negative SPI indicates drier-than-average conditions. The magnitude of the SPI values reflects the severity of the wet or dry anomaly.

Key Points:

- Longer time scales (e.g., 12-month) are more suitable for assessing long-term drought conditions.
- Shorter time scales (e.g., 3-month) are more sensitive to recent precipitation patterns and can be useful for early warning of drought onset.
- The choice of time scale depends on the specific application and the hydrological characteristics of the region.

Annex A5: Approach for Determining Precipitation Events and Other Extreme Phenomena

1. Precipitation-related events

All the descriptions and results are based on a literature review of heavy monsoonal rainfall events that lead to flash floods, typhoons, tropical storms, and thunderstorms. The literature sources comprise research papers, review articles, and official reports from trusted bodies such as the Mekong River Commission (MRC), the Royal Government of Cambodia (RGC), the Asian Development Bank (ADB), and the Japan International Cooperation Agency (JICA). The literature quantified the frequencies of those events and damages in key sectors of the economy, such as agriculture, fisheries, and livelihoods. National and international news was also used to develop a comprehensive catalog of historical tropical storms impacting Cambodia. The news listed essential numerical and descriptive information to indicate the intensity of each tropical storm hitting parts of the country.

2. Other extreme phenomena

Extreme phenomena include, but are not limited to, El Nino, La Nina, and landslides. A wide array of literature was collected to provide evidence on the impacts of such phenomena at a national scale. Most of the literature is research articles that adopted process-based models and techniques to measure changes in precipitation during El Nino and La Nina years compared with neutral years and make predictions on the impacts on sectors such as agriculture, fisheries, and overall economic growth. Landslides were moderately discussed, as not many studies have been conducted on the topic. However, relationships between geography, season, and risks of landslides were formed to provide a picture of risk, frequency, and intensity of landslides in some regions of Cambodia.

3. Temperature-related events

Temperature-related events comprise heatwaves, urban heat islands, and droughts. Literature was collected to provide a clear overview of how such events have affected and will impact rural and urban areas. Since not many studies have been conducted on these topics, news articles were used to provide supportive evidence. Studies focusing on droughts are also relevant to studies on El Nino. The report also used predictions using observed data, historical and future climate datasets generated by regional climate model (RCM) based on selected emission scenarios, coupled with time series graphs and linear trends with significance.

4. Trends and Changes in Tropical Hurricanes, Typhoons, and Cyclones Frequency, Intensity, and Trajectory

Studies focusing on trends and changes in storms on a country level are unfortunately scarce. As a result, this section leverages all relevant literature on a regional level (Asia and Mekong River Basin) that studied historical trends of frequency and intensity and also predicted changes in the region. In addition, by using numerical models, those studies managed to quantify precipitation intensity induced by tropical cyclones/depressions and segregated the precipitation from the contribution of tropical cyclones/depressions. Methods involve correlation and linear regression analyses on multiple precipitation products, the use of climate indices and atmospheric data, and statistical tests to find significant trends and normality of data.

Annex A6: Approach for Determining Projections of Cambodia's Future Climate Change

1. Data and Method for Temperature Projection

Regarding temperature projection, the NASA Earth Exchange Global Daily Downscaled Projections (NEX-GDDP-CMIP6) dataset was also used. The Bias-Correction Spatial Disaggregation (BCSD) method used to generate the NEX-GDDP-CMIP6 dataset is a statistical downscaling algorithm specifically developed to address these limitations of global GCM outputs (Wood et al. 2002; Wood et al. 2004; Maurer et al. 2008; Thrasher et al. 2012). The algorithm compares the GCM outputs with corresponding climate observations over a common period and uses information derived from the comparison to adjust future climate projections so that they are progressively more consistent with the historical climate records and, presumably, more realistic for the spatial domain of interest. The algorithm also utilizes the spatial detail provided by observationally-derived datasets to interpolate the GCM outputs to higher-resolution grids.

For data pre-processing, because the BCSD method does not explicitly adjust trends (in particular, slopes) in climate variables produced by GCMs, we extract the monthly large-scale climate trends from the GCM temperature data. This is calculated as a 9-year running average for each individual month (e.g. the trend for all January taken together). These trends are preserved and added back to the adjusted data after the bias-correction step.

2. Method Assessment for Rainfall Downscaling in Cambodia

2.1. Dataset

Statistical downscaling employs statistical relationships between observations and climate models to replicate a climate condition over a specific region in more detail. Two types of datasets were used in this research: observed data and climate model data (Table 1). Five climate models from CMIP6 were selected by choosing one model or one ensemble from each institution to ensure that they are independent from each other, to avoid inter-model dependency. Those models are Euro-Mediterranean Centre for Climate Change (CMCC), Model for Interdisciplinary Research on Climate (MIROC), Max Planck Institute for Meteorology (MPI), Meteorological Research Institute (MRI), and Nanjing University of Information Science and Technology. In addition, the observational data were obtained from Multi-Source Weighted-Ensemble Precipitation (MSWEP).

Table A6.1: Detailed information on the dataset.

Data Center	Model Acronym	Resolution	Frequency	Available Period	Data Type
MSWEP	MSWEP	0.1°	daily	1979 to present	Observation
CMCC	CMCC-CM2-SR5	1.25°	daily	1850–2100	Climate Model
MIROC	MIROC6	1.4°	daily	1850–2100	Climate Model

MPI	MPI-ESM1-2-HR	0.94°	daily	1850–2100	Climate Model
MRI	MRI-ESM2-0	1.13°	daily	1850–2100	Climate Model
NUIST	NUIST-NESM3	1.88°	daily	1850–2100	Climate Model

In this report, downscaling is applied to each of the five climate models above by correcting the model data toward the observation data, that is MSWEP. In context of climate projection, multi-model information is very useful for overcoming uncertainty rather than relying on a single model. Thus, we select the above five models to investigate the consistency among the five models and focusing on multi-model ensemble information.

2.2. Bias-Corrected Spatial Disaggregation

The climate model from CMIP6 has a relatively coarse resolution, which is not suitable for extreme precipitation analysis in the local area. Therefore, downscaling the climate model is essential before applying it to local-scale studies, as it helps to reduce large biases in the model output. In this study, we applied a statistical downscaling method called "Bias-Corrected Spatial Disaggregation" (BCSD). The process of BCSD method contains three main steps. The flowchart in Figure A6.1 shows the detailed process of the BCSD method. Step 1 is to interpolate the observation data to the same spatial scale as that of the climate model. Step 2 is to use the upscaled observation to bias-correct the climate model, using the quantile mapping method. Step 3 is to perform spatial disaggregation on the bias-corrected climate model to a finer resolution.

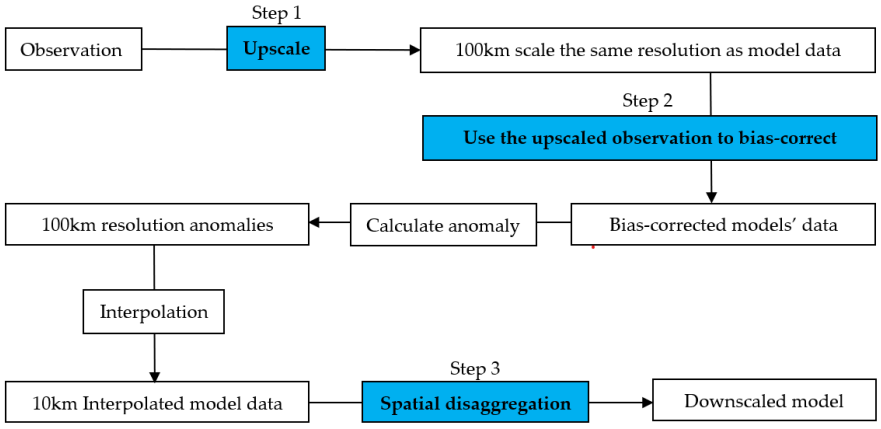

Figure A6.1: Flowchart describing the BCSD process.

2.2.1. Spatial Linear Interpolation of the Observed Data

The observed data were interpolated from the original scale to the same scale as the model data by using the bilinear interpolation method. Note that this process was done without any intervention of bias correction and spatial disaggregation. Afterward, the interpolated observed data were used to bias-correct the model data to remove as much of the model bias as possible.

2.2.2. Quantile Mapping

Quantile mapping (also referred to as quantile matching, cumulative distribution function matching, quantile-quantile transformation) attempts to find a transformation of a model

variable such that its new distribution equals the distribution of the observed variable. Quantile mapping is an application of the probability integral transform and if the distribution of the variable of interest is known, the transformation is defined as:

$$X_{m-corrected} = F_o^{-1}\big(F_m(X_m)\big),$$

Where X_m is a model variable, $F_m$is the cumulative distribution function of model variable, $F_o^{-1}$is the inverse cumulative distribution function (or quantile function) of the observation variable.

Quantile mapping was employed for bias correction. In other words, quantile mapping enhances the reliability of climate models by adjusting the distribution of their outputs to more closely match the observed distribution of climate variables. Quantile mapping was achieved by identifying a transfer function that captures the relationship between the observed and climate model data. Once the transfer function is determined, it can be used to calibrate climate model outputs that accurately resemble the observed data during the calibration period. Then, the calibrated relationship between the model and observed data was applied to the validation period or future period.

2.2.3. Spatial Disaggregation

After bias-correcting the climate model, the long-term mean of the model was removed to obtain the anomalous field, by dividing the data by the daily long-term mean. The daily long-term mean was calculated using a 30-day running window centered on each day of the year. The anomalous field of the bias-corrected model data was then interpolated to a fine scale that matches that of the observation. Next, the interpolated anomalous field was scaled by the long-term mean of the observation to align the model's spatial feature with the spatial pattern of the observation. Finally, the downscaled climate model data were obtained.

2.3. BCSD Method Performance

Before applying the BCSD method to downscale climate models for climate change projection, we evaluated the performance of the method. We employed statistical indicators such as time-series correlation, pattern correlation (correlation of 2D map rearranged into 1D), and root mean square errors (RMSE) to evaluate the performance of the BCSD method. Additionally, we also checked the performance in terms of climatological annual cycle pattern.

The correlation coefficient can be calculated using the expression below:

$$\mathrm{R} = \frac{\sum_{\mathrm{I}=1}^{\mathrm{N}}\left(|\mathrm{S_i}-\overline{\mathrm{S_i}}|(|\mathrm{O_i}-\overline{\mathrm{O_i}}|)\right)}{\sqrt{\sum_{\mathrm{i}=1}^{\mathrm{N}}(|\mathrm{S_i}-\overline{\mathrm{S_i}}|)^2}\times\sqrt{\sum_{\mathrm{i}=1}^{\mathrm{N}}(|\mathrm{O_I}-\overline{\mathrm{O_i}}|)^2}}$$

The value of RMSE can be determined using the equation below:

$$\mathrm{RMSE} = \sqrt{\frac{1}{\mathrm{n}}\sum_{\mathrm{i}=1}^{\mathrm{N}}(\mathrm{S_i}-\mathrm{O_i})^2}$$

Where:

- N is the number of samples
- n is the observed rainfall data
- S is the model-simulated rainfall data
- O_i and S_i are the averages of the corresponding data during N events

2.4. Climate Change Projection

After downscaling the climate models, we predicted climate patterns in the near-future period (2015–2045) and far-future period (2070–2100) under two climate change scenarios, using the downscaled climate model data. This research employed two Shared Socioeconomic Pathways scenarios (SSPs), namely SSP2-4.5 and SSP5-.85. SSP2-4.5 is a climate change scenario that assumes moderate socioeconomic development and moderate climate change mitigation. The number 4.5 refers to the radiative forcing of 4.5 watts per square meter by the year 2100. SSP5-8.5 is the worst-case climate change scenario that assumes high greenhouse gas emissions and high temperatures. The number 8.5 refers to the radiative forcing of 8.5 watts per square meter by the end of the year 2100. The main objective of this study was to project the changes in mean precipitation and extreme rainfall events, using extreme climate indices.

2.5. Extreme Climate Indicators

In this study, we projected two types of precipitation change information over Cambodia, after downscaling the coarse-resolution climate model to 10 km resolution. Firstly, we calculated the mean precipitation changes. Secondly, the CDD and CWD were calculated alongside the rx1day and nR50mm (See more explanation in Annex A3). These climate indicators are important for climate change projection linked to flood, drought, and rainfall pattern changes. The CDD is an indicator used for measuring drought severity and monitoring the changes in precipitation patterns over time. The CWD is a climate index that measures the longest period of consecutive days with at least 1 mm of precipitation, as defined by the ETCCDI. Rx1day is a climate index used for measuring the amount of precipitation that falls in a single day. Rx1day can be used to assess flood risk; monitor changes in precipitation patterns; and predict the likelihood of future flood events, such as flash floods or riverine floods. NR50mm is the index linked of frequency of days with rainfall more than moderate level (50mm). This index link flood risk and frequency of the event.

Furthermore, the multi-model-mean of each climate indicator was calculated. The process was one by dividing the downscaled climate model of the future time frame into two periods, which are the near future (2015–2044) and far future (2071–2100), and subtracting from the baseline period (1980–2014). Then, the median of the five climate models was calculated (multi-model ensemble) to determine a more reasonable outcome of precipitation change projection rather than showing the individual results of climate model.

2.5.1. Performance Evaluation of BCSD Method

Downscaling is very important in this study; therefore, we performed a cross-validation of the BCSD method on the historical data from CMIP6 models and compared it with observed data (Duong et al., 2023). The evaluation process used the data from 1980 to 2014 and divided them into two time periods: calibration or baseline period (1980–2004) and validation or future period (2005–2014). Thus, the performance of BCSD relies more on the validation outcomes as the climate projection is done for future periods.

Figure A6.2 presents the improvement of the climate models after downscaling in terms of pattern correlation and RMSE of the climatological annual cycle map. Figure A6.3a shows the pattern correlation of the climatological annual cycle map of the raw model and the downscaled model with observation. It can be seen that the correlation of the downscaled model with observation improves drastically from January to December. Additionally, Figure A6.3b shows the RMSE of raw and downscaled models with observations. The RSME of the downscaled model with observation reduces significantly each month compared to the raw model. However, in November and December, the RSME of the downscaled model slightly surpasses the raw model.

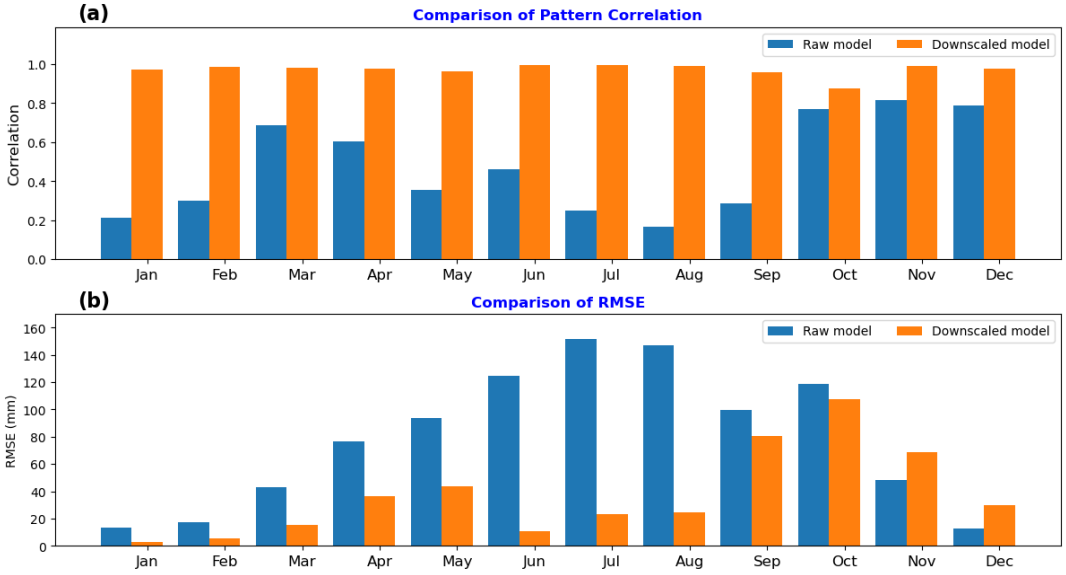

Figure A6.2: Pattern correlation (a) and RMSE of climatological annual cycle for the MPI-ESM1-2-HR model (b). Sample size for correlation calculation is 2500, which is the number of grid cells over Cambodia. Raw model data are bilinear interpolated to the same resolution as downscaled model data.

Figure A6.3 shows the correlation between the downscaled data and observed data. As seen on each map plot, the correlation of each climate model indicated a good relationship, with an average value of more than 0.7. Moreover, the highest correlation mostly occurs in the high-elevation area (northeastern region of the country) and coastal area (southwestern region).

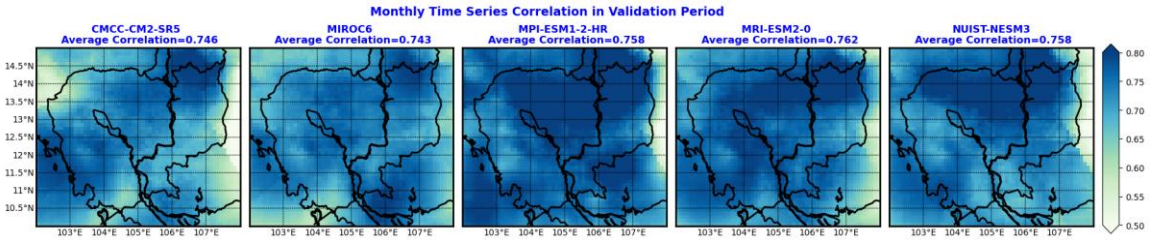

Figure A6.3: Correlation of monthly time series on each grid cell in validation period (2005–2014). Sample size for correlation calculation is 120, which is the number of months during the 10-year validation period.

Figure A6.4 illustrates the root mean square errors of downscaled and observed data. The highest error mostly occurs in the coastal area (southwestern region), resulting from the orographic effect varying the rainfall amount. Similarly, there are slight biases over the

high-elevation area (northeastern region), while the low-land area shows the smallest biases (central part of the country).

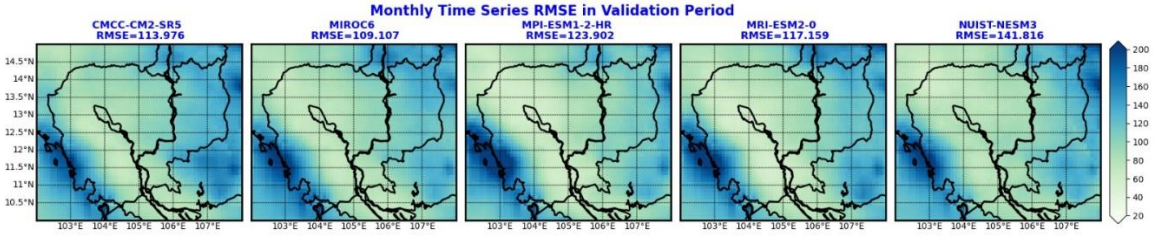

Figure A6.4: RMSE of monthly time series on each grid cell in validation period (2005–2014).

In summary, the results of cross-validation indicated the satisfactory performance of the BCSD method, which is suitable for application in Cambodia.